UNIVERSITÀ DEGLI STUDI DI GENOVA

Doctorate in Sciences and Technologies of Chemistry and Materials
Curriculum: Pharmaceutical, Food and Cosmetic Sciences

PhD Thesis

Development of quinone-based systems as new ligands for the treatment of Alzheimer's disease

Marta Campora

Advisors: Prof. Bruno Tasso **-** Prof. Michele Tonelli
Defense date: 30th March 2021

Table of content

List of abbreviations

3-APS	3-Amino-1-propanesulfonic acid
5-HT$_4$R	5-hydroxytryptamine 4 receptor
Acetyl-CoA	Acetyl-coenzyme A
Ach	Acetylcholine
AChE	Acetylcholinesterase
AChEI(s)	Acetylcholinesterase inhibitor(s)
AD	Alzheimer's disease
ADAM(s)	A disintegrin and metalloprotease(s)
ADDL(s)	Aβ-derived diffusible ligand(s)
ADE(s)	amyloid-degrading enzyme(s)
ADI	Alzheimer's disease International
ADRDA	Alzheimer's Disease and Related Disorders Association
AFM	Atomic force microscopy
AGE(s)	Advanced glycosylation end product(s)
AICD	APP intracellular domain
ApoE	Apolipoprotein E
APP	Amyloid precursor protein
AQ(s)	Anthraquinone(s)
Aβ	Amyloid beta
BACE	β-site APP cleaving enzyme
BBB	Blood-brain barrier
BChE	Butyrylcholinesterase
CAS	Catalytic active site
CD33	Cluster of differentiation 33
CDK5	Cyclin-dependent kinase 5
CGC(s)	Cerebellar granule cell(s)
ChAT	Choline acetlytransferase
ChE(s)	Cholinesterase inhibitor(s)
CK1	Casein kinase-1
CLU	Clusterin
CNS	Central nervous system
Cpd(s)	Compound(s)
CR1	Complement receptor 1
CSF	Cerebrospinal fluid exams
CT	Cranial computed tomography
DAPT	(2S)-N-[(3,5-difluorophenyl)acetyl]-L-alanyl-2-phenyl]glycine-1,1-dimethylethyl ester
DMT1	Divalent metal transporter 1
DSM	Diagnostic and statistical manual of mental disorders
DYRK-1A	Dual specificity tyrosine-phosphorylation-regulated kinase-1A
eeAChE	Electric eel acetylcholinesterase
EMA	European medicines agency
EOAD	Early onset Alzheimer's disease
EOFAD	Familial early onset Alzheimer's disease

ER	Endoplasmic reticulum
ERK1/2	Extracellular regulated protein kinase1/2
esBChE	Equine serum butyrylcholinesterase
FAD	Familial Alzheimer's disease
FAD	Flavin adenine dinucleotide
FDA	Food and drug administration
FPN	Ferroportin
GABA	γ-aminobutyric acid
GSH	Glutathione
GSH-Px/Rd	Glutathione peroxidase/reductase
GSK-3	Glycogen synthase kinase-3
GSMs	γ−secretase modulators
GWASs	Genome-wide association studies
hBChE	Human butyrylcholinesterase
HFIP	Hexafluoroisopropanol
IDE	Insulin-degrading enzyme
JNK	c-Jun N-terminal kinase
LDH	Lactate dehydrogenase
Lf	Lactoferrin
LOAD	Late-onset Alzheimer's disease
LRP1	Low-density lipoprotein receptor-related protein-1
MAO(s)	Monoamine oxidase(s)
MAP(s)	Microtubule-associated protein(s)
MAPK(s)	Mitogen-activated protein kinase(s)
MARK(s)	Microtubule affinity-regulating kinase(s)
MBD	Microtubule-binding domain
MCI	Mild cognitive impairment
MD	Molecular dinamics
MMSE	Mini-Mental State Examination
MRI	Magnetic resonance imaging
MTC	Methythioninium chloride
MTDL(s)	Multitarget directed ligand(s)
MTT	3-(4,5-dimethylthiazol-2-yl)-2,5-diphenyltetrazolium bromide
NADPH	Nicotinamide adenine dinucleotide phosphate
NASSA	Noradrenalin and selective serotonin antidepressant
NEP	Neutral endopeptidase
NFT(s)	Neurofibrillary tangle(s)
NINCDS	National institute of neurological and communicative disorders and stroke
NMDA	N-methyl-D-aspartate
NO	Nitric oxide
NOS	Nitric oxide synthase
NOX	NADPH oxidase
NQ(s)	Naphthoquinone(s)
OX	Xanthine oxidase
PAS	Peripheral anionic site
PDB	Protein data bank

PET	Positron emission tomography
PHF(s)	Paired helical filament(s)
PICALM	Phosphatidylinositol binding clathrin assembly protein
PKA	Cyclic AMP-dependent protein kinase A
PNS	Peripheral nervous system
PP1/2A/5	Protein phosphatase 1/2A/5
PS1/2	Presenilin-1/2
PSEN1/2	Presenilin-1/2 gene
p-tau	Hyperphosphorylated tau
RAGE(s)	Receptors for advanced glycosylation end product(s)
RNS	Reactive nitrogen species
ROS	Reactive oxygen species
RyR	Ryanodine receptor
SAR	Structure-activity relationship
SERCA	Sarco-Endoplasmic Reticulum Calcium ATPase
SOD	Superoxide dismutase
SORL1	Sortilin-related receptor
SR	Sarcoplasmic reticulum
SSRI	Serotonin reuptake inhibitors
T2D	Type 2 diabetes
TACE	Tumor necrosis factor-α converting enzyme
Tau	Tubulin-associated unit
TcAChE	Torpedo californica acetylcholinesterase
Tf	Transferrin
ThT	Thioflavin T
TNFa	Tumor necrotic factor a
TREM2	Triggering receptor expressed on myeloid cells 2
VAChT	Vesicular acetylcholine transporter
VaD	Vascular Dementia
WHO	World Health Organization
XR	Extended release

Summary

Alzheimer's disease is a neurodegenerative disorder characterized by a neuronal and synaptic loss of the cholinergic system and by the accumulation of amyloid β aggregates and hyperphosphorylated tau protein. There are two main forms of the disease, namely the familial form, which affects people younger than 65 and presents a genetic inheritance, and the sporadic form, which includes the remainder of Alzheimer's cases that usually occur in adults aged 65 and older.

Since current therapies offer only temporary benefits to patients, new strategies have been formulated on the basis of the complex nature of Alzheimer's disease. One of the leading approaches is the development of multi-target ligands, which are able to modulate simultaneously different pathogenic processes. On the pattern of the previously identified multi-target leads, which displayed the ability to inhibit both cholinesterases and amyloid β aggregation, the efforts of my PhD work have concerned the design and synthesis of four different series of naphtho- and anthraquinone derivatives connected through a polymethylene chain of variable length to an (hetero)aromatic ring or a basic moiety.

The first set is characterized by the presence of hydrophobic features selected for an efficient interaction with a sequence of aromatic amino acids of amyloid β, implicated in the initial phases of aggregation. For the others set, the scaffold has been decorated exploiting the piperazine or piperidine ring as basic feature in order to improve the inhibition of cholinesterases. All the compounds have been evaluated *in vitro* for the inhibitory activities towards amyloid β aggregation and both cholinesterases. The first set was subsequentially evaluated towards other targets such as Tau and MAO. Since most of the derivatives have been shown a multi-target mechanism of action, some promising compounds of the second set have been selected for further biological studies that I performed at the University of Bath (UK) to establish their safety profile and their value as potential neuroprotective agents and γ-secretase inhibitors.

The encouraging results gathered show that these derivatives may exert different potential benefit as non-toxic agents against Alzheimer's disease, thus fulfilling the fundamental requirement for a multi-target mechanism of action. The challenge will be to move from early biological evaluation (enzyme and cellular level) to the next *in vivo* stage.

Introduction

1. GENERAL OVERVIEW

Alzheimer's disease (AD) is one of the most common neurodegenerative diseases and deemed by World Health Organization (WHO) as 60-70% of total dementia cases in elderly people[1]. AD is characterized by a progressive decline in cognitive function, which typically begins with memory deterioration. Usually, individuals with this disorder become dependent on caregivers before death.

Alzheimer's main features are the deposit of amyloid beta (Aβ) peptides in the extracellular surface of neurons and the formation of neurofibrillary tangles (NFTs) arising from the intracellular accumulation of hyperphosphorylated Tau protein.

Alzheimer's disease international (ADI) estimates that currently over 50 million people worldwide are afflicted by dementia, a global community around the size of Spain; and, as a result of life expectancy increase over the next decades, that community is likely to rise to about 152 million people by 2050, to one that is more the size of Russia[2] (**Figure 1**).

Someone in the world develops dementia every three seconds, and the current cost of the disease is about a trillion US dollars a year, which is forecast to double by 2030. This means that if global dementia care were a country, it would be the 18th largest economy in the world. The annual costs of this disease are comparable with the market values of company like Apple and Google[2].
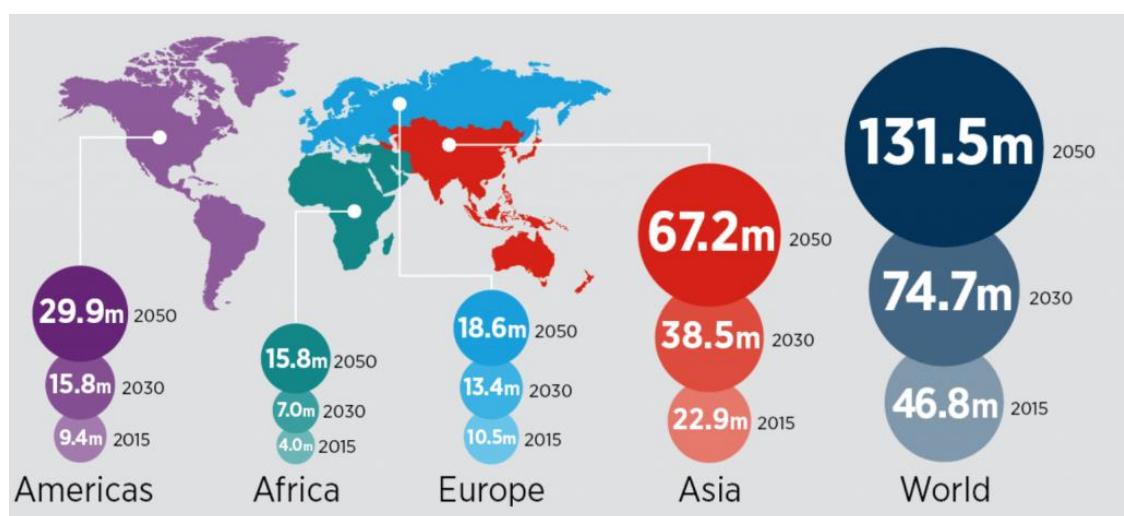
FIGURE 1| The projected number of people living with dementia by 2050 according to the World Alzheimer's Report published by Alzheimer's Disease International[2].

1.1 Dementia

Dementia is the generic term to describe a clinical syndrome defined by the loss of cognitive functions and everyday life skills and competencies. The main risk factor due to the development of dementia is age. Dementia mainly affects older people, but 2 to 10% of all cases are estimated to start before the age of 65 years. This irreversible syndrome is due to diseases of the brain, usually of a chronic or progressive nature, in which there is an impairment of functions including memory, thinking, orientation, comprehension, language, learning capacity and judgement. The impairment is often accompanied, and occasionally preceded, by deterioration in emotional control, social behavior or motivation. Because of the heterogeneity of clinical presentation and complexity of disease neuropathology, dementia classification remains controversial. The most common classification include: Alzheimer's disease, vascular dementia[3], dementia with Lewy bodies[4], frontotemporal dementia[5] and mixed dementias[6] (**Figure 2**). While each of these dementing conditions has their unique pathological signature, one common etiology shared among these disorders is small-vessel disease or cerebrovascular dysfunction at some point during the disease process. Furthermore, all dementia types share molecular mechanisms, such as hypoxia, oxidative stress, neuroinflammation and blood-brain barrier (BBB) altered permeability, responsible for the disease etiology and progression[7].

	Dementia		
Vascular dementia	**Alzheimer's disease**	**Dementia with Lewy bodies**	**Frontotemporal dementia**
Proportion of dementia cases 20-30 %	50-75 %	< 5 %	5-10 %
Neuropathology Cerebrovascular disease.	Cortical amyloid plaques and neurofibrillary tangles.	Cortical Lewy bodies (alpha-synuclein).	No single pathology – damage limited to frontal and temporal lobes.
Characteristic symptoms Similar to AD, but memory less affected, and mood fluctuations more prominent. Stepwise onset.	Impaired memory, apathy and depression with gradual onset.	Marked fluctuation in cognitive ability. Visual hallucinations. Parkisonism (tremor and rigidity).	Personality changes. Mood changes. Language difficulties.

FIGURE 2| Classification of dementia subtypes and associated neuropathological features. A mixed phenotype represented by double-sided arrows indicates a shared disease neuropathology between two dementia types.

1.2 History of Alzheimer's disease

Alzheimer's disease was first reported by Alois Alzheimer, a German neurologist and psychiatrist, in 1901, who described the pathology as an "unusual disease of the cerebral cortex" which affected a woman in her fifties, Auguste D., and caused memory loss, disorientation and hallucinations. He followed her care for five years, until her death in 1906, aged 55. The post-mortem showed abnormalities such as a shrinkage of the cerebral cortex which was also thinner than normal. He also reported the presence of a collection of dense deposits or plaques outside the neurons and bands of fibers or tangles within the brain cells, two figures which have become indicative of AD. The condition was first discussed in medical literature in 1907[8] and named after Alzheimer in 1910.

2. DISEASE PRESENTATION

The clinical manifestations of AD are characterized by progressive memory deterioration and cognitive decline, related with gradual neuronal death and the loss of cholinergic function[9].

The anatomopathology of AD has been described by progressive loss of synaptic neurons triggering atrophy in the hippocampus and frontal and tempo-parietal cortex (**Figure 3**). The brain areas most affected are basal forebrain, cortex and amygdala, which are all involved in memory, attention and emotions. However, among elderly subjects, especially those of advanced age, there is considerable overlap between brain weight as well as measures of cerebral cortical thickness between age-matched individuals with normal cognitive function and those with AD. Indeed, it is only upon the histological examination of the brain specimen that a definitive diagnosis of Alzheimer's disease can be made.

The loss of synaptic components is a change that clearly has a significant impact on cognitive function and represents another important morphological alteration. Other lesions include poorly understood changes such as granulovacuolar degeneration and eosinophilic rod-like bodies (Hirano bodies)[10]. Microscopically it is possible to observe the formation of amyloid plaques, or senile plaques, which are amorphous structures of Aβ, and accumulation of hyperphosphorylated Tau protein, which implies the formation of neurofibrillary tangles, and extensive neuronal loss[10,11].
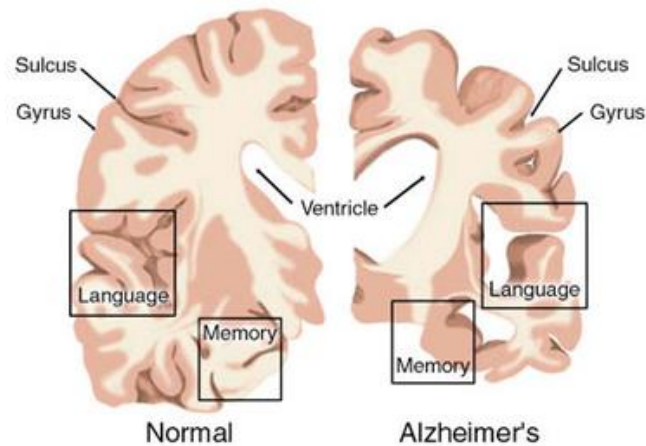
FIGURE 3| Macroscopic changes. Atrophy of the hippocampus and cerebral cortex.

It is now clear that Alzheimer's disease is a slowly progressive disorder whose lesions accumulate within the brain over a period of many years. However, the brain changes underlying AD, such as atrophy and loss of synaptic transmission, probably develop over a period of year, if not decades, before symptoms[12], and this period of time is called preclinical AD (usually identified only in research settings). How long it takes before a sufficient extent of neuropathological damage produce a degree of functional impairment that might allow a clinical diagnosis is not known, but it is likely to take many years for this to occur.

2.1 Symptoms

Symptoms vary between AD and other types of dementia, but there are broad similarities among them all. The individual personality, general health and social situation are important factors in determining the impact of dementia on the patient; that is the reason why dementia affects people differently, namely no two people will have symptoms that develop in exactly the same way.

The most common warning signs are the loss of memory and practical abilities, which can lead to withdrawal from work or social activities. The early symptoms include a decline of short-term memory, difficulty to complete everyday tasks, decreased judgement, problems with language, misplacing things and rapid changes in mood or behavior for no apparent reason (**Figure 4**).
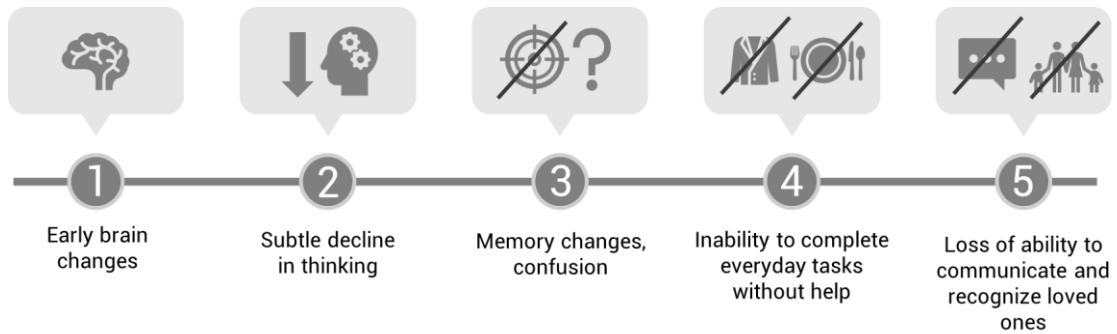
FIGURE 4| Alzheimer's disease symptoms timeline.

Disease progression occurs through three different stages, each with its own challenges and symptoms. By identifying the current stage of the disease, it is possible to predict what symptoms can be expected in the future and the possible courses of treatment.

- *Early-Stage Alzheimer's disease* - The disease is often first diagnosed in this mild stage, which usually lasts 2 to 4 years. In this period of time, family and friends may begin to realize that there has been a decline in the patient's cognitive ability. Common symptoms are difficulty with retaining new information and problem solving or decision making, personality changes and difficulty expressing thoughts. Cholinergic neurons in the limbic system are affected and the hippocampus shrinks by approximately 25% of its volume.

- *Moderate Alzheimer's Disease* - Lasting 2 to 10 years, is the longest stage of the disease. Patients experience increased difficulty with memory and may need help with activities of daily living. Symptoms frequently include increasingly poor judgment and confusion. The patients may begin to confuse family members and lose orientation to time and place. Moreover, they may begin wandering, making it unsafe for them to be left alone. Other symptoms involve difficulty to complete tasks and many of the activities of daily living, greater memory loss and significant personality changes. Additionally, patients may become withdrawn from social interactions and develop unusually high suspicions of caregivers.

- *Severe Alzheimer's Disease* – It is the final stage of the disease, which can last between 1 and 3 years on average, and ends with the death of the patient. Cognitive capacity continues to decline and physical ability is severely impacted. Due to the family's decreasing ability to care for the patient, this stage often results in long-term care facility placements. Patients lose the ability to communicate and gradually need others for personal care, such as eating, bathing and dressing. They may be also unable to walk or sit

13

independently; muscles may become rigid and swallowing can eventually be impaired. The destruction of stored memories is associated with degeneration of cholinergic neurons throughout the cerebral cortex. The person forgets his past, friends and family. Additionally, no information recovery is possible due to the interference of the disease in the limbic system.

2.2 Risk factors and prevention

Although it is not currently understood why people develop AD, there are many genetics and environmental factors suggested to be linked to the development of the condition. Some are risk factors, while others appear to be protective[13].

Risk factors can be defined as characteristics related to the development of a disease: if these risk factors are present, there is an increased chance, but not a certainty, that the disease will develop. These include family background or exposures to a substance or product. Some risk factors can be modified, for example lowering blood pressure reduces the risk of a stroke; other risk factors cannot be modified, for example age or family history. Furthermore, risk factors may be related to AD through different pathways, namely through the affection of one specific step on the cascade (amyloid, tangles, neurodegeneration), through the modulation of other pathology related to AD, or independently of known pathology.

2.2.1 Age

Epidemiologically, AD affects approximately 5% of individuals over 65 years and 20% of those over 80 years. This means that the rate of prevalence doubles every 5 years. Thus, AD has a progressive increase proportional to aging and age is considered to be a prevalence factor.

The majority (>95%) of patients who develop this disease are aged >65 years, so-called late onset AD (LOAD), with 1−5% of AD cases exhibiting an earlier onset, typically in the late 40s or early 50s, so-called early onset AD (EOAD). Late onset and early onset AD are clinically indistinguishable; however, the latter is generally more severe than the former and it is associated with a more rapid rate of pro-gression[14]. Moreover, the two forms of AD are associated with different patterns of genetic epidemiology.

Early onset Alzheimer's disease is usually characterized by the Mendelian inheritance pattern; this rare form of the disease is called familial early onset Alzheimer's disease (EOFAD) and it affects less than 10% of AD patients; however, EOAD patients have also been reported without any family history (termed

"sporadic EOAD"). In late-onset Alzheimer's disease, several genes, which are not inherited in a Mendelian fashion, have been described as potential risk factors, but non-genetic factors may also be involved in the disease's progression[15].

2.2.2 Genetics

There are two main form of the disease: familial AD and sporadic AD. Familial AD (FAD) develops much faster and is caused by mutations in components of the amyloid pathway, such as amyloid precursor protein (APP), presenilin-1 (PS1) and presenilin-2 (PS2). In sporadic AD, there does not appear to be a genetic pattern of inheritance; a connection has been found between a gene called Apolipoprotein E (ApoE) and the development of AD.

2.2.2.1 Familial AD

Early-onset familial Alzheimer's disease is a condition characterized by early onset dementia (age at onset <65 years) and a positive family history for dementia. Occurrence of familial Alzheimer's disease represents the minority (about 5 %) of all AD cases. Compared with sporadic AD, EOFAD has some distinctive features, including onset at early age, positive familial history, a variety of non-cognitive neurological symptoms and signs, and a more aggressive course. Notably, among different mutations of EOFAD, there is a marked phenotypic heterogeneity. EOFAD diagnosis is based on family and clinical history, neurological symptoms and examination, biomarker features, as well as genotyping in some cases. EOFAD individuals may benefit from new therapeutic agents targeting amyloid formation[16]. Three genes are considered the main risk factors for EOFAD: *amyloid precursor protein* (APP), *presenilin 1* (PSEN1), and *presenilin 2* (PSEN2) (**Figure 5**). All three causal AD genes lend support to a common pathogenic AD pathway, with a pivotal role for Aβ, leading to apoptosis of the neurons and dementia[17,18]. Mutations in these three genes can be considered as "diagnostic biomarkers" of the disease, since they show an autosomal dominant inheritance and lead with certainty to Aβ aggregation and early-onset disease.

- *APP mutations* account for <0.1% of AD cases. The *APP* gene is located on chromosome 21. Triplication of chromosome 21 results in the triplication of the *APP* gene, which might enhance APP expression and Aβ accumulation. Down syndrome patients have been reported to develop AD pathology (deposition of senile plaques and neurofibrillary tangles) earlier than those without Down syndrome[19]. This finding suggests that overexpression of APP might be related to AD pathology. The *APP* gene contains 19 exons for

encoding the APP protein. The Aβ peptide is encoded by exons 16 and 17. Most of the pathogenic *APP* mutations are located near the cleavage sites of α, β, and γ secretase enzymes, suggesting they might be involved in the onset of AD through altering the proteolysis of the Aβ peptide[20]. In addition to these dominant mutations, the APP mutation spectrum extends to two recessive mutations, which only cause disease in the homozygous state, and APP locus duplications, underscoring the importance of APP gene dosage in AD[14].

- *PSEN1 and PSEN2*, two highly homologous genes, were identified in 1996 through linkage analyses, as probably involved in the onset of AD[21,22]. The structures of *PSEN1* and *PSEN2* are similar, sharing a homology of 67%. Both of them contain 12 exons with ten coding exons (exons 3–12) for a protein of ~450 amino acids. PS1 and PS2 are transmembrane proteins with at least seven transmembrane domains[21]. Presenilins are functionally involved in the γ-secretase-mediated proteolytic cleavage of *APP*[22]. The majority of AD-linked *PSEN1* and *PSEN2* mutations are single-nucleotide substitutions, but small deletions and insertions have been described as well. Mutations in *PSEN1* and *PSEN2* impair the cleavage and cause an increase in the $Aβ_{42}$: $Aβ_{40}$ ratio. This rise might occur through either an increase in $Aβ_{42}$ levels, as indicated in plasma and fibroblast media from *PSEN*-mutation carriers[23], or a decrease in $Aβ_{40}$ levels.

Most AD risk-factor mutations have been detected in *PSEN1* (approximately 30–70% of EOFAD), which is located on chromosome 14. More than 180 mutations were found in *PSEN1* in association with FAD, but they might be involved in sporadic AD or LOAD. Patients with *PSEN1* mutations might develop AD symptoms in their 40s or early 50s, with a few cases occurring in persons in their late 30s and early 60s. *PSEN2*, on chromosome 1, is another risk-factor gene for AD, especially EOAD. A few *PSEN2* mutations, such as Leu143His or Arg143His, have not been associated with any neurodegenerative phenotype[24]. Two *PSEN2* mutations, may be involved in breast cancer, although the pathomechanism is still not clear[25].
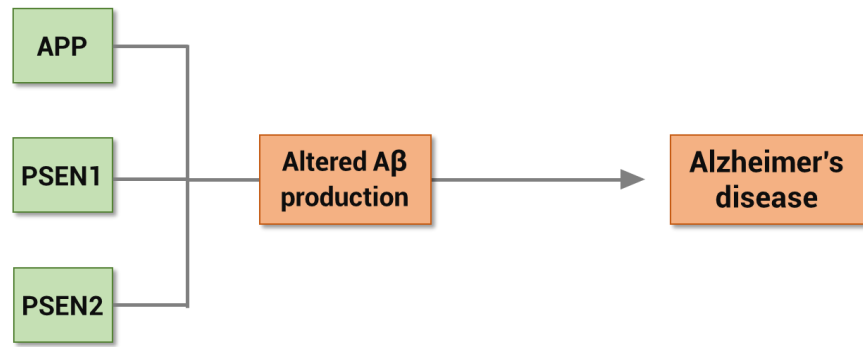
FIGURE 5| Schematic of the three genes involved in the early onset AD.

2.2.2.2 Sporadic AD

Sporadic AD is characterized by a severe progressive decline in cognition and increased neuronal cell death and it accounts for the most part of AD cases. The prevalence of sporadic AD cases shows a late onset, is related to a complex combination of genes, environment and lifestyle, and it has not a specific familiar connection (**Figure 6**). An important genetic risk factor for late onset sporadic AD is the *APOE* gene, located on chromosome 19, and its importance has been validated from population studies. ApoE protein is the main cholesterol carrier in the brain, involved in neuronal maintenance and repair. This protein binds to several receptors on the cell surface, implicated in lipid delivery and transport, glucose metabolism, neuronal signaling, and mitochondrial function. In physiological condition, ApoE binds to Aβ peptide and plays a role in its clearance[26]. Two polymorphic sites, located at codon 112 and 158, have been described in the human *APOE* gene. At least three main variations of the *APOE* gene have been identified, called "E2," "E3," and "E4" alleles. E3 was defined as a normal allele with Cys at codon 112 and Arg at codon 158, while the two other *APOE* alleles, the E2 and E4 alleles, carry Arg158Cys and Cys112Arg polymorphisms, respectively[27]. Six different genotypes can be distinguished with the following combinations: homozygous − E4/E4, E3/E3, and E2/E2 − and heterozygous − E2/E3, E2/E4, and E3/E4. E3 is the most common variant (77%), while E2 (8%) and E4 (15%) alleles have been detected less frequently. Higher frequencies of the E4 allele have been found among AD patients, and increased risk of AD can be found in patients with both homo- and heterozygous alleles[26]. Despite the studies linking E4 with AD, the presence of this allele is neither necessary nor sufficient for developing the disease[28]. The pathogenic nature of the E4 allele might be associated with the structural change of ApoE protein. ApoE protein has two major functional domains: a 22 kDa N-terminal and a 10 kDa C-

terminal domain, connected by a hinge region. The E4 allele can promote domain interactions through altered orientations in the N-terminal domain. Arg112 can interact with the Glu255 in the C-terminal domain, resulting in structural changes of ApoE protein, neuronal death, and neurodegeneration.

The prevalence of the E2 allele has been found to be significantly lower in individuals with dementia[29]. Indeed, E2 allele was suggested to be protective against AD. Further, *APOE* E2 and E3 may participate in neuronal maintenance and repair[30].
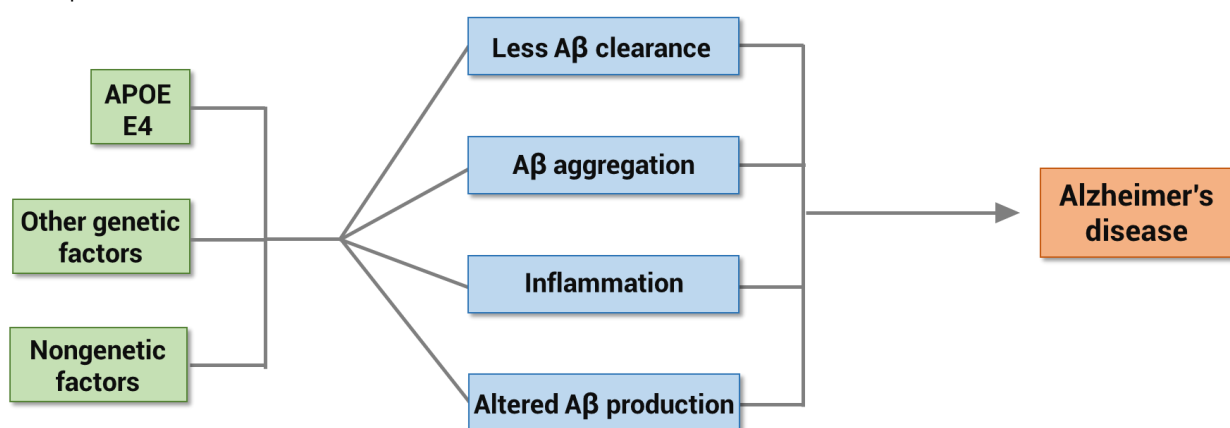
FIGURE 6| Schematic of factors involved in the sporadic late onset AD.

2.2.2.3 Additional genetic risk variants for LOAD

Studies conducted in families of patients with AD support the presence of at least four to six additional major AD risk genes. Indeed, genome-wide association studies (GWASs) have identified several genes that might be potential risk factors for AD, including *clusterin* (*CLU*), *complement receptor 1* (*CR1*), *phosphatidylinositol binding clathrin assembly protein* (*PICALM*), and *sortilin-related recepto*r (*SORL1*). Additionally, recent studies have discovered novel genes that might be involved in late-onset AD, such as *triggering receptor expressed on myeloid cells 2* (*TREM2*) and *cluster of differentiation 33* (*CD33*).

- *Clusterin* (*CLU*) is a major inflammatory-related apolipoprotein that is expressed in all mammalian tissues. Clusterin may play a protective role against apoptosis, cell damage, or oxidative stress. Its expression has been found to be upregulated in the brains of AD patients. Animal models have suggested it might be secreted with soluble Aβ. Clusterin can act as a molecular chaperon, which might prevent Aβ oligomerization and fibrillization. GWASs have determined a strong association between *CLU* mutations

(located on chromosome 8) and LOAD. Additionally, a significant association has been found between the *APOE* E4 allele and *CLU* mutations[31].

- *Complement receptor 1* (*CR1*) gene, located on chromosome 1, encodes the receptor for C3b complement protein. CR1 and C3b can be involved in Aβ clearance and in the prevention of Aβ aggregation. Risk-factor mutations for LOAD have been found in CR1 (rs6656401 and rs3818361). The functional role of CR1 mutations in AD pathogenesis is not determined yet, and further studies are needed to find out the effect in Aβ deposition[32].

- *Phosphatidylinositol binding clathrin assembly protein* (PICALM), located on chromosome 11, may be a putative LOAD risk-factor gene. PICALM can play a role in APP endocytosis and Aβ generation. Additionally, its overexpression may increase Aβ cleavage and aggregation[33].

- *Sortilin-related receptor 1* (*SORL1*) gene is the best-validated gene modulating late-onset AD risk after *APOE*. It is located on chromosome 11q23 and may be involved in Aβ recycling. SORL1 belongs to a group of five type I transmembrane receptors that are highly expressed in the central nervous system (CNS) and are characterized by a luminal, extracellular vacuolar protein sorting 10 domains. The under-expression of SORL1 can increase Aβ generation[34].

- *Triggering receptor expressed on myeloid cells 2* (*TREM2*), located on chromosome 6, is a member of immunoglobulin family and it contains a single variable domain. TREM2 is located on the membrane of several immune cells, such as macrophages and dendritic cells. Functions of TREM2 protein can include the clearance of apoptotic cells and immunosuppression. In an Icelandic population, a rare variant (Arg47His) has been suggested to increase the risk of impairment in inflammation, leading to LOAD[35]. Other variants located in exon 2 have been shown higher percentage in AD patients. AD associated with *TREM2* can be associated with chronic brain inflammation with aberrations in microglial phagocytosis or inflammatory pathways[36].

- *Cluster of differentiation 33* (CD33), located on chromosome 19, is a transmembrane glycoprotein that is expressed on the surface of myeloid progenitor cells, mature monocytes, and macrophages. It can function as a lectin, a carbohydrate-binding protein, which inhibits cellular activity. The *CD33* locus is related to an altered monocyte function, which suggests it can be involved in innate immunology, leading to AD progression. Elevated CD33 expression may lead to cognitive decline. Mutations in *CD33* can be

associated with disturbances in myeloid function and amyloid pathology, thus may be involved in the progression of early AD[37].

Identification of new AD-related genes is important for better understanding the pathomechanisms leading to neurodegeneration, and finding the potential genes involved in AD progression is an essential step in molecular diagnosis. Since the differential diagnoses of neurodegenerative disorders are difficult, especially in the early stages, genetic testing is essential for diagnostic processes[15]. Indeed, disease-modifying therapies are more likely to be effective in the earlier stages of AD, especially before the clinical symptoms appear. Genetic testing in the family members of patients should also be important to predict the risk for disease onset in the future. Using disease markers with genetic testing together may provide more effective disease diagnosis.

2.2.3 Coexisting Health Problems

2.2.3.1 Cerebrovascular disease

The link between heart health and brain health has been firmly established, and many cardiovascular risk factors are clearly related to risk for cerebrovascular disease and vascular dementia (**Figure 7**). Indeed, cerebrovascular changes such as hemorrhagic infarcts, small and large ischemic cortical infarcts, and vasculopathies all increase the risk of dementia. Stroke could lead to cognitive impairment and AD through several mechanisms. First, stroke may lead directly to damage of brain regions that are important in memory function, such as thalamus and thalamocortical projections. Second, stroke might increase Aβ deposition, which in turn can lead to cognitive decline. Third, the onset of stroke may induce inflammatory responses that impair cognitive function. And last, hypoperfusion can lead to overexpression of cyclin-dependent kinase 5 (CDK5), a serine−threonine kinase that is critical to synapse formation and synaptic plasticity and, hence, to learning and memory. Aberrant CDK5 activation is associated with neuronal apoptosis and death[38].This kinase may also be involved in the abnormal phosphorylation of tau, thereby contributing to the formation of NFTs[39], and might be a key protein linking NFT pathology to amyloid plaques.
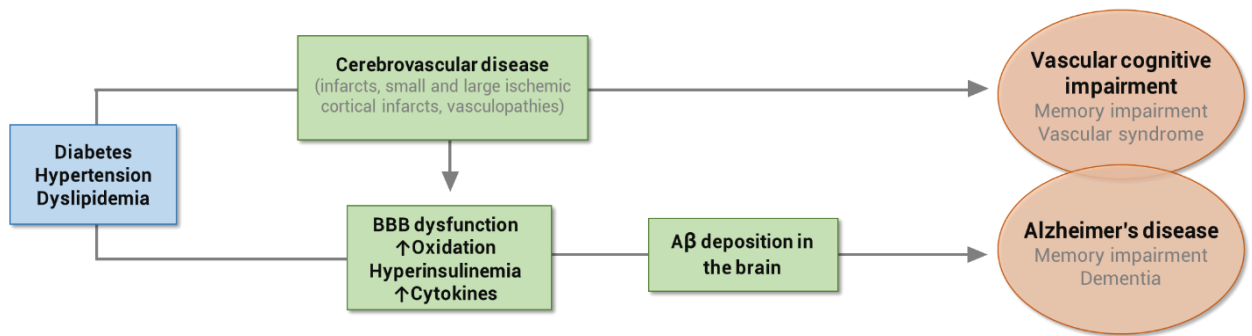
FIGURE 7| Potential mechanisms linking vascular and other risk factors to cognitive impairment. At least two pathways exist: the development of cerebrovascular disease may lead to vascular cognitive impairment syndromes, and deposition of Aβ may lead to other distinct amnestic clinical syndromes, including Alzheimer's disease. In addition, these pathways may overlap and interact, resulting in mixed cognitive syndromes.

2.2.3.2 Blood pressure

Hypertension is a shared risk factor of AD and VaD associated with significant memory impairments in late life[40]. Chronically elevated blood pressure promotes cerebrovascular remodeling, leading to a reduction in the lumen diameter by an increase in the wall-to-lumen ratio. Additional consequences of prolonged systemic blood pressure include altered morphology of small cerebral arterioles that supply vulnerable brain regions necessary for cognitive function. In middle age, elevated blood pressure increases the risk of cognitive impairment, dementia and AD (**Figure 7**). Hypertension may increase the risk of AD by decreasing the vascular integrity of the BBB, resulting in protein extravasation into brain tissue[41]. In turn, protein extravasation can lead to cell damage, a reduction in neuronal or synaptic function, apoptosis, and an increase in Aβ accumulation, resulting in cognitive impairment[42]. With increasing age, the effect of elevated blood pressure on AD risk diminishes and may even become inverted, with an increase in blood pressure showing a protective effect. This observation might be explained by the fact that following the onset of AD, blood pressure begins to decrease, possibly as a result of vessel stiffening, weight loss and changes in the autonomic regulation of blood flow.

2.2.3.3 Type 2 diabetes

In observational studies, type 2 diabetes (T2D) has been found to nearly double the risk of AD[43] (**Figure 7**). Various mechanisms have been proposed whereby diabetes might influence the development of AD. In cases of hyper insulinemia accompanying diabetes, insulin may compete with Aβ for the insulin degrading

enzyme, which is involved in Aβ clearance, thereby hindering clearance of Aβ from the brain[44].

Moreover, diabetes and impairment of glucose tolerance lead to the formation of advanced glycosylation end products (AGEs), and amyloid plaques and NFTs contain receptors for AGEs (RAGEs). Glycation of Aβ enhances its propensity to aggregate *in vitro*. In addition, RAGEs may facilitate the neuronal damage caused by Aβ[45], as the latter is a high-affinity ligand for cell-surface RAGEs.

2.2.3.4 Others

Many others risk factors have been found to be probably associated with dementia and/or AD. However, the mechanism linking these factors to the development of the disease remains unclear and in literature conflicting data are reported. One example is the level of plasma lipids: evidences assert that depletion of membrane cholesterol inhibits secretase cleavage of APP[46], thereby lowering Aβ accumulation. Nevertheless, dyslipidemia increases the risk of vascular disease[47], which in turn is associated with a higher risk of AD. A second example is smoking, which could affect the risk of AD via several mechanisms. It may increase the generation of free radicals, leading to high oxidative stress, or affect the inflammatory immune system, leading to activation of phagocytes and further oxidative damage[48] or it may promote cerebrovascular disease. However, evidences that smoking can have a protective effect against AD also exist. Indeed, nicotine has been suggested to induce an increase in the level of nicotinic acetylcholine receptors, thereby counterbalancing the loss of these receptors, and subsequent cholinergic deficits, observed in AD[49]. The last example is depression; studies have found an increase in the risk of AD or mild cognitive impairment in individuals with a history of depression[50,51], but others have been unable to link AD with this mood disorder[52]. However, depressive symptoms occur in 40–50% of patients with AD. The mechanisms underlying the possible association between these conditions might involve vascular pathways and still have to be clarified.

2.2.4 Prevention

Because there are no established diagnostic biomarkers of dementia-related brain damage, and the mechanisms linking this damage to the expression of dementia symptoms are not fully understood, prevention of dementia is commonly conceived as the delay of the clinical onset of the disease rather than a slowing or avoidance of the development of the neuropathology.

A large variety of potential risk and protective factors for dementia and cognitive impairment have been investigated in epidemiological and experimental studies[53]. The current focus on modifiable risk factors is justified by their potential to be targeted for prevention. However, there is still no evidence strong enough at this time to claim that lifestyle changes will prevent dementia on an individual basis.

A wide variety of activity, including physical, cognitive, and social or leisure activities, has been linked to a reduction of risk for dementia[54,55]. These activities work through a wide variety of mechanisms, ranging from cardiovascular benefits of physical activity to the potential building of reserve capacity through cognitive stimulation.

Education has long been connected to a lowered risk of AD. In fact, several clinical-pathologic studies showed that education is associated with cognitive decline or dementia regardless of AD pathology[56,57] or that education modifies the relationship between AD pathology and cognition[58,59]. The evidences support the hypothesis that education, and the related construct of occupational complexity, impart resilience to pathology and a neural reserve capacity.

Following initial reports that elderly people with higher levels of education had a lower incidence of dementia than individuals with no education, cognitively stimulating activities such as reading, puzzles, and games were suggested to decrease the risk of cognitive decline and are posited to build reserve capacity much like education. Studies have shown that early-life and late-life cognitive activities are independently associated with cognitive decline after adjustment for AD and other pathologies and even that cognitive activities in adulthood are more strongly related to reserve (residual variance in cognition after adjusting for AD and other pathologies) than is education[60].

Social or leisure activity is another lifestyle activity that has been linked to dementia, though, to date, the association has rarely been explored in the context of AD pathology. Socializing, specifically, does appear to confer benefits to the brain. Studies have shown that larger social networks positive modify the relationship between AD pathology and cognition[61].

Epidemiological and experimental data suggest that also physical exercise may promote brain health. Conflicting results have, however, emerged from observational studies that examined the relationship between exercise levels and cognitive decline or dementia: while some studies indicated that physical activity has a beneficial effect on brain health, others showed no association between these variables[62]. Physical activity could affect cognition via multiple mechanisms. An improvement in aerobic fitness increases cerebral blood flow,

oxygen extraction and glucose utilization, and activates growth factors that promote structural brain changes, such as an increase in capillary density[63]. In addition, rodent studies suggest that physical activity decreases the rate of amyloid plaque formation[64].

2.3 Diagnosis

Researches show that most people currently living with dementia have not received a formal diagnosis. Indeed, in high income countries, only 20-50% of dementia cases are recognized and documented in primary care. This "treatment gap" is certainly much greater in low and middle income countries, with one study in India suggesting 90% remain undiagnosed[65]. This means that approximately three quarters of people with dementia have not received a diagnosis, and therefore do not have access to treatment, care and organized support that getting a formal diagnosis can provide. Moreover, in the cases in which diagnosis occurs, this is typically at a relatively late stage in the disease process, when progressive decline has had noticeable impacts upon patient's ability to carry out important everyday activities.

Despite neurodegenerative changes can begin decades before the onset of symptoms, the time from first symptoms to the correct diagnosis may take up to 2 years[66]. The reasons for a delayed diagnosis may include that older patients themselves tend to play down their symptoms because they consider memory problems part of "normal" aging, and because of concerns associated with a dementia diagnosis, such as fear of limited autonomy, need for a caregiver and the false belief that nothing could be done. All these issues result in inactivity in seeking help. On the other hand, another factor contributing to low rates of detection of dementia is that medical practitioners may also neglect the diagnosis of dementia because of a misconception of memory problems as normal in persons of advanced age, lack of (neuro)geriatric training, ageism or fear of constraining the patient's independence. However, the recognition and correct diagnostic assessment of dementia are important for enabling targeted treatment and management as well as advance care planning[65].

Unfortunately, there is not a simple test to make a diagnosis. Despite significant improvements in brain imaging, dementia can only be confirmed with certainty by examining the brain after death. Thus, the diagnosis of AD in living patients is based upon clinical examination (**Figure 8**). There is new research on development of tests that can detect Alzheimer's disease biomarkers, but this remains at an

early stage[67,68]. When making a diagnosis, it is important to exclude other treatable conditions that cause memory loss such as depression, urinary infection, vitamin deficiency and brain tumor.

The criterions for diagnosing mental disorders can be found in the Diagnostic and Statistical Manual of Mental Disorders (DSM-IV), published by the American Psychiatric Association, and are also established by the National Institute of Neurological and Communicative Disorders and Stroke (NINCDS) concomitant with Alzheimer's Disease and Related Disorders Association (ADRDA)[69].
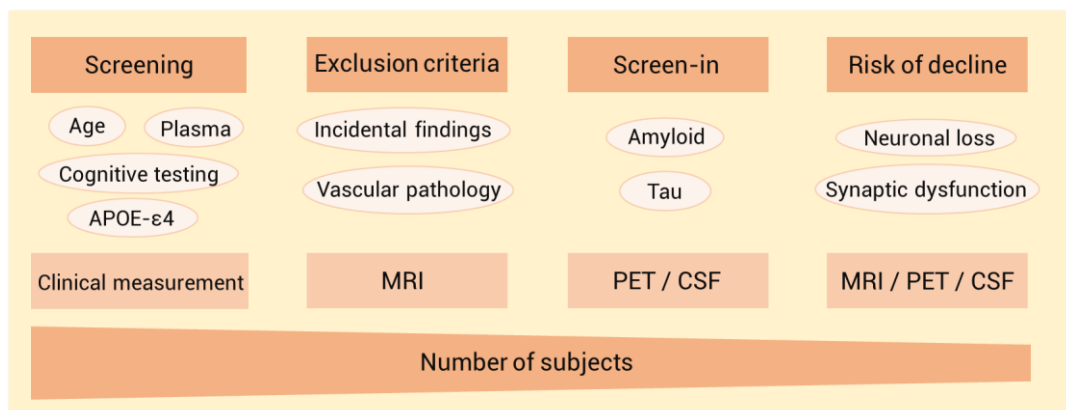
The first step in finding a diagnosis is obtaining the patient history. Namely, the family history of illness, what symptoms are present, when they began and how they have progressed over time. Then both neuropsychological and psychometric tests are performed to analyze the cognitive functions of patients. Particularly, for global cognitive function, the main clinical examination established by NINCDS-ADRDA is the Mini-Mental State Examination (MMSE). Prepared by Folstein *et al.*[70], MMSE test can be used by clinicians to help diagnose dementia and to help assess its progression and severity. It consists of a series of questions and tests, each of which scores points if answered correctly, with a score out of 30 possible points (a score of less than 12 indicates severe dementia). It tests a number of different mental abilities, including a person's memory, attention and language. This test can be used alone or coupled with other tools to assess the cognitive level of patients. MMSE can also be used to assess changes in a person who has already been diagnosed with dementia, as AD patient's scores typically decrease 2 to 4 points every year. Therefore, it can help to give an indication of how severe a person's symptoms are and how quick dementia is progressing. Undoubtedly, MMSE is only one part of assessment for dementia and the result should be considered alongside other measures of how the person is coping together with clinical judgement. Apart from MMSE test, several others neuropsychological tests exist, aimed to evaluate specific cognitive function as memory assessment, attention, conceptualization and abstraction and constructive skills[71]. Two notable issues surround the use of neuropathological studies to inform the diagnosis of AD. First, neuropathological studies are usually end-stage disease investigations and extrapolation of the findings of such studies to living patients in earlier stages of disease can be difficult. Second, neuropathological findings can differ between patients with similar clinical profiles before death. Thus, clinical diagnoses are not always in agreement with clinicopathological diagnoses, which indicates that the relationship between clinical profiles and age is not stable[14].

The standard diagnostic work-up also includes laboratory screening such as blood tests, urinalysis and other physical examination to rule out comorbidities or primary cause of dementia as hormone imbalance, vitamin deficiency, hypothyroidism and urinary tract infections. Genetic studies are also important complementary tests that can integrate a more complete diagnosis of the disease. In the differential diagnosis of cognitive decline, brain imaging plays an important role. The goals of imaging are: (i) to exclude a potentially treatable disorder as frontobasal meningioma; (ii) to detect vascular alterations as small vessel disease; (iii) to demonstrate evidence of temporal or frontal atrophy indicative of AD or frontotemporal dementia, respectively; (iv) to detect both atrophic and vascular changes, features of mixed dementia[72].

In most patients the imaging diagnosis is based on cranial computed tomography (CT) and magnetic resonance imaging (MRI) as these exams provide information about the shape and the volume of the brain. Other imaging modalities enable evaluation of molecular alterations by using specific radiopharmaceuticals. The metabolism of glucose visualized by positron emission tomography (PET) can be evaluated to detect molecular alterations, such as amyloid beta and tau deposit[73], and microglial cells driving neuronal destruction.

Cerebrospinal fluid exams (CSF) analyze the changes in two biomarkers: reduced $A\beta_{42}$ and increased levels of Tau protein, total and phosphorylated, that is related to neuronal decay[74].

According to INCDS-ADRDA criteria, information gathering from all the tests and exams above mentioned result in a diagnosis of definite, probable or possible Alzheimer's disease. As the brain pathology develops, then so do the symptoms and signs, that may, with progression, ultimately validate the diagnosis of dementia.

Screening	Exclusion criteria	Screen-in	Risk of decline
Age Plasma Cognitive testing APOE-ε4	Incidental findings Vascular pathology	Amyloid Tau	Neuronal loss Synaptic dysfunction
Clinical measurement	MRI	PET / CSF	MRI / PET / CSF

Number of subjects

FIGURE 8| Diagnostic set of images of patients with cognitive decline at various disease stages and ages.

3. ETIOPATHOGENESIS

The most important neuropathological event in Alzheimer's patients is a neuronal and synaptic loss at the level of different neurotransmitter systems, the first of which is the cholinergic system, although major alterations are also observed in neuronal systems that use as neurotransmitter noradrenaline, serotonin, glutamate, substance P and somatostatin. AD is also characterized by the loss of function and death of neurons in different areas of the brain due to the accumulation of β-amyloid (Aβ) aggregates and hyperphosphorylated tau proteins, which lead to the formation of extracellular amyloid plaques and intracellular fibrillary tangles, respectively. Despite the continuing efforts of researchers, the pathogenesis of this neurodegenerative disorder is not yet fully understood, and during the years different hypothesis have been formulated. Currently the scientific consensus is quite firm in describing AD as a multifactorial disease caused by several elements (**Figure 9**). These elements include: loss of cholinergic transmission, excessive protein misfolding and Aβ aggregation, oxidative stress and free radical formation, metal dyshomeostasis, excitotoxic, and neuroinflammatory processes[75].
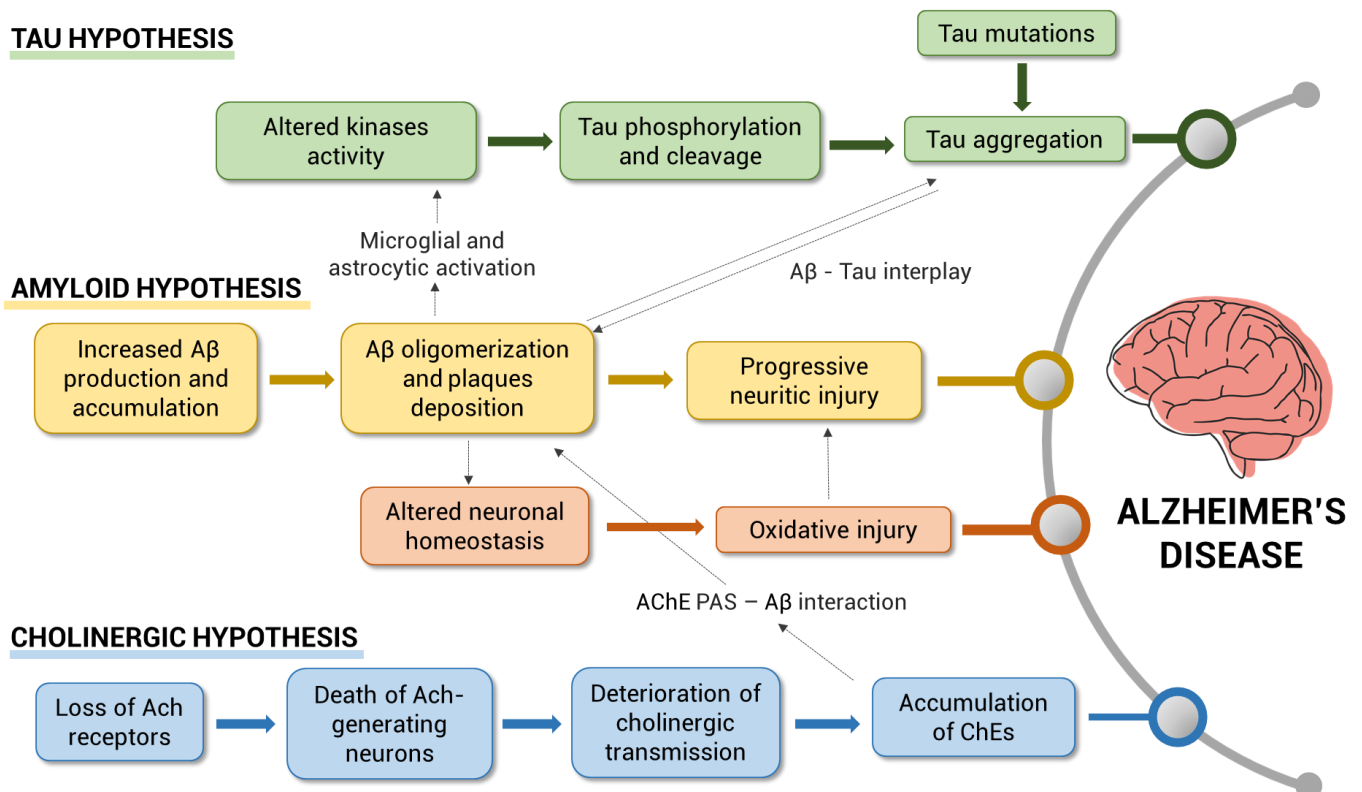
FIGURE 9| Schematic representation of some biological pathways involved in AD pathogenesis.

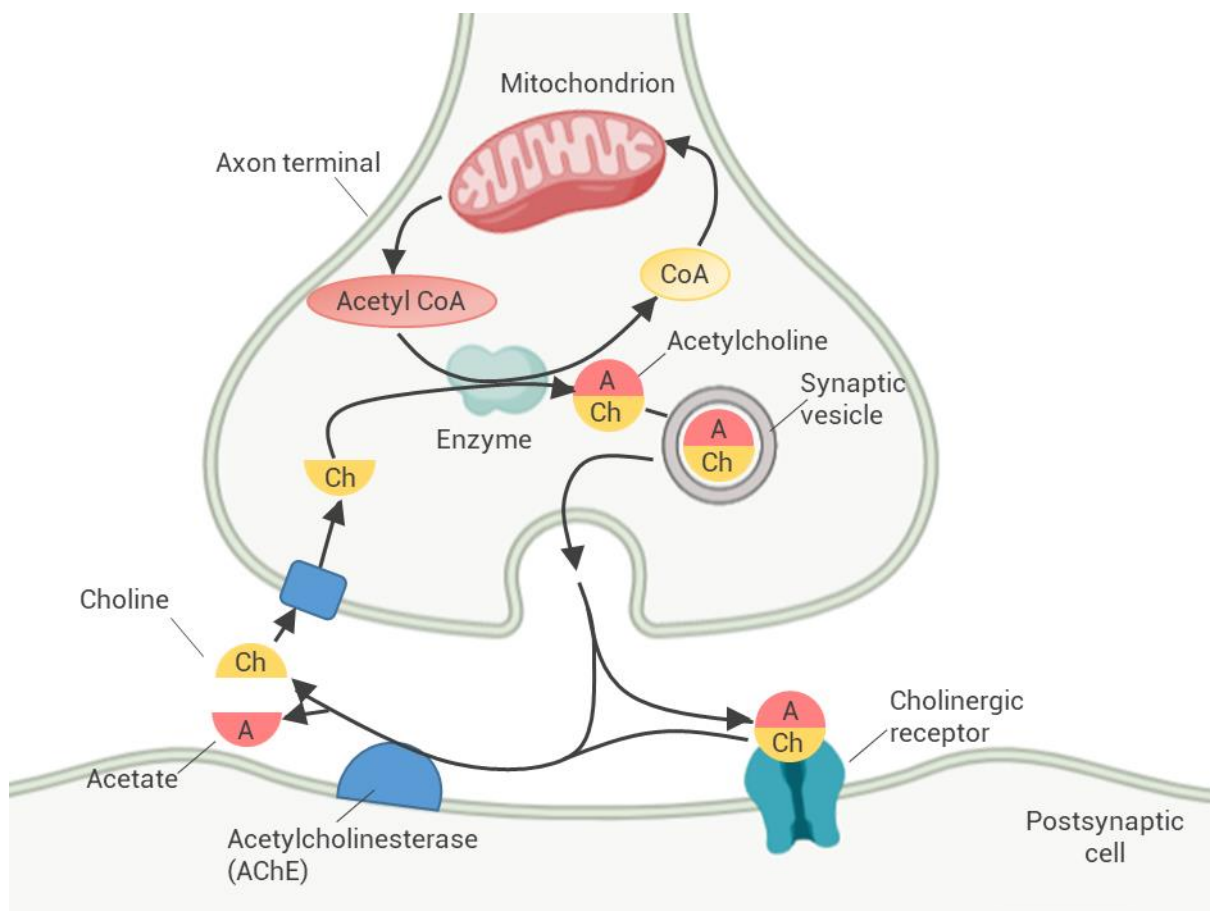## *3.1 Cholinergic hypothesis*

The cholinergic hypothesis was proposed to explain the etiology of AD in 1970 after the observation of postmortem brain of patients. The first physiological evidence for the involvement of the cholinergic system in the pathology was a reduction in pre-synaptic acetylcholine (ACh), and a reduced activity of choline acetyltransferase (ChAT) in the septal nuclei and basal forebrain of patients[76]. ChAT is the enzyme responsible for the synthesis of the neurotransmitter ACh in the brain, which has a significant role in the neuromodulation of memory, learning and other cognitive functions. According to the cholinergic theory, the development of AD symptoms is related to structural alterations in cholinergic synapses, loss of ACh receptors, death of ACh-generating neurons and the deterioration of cholinergic transmission. Taken together, all these issues lead to the accumulation of the enzyme responsible for ACh hydrolysis, acetylcholinesterase (AChE).

3.1.1 Cholinergic neurotransmission

Cholinergic neurotransmission is based on proteins involved in ACh synthesis, storage, transport, and degradation (**Figure 10**). Acetylcholine is synthesized from choline and active acetate, partly in the cytoplasm of cholinergic neurons, but mostly at the terminal buttons[77]. Choline originates from lipid degradation (especially from lecithin) as well as from acetylcholine hydrolysis and it is captured from outside the neuron by axonal termination via a specific transport mechanism. Acetyl-coenzyme A (acetyl-CoA) is formed in the mitochondria starting from pyruvate. Choline acetyltransferase, which is present in high concentration in the cytoplasm of cholinergic nerve endings, catalyzes the esterification between choline and acetyl-CoA. The activity of ChAT is regulated by neuronal depolarization, influx of calcium ions and phosphorylation of the enzyme[77]. The biosynthesized ACh is transported by vesicular ACh transporter (VAChT) which facilitates its storage into synaptic vesicles. The release of acetylcholine occurs by exocytosis of the synaptic vesicles. The vesicles fuse with the pre-synaptic membrane and eliminate the neurotransmitter in the synaptic cleft, where it can activate two different types of receptor: muscarinic and nicotinic. The release activity is due to the influx of calcium ions, which occurs as a result of the opening of the slow channels in the pre-synaptic membrane, controlled by depolarization[78]. Then acetylcholine crosses the synaptic cleft and enters with its cationic end in the anionic site of the active receptor surface, and it is subsequentially fixed with its ester group by the esterophilic site of the enzyme.

ACh acts by activating the receptors causing stimulation or inhibition, depending on the neuronal type and localization of the receptor; the cellular effectors of these receptor are sodium ion channels and membrane proteins modulated by G proteins. Acetylcholine that breaks down from the cholinergic receptor complex is rapidly hydrolyzed and inactivated thanks to acetylcholinesterase (AChE), an enzyme presents in the synaptic cleft, either free or bound to the basal lamina. The final step is the uptake of the choline in the presynaptic neuron, and then the process is repeated for the neurotransmission.

FIGURE 10| Schematic of the synthesis of acetylcholine and the cholinergic neurotransmission.

3.1.2 Cholinesterases

There are two types of cholinesterase: acetylcholinesterase (AChE) and butyrylcholinesterase (BChE). Both enzymes are α,β-hydrolases folded with α-helices surrounding the central β-sheet which contains the catalytic domain[79] (Figure 11). In mammals, gene with chromosome location 7q23 encodes AChE, while BChE is encoded by the gene with chromosome location 3q23. Within species, the overall tertiary structure of cholinesterase enzymes was found to be similar with ~50% amino acids identity[80].
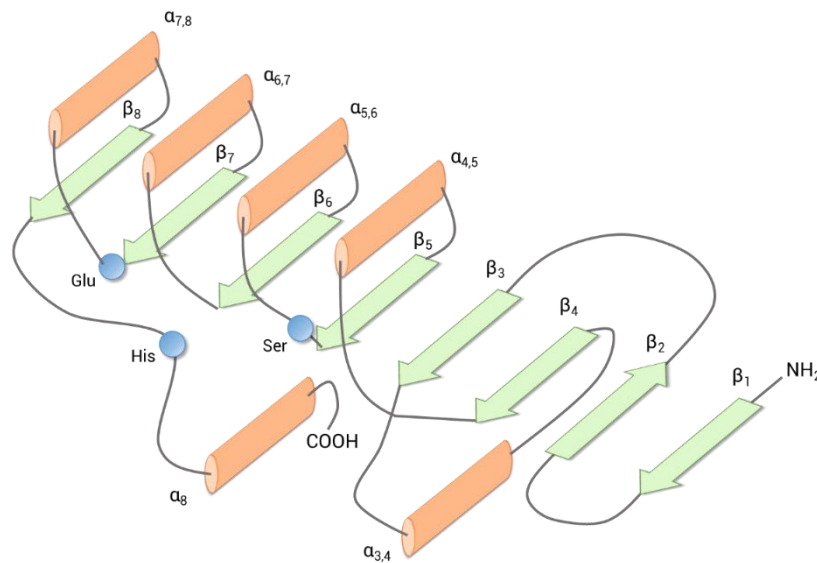
FIGURE 11| Schematic diagram of the topological secondary structure of the α,β-hydrolase fold. The α-helices are shown as orange cylinders, the β-strands as green arrows, and the three residues making up the active site are shown as blue circles (the labels Ser, Glu and His correspond to the catalytic-triad of the AChE active-site).

Although AChE and BChE are structurally similar, both their significance and location are substantially different. AChE is predominantly observed in the neuronal synapses and blood, whereas BChE, at the level of the human brain, is located close to glial cells and neurons or in tangles and neuritic plaques in AD patients[81]. Another difference between the two cholinesterases is the preference for the substrate they hydrolyze. In physiological conditions, AChE is the main enzyme responsible for ACh hydrolysis, while BChE plays a supportive role and hydrolyzes butyrylcholine. AChE performs the hydrolysis of the small substrate ACh into acetic acid and choline. Whereas, BChE adapts the bulkier substrate like benzoyl- or butyrylcholine for their catalytic decomposition. BChE also significantly catalyzes other esters, namely cocaine, acetylsalicylic acid, heroin, physostigmine, and organophosphates[82]. In addition, both these enzymes are

involved in cell differentiation and development activities. There seems to be an increasing appreciation of the potential importance of BChE in dementia. BChE, indeed, showed to be capable to compensate for some functions of AChE in a AChE knockout mice, maintaining the structural integrity of central and peripheral cholinergic neurotransmission. The same compensatory effect is also reported in AD patients. In fact, through AD progression, AChE activity is greatly reduced (by up to 85%) in specific brain regions, whereas BChE activity increases, likely compensating for AChE decrease[83]. The increasing role of BChE in the hydrolysis of ACh, as the ratio AChE/BChE gradually decreases in these patients, makes BChE an increasingly important therapeutic target with the disease progress. It has been suggested that dual inhibition of AChE and BChE could increase the efficacy of treatments and broaden the indications or even confer additional neuroprotective benefits[84]. Thus both enzymes have drawn the attention of researchers towards the design of dual AChE and BChE inhibitors in the interest of a better disease outcome[85] (**Figure 12**).
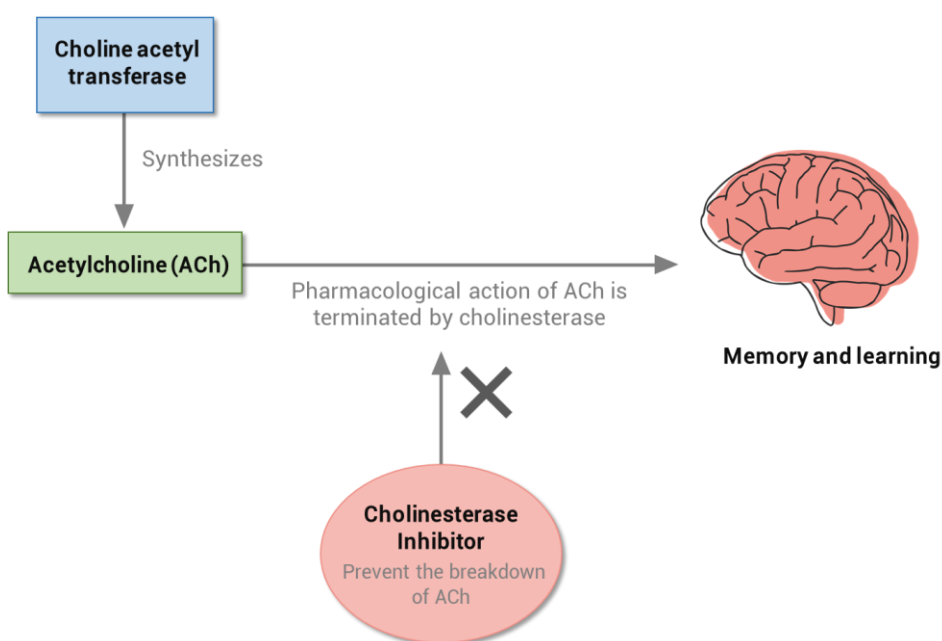
FIGURE 12| Cholinesterase hypothesis of memory and learning.

Cholinesterases present three distinct domains, confirmed by molecular modeling and site-specific mutagenesis studies, which contribute to the binding of ChE inhibitors into the active site of ChEs. Each domain contains the clusters of aromatic amino acid residues which contribute to substrate and inhibitor specificities. AChE is an enzyme found in globular, monomer and homodimer forms and can be either free or bound to lipid membranes. Free AChE can be manipulated and successfully crystalized to study; for this reason, it was one of

the first enzymes to be characterized by X-ray diffraction, and currently, there are more than 300 AChE structures located in the Protein Data Bank (PDB, http://www.pdb.org/). The first crystal structure of AChE was given in 1991[86], consisting of 537 amino acids and containing 12 β-sheets surrounded by 14 α-helices, successfully crystallized in Torpedo californica (TcAChE) (PDB ID:1EVE)[87]. The crystal structure of human BChE (hBChE) (PDB ID: 1P0I) is very similar to TcAChE and consists of 529 amino acids[80]. The difference between these two crystal structures is that hBChE does not form the dimer as observed for TcAChE. The TcAChE has four-helix structure, which are commonly involved in the interaction of subunits.

The active site gorge of both ChEs is deep ~20 Å length, wherein the catalytic site is located at the bottom of the gorge (~4 Å above the base of gorge) (**Figure 13**). The outer gorge of AChE is termed peripheral anionic site (PAS) or β-anionic site, and it is known to allosterically modulate the enzyme activity. The entrance of PAS is lined by numerous aromatic amino acid residues, namely Tyr70, Tyr72, Tyr121, Tyr279, and Tyr334 for TcAChE and Asp70, Tyr332 for hBChE, which are responsible for the π interactions with inhibitors. Thus, in BChE, lining of the gorge has lesser aromatic amino acid residues, six in number compared to 14 in AChE. PAS enhances the catalytic efficiency by trapping the substrate or the inhibitor toward the active site. Moreover, this region has been reported to play an important role in AD since it contains a motif that promotes Aβ fibril formation: the interaction of the Aβ peptide with the PAS contributes to the formation of amyloid plaques by accelerating the aggregation process. The PAS sequence responsible for triggering Aβ aggregation has been identified as a hydrophobic AChE sequence (aa 281−315) which contains a highly conserved key residue, Trp279[88]. Thus, inhibitors targeting both the active site and the PAS, along with the AChE inhibition activity, they also prevents the Aβ production and deposition[89]. Donepezil, a clinically approved drug for AD treatment, presents a structure which spans the entire active site, interacting with both the catalytic active site and the PAS residues at the same time[90].

The inner gorge portion of the active site in cholinesterase consists of four subsites: catalytic active site (CAS), oxyanion hole, acyl binding pocket and anionic subsite.

- The *catalytic active site* catalyzes the hydrolysis of the ester bond of the neurotransmitter and includes a catalytic triad of aminoacidic residues, Ser200, His440 and Glu327 in TcAChE and Ser198, Glu325 and His438 in hBChE. These residues of the CAS help in designing inhibitors. Inhibitors

32

directed to the active site prevent the binding of a substrate molecule, or its hydrolysis, either by occupying the site with a high affinity, as for tacrine, or by reacting irreversibly with the catalytic serin, as for organophosphates and carbamates[91].

- The *oxyanion hole* is the crucial determinant in active site geometry, which accommodates the acetyl group of ACh[92]. The oxyanion hole is responsible for the stabilization of the transition state of the enzyme-substrate complex. The crystal structure of AChE revealed that three-pronged oxyanion hole is created by peptidic NH group of Gly118, Gly119 and Ala201 residues present in TcAChE. The oxyanion hole in hBChE is similar to TcAChE and consists of highly conserved Gly116, Gly117, and Ala199.

- The *acyl binding pocket* in cholinesterases is responsible for substrate specificity. In TcAChE, acyl binding pocket consists of aromatic residues, namely Trp233, Phe288, Phe290, and Phe331. During catalysis, acyl group of choline esters are accommodated in this area. Whereas, in hBChE, two of these phenyl residues were replaced with valine and leucine to create a larger pocket. This larger pocket, made by Trp231, Val288, Leu286, and Phe329, allows BChE to hydrolyze bulkier substrate and ligands compared to AChE, resulting in its lower specificity.

- The *anionic subsite* accommodates the quaternary amine of ACh, ensuring its correct orientation, by aromatic residue tryptophan with cation–π interactions. The substrate is guided inside the active gorge via interaction with a phenylalanine residue. In TcAChE, this gorge consists of Trp84, Glu199, and Phe330 residues. In hBChE, Phe330 residue is replaced by Ala328. Lack of this phenylalanine residue in BChE influences the affinity for some inhibitors.

The catalytic mechanism of cholinesterases is similar to that of other hydrolases; the hydroxyl group of the serine becomes highly nucleophilic by a charge-retransmission mechanism involving the carboxylate anion of glutamate, the imidazole anion of histidine, and the hydroxyl anion of the serine. During the enzymatic attack on acetylcholine, which is an ester with trigonal geometry, a tetrahedral intermediate is formed between the enzyme and the substrate.
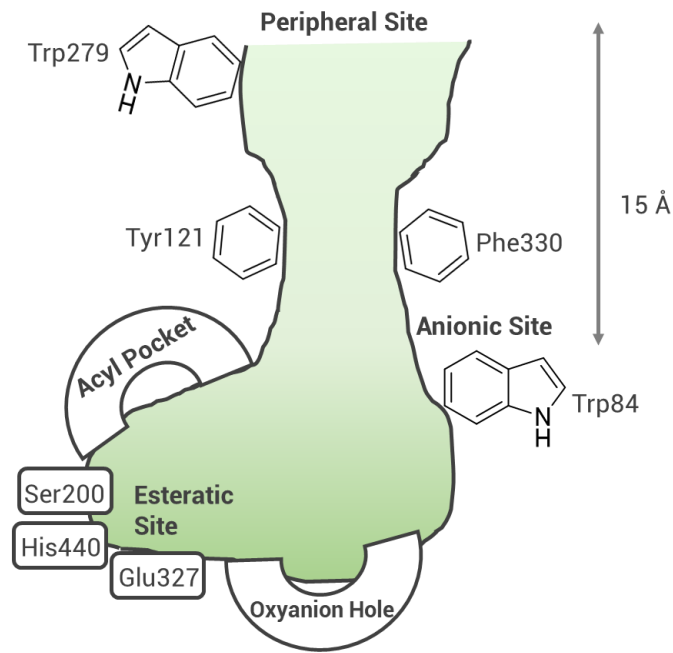
FIGURE 13| Schematic view of the active-site gorge of TcAChE. The bottom of the gorge is characterized by several sub-sites: the anionic site, which interacts with the choline moiety of ACh; the esteratic site, which contains the three residues of the catalytic triad; the oxyanion hole, and the acyl pocket, which confers substrate specificity. The PAS is located ~15 Å above the active site, close to the mouth of the gorge.

Acetylcholine decomposes to an acetyl conjugate of the enzyme with concomitant release of choline. Acetyl CoA is highly labile to hydrolysis after which acetate and the active enzyme are formed. AChE is a very efficient enzyme as one molecule can hydrolyze 6×10^5 molecules of acetylcholine/minute; thus, the recovery time of the enzyme is 100 microseconds[93].

3.1.2 Cholinesterases as therapeutic target

From decades, cholinesterase hypothesis is widely approved for its role in dementia and neurological disorders. It can be detected histopathologically through the loss of neurons and neurochemically by the deficit of marker enzymes involved in ACh synthesis and degradation. The hypothesis has been also validated by the use of acetylcholinesterase inhibitors (AChEIs) drugs as pharmacological treatment available for AD.

Even though this pharmacotherapeutic approach leads to a partial stabilization of cognitive function and improvement of the quality of life, these compounds have beneficial effects only for a short period of time, which usually lasts 1-3 years, and they are not able to influence the disease evolution[94].

The question remains whether it may be more clinically beneficial for the treatment of AD to have a selective cholinesterase inhibitor for AChE or BChE as

opposed to the non-specific inhibitors. *In vitro* kinetic studies have demonstrated that the marketed drug donepezil, rivastigmine, and galantamine inhibit both AChE and BChE[95]. Despite differences in potency, degree of selectivity and also mechanism of action, these cholinesterase inhibitors demonstrate comparable clinical efficacy for the treatment of AD[96]. In addition to their cholinesterase inhibitory activity, several of these compounds also display modulatory activity on Aβ and, thus, may influence AD through effects on this pathway. In particular, tacrine and rivastigmine, both of which more strongly inhibit BChE over AChE, lower Aβ levels in cell culture models[97,98].

Although its precise role in the pathogenesis of AD is not fully understood, BChE has been consistently found to be associated with the neuropathological structures of AD, neuritic plaques and neurofibrillary tangles[99]. Especially, given the decreasing levels of AChE with AD progression, inhibition of this enzyme may yield diminishing returns for increasing brain acetylcholine levels that are declining due to cholinergic neurotoxicity. In particular, selective inhibition of BChE has been shown to raise acetylcholine levels in the brain[100]. This has prompted the suggestion that BChE may be a better target than AChE for treatment of AD[96]. To date, no conclusive studies have demonstrated the benefit of BChE-selective inhibition for the treatment of AD. Further clinical studies are required to adequately evaluate the efficacy of BChE-selective inhibitors for the treatment of AD compared with the effectiveness of non-selective inhibitors currently in use.

3.2 Amyloid hypothesis

The amyloid cascade hypothesis was first proposed in 1992 by Hardy and Higgins[101]. Originally, this hypothesis simply described the harmful effects of β-amyloid (Aβ), suggesting that accumulation of Aβ peptides in the brain is an early event in AD which leads to the formation of senile plaques and, subsequentially, neurofibrillary tangles, causing neuronal cell death and ultimately dementia. Various experimental studies have supported this hypothesis which has dominated research for more than 25 years[102].

3.2.1 Aβ peptide

Aβ is a protein consisting in 40-42 amino acids, formed by proteolytic cleavage of a 695 amino acids long type I transmembrane protein, known as amyloid precursor protein (APP)[103]. APP is a type I cell surface glycoprotein of up to 770 amino acids involved in nuclear signaling which may also have a growth-stimulating function and importance in wound repair. The APP gene, localized on

chromosome 21q21.2, is a house-keeping gene as it is expressed abundantly in a variety of tissues. After its synthesis on ribosomes, a small fraction of APP molecules reaches the plasma membrane where they undergo a specific endoproteolysis by three proteases: α-, β-, and γ-secretases. The α-secretase activity is exerted by three members of the ADAM (a disintegrin and metalloprotease) family: ADAM-9, ADAM-10, and TACE (tumor necrosis factor-α converting enzyme)/ADAM-17[104]. The protein responsible for β-secretase activity is as an aspartyl protease called BACE (β-site APP cleaving enzyme)[105]. A large complex of different proteins, including neprilysin, insulin- degrading enzyme, and presenilins as the part of catalytic center, is suggested to be responsible for the γ-secretase cleaving activity[106].

The proteolytic cleavage can take two different pathways (**Figure 14**). In physiological conditions, it occurs via the major non amyloidogenic pathway. α-secretase cleaves APP to form soluble α-APP, which is removed from the brain, and C83, a peptide consisting of 83 amino acids which remains anchored in the membrane. A second enzyme, γ-secretase, located within the transmembrane zone, then cleaves the membrane peptide into two small peptides, APP intracellular domain (AICD) and P3, which are not amyloidogenic. As previously mentioned, the process of APP cleavage has been shown to be impaired in genetically determined forms of AD[20].

The amyloidogenic pathway begins with the cleavage of the extracellular part of APP by β-secretase, which forms soluble β-APP and a residual membrane peptide consisting of 91 instead of 83 amino acids. This process is followed by the formation of AICD and the pathological β-amyloid by γ-secretase, which accumulates in the brain forming cellular fibrillar deposits known as amyloid plaques. The γ-secretase processing is a heterogenous event forming Aβ with different C termini; $A\beta_{40}$ and $A\beta_{42}$ are the most common forms, resulting from the cut of γ-secretase at Val at position 40 or/and at Ala at position 42[107].
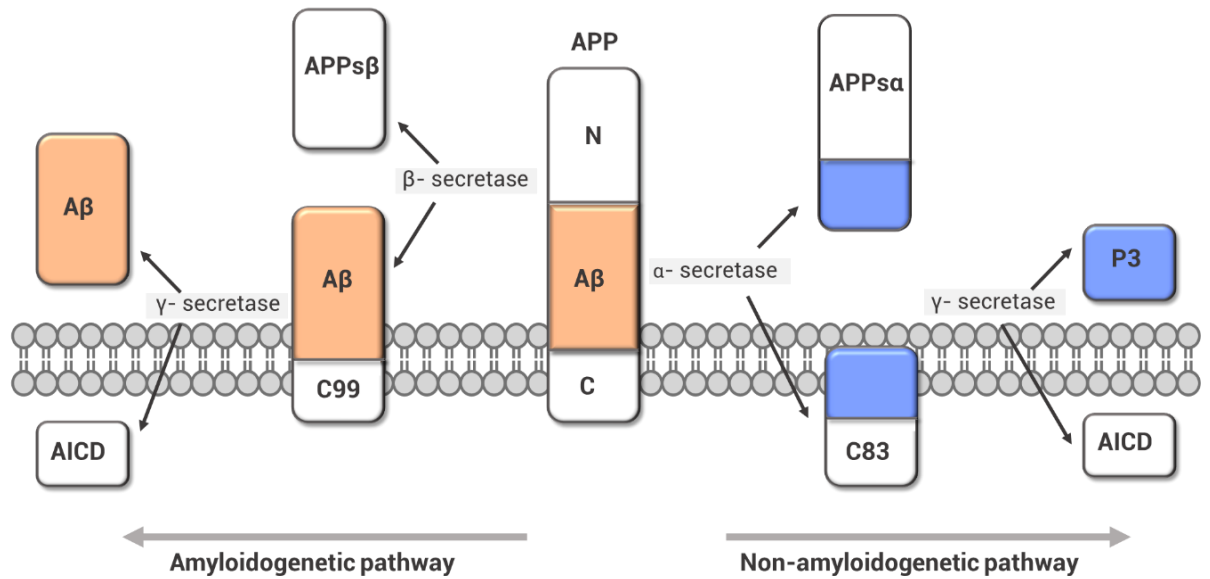
FIGURE 14| Endoproteolytic cleavages of the amyloid precursor protein (APP) leading to the formation of the non-amyloidogenic or amyloidogenic products, which are essential for the pathogenesis of Alzheimer's disease.

The amino acids sequence of Aβ peptide was discovered in 1984, from extracellular deposits and amyloid plaques[108]. The $A\beta_{40}$ peptide contains 17 hydrophobic, 11 polar and 12 charged residues. $A\beta_{42}$ peptide includes two additional hydrophobic residues at the C-terminal residue (**Figure 15**), which makes the $A\beta_{42}$ peptide more toxic and aggregation prone[109].


FIGURE 15| Amino acids sequence of $A\beta_{40}$ and $A\beta_{42}$ peptides. Negatively charged residues have been shown in red, positively charged residues have been shown in green, polar residues have been shown in black and nonpolar residues have been shown in light blue colour.

3.2.2 Aβ aggregation

The fibrillization of Aβ into senile plaques is a complex process involving several discrete steps, in which Aβ peptide sustains a series of transitions, from a structure rich in α−helix to one in which β-strands prevail. The total Aβ concentration may be the critical determinant of fibril formation. In young and healthy brains, Aβ is fully catabolized immediately after its secretion from the cell before it can be deposited. In the aging brain, enhanced production of Aβ and its reduced clearance may lead to Aβ deposition. Three types of Aβ oligomers have been identified thanks to *in vitro* studies: i) very short oligomers ranging from dimer to hexamer size[110]; ii) Aβ-derived diffusible ligands (ADDLs), small oligomers of 17-42 kDa[111]; iii) protofibrils, short fibril intermediates of <8 nm in diameter and <150 nm in length[112]. Detailed relationships between these different oligomers are still not clear. The two predominant *in vivo* Aβ alloforms, $Aβ_{40}$ and $Aβ_{42}$, have distinct behavior at the earliest stage of assembly[113]. Studies of the kinetics of Aβ fibril formation have shown that $Aβ_{42}$ forms fibrils much faster than $Aβ_{40}$[114,115]. Thus, $Aβ_{42}$ is more fibrillogenic and more neurotoxic than $Aβ_{40}$. The initial phase of oligomerization of $Aβ_{42}$ monomers involves the formation of pentamer/hexamer units, so-called paranuclei[113] (**Figure 16**). Paranuclei are initial and minimal structures that can oligomerize to larger forms, namely large oligomers, protofibrils, fibrils. Monomers, paranuclei and large oligomers are predominately unstructured with only short β-sheet/β-turn and helical elements. During protofibril formation essential conformational changes occur when the unstructured, α-helix, and β-strand elements transform into β-sheet/β-turn structures. Paranuclei could not be observed for $Aβ_{40}$ at similar concentrations of the peptide[116].

Moreover, it has been suggested that $Aβ_{42}$ might directly aggregate into fibrils without previous association into oligomers; thus indicating that oligomers are not an obligate intermediate in the fibril formation pathway, but oligomerization and fibrillization are independent and distinct pathways[117].
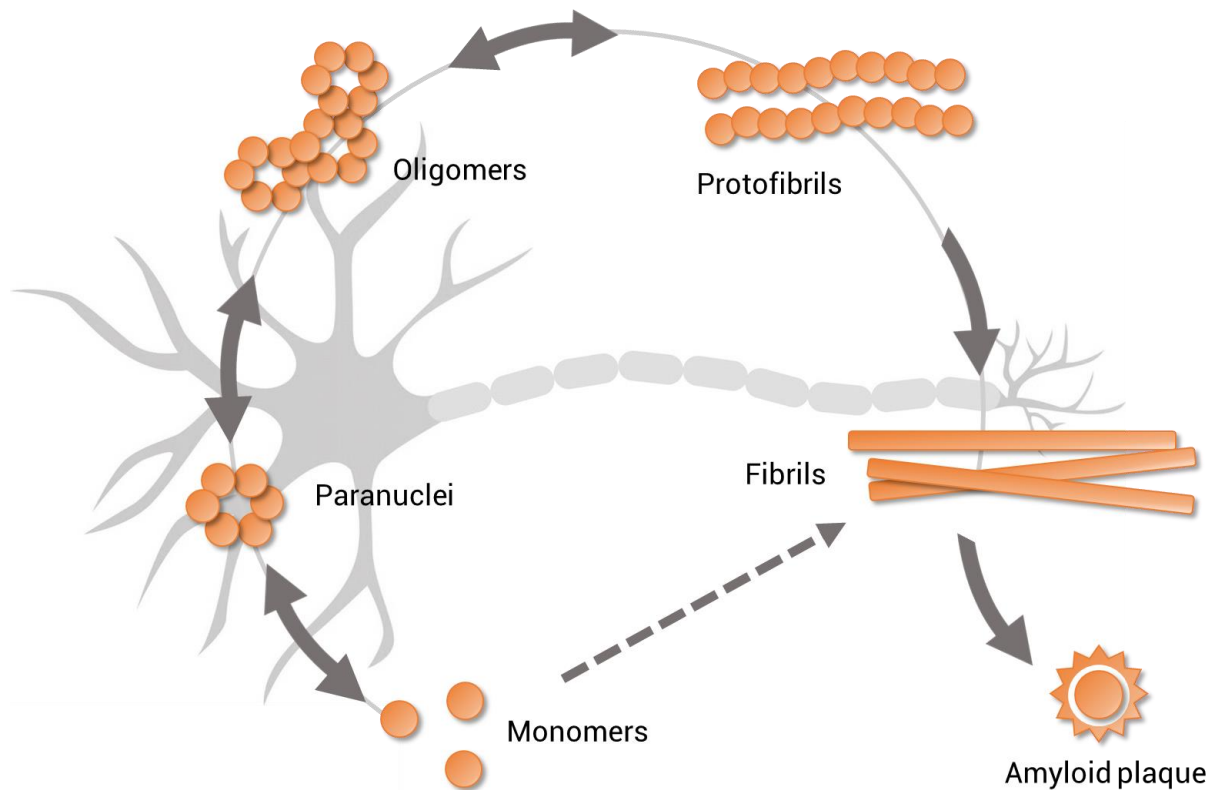
FIGURE 16| Simplified representation of $A\beta_{42}$ aggregation. The equilibrium between monomer and paranuclei is rapid and reversible. The conversion to protofibrils is slower but also reversible. The further oligomerization of protofibrils into fibrils appears irreversible. Monomers, paranuclei and large oligomers are predominately unstructured with only some β-sheet/β-turn and helical elements. During protofibril formation essential conformational changes occur when the unstructured, α-helix, and β-strand elements transform into β-sheet/β-turn structures. Recently, it has been suggested that $A\beta_{42}$ might directly aggregate into fibrils without previous association into oligomers.

3.2.3 Aβ as therapeutic target

Until recently, the fibrillar $A\beta_{40/42}$ was considered the only toxic form of this peptide, but it is now clear that Aβ oligomers and protofibrils are more neurotoxic than mature Aβ fibrils or amyloid plaques. The neurotoxicity of the prefibrillar aggregates appears to result from their ability to trigger a whole cascade of harmful mechanisms, including the neuroinflammatory process, oxidative stress, and excitotoxicity, which leads ultimately to loss of synapses, intraneuronal connections, and neuron death[116] (**Figure 17**). The strong cytotoxicity of the pre-fibrillar amyloid aggregates may be a direct consequence of their interactions with cell membranes causing membrane damage *via* the formation of non-specific ion channels, already described for Aβ peptide[118]. They could disrupt cellular

homeostasis impairing fundamental cellular processes by oxidative stress and by increasing free Ca^{2+} that eventually cause apoptotic cell death[119].

On the contrary, some authors hypothesize the cores of amyloid in the AD brain as a mechanism of defense, which in the end lead to catastrophic consequences[120].
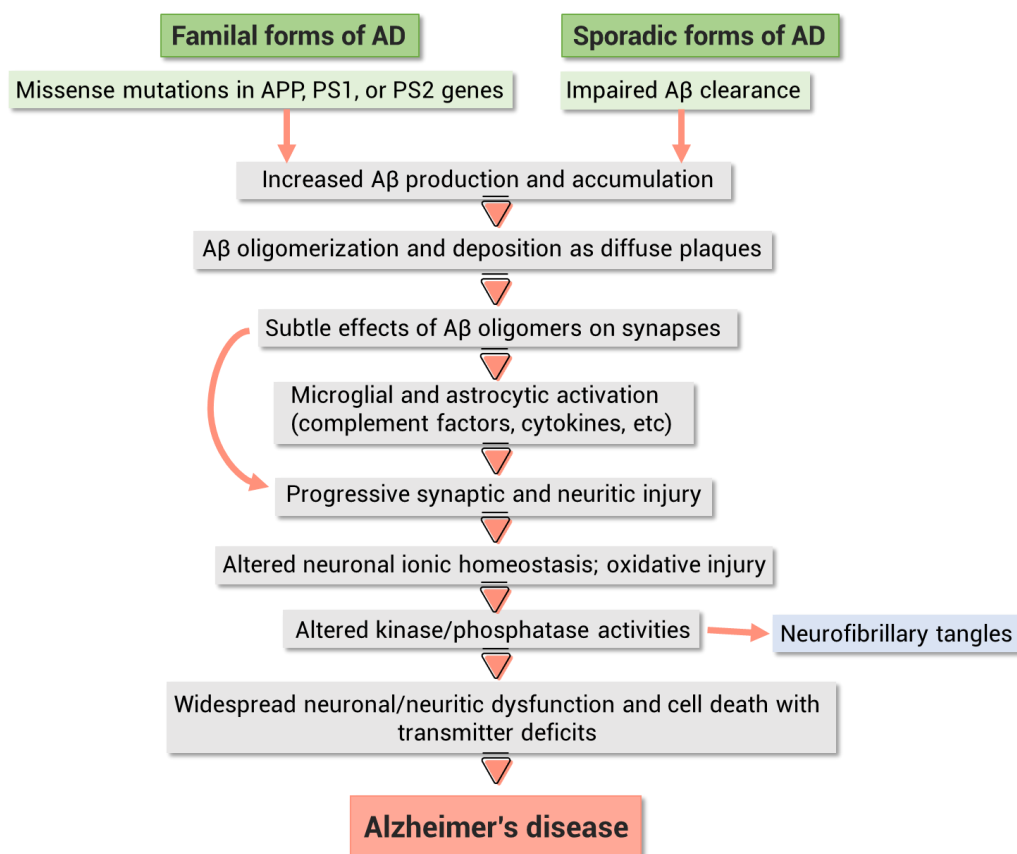
FIGURE 17| The sequence of pathogenic events leading to AD proposed by the amyloid cascade hypothesis. The curved arrow indicates that Aβ oligomers may directly injure the synapses and neurites of brain neurons, in addition to activating microglia and astrocytes.

As previously mentioned, the mutations responsible for the familial Alzheimer's disease have a direct effect on Aβ fibril formation[17]. Both APP and PS mutations affect the activity of α-, β-, and γ-secretases during APP processing, leading to overproduction of amyloidogenic $A\beta_{42}$[121]. A significant increase in the $A\beta_{42}/A\beta_{40}$ concentration ratio is observed in the majority of familial cases determined by the mutations. Conversely, no evidence of an altered Aβ generation in sporadic late-onset AD, the major form of the disease, has been provided. Therefore, it is reasonable to assume that Aβ aggregation in sporadic AD may be induced by a yet unknown post-translational modifications of Aβ and/or by an altered mechanism of Aβ clearance. Aβ clearance is principally mediated by two distinct

mechanism, namely, through its hydrolysis by cerebral proteases, both intra and extracellular, and independently by transport from the brain and subsequent proteolytic removal in the periphery. The proteolysis occurs by a family of amyloid-degrading enzymes (ADEs), the majority of which are zinc metalloproteases, as the plasma membrane peptidase neprilysin (neutral endopeptidase, NEP) and the cytosolic insulin-degrading enzyme (IDE)[122]. In addition to extracellular and neuronal metabolism of Aβ, another significant pathway for its removal is represented by the uptake and clearance by glial cells, particularly microglia and astrocytes. Extrusion of Aβ from the brain can occur by enzymic way, for example through the potent binding of Aβ oligomers with the triggering receptor expressed on myeloid cells 2 (TREM2). Alternatively, the extrusion can occur by nonenzymic pathways, as the interaction of Aβ with the low-density lipoprotein receptor-related protein-1 (LRP1), which is primary responsible for Aβ transport peripherally, or the soluble form of the receptor of advanced glycation end products (RAGEs)[123]. After its transport in the plasma, Aβ is cleared mainly in the kidney, which is highly enriched in the Aβ-degrading peptidase NEP, and in the liver[124]. Levels of Aβ in the periphery and brain are in equilibrium and enhancing Aβ cleavage peripherally may result in reduced brain Aβ levels.

Targeting the Aβ peptide cascade has been at the heart of therapeutic development in AD research since its formulation in 1992, even if drugs based on this hypothesis have not reached commercialization yet. In the last few years, several phase 3 clinical trials of agents directed against the Aβ protein in symptomatic patients with late-onset Alzheimer's disease have failed to achieve their prespecified primary endpoints. This disappointing outcome automatically leads to further questioning of the validity of the amyloid hypothesis.

A probable explanation for the clinical failures is that most trial participants may have had too advanced pathobiology to have the process slowed noticeably when averaged across all participants over 18 months. Even very mildly symptomatic patients may have had too much biochemical and neuropathological abnormality, including microgliosis, astrocytosis and synaptic loss, to experience a measurable cognitive benefit from clearing some or many forms of Aβ. This explanation suggests that the anti-amyloid agents may exert the most beneficial effects in presymptomatic subjects with demonstrated Aβ dishomeostasis[125].

Essentially, there are three different ways to approach Aβ as a therapeutic strategy. The first is based on the limitation of Aβ production through the inhibition of β- and γ-secretase or the activation of α-secretase[126,127]. The second lies in inhibiting Aβ oligomerization and fibrillization and/or destabilizing preformed Aβ

fibrils[126]. The last focuses on the regulation of Aβ levels through targeting Aβ clearance[122].

3.3 Tau protein

Tau (tubulin-associated unit) protein is known as an unfolded protein primarily expressed in neurons, which in its physiological form is bound to microtubules of neurons. Together with the other microtubule-associated proteins (MAPs), tau exerts important effects to create and stabilize the network of neuronal microtubules in the cytoskeleton[128]. Dysfunction and intraneuronal accumulation of the microtubule-related protein tau in the form of insoluble paired helical filaments (PHFs) and neurofibrillary tangles (NFTs) proved to be involved in early stages of the AD pathogenesis. Hence tau hypothesis of AD suggests that oligomerization, hyperphosphorylation, and propagation of tau have important roles in the pathological pathways leading to cellular disintegration and the consequent neurodegeneration. Contrary to the levels of senile plaques made by Aβ aggregates, the typical brain-regional occurrence and progression of tau pathology correlates temporally and spatially with neuronal and cognitive dysfunction[129]. Moreover, the levels of phosphorylated Tau also correlates to CSF concentration[130]. However, the crucial question remains whether the protein Tau should be placed downstream in the amyloid cascade hypothesis, at the same level or even upstream of amyloid. According to the Aβ hypothesis already discussed, NFTs formation is preceded by Aβ deposits, whereas other authors suggest tau as the prime cause of synaptic and neuronal degeneration in AD[131]. Only recently, a better view of how these two main AD hallmarks could be linked mechanistically has gained.

Tau protein is encoded by a single gene (MAPT) made of 16 exons on chromosome 17, resulting in six isoforms in the CNS and six additional isoforms in the peripheral nervous system (PNS). Alternative splicing of exons 2, 3 and 10 leads to the six isoforms found in CNS, which are made of 352-441 amino acids residues. Tau protein presents four different parts (**Figure 18**): (i) the N-terminal domain; (ii) the proline-rich domain, which together with the N-terminal constitutes the projection domain as it is not linked to the microtubules; (iii) the microtubule-binding domain (MBD), which contains three or four repeats of a sequence of 31 or 32 amino acids residues, depending on the isoforms; (iv) the C-terminal region. Alternative splicing primarily affects the N-terminal and MBD, yielding 3R and 4R tau isoforms, which display three or four repetitions of the

amino acids sequence in the MBD, respectively. Therefore, the 4R isoform, with four repetitions, shares a stronger interaction with the microtubules, thus conferring them a better stability[128]. In physiological condition, these two isoforms are present in ratio 1:1 in adult human brains. The disruption of this ratio is at the base of several tauopathies, AD included. Moreover, several tau mutations have been observed and numbered by their locations in 2N4R human tau and are associated with the emergence of tauopathies. These mutations could impact tau post-translational modifications, protein folding and aggregation[132].
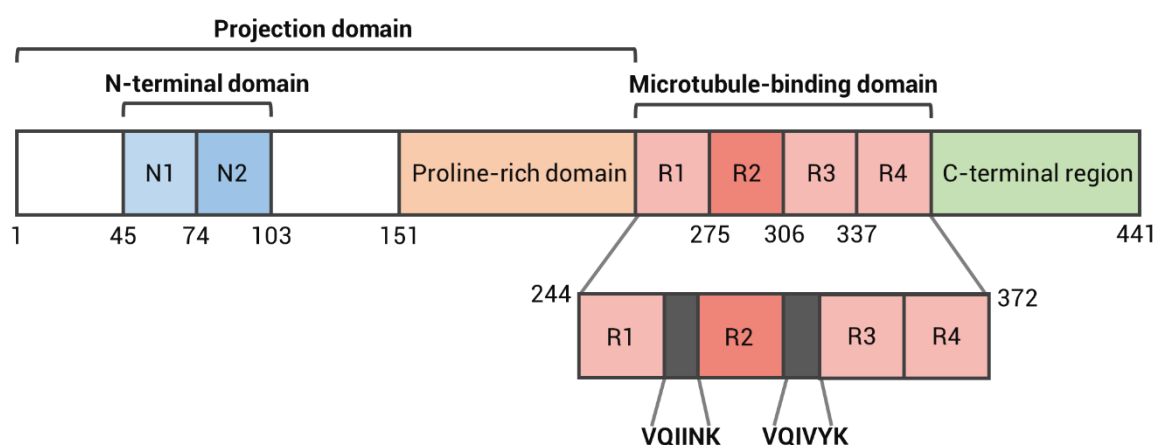
FIGURE 18| Domains of 2N4R tau. Tau protein comprises four primary domains, the N-terminal domain (blue), the proline-rich domain (orange), the microtubule-binding domain (pink), and the C-terminal region (green). Alternative splicing of the N-terminal and microtubule-binding domains yields six isoforms in the CNS. Repeat domains R1, R3 and R4 (light pink) are constitutive, while R2 (dark pink) is incorporated only in the three 4R isoforms. N1 and/or N2 may be skipped, but inclusion of N2 requires that N1 also be included. The final variants become: 0N3R, 1N3R, 2N3R, 0N4R, 1N4R, and 2N4R tau.

The molecular understanding of the role played by abnormal structural features of tau protein in human tauopathies, should be based on the knowledge of its normal cellular functions. The major, and as far as we know, the only physiological function of tau involves its capacity to bind to microtubules to control or affect spacing, stabilization and dynamics[133]. The cytoskeleton, which is a complex network of cytoplasmic protein filaments, allows cells to adapt to a wide variety of morphological changes and to undertake coordinated movements. It constitutes of three types of protein filaments: actin filaments, microtubules and intermediate filaments. Microtubule formation is stabilized by a family of protein called microtubules-associated proteins (MAPs). A major member of the MAPs is tau protein which, by binding with tubulin dimers constituting the microtubules, takes

part in their association-dissociation. This therefore grants them an essential dynamic in neuronal transport[134].

In its native form, tau protein is disorganized, soluble, flexible and resistant to aggressive treatments such as high temperatures and acid treatments[135]. In many of neurodegenerative diseases known as tauopathies, of which AD is the most common, abnormally phosphorylated forms of tau protein aggregate in filaments. When it becomes pathological, tau protein undergoes different post-translational modifications such as glycosylation, cleavage, nitration, ubiquitination, glycation or hyperphosphorylation, with the latter as the main one. Tau phosphorylation and cleavage are the are early steps that trigger and precede aggregation. Tau protein is considered hyperphosphorylated when it is phosphorylated in greater quantities than in normal adult brains at physiological level. This process is caused by a deregulation of the kinases and phosphatases acting on tau protein. The phosphorylation process can take place at diverse unique site of the protein and through multiple pathways. Tau contains 85 potential serine, threonine, and tyrosine phosphorylation sites, mainly found in the proline-rich domain of tau near the MBD. A large number of different kinases and phosphatases are implicated in tau phosphorylation regulation, including glycogen synthase kinase-3 (GSK-3), cyclin-dependent kinase 5 (CDK5), mitogen-activated protein kinases (MAPKs), casein kinase-1(CK1), microtubule affinity-regulating kinases (MARKs), cyclic AMP-dependent protein kinase A (PKA), dual specificity tyrosine-phosphorylation-regulated kinase-1A (DYRK-1A), tyrosine kinases such as Fyn, Abl and Syk, and phosphatases such as protein phosphatase-1, -2A, and -5 (PP1, PP2A, and PP5)[136].

Tau hyperphosphorylation negatively influences its physiological ability to stimulate the physiological microtubules assembly, resulting in the destabilization of cytoskeleton and degeneration of nerve cells. Moreover, among the kinases listed above, GSK3 appears to be directly involved in the AD pathogenesis, since it also contributes to the production of Aβ and Aβ-associated neuronal death[137]. It has also been reported that CK1 and CDKs play important roles in the tau hyperphosphorylation and formation of intracellular tangles, and secondarily Aβ peptides aggregation[138]. Furthermore, tau can be cleaved by many proteases: caspase-3 cleaves tau at Asp421 while calpain-1 and caspase-6 are responsible for the N-terminal cleavage. The resulting tau fragments have been detected in AD brains; in fact, caspase-cleaved tau fragments are known to be prone to aggregation, while cleavage of tau by calpain appears to partially inhibit the aggregation processes. Thus, phosphorylation and caspase-mediated cleavage

of tau should be considered also as important events in triggering the NFTs formation in AD[136].

As happens for Aβ peptide, the mechanism of tau aggregation is constantly being updated by new research findings, making difficult to establish a single mechanism. Fibrillogenesis is a slow process evolving over several phases, and one of its proposed mechanism include the protein dimerization (through disulphide bridges or ionic bonds), followed by a nucleation phase in which the dimers form oligomers, and finally the elongation phase in which the oligomers grow. Intracellular tau aggregate formation is mediated by the MBD, in a region between Ser214 and Glu372 which binds microtubules tethering tubulin dimers together. MBD region contains a tau repeat domain, which spans residues 243 to 365[139]. The third repeat contains the hexapeptide motif $_{306}$VQIVYK$_{311}$ which, along with the second hexapeptide motif $_{275}$VQIINK$_{280}$, is the most important for fibril assembly since these two sequences initiate and stabilize fibrillization[140]. Moreover, they promote the formation of β-sheet structures and consequent tau aggregation. The occurrence of tau mutations that destabilize local structure around these motifs could trigger spontaneous aggregation, leading to tauopathies[132,139].

In AD, NFTs are mostly constituted by bundles of paired helical filaments which are formed by two filaments twisted around one another with a crossover spacing of approximately of 80 nm and a width of 2-20 nm[135].

Based on tau hypothesis, researches are ongoing in order to explore different aspects of tau pathogenesis, such as modulation of tau gene expression, modulation of post-translational modifications, tau immunotherapy, and microtubule stabilization[141]. In addition, also anti-tau immunotherapy might effectively become a promising strategy in AD treatment[142].

3.4 Oxidative stress

The exacerbated production of reactive oxygen species (ROS) triggers the process called oxidative stress, which increases neuronal cell abnormalities, most often followed by apoptosis, leading to cognitive dysfunction and dementia. It is demonstrated that the brain of AD patients shows a significant extension of oxidative impairment. In this context, the oxidative stress plays a crucial role in the origin and development of AD. However, it is not clear whether this is a disease triggering event or it is a side effect[143].

Reactive oxygen species (ROS) are generated in the cell of living organisms and function as a second messenger in the intracellular signaling cascade[144]. This is a normal outcome of cellular metabolism, being essential in the maintenance of cellular homeostasis. In physiological conditions, low to moderate concentrations of ROS are important for diverse activities, such as immune response, inflammation, among others[145]. However, a redox imbalance or a dysfunction of the antioxidant system, called oxidative stress, cause an excessive generation of ROS, which may lead to loss of function and cellular apoptosis[146].

Since the brain is one of the organs that requires the highest oxygen demand to perform its activities properly, it is susceptible to the action of ROS. In addition, the brain is rich in polyunsaturated fatty acids that are exposed to peroxidation, presenting a high level of iron, which is a potent ROS catalyst. Moreover, the brain has a small amount of enzymes and other antioxidant substances[147].

The ROS are highly reactive molecules since they have one or more unpaired valence shell electrons. These species can be free radicals derived from oxygen, such as superoxide anion ($O_2 \cdot$) and hydroxyl radical ($\cdot OH$), or non-radical molecules as hydrogen peroxide (H_2O_2).

In the brain, these species can be generated by both exogenous and endogenous sources. Example of exogenous sources are drugs (wherein the mechanism of action is mediated by ROS), ionizing and UV radiation, environmental pollutants, inflammatory cytokines, chemicals found in tobacco smoke and environmental toxins. As for the endogenous sources, where ROS production is mediated by mitochondrial and non-mitochondrial enzymes, they include nicotinamide adenine dinucleotide phosphate—NADPH oxidase (NOX), xanthine oxidase (XO), granular endoplasmic reticulum cytochrome P450 and flavo-oxidase. The main source of endogenous generation is the respiratory chain and reduction—oxidation systems. In fact, the superoxide radical is the most commonly found, and its main source of generation is the electron transport chain[148].

Mitochondria are organelles that are the bigger consumers of intracellular oxygen, and, as a consequence, they are exposed to ROS. During the process of mitochondrial respiration, many reactive species such as hydrogen peroxide and superoxide anion are formed. The superoxide radical can also react with a reactive nitrogen species (RNS), nitric acid, which is produced by nitric oxide synthase (NOS) during cell signaling, resulting in others powerful reactive species.

In order to prevent their formation, hydrogen peroxide is deactivated by antioxidant molecules such as glutathione peroxidase and catalase enzymes.

An increase in ROS stops the activity of the electron transport chain in mitochondria, resulting in the oxidation of molecules such as DNA and lipids. In this sense, mitochondrial dysfunction is observed in several neurodegenerative diseases[148].

The free radicals amount in the body is regulated by an antioxidant protection system, which has the function of protecting healthy cells against free radicals.

Antioxidants can act against free radicals either inhibiting their formation or repairing the damage already caused. The first way is related to the inhibition of chain reactions involving their formation; and the second one, in the removal of damaged cells, followed by reconstitution of cell membranes. In this context, the human body presents two antioxidant self-defense systems, namely the enzymatic (endogenous) and non-enzymatic (exogenous) systems.

The enzymatic system is formed by a set of enzymes naturally produced by the body. The first antioxidant enzyme system consists of two types of SOD enzymes which catalyze the dismutation of the superoxide anion radical O_2^-, converting it into oxygen and hydrogen peroxide. The second antioxidant system is formed by the catalase enzyme that acts in the dismutation of the H_2O_2 into oxygen and water. The last system consists of glutathione (GSH) together with two enzymes, glutathione peroxidase (GSH-Px) and glutathione reductase (GSH-Rd). This system also catalyzes the dismutation of hydrogen peroxide into water and oxygen, and glutathione operates in cycles between its oxidized and reduced form[149].

In turn, the non-enzymatic system is made up of different substances such as vitamins, plant substances and minerals that can be obtained through the diet.

However, the endogenous self-defense system tends to be reduced with the natural aging process, as over the years the production of antioxidant enzymes loses its efficiency. Therefore, it is important to maintain the quality of the non-enzymatic defense system by eating antioxidant-rich foods. That is the reason why the use of vitamin-rich diets is an important adjunct in the treatment of AD

and other neurodegenerative diseases. Vitamins are powerful antioxidants that directly influence the fight against free radicals, reducing oxidative stress, inflammatory processes and loss of neurons[150].

As ROS production is increased within the mitochondria under some conditions of stress, in addition to aging, and along with the absence of an effective antioxidant system, there is an increased probability of developing AD. Various molecular mechanisms explaining the association between oxidative stress and other AD's features have been identified, most of which involve the alteration of Aβ homeostasis (**Figure 19**). Firstly, most biomolecules can undergo oxidation, and in the case of AD, these biomolecules are mainly those from the neuronal membrane, which involves the oxidation of lipids, fatty acids, and proteins[151]. If ROS are very unstable and reactive, presenting a very short half-life, the species they generate, after oxidizing biomolecules, are much more stable than themselves and can be used as biomarkers of oxidative damage. Examples of biomarkers include lipids, nucleic acids, and proteins in their oxidized states. In this context, the oxidative stress plays a crucial role in the origin and development of AD, and altered levels of biomarkers may indicate AD. Altered levels of antioxidant enzymes, such as catalases, superoxide dismutase, and glutathione peroxidase, as well as other antioxidant substances, can also be considered biomarkers[152]. Among the molecules that may undergo oxidation, there are also Aβ and tau, the two AD hallmark proteins. Moreover, Aβ itself is reported to induce the formation of ROS through different pathways. A number of genetic factors have been identified to play a role in AD-related failure to maintain physiological ROS levels within strict limits. For example, clusterin, apolipoprotein E and other enzymes involved in the APP processing are related, either directly or indirectly, to oxidative stress[143]. Another association identified as key feature in AD-related oxidative stress is the potent interaction of Aβ with Cu^{2+} [153]. But the relationship between Aβ and oxidative stress accounts also various other mitochondria-associated factors, including mitochondrial permeability transition pore formation, regulation of cellular metabolic pathways and Ca^{2+} signaling[143]. Additionally, oxidative stress could be involved in the clearance of Aβ, as the oxidation of biomolecules in AD context is mostly related to the neuronal membrane molecules and to the disruption of membrane integrity. There are indications that Aβ may promote the oxidation of the low-density lipoprotein receptor-related protein (LRP1), the protein responsible for Aβ efflux from the brain through the BBB, whose activity is decreased in AD. As a consequence, Aβ, through LRP1 oxidation, might potentially disrupt its own clearance, resulting in an increased accumulation

of Aβ in the brain. Therefore, the association between oxidative stress and AD appears complex, bi-directional, and self-reinforcing.
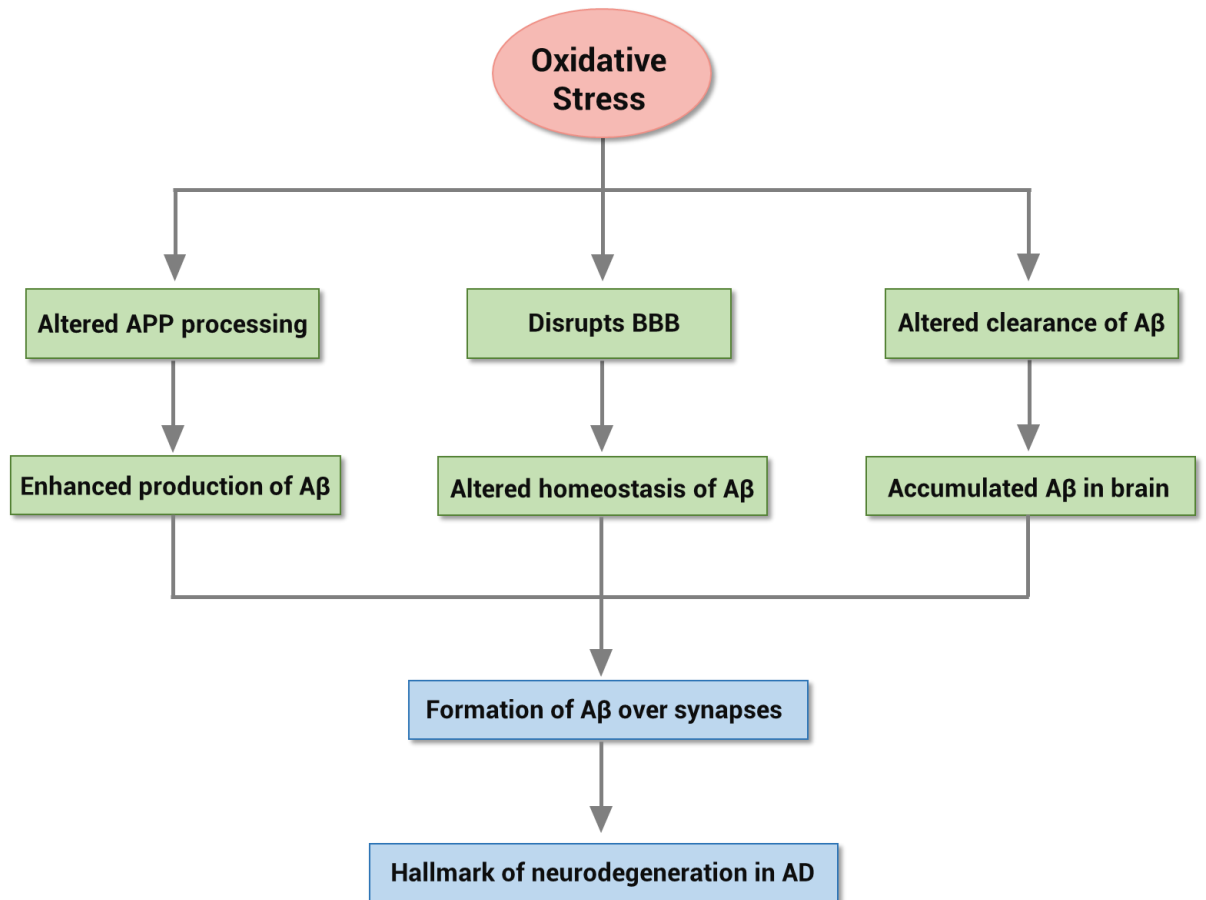
FIGURE 19| Oxidative stress dependent altered amyloid-β homeostasis in AD.

3.5 Monoamine Oxidases

Another feature associated to AD is represented by monoamine oxidases (MAOs). MAOs are flavin adenine dinucleotide (FAD)-containing enzymes that catalyze the oxidative deamination of primary, secondary, or tertiary amines, producing the corresponding aldehyde, hydrogen peroxide and ammonia. There are two isoforms of MAO in mammals, MAO A and MAO B, which share ~70% sequence identity and are encoded by separate genes located on the X chromosome. The C-terminal regions of MAOs are transmembrane α-helices that anchor the enzymes to the mitochondrial outer membrane, leaving the rest of the protein exposed to the cytoplasm. MAO-A catalyzes the deamination of neurotransmitters like serotonin, norepinephrine and dopamine, while phenyl ethylamine and benzylamine are mainly degraded by MAO-B. Both enzymes are involved in the etiology of AD, particularly MAO-B has been considered as a biomarker, being associated with the formation of Aβ peptide and responsible for cognitive dysfunction and disorders of the cholinergic neurons[154]. MAO B levels continue to increase throughout the lifetime and in AD progression, and in AD patients MAO B activity represents more than 80% of the total MAOs activity in the brain[155]. The activity and gene expression of MAO-A are also up-regulated in different brain areas. High levels of MAOs catalyze oxidative deamination and increase the production of hydrogen peroxide and ROS which are responsible for oxidative injuries and the toxic environment characteristics of neurodegeneration. Moreover, the increased MAO-B levels can enhance astrogliosis in the brain[156]. MAO-A inhibitors are used in the clinic to treat anxiety and depression, which are also common symptoms considered to be risk factors in AD progression[157], while MAO-B inhibitors are used in the treatment of Parkinson disease. Since in AD the loss of neuronal connection leads to a decrease in all neurotransmitter, the use of an anti-MAO-B, which prevents removal of dopamine by metabolism, could be beneficial. In addition to the increase of monoaminergic neurotransmission, MAOs inhibitors can decrease ROS formation and exert pharmacological effects including antioxidation, neuroprotection and cognitive improvement[158], which are all potentially valuable for the treatment of AD. Thus, both MAO isoforms can be considered as targets for the treatment of AD[154,159].

3.6 Metal ions dyshomeostasis

The homeostasis of metal ions, such as iron, copper, zinc and calcium, is crucial for maintaining normal physiological functions. Studies have proved that an imbalance of these metal ions levels in the brain is closely related to the onset and progression of AD[160] (**Figure 20**). In particular, changes in the balance of the metal ions in the brain of AD patients, are closely related to the Aβ deposition and tau hyperphosphorylation/accumulation, suggesting a crucial role of the metals in AD pathogenesis. The Aβ peptide itself has shown to be a strong redox-active catalyst able to produce hydrogen peroxide and OH⁻ in presence of copper or iron, which, in turn, are enriched in the amyloid cores of senile plaques[161]. Metal ions canal so interacts with Aβ peptide enhancing its self-aggregation and oligomerization at low physiological concentrations. Moreover, metals can promote tau hyperphosphorylation and subsequent formation of NFTs by inducing aggregation upon tau interaction with Aβ and by activating protein kinases, GSK-3, CDK5, MAPKs, etc., and/or inhibiting protein phosphatase 2A (PP2A)[162]. In addition, erroneous deposition/distribution of the ions in different brain regions induces oxidative stress. Redox-active metals, especially Fe^{2+} and Cu^{2+} are capable of stimulating free radical formation via the Fenton reaction, thereby increasing protein and DNA oxidation and enhancing lipid peroxidation.

The metal ions imbalances can also directly or indirectly disrupt organelles, causing endoplasmic reticulum (ER) stress and both mitochondrial and autophagic dysfunctions, which in turn can cause or aggravate Aβ and tau aggregation/accumulation and impair synaptic functions. The vicious cycles between metal ions dishomeostasis and Aβ/tau abnormalities might lead to a chronic neurodegeneration and cognitive deficits.

As both increase and decrease as well as mislocalization of the metal ions have been observed in AD, application of metal ions chelators has been studied for ameliorating the pathology and the cognitive functions. In this context, several clinical trials by supplementing or chelating or modulating the metal ions have been carried out in AD patients[163]. An effective metal chelator should be able to pass through the BBB, be specific for a single metal ion, and not show interference to the normal metabolism of the metal ions.
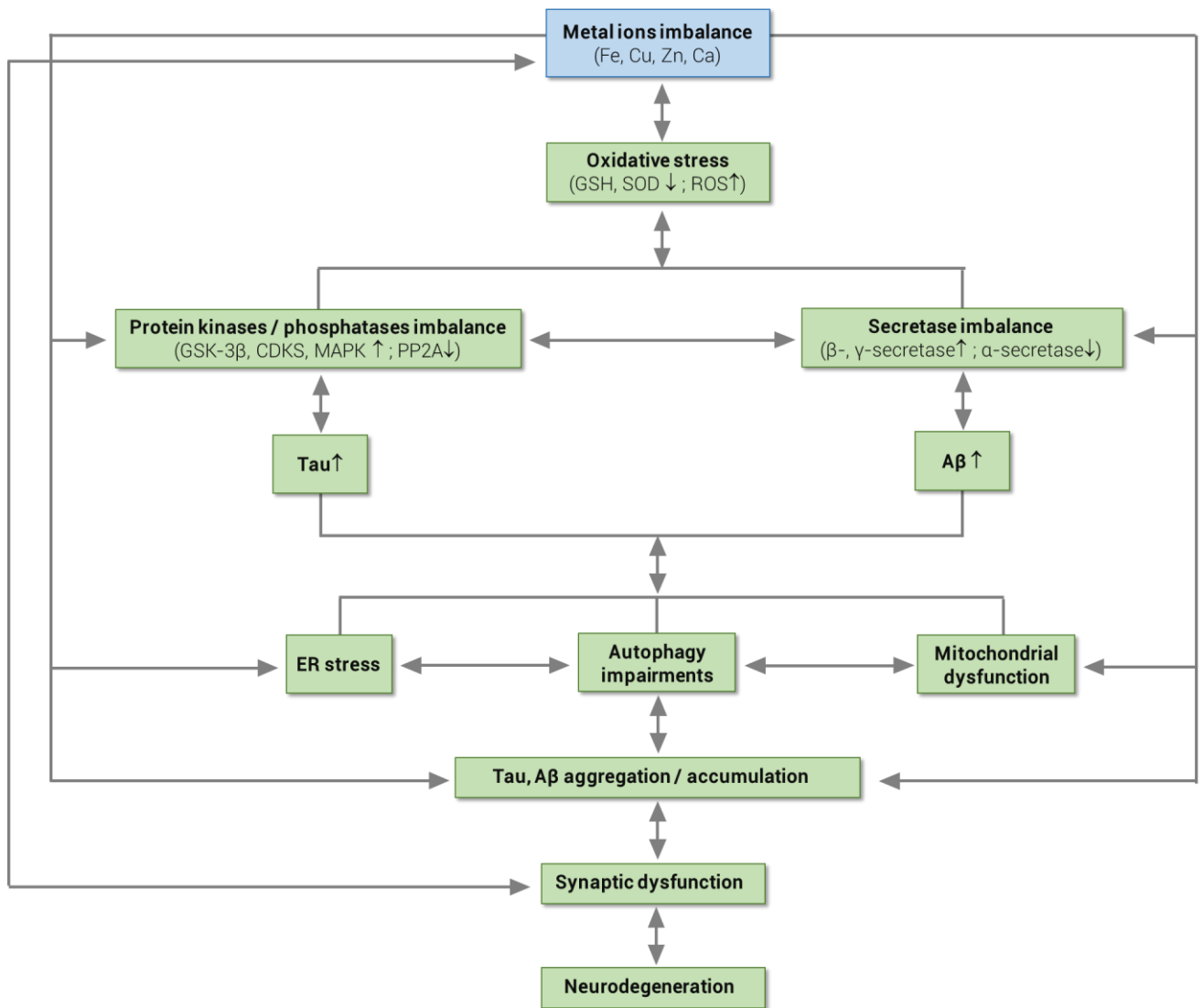
FIGURE 20| Metal ions imbalance in AD. The metal ions (Fe, Cu, Zn and Ca) imbalance induces oxidative stress, as demonstrated by the reduced level/activity of GSH and SOD1 and the increased level of ROS. Oxidative stress can in turn induce tau hyperphosphorylation by activating protein kinases, such as GSK-3β, CDK5, MAPK, etc., and/or inhibiting PP2A; it can also promote Aβ overproduction by activating β- and γ-secretases and/or inhibiting α-secretase. Together with the imbalanced metal ions and oxidative stress, or independently, the hyperphosphorylated tau (p-tau) and overproduced Aβ could induce ER stress, mitochondrial dysfunction, and autophagic impairments, leading to p-tau and Aβ aggregation and accumulation. Again, together with p-tau/Aβ accumulation, autophagic/mitochondrial deficits, ER stress and oxidative stress, or independently, the imbalanced metal ions can induce synapse damages. Synapse damages cause synaptic dysfunction, neurodegeneration, and eventually learning and memory deficits. As indicated in the figure by the double-sided arrows, many of these pathological processes occur in a bi-directional way thus forming a vicious cycle[160].

3.6.1 The role of Copper

Copper is an essential trace element for the human body and its levels are controlled by homeostatic mechanisms to prevent an excess, or a deficiency, that may trigger adverse health effects. Copper can undergo redox cycling between Cu^{1+} and Cu^{2+} and it is an effective catalyst, which serves as an active component for over 30 enzymes. The activities of some copper-containing enzymes, including superoxide dismutase (SOD) and cytochrome-c oxidase have important biological functions. However, copper is also involved in the formation of free radicals by the Fenton reaction, in which free copper catalyzes the formation of toxic hydroxyl radicals starting from physiologically available hydrogen peroxide[160]. In AD pathology, copper is mislocalized in the brain, where decreased levels of this metal have been reported in affected regions with enrichment in amyloid plaques and tangles[164]. Copper ions can bind to Aβ and promote oligomer formation, and eventually lead to Aβ aggregation. Cu^{2+}-stabilized $Aβ_{42}$ then interacts with the lipid bilayer increasing the permeability of membrane[165]. Furthermore, Cu^{2+} significantly affects the amyloid cascade through the interaction with APP via a Cu^{2+}-binding domain[166]. In addition, APP and Aβ display copper binding sites, and their interaction with copper can produce ROS, including •OH. Moreover, elevated copper reduces the level of GSH, enhancing the production and cytotoxic effects of ROS. The expression of copper dependent enzymes, as the SOD1 is reduced in AD patients, and, since in addition to the antioxidant role SOD1 also has anti-inflammatory functions, reduced expression of SOD1 can exacerbate ROS accumulation and the chronic neuroinflammation[167]. Finally, excess copper can promote tau phosphorylation and aggregation, as shown in a mouse model of AD[168]; while suppressed levels of copper in plasma and brain resulted in an attenuation of tau phosphorylation in a transgenic mouse expressing human tau, as well as copper chelating agents in human neuroblastoma cells[160].

3.6.2 The role of Zinc

Zinc is an essential component for many enzymes and transcription factors. In healthy conditions, most of the zinc content is located in membrane-bound metalloproteins, loosely bound to zinc within the cytoplasm, and vesicular zinc, enriched in synapses. It has several functional roles in signal transmission. Synaptic transmission releases high concentrations of zinc into the synaptic cleft, where it acts as an antagonist of γ-aminobutyric acid (GABA) and N-Methyl-D-aspartate (NMDA) receptors and activates the G-protein-coupled receptor GPR39.

Regarding the alterations or role of zinc in AD, large numbers of controversial results have been reported. Some authors demonstrated that zinc concentration in senile plaques increased 2~3-fold compared to the controls, while others showed a decreased zinc concentration in hippocampus or amygdala of AD patients. The reasons for the discrepancy are not still very clear, but the different experimental systems used for the studies could be at least one of them. These evidences strongly suggest that zinc is required for normal neural functions while excessive or misdirected zinc is harmful to the neural cells[160].

Aβ can directly bind to zinc at residues 6-28 with up to three zinc ions inducing Aβ aggregation. The binding between zinc and Aβ also reduces the Aβ solubility, and, together with the increase of Aβ aggregation, exacerbates damage to neurons[169]. Therefore, zinc, like copper, is able to accelerate Aβ induced toxicity and zinc sequestration into amyloid deposits. Zinc ions may also interfere with APP processing and function, as these processes are coordinate by secretases under the zinc regulation. Particularly, ADAM10, which can catalyzes the non-amyloidogenic α-secretase cleavage of the APP, can be activated by zinc[170]. Moreover, zinc is also associated with the impairment of Aβ clearance, as its direct binding to Aβ hides the proteolytic cleavage site, thus inhibiting the degradation of Aβ by proteases[171].

Excessive of zinc induces tau aggregation and formation of NFTs, as zinc can directly bind to tau monomers altering their conformation and inducing both aggregation and fibrillation of tau protein[172]. Moreover, it can modulate the phosphorylation of tau proteins by activating GSK-3β, extracellular regulated protein kinase1/2 (ERK1/2), and c-Jun N-terminal kinase (JNK)[173]. Zinc also induces PP2A inactivation and tau hyperphosphorylation through Src-dependent pathway, which ultimately leads to a net increase in phosphorylated tau that may exacerbate AD-like tau pathologies.

Although zinc is recognized as a redox-inert metal ion, evidences show its active involvement in redox metabolism. Under pathological conditions, excessive zinc is released from presynaptic neurons and astrocytes, which causes NADPH-oxidase activation, ROS production in neurons, microglial activation, and eventually exacerbates neuronal death. The mitochondrial respiratory chain is particularly sensitive to Zn^{2+}, and elevated Zn^{2+} in mitochondria promotes ROS production. Excessive zinc, which can be a consequence of an increased release from metalloproteins, can induce, as mentioned, Aβ production and deposition, and thereby triggering a cascade reaction. Therefore, oxidative and nitrosative stresses can cause an uncontrolled zinc elevation and Aβ deposition, while zinc

and Aβ accumulation can conversely lead to oxidative stress and cytotoxicity, forming a vicious cycle[160].

3.6.3 The role of Iron

Iron is a fundamental element in biology for oxygen transport and energy metabolism. It is a transition element that exists in oxidative states from −2 to +8, although in biological systems only ferrous (Fe^{2+}) and ferric (Fe^{3+}) states normally exist. The cycling between ferric to ferrous states is used in biology for various redox reactions essential to life. However, deleterious reactions with oxygen, such as Fenton reaction, which is catalyzed by the free ferrous iron, are a source of oxidative stress. In the brain, iron is involved in development, metabolic and neurotransmitter systems. Iron is transferred into neurons via transferrin (Tf), divalent metal transporter 1 (DMT1), and lactoferrin (Lf), while it is transferred out of neurons by ferroportin (FPN). As a multifunctional iron-binding globular glycoprotein, Lf has high affinity for Fe^{3+}. Iron can be transported to tissues and organs with blood circulation by bounding to Tf. Therefore, the dysregulation of DMT1, Lf, Tf and FPN not only affects the distribution, but also the accumulation of iron in the brain[160].

An increased iron level is correlated with the amount of Aβ plaques and tau pathologies, and, in AD brain, iron is enriched in both senile plaques ad NFTs. The binding of iron to Aβ or to tau induces Aβ aggregation and tau hyperphosphorylation, leading respectively to the formation of senile plaques and NFTs[174]. Fe^{2+} ions binding to the N-terminal region of Aβ can modify Aβ, impeding its ordered aggregation[175], and generate oxygen radicals that induce damages on the membrane surface[176]. Fe^{2+} can promote tau phosphorylation by activating CDK5 and GSK-3β. Iron-mediated tau hyperphosphorylation may be caused by the activation of ERK1/2 and MAPK pathway[177]. Conversely, it was observed that treatment of the cultured hippocampal neuron with Fe^{3+} decreases tau phosphorylation, which correlates with a decreased activity of CDK5[178].

3.6.4 The role of Calcium

The dysregulation of intracellular Ca^{2+} is an early manifestation of AD. Ca^{2+} concentrations near Aβ deposits are significantly increased, and the increase of Ca^{2+} likely plays a key role in the cognitive deficits associated with AD[179]. Calcium elevation promotes Aβ production and the cellular toxicity of Aβ, while the elevation of Aβ in turn promotes the opening of voltage-dependent calcium channels contributing to the increased intracellular Ca^{2+}. Moreover, an increased

intracellular Ca^{2+} concentration promotes the overexpression of L-type calcium channel subtype in the hippocampal cell membranes in models of AD, which further promote the Ca^{2+} influx[180]. Majority reports suggest that the intracellular calcium overload can promote Aβ production and aggregation. For instance, the elevated cytoplasmic Ca^{2+} by inhibiting the sarcoplasmic/endoplasmic reticulum (S/ER) calcium ATPase (SERCA) or liberating Ca^{2+} release via the ryanodine receptor (RyR), can robustly activate β-secretase and thus increase Aβ production[181]. Hence, a positive feedback loop may exist between Ca^{2+} and Aβ, which may exacerbate the neurodegeneration and cognitive deficits in AD patients[160]. In fact, inhibition of Ca^{2+} influx can reduce the levels of insoluble $Aβ_{40}$ $_{/42}$ in the hippocampus of AD transgenic mice[182]. Other studies demonstrated that Ca^{2+} ions actively participate in Aβ-related membrane damage, namely, Ca^{2+} ions inhibit Aβ-mediated membrane poration but enhance membrane fragmentation by lipid loss due to fiber growth on the membrane surface[183]. Finally, given that many kinases can be activated by Ca^{2+}, the dysregulation of calcium homeostasis can increase tau phosphorylation[160].

3.7 Inflammation

Increasing evidences suggest that AD pathogenesis involves strong interactions with immunological mechanism in the brain. Inflammation is a defensive mechanism of the body against multiple threats such as infections and injury. It is a complex event that involves both soluble factors and specialized cells. Similar inflammatory processes occur in the brain and peripheral tissues. In the brain, glial cells, including astrocytes and microglia, undergo activation under pro-inflammatory conditions by the increase in the production of inflammatory cytokines in the CNS, which becomes deleterious and leads to progressive tissue damage in degenerative diseases[184].

Microglia are ubiquitously distributed in the brain and constantly use highly motile processes to survey their assigned brain regions for the presence of pathogens and cellular debris. Moreover, they simultaneously provide factors that support tissue maintenance. At the same time, microglia are involved in the maintenance and plasticity of neuronal circuits, contributing to the protection and remodeling of synapses[185]. When activated by pathological triggers, as neuronal death or protein aggregates, microglia extend their processes to the site of injury, and migrate to the lesion, where they initiate the innate immune response (**Figure 21**). Microglia can bind to Aβ oligomers and fibrils through cell-surface receptors,

including SCARA1, CD36, CD14, α6β1 integrin and CD47, and this process is thought to be part of the inflammatory reaction in AD[186]. Binding of Aβ with CD36, TLR4, and TLR6 results in activation of microglia, which start to produce pro-inflammatory cytokines and chemokines[187]. As a consequence of receptor ligation, microglia start to engulf Aβ fibrils by phagocytosis, and these fibrils enter the endolysosomal pathway. If fibrillar Aβ is mostly resistant to enzymatic degradation, soluble Aβ can be degraded by various extracellular proteases as neprilysin and insulin-degrading enzyme (IDE) which are of major importance in microglia. However, as previously mentioned, in sporadic AD an inefficient clearance of Aβ has been identified. Moreover, an increased concentration of cytokines, by downregulation of expression of Aβ phagocytosis receptors, are suggested to be responsible for insufficient microglial phagocytic capacity[188].

Pathological responses of astrocytes include reactive astrogliosis, a complex, multistage and pathology specific reaction, whereas remodeling of astrocytes is generally aimed to neuroprotection and recovery of injured neural tissue. Next to activated microglia, hypertrophic reactive astrocytes accumulate around senile plaques and are often seen in post-mortem human tissue from AD patients[189], as well as in animal models of the disorder[190]. Glial cells activation might occur early, even before Aβ deposition[191]. Infiltration by peripheral macrophages may also occur[192]. Microglia and astrocytes release cytokines, such as tumor necrotic factor a (TNFa), interleukins, nitric oxide (NO), ROS, and other potentially cytotoxic molecules after exposure to Aβ, thereby exacerbating the neuroinflammatory response and eventually promoting neuronal death[193]. The important role of neuroinflammation is also supported by findings that gene for immune receptors, as TREM2 and CD33, are associated with AD[36,37].

Therefore, in AD, neuroinflammation do not appear a passive system activated by emerging senile plaques and neurofibrillar tangles, but instead contributes actively to pathogenesis as do plaques and tangles themselves. Understanding and controlling the interactions between the immune system and the nervous system might useful for the prevention or delay of most late-onset AD.
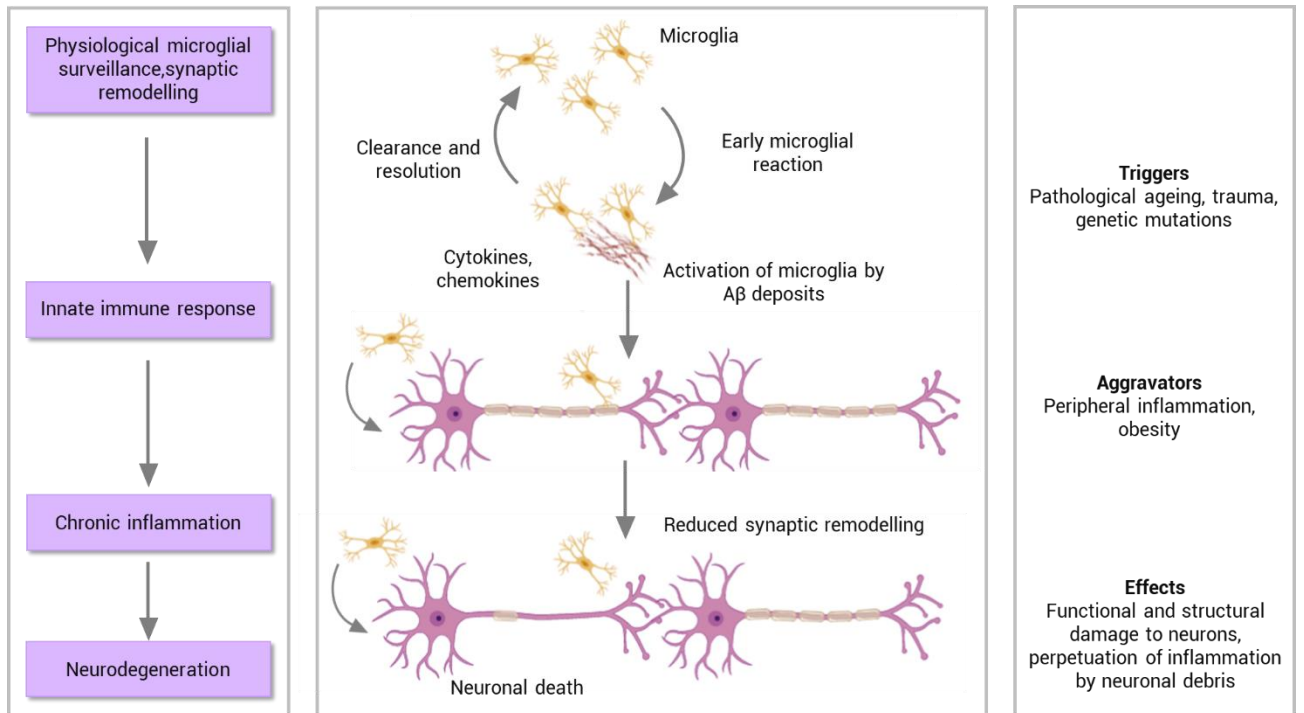
FIGURE 21| Pathomechanism sequence of microglia activation. Physiological functions of microglia, including tissue surveillance and synaptic remodelling, are compromised when microglia detect pathological Aβ accumulation. The acute inflammatory response initially mediates a response aimed to restore tissue homeostasis. Triggers and aggravators promote sustained exposure and immune activation leading ultimately to chronic neuroinflammation. Perpetuation of microglia activation and persistent exposure to pro-inflammatory cytokines cause structural and functional changes which lead to neurodegeneration.

4. TREATMENT

Unfortunately, there is still no cure available for AD, as the currently approved medications offer only a temporarily delay of the progression of symptoms and improvement of the quality of patients' life. The nebulous and complicated pathogenesis of AD makes difficult to develop new drugs, and also leads to the failure of many promising drug candidates when tested in clinical trials, resulting in unpredictable clinical manifestations. Despite these challenges, research of AD is still a hot topic, and the efforts and attempts of scientific groups worldwide are continuing, with the aim of finding an effective treatment. On the clinical front, the approach that has so far produced the majority of marketed drugs is the cholinergic hypothesis. Moreover, these medicaments are largely used in combination therapy with agents that have non overlapping or even synergistic mechanisms of action.

4.1 Current options

There are two main domains of intervention that may be relevant in early-stage AD, namely, pharmacological interventions, which include symptomatic treatments and other treatments targeting underlying disease mechanisms, and non-pharmacological interventions, which include interventions aimed to support and enhance cognitive abilities, and psychological interventions to support both the patients and their caregivers (Figure 22).
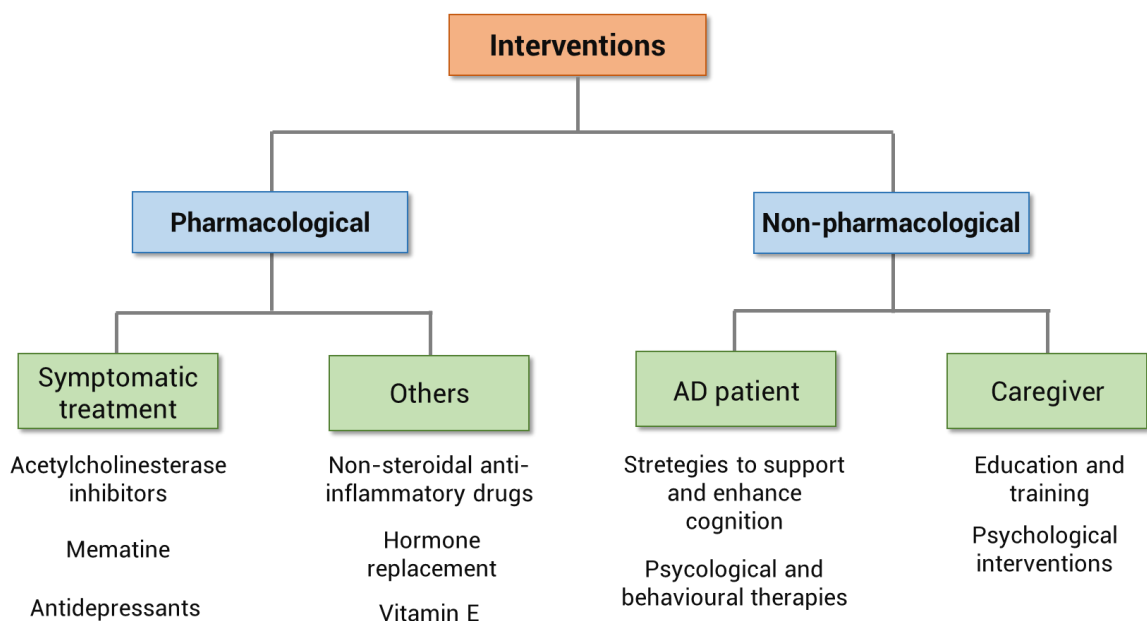
FIGURE 22| Classification of interventions.

4.1.1 Pharmacological interventions

As mentioned, current therapies are only able to mitigate symptoms and not to influence the progression of the disease (**Figure 23**). Symptoms can be divided into cognitive and behavioral categories. Cognitive symptoms affect memory, language, judgment and thought processes, while behavioral symptoms alter actions and emotions of the patients and include anxiety, sleeplessness and depression. Possible treatment methods involve medications and non-drug interventions. To set appropriate expectations and improve medication adherence, patients and families should be counseled that the expected goal of these agents is to stabilize the patient's cognitive symptoms rather than achieve noticeable improvement.
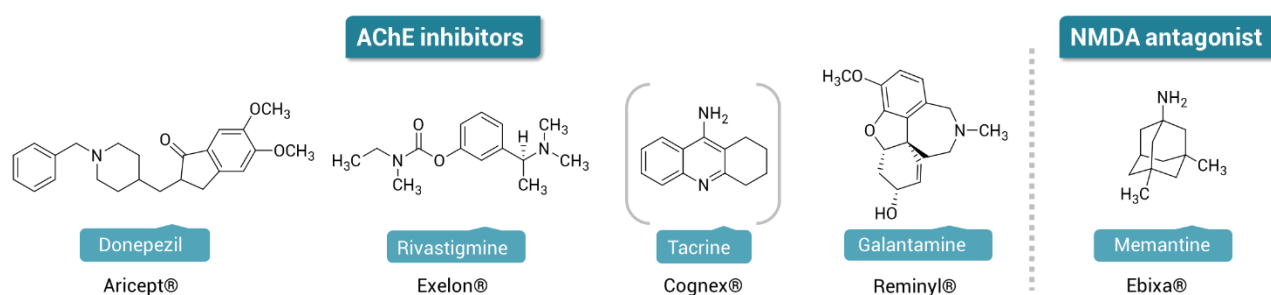
FIGURE 23| Overview of currently approved cognitive enhancing medications and Tacrine, which was withdrawn from use in 2013.

4.1.1.1 Cholinesterase inhibitors

Attempts to enhance cholinergic neurotransmission represented an early approach to treating AD. Though agonists of muscarinic receptors have previously been unsuccessful in human trials, and a trial of a nicotine transdermal patch is currently in phase 2 (ClinicalTrials. gov Identifier: NCT02720445), inhibitors of acetylcholinesterase are the only examples of this approach that have thus far shown some success. Acetylcholinesterase inhibitors (AChEIs) work by inhibiting AChE, the enzyme primarily responsible for synaptic recycling of acetylcholine, thereby prolonging the action of endogenous acetylcholine. Three inhibitors are currently in clinical use: donepezil (Aricept®), rivastigmine (Exelon®), and galantamine (Razadyne®) (**Table 1**). A fourth, tacrine, is no longer in use, largely due to its side effects, particularly hepatotoxicity[194].

AChEIs are overall relatively well tolerated. Gastrointestinal side effects are fairly common, occurring in 5-33% of patients in clinical trials, and include anorexia, nausea, vomiting, and diarrhea[195]. Other common adverse effects are dizziness/vertigo, fatigue, insomnia, hallucinations, bradycardia, and muscle

cramps[196]. The rivastigmine patch can also cause skin irritation at the application site.

Table 1. Administration, mechanism of action and adverse effects of currently approved cognitive enhancing medications.

Medication (trade name)	Administration	Mechanism of action	Adverse effect
Donepezil (Aricept)	Oral immediate release, oral disintegrating tablet, oral sustained release	Reversible non-competitive acetylcholinesterase inhibitor	Nausea, vomiting, loss of appetite, weight loss, diarrhea, bradycardia, dizziness, insomnia, fatigue, headache, muscle cramps
Rivastigmine (Exelon)	Oral, transdermal patch	Acetylcholinesterase and butyrylcholinesterase inhibitor	Nausea, vomiting, loss of appetite, weight loss, abdominal pain, tremor, diarrhea, bradycardia, dizziness, insomnia, fatigue, headache, allergic dermatitis, irritation at application site (patch)
Galantamine (Razadyne)	Oral immediate release, oral extended release	Reversible and competitive acetylcholinesterase inhibitor	Nausea, vomiting, loss of appetite, weight loss, abdominal pain, diarrhea, bradycardia, dizziness
Memantine (Ebixa)		Non-competitive NMDA antagonist	Both hypertension and hypotension, constipation and diarrhea, rare hypersensitivity reactions

Donepezil was approved by the Food and Drug Administration (FDA) in 1996 and by the European Medicines Agency (EMA) in 1997 and it is currently one of the most commonly prescribed drugs for the treatment of mild to moderate AD. It is a selective reversible non-competitive inhibitor of AChE, and it was developed, synthesized and evaluated by a Japanese pharmaceutical industry. However, its combination with other drugs should be cautious, since donepezil use cytochrome P450 in its metabolism. Donepezil was also found to be effective in inhibiting Aβ aggregation[197] and increasing the expression of nicotinic receptors in the cortex[198]. It has oral bioavailability of about 100% with a long half-life ($t_{1/2}$ = 70−80 h)[199]. Donepezil can be considered the first drug approved for AD treatment acting as a dual binding site inhibitor, namely is able to simultaneously bind both peripheral and catalytic site of AChE. Inspection of the X-ray crystallographic structure of the AChE-donepezil complex (PDB ID:1EVE)[200] shows that this compound extends from the catalytic site to the peripheral one along the gorge.

The benzyl ring establishes stacking interaction with Trp84, and the piperidine ring, whose nitrogen atom is protonated at physiological pH, lies onto the benzene moiety of Phe330. Moreover, there can be a stabilizing electrostatic interaction with Asp72. The indanone ring partly stacks against the indole ring of Trp279, whose orientation also mimics the arrangement found in the complexes with catalytic and peripheral site inhibitors[201].The discovery of donepezil started with the development of N-benzylpiperazine derivatives that showed micromolar inhibitory potential. Subsequentially, the replacement of the piperidine nucleus instead of piperazine ring dramatically increased the potency. Finally, among several substitutions, 4,5-dimethoxyindanone nucleus showed significant inhibitory potential and devoid of any side effect. The ring expansion of indanone nucleus decreased the activity drastically, and the 4,5-dimethoxy substituents showed maximum inhibitory potential. Moreover, the carbonyl group in indanone is also essential for activity and its replacement with indanol or indene nucleus, remarkably decreased the activity. Currently donepezil is an extensively investigated molecule, and its detailed structure-activity relationship (SAR) study has been conducted.

Rivastigmine is a combined AChE and BChE inhibitor that achieved FDA approval in 2000 and is available in oral and transdermal forms. Its half-life is 1.5 h, but the duration of clinical effect from oral administration is approximately 10 h because of the "pseudo-irreversible" nature of the inhibition, allowing for twice daily dosing. A more slowly absorbed patch form, which is applied once per day, was subsequently developed[202]. Since rivastigmine does not involve the cytochrome P450 system in its metabolism, the possibility of occurrence of drug-drug interactions is reduced.

Galantamine is a tertiary alkaloid extracted from various species of Amaryllidaceae, accidentally discovered in 1950. It is a competitive and reversible inhibitor of acetylcholinesterase and therefore theoretically has greater effect in areas of the brain with low levels of acetylcholine. It is also an allosteric modulator that enhances the effect of acetylcholine at nicotinic cholinergic receptors[203]. It is available in immediate and extended release oral formulations.

4.1.1.2 Memantine

Memantine is a low affinity and non-competitive NMDA receptor antagonist, and thus memantine regulates the activity of glutamate in the brain. Glutamate is an excitatory neurotransmitter involved in learning and memory. Overstimulation of nerves by glutamate may be the cause of the neuron degeneration seen in AD, called excitotoxicity. Glutamate binds to NMDA receptors on the surface of brain cells. Memantine functions by blocking the NMDA receptors and therefore protecting the nerves from excessive glutamate stimulation[204]. The exact mechanism of action in AD is uncertain but has been hypothesized that in addition to mitigate glutamate-induced excitotoxicity, memantine decreases hyperphosphorylation of tau protein and protects against the toxicity induced by Aβ peptide[205,206]. It is available as immediate and extended release (XR) formulations (Ebixa©) (**Table 1**) and as combination pill of memantine XR 28 mg daily and donepezil 10 mg daily (Namzaric©, approved by the FDA in 2014). Memantine, although frequently prescribed in the US for mild AD, has no consistent measurable benefit until the disease reaches the moderate stages. At that point, the modest benefit on cognition seems to be additive to that provided by acetylcholinesterase inhibitors, and, given the lack of significant adverse effects, combination therapy is appropriate for most patients[207].

4.1.1.3 Others

In regard to the pharmacological treatment, in addition to AChEIs and memantine, there are other approaches that might collaborate in the process of stabilization of the disease, such as the use of anti-inflammatory, antioxidant and estrogenic replacement, among others.

The use of anti-inflammatory drugs, as indomethacin and ibuprofen, that act by reducing the inflammatory response in the brain, is suggested to be able to reduce Aβ formation. However, prolonged use of these drugs can cause many side effects such as kidney and stomach problems[208].

Since depression is a common problem in old age, with a particularly high prevalence among people with dementia, the prescription of antidepressants is sometimes practiced in AD patients. The classes commonly used to treat depression in dementia are selective serotonin reuptake inhibitors (SSRI) and noradrenalin and selective serotonin antidepressant (NASSA).

Antioxidant prevent free radical formation, reducing oxidative stress and thus exerting a probable neuroprotective effect. The vitamin E demonstrated benefit on AD, and other examples of antioxidant are some flavonoids, which are the active

components of Gingko Biloba leaf extract. Evidence for the efficacy of vitamin E supplementation and medical foods is weak but might be considered in the context of cost, availability, and safety in individual patients.

Similar to antioxidant, the estrogen-replacement therapy also acts through neuroprotective mechanism. Estrogens exert effects on various receptors on the neuronal surface, promoting the neurotransmitters release and increasing the cerebral blood flow[71].

4.1.2 Non-pharmacological interventions

Evidences suggest that is possible to produce short-term improvements in cognitive functions and/or reduce cognitive decline in AD patients using non-pharmacological approaches. The strongest evidence for efficacy is related to interventions which apply principles of cognitive stimulation and/or reality orientation[65]. Cognitive stimulation targets cognitive and social function, through reality orientation, activities, games and discussions. It can be administered by professional therapists or by caregivers who have been trained.

Another non-pharmacological intervention involves psychological and psychosocial treatments, including cognitive behavioral therapy aimed to treat depression and anxiety. However, the evidence base for the effectiveness of these intervention for AD patients is limited[65].

Despite there is evidence that midlife exercise is associated with a reduced risk of AD, the benefits of exercise after onset of dementia are unclear, and the data are limited by the lack of consistent use of biomarkers. For patients with mild cognitive impairment, limited evidences suggest that exercise should be recommended since it promotes cognitive health, but the direct effect on AD pathology remains uncertain. Thus, while exercise may be recommended for the patient's overall physical health, data do not support its prescription to specifically improve cognitive function in AD patients[207].

4.2 State of the art – future perspectives

Since the number of AD cases will continue to rise in the next few decades as the result of life expectancy increase, there is an urgent need to develop a treatment able to modify the course of the disease more effectively. In the period between 1998 and 2011, ~100 compounds failed to demonstrate efficacy in modifying the AD course in the clinical development phase[209,210]. The reason why these compounds failed to show efficacy might be the related to the multifactorial aetiology and intricate pathophysiology of AD. Finding a suitable drug that is also

effective in the entire trial population is not an easy task. Although several key aspects of AD pathogenesis have not been resolved yet, scientific progresses in the last years allowed to establish different rational strategies for developing safe and effective treatments able to modify AD course. As a consequence of the current knowledge in the framework of new therapeutic intervention targets, there are multiple hypotheses around which therapeutic agents can be developed[211]. Currently are being proposed or utilized in disease prevention trials drugs that interfere with the synthesis, deposition and aggregation of β-amyloid protein[212], or with the hyperphosphorylation of tau protein[213], anti-inflammatory agents[193] and antioxidants[149,214], among the others. Out of all of these treatment strategies, those aimed at reducing Aβ formation and tau phosphorylation are the most important, as the greater advance in AD field have had to do with these two types of processes, and findings in this area may be the key to AD treatment in the near future.

4.2.1 Anti-amyloid strategies

Over the past two decades, research has mainly focused on development on compounds aimed to play a role interfering with Aβ, in line with the amyloidogenic hypothesis[126]. Although the repeated clinical failures of compounds developed led researchers to question the amyloidogenic hypothesis, it is believed that the past failures may be due to the lack of biomarkers able to facilitate patient recruitment for clinical trials before they have reached advanced stages of AD, in which any type of therapeutic intervention might be useless[209]. In this context, both new compounds and new tools for AD diagnosis that take into account Aβ role are currently being investigated (**Figure 24**).
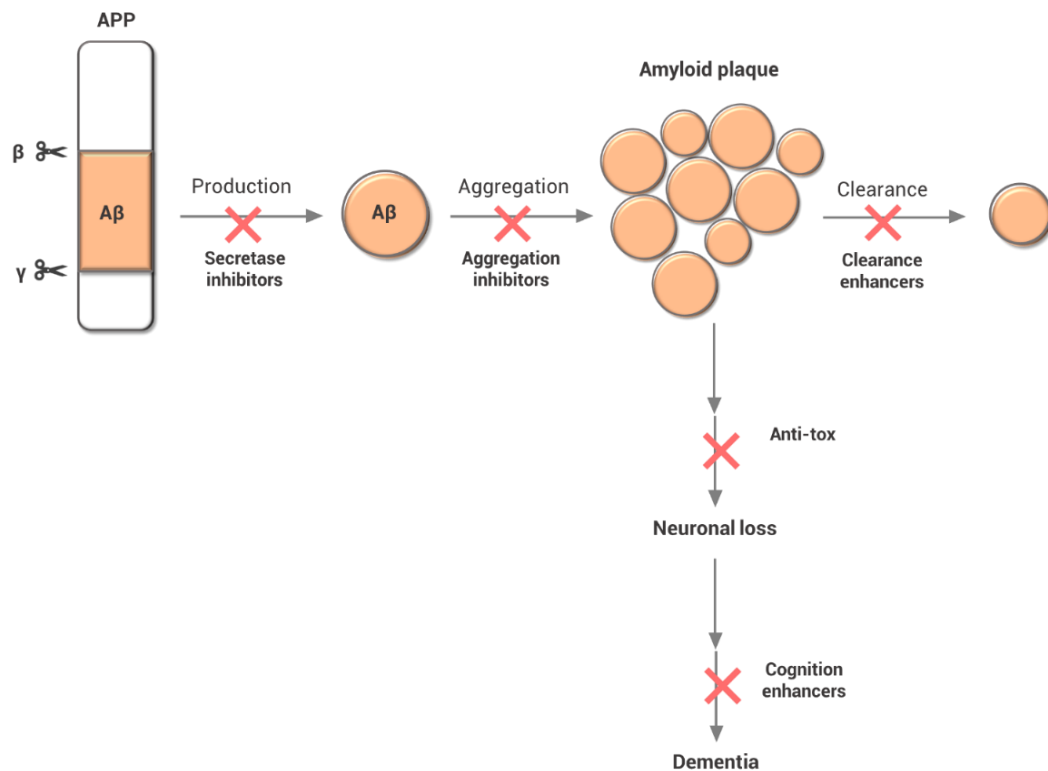
FIGURE 24| Therapeutic approaches targeting the amyloid cascade hypothesis.

4.2.1.1 Secretase modulators

The first strategy intended to reduce Aβ production is focused on modulate APP processing, namely, to inhibit γ− and/or β-secretase and to activated α-secretase.

β-secretase is a transmembrane aspartic protease that cleaves APP in the lumina, and its inhibition provides multiple advantages, among which is the prevention of Aβ formation at an early stage of APP processing. Developing an inhibitor of BACE1 is a hard challenge, as, in addition to APP, BACE1 has many other substrates important for synaptic plasticity and homeostasis, as neuregulin-1 which is involved in myelination of peripheral nerves. Moreover, BACE1 presents similarities with other aspartyl proteases, such as BACE2, pepsin and rein; thus, achieving selectivity in BACE1 inhibition without affecting other proteases, is crucial for eliminating off-target side effects[215]. Furthermore, an additional challenge is related to the size of the active site of BACE1, which is known to be relatively large. Therefore, having a small hydrophilic molecule able simultaneously to occupy the active site and cross the BBB represents a grand challenge[216]. Despite all these issues in the design of BACE1 inhibitors, many laboratories succeeded in developing selective, potent and bioavailable inhibitor agents; and many of these compounds showed promising clinical effects (**Table**

2); however, none of them have passed the final stages of clinical trials yet to receive FDA approval and reach the market[217].

Despite BACE1 inhibitor clinical trials conducted so far being discontinued for either futility or safety reasons, BACE1 still remains a validated therapeutic candidates for AD[105].

Table 2. BACE1 inhibitors currently in different stages of clinical trials.

Drug [Clinicaltrials.gov registry name]	Structure	Clinical trial phase	Status	Results
Verubecestat (MK-8931) [NCT01739348]		Phase III	Launched in November 2012; ended in April 2017	The trial ended 5 months earlier than expected as it was non effective and associated with adverse effects
Lanabecestat (LY2886721) [NCT02245737]		Phase II/III	Launched in September 2014; ended in October 2018	Studies stopped due to the lack of efficacy, no cognitive improvement were observed
Atabecast (JNJ-54861911) [NCT02406027]		Phase II/III	Launched in July 2015; ended in June 2018	Studies stopped due to liver toxicity
Elenbecestat (E2609) [NCT03036280]		Phase III	Launched in December 2016; estimated study competition November 2023	
CNP520 (Umibecestat) [NCT02576639]		Phase II/III	Launched in August 2017; ended in March 2020	Results not available

The enzyme γ−secretase is responsible for the final stage in APP processing, producing $A\beta_{40}$ and $A\beta_{42}$. Although achieving the inhibition of this enzyme was seen as promising approach for the disease modification, the development of a γ−secretase inhibitor shares the same hard challenges as for BACE1[218]. In fact, in addition to APP, γ−secretase acts to process other proteins, as the Notch protein,

which is involved in cell proliferation, development, communication and survival[219]. For this reason, nonspecific inhibitors would result in severe adverse effects. As a consequence, the attention of researchers is more oriented towards BACE1. One solution devised to prevent the adverse effects derived from γ–secretase inhibition was the study and use of selective γ–secretase modulators (GSMs), which block the enzyme to alter APP processing while sparing signaling on other pathways. The development of GSMs began with the observation that some non-steroidal anti-inflammatory drugs decreased levels of Aβ in cell cultures and in rats[220]. These drugs include ibuprofen, sulindac, indomethacin and flurbiprofen. In contrast, both tarenflurbil (R-flurbiprofen) and ibuprofen failed to show efficacy in their respective clinical trials[221,222].

CHF-5074 is a nonsteroidal anti-inflammatory derivative which proved to reduce $A\beta_{42}$ production *in vitro* by modulating γ–secretase. Subsequent preclinical studies proposed other mechanisms of action, such as restoring neurogenesis, reorganizing the astrocytic cytoskeleton, reducing tau, rescuing synaptic plasticity and acting on microglia to counteract inflammation[223]. CHF-5074 was submitted to two different phase II trials (ClinicalTrials.gov Identifier: NCT01723670, NCT01303744). The second phase II trial was withdrawn from ClinicalTrials.gov reportedly to be placed on hold to await the outcome of licensing negotiations.

The natural occurring molecule NIC5-15 is one example of selective GSM, which was found to decrease functional deficit and improve cognitive memory in preclinical models of AD. NIC5-15 (ClinicalTrials.gov Identifier: NCT00470418) entered in a phase II trial in 2007 which ended in 2010. Researchers are now examining its potential role as an inhibitor of the inflammatory process, especially referring to inhibition of microglial activation[126].

Activation of the α-secretase provides an attractive strategy for the development of disease-modifying drugs as it leads to APP being processed by the non-amyloidogenic pathway. With this aim, different compounds have been investigated, including agonist of muscarinic, glutamatergic and serotonergic receptors, and protein kinase C activators. However, only a limited number of compounds proved to modulate this pathway in animal models, thus very few compounds have reached the clinical trial stage[126]. In this context, a clinical trial of phase III (ClinicalTrials.gov Identifier: NCT00951834) is currently underway to evaluate the efficacy of epigallocatechin gallate in early stages of AD. It is reported that epigallocatechin gallate, a polyphenolic compound extracted from green tea leaf, displays beneficial effects ranging from anti-neoplastic to anti-inflammatory

and neuroprotective properties; and, in addition, it may have positive effects on cognitive function[224].

4.2.1.2 Amyloid aggregation inhibitors

The large amount of evidence about the neuronal and synaptic toxicity of amyloid deposits provides the basis for the development of inhibitors of Aβ aggregation. Unfortunately, only few Aβ aggregation inhibitors have reached clinical trials. One example is the synthetic glucosaminoglycan 3-amino-1-propanesulfonic acid (3-APS, tramiprosate, Alzhemed™), that acts antagonizing the interaction of Aβ with endogenous glycosaminoglycans[225]. Glycosaminoglycans have been reported to promote Aβ aggregation and plaque stability[226], and thus is reported 3-APS is able to prevent β-sheet formation. After a phase II study in which the drug appeared safe and reduced CSF $A\beta_{42}$ after three months, in June 2004, Alzhemed™ became the first anti-amyloid drug to enter phase 3 (ClinicalTrials.gov Identifier: NCT00088673). However, in 2007, it was announced the trial had failed to measure an improvement in cognition in the North American trial. As a consequence, it was stopped also the European trial, but the open-label extension of the North American trial continued. Results were subsequently published in 2011 by Aisen *et al.*[227].

4.2.1.3 Promotors of amyloid clearance

The last strategy pursuing the amyloidogenic pathway targets the clearance of Aβ aggregates and deposits. To this end, three different approaches can be pursued. The first one is to activate the enzymes responsible for the breakdown of amyloid plaques, such as neprilysin, IDE and endothelin converting enzyme, since their levels drop in AD[228]. However, no protease activators have been evaluated at present, and this is probably due with their lack of specificity[126].

The second approach is to modulate Aβ transport from the brain to the periphery. Aβ transport is regulated by apolipoproteins (APOEε4 included), that promote the transfer of Aβ from the blood-stream to the brain, low density lipoprotein receptor-related protein, that increase the transfer of Aβ from the brain to the blood-stream, and the RAGE, which facilitates Aβ penetration in the brain[229,230]. Although different proposed strategies exist, only the compounds aimed to inhibit or modulate RAGE have reached the clinical development stage. One example is PF-04494700 which blocks the interaction between RAGE and Aβ; hence the rationale is that it could provide a combined treatment effect across glial inflammatory and amyloid-related processes[231]. Currently PF-04494700 is undergoing a phase III clinical trial

(ClinicalTrials.gov Identifier: NCT03980730). Another example is TTP4000, which underwent a phase I clinical trial (ClinicalTrials.gov Identifier: NCT01548430), and despite study ended in 2013, the results have not been published yet.

The last approach, which is the most studied approach to reduce Aβ, is based on immunotherapy aimed to improve Aβ clearance. Immunotherapy can be either active or passive. Active immunization (vaccination) with $Aβ_{42}$ or with other synthetic fragments, has been successful in transgenic mouse model of AD. These trials are typically based on stimulating T and B cells and generating an immune response by activating the phagocytic capacity of microglia. If initial results from these type of trials were promising, some studies have been suspended since some patients developed meningoencephalitis[232]. By designing second generation vaccines, researchers attempted to prevent a nonspecific immune response to immunization with complete $Aβ_{42}$ peptides. As a consequence, the new vaccines employed shorter segments of the Aβ peptide, that would promote a humoral response to the cellular immune response. The first second-generation vaccine to reach clinical development stages was CAD-106[233]. Two phase II randomized and placebo-controlled clinical trials of CAD106 (ClinicalTrials.gov Identifier: NCT00733863 in Europe, and NCT00795418 in the U.S, both sponsored by Novartis) were initiated in 2008, and their open-label extension studies (ClinicalTrials.gov Identifier: NCT00956410 and NCT01023685) lasted through to 2011 and 2012, respectively. A Phase 2/3 clinical trial (ClinicalTrials.gov Identifier: NCT02565511) is currently underway. The study was designed to separately test CAD106 and another investigative medication, CNP520 from Amgen.

Passive immunization is another type of immunotherapy which in this context consists in the passive administration of monoclonal or polyclonal antibodies targeting Aβ. This method provokes an anti-Aβ immune response with no need for pro-inflammatory reaction T-cells mediated[234]. Bapineuzumab and solanezumab are two monoclonal anti-bodies that, among other, reached the most advanced stages of clinical development. However, both failed to show the expected clinical benefits in patients with mild to moderate AD in phase III studies in 2012. Bapineuzumab is a humanized monoclonal antibody that binds to the N-terminus of $Aβ_{1-5}$, while solanezumab is designed to bind the central part of the protein, $Aβ_{12-28}$ [235,236]. At present, new phase III clinical trials are being carried out on solanezumab (ClinicalTrials.gov Identifier: NCT02008357). Gantenerumab is another monoclonal antibody tested for its disease-modifying potential in phase III clinical trial (ClinicalTrials.gov Identifier: NCT01224106). Results gathering from

the study seem to indicate a tendence towards cognitive improvement, however, this trend does not seem statistically significant. Gantenerumab is a fully human IgG1 antibody with high affinity for a conformational epitope expressed on Aβ fibrils[237]. The therapeutic basis for this antibody, supported by experimental studies in transgenic mice[238], is that it acts by breaking down amyloid plaque with a process that involves microglial recruitment and activation of phagocytosis.

Finally, aducanumab is a human monoclonal antibody that selectively targets Aβ aggregates, including soluble oligomers and insoluble fibrils. It has been evaluated in several clinical trials on mild Alzheimer's disease and mild cognitive impairment, including the ENGAGE, EMERGE and PRIME trials[239−241]. Based on a later analysis of additional follow-up data and other supportive findings, Biogen submitted a biological license application to the FDA requesting the therapy's approval for the treatment of AD. Since 7 August 2020, Aducanumab has been under priority review at the US FDA. On 4 November 2020, the FDA released documents noting support for the safety and efficacy of Biogen's treatment for AD, aducanumab. However, on 6 November 2020, the FDA discussed aducanumab during a meeting of Peripheral and Central Nervous System Drugs Advisory Committee (which is charged with reviewing and evaluating data concerning the safety and efficacy of drugs for AD), and the committee voted against the approval. The FDA will now continue the review process, with a final decision on approval whether aducanumab's solution for intravenous infusion will attain its biologics license firstly due by 7 March 2021 and currently postponed to 7 June 2021. If approved, the drug will become the first new AD therapy to be approved in 17 years.

4.2.2 Tau

Another potential strategy to target AD is the inhibition of tau aggregation by small molecules to avoid the development of tau lesions, but, unfortunately, this approach lacks a complete understanding of the pathology of tau[242].

While extensive research is directed to interpret the relations between Aβ, tau and the kinase and proinflammatory cytokines that modulate tau phosphorylation, the therapeutic potential of this target interconnection is strengthened further by the case study of methylene blue (methythioninium chloride, MTC) (**Figure 25**). Methylene blue, the first synthetic drug ever used as an antiseptic in medicine, is a molecule able to cross the BBB which has neuroprotective effects in AD[243,244]. The hypothesis that methylene blue could have a therapeutic potential against AD arise from the observation that Tau filaments could be dissolved by this compound and its demethylated derivatives, such as Azure A, Azure B and

tolonium chloride[245]. Methylene blue also accumulates in the mitochondria, intervening in electron transport and improving mitochondrial respiration. Starting from methylene blue, two purified preparations have been developed, namely Rember® and TRx0237 (LMTX™) (**Figure 25**). The latter is an inhibitor of the Tau protein aggregation for the treatment of both AD and frontotemporal dementia[246], and it is a replacement formula for Rember®, the first patented formulation of methylthioninium chloride. Several clinical trials (ClinicalTrials.gov Identifier: NCT01689233) evaluating the efficacy and safety of TRx0237 in the treatment of mild AD are currently in phase III.
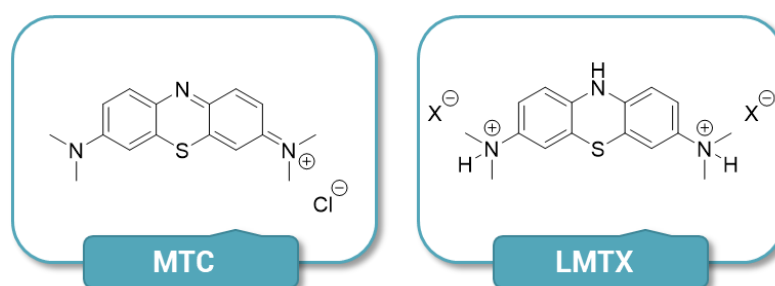
FIGURE 25| Structures of methylene blue (MTC) and its reduced form LMTX™.

Another strategy aimed to target tau toxicity consists in immunotherapy. The first example is AADvac1, a synthetic peptide derived from tau protein sequence, which is labeled with hemocyanin and uses aluminum hydroxide as adjuvant. AADvac1 is expected to reduce the number of neurofibrillary tangles, eliminate hyperphosphorylated Tau protein and reduce the amount of oligomerized Tau in the brain. Therefore, this vaccine should prevent cognitive impairment. Results gathering from preliminary phase I clinical trials, showed a tendency towards improved cognition and brain atrophy[247]. However, more placebo-controlled studies are necessary to confirm the efficacy of this compound significantly. A phase II study (ClinicalTrials.gov Identifier: NCT02579252) ended in June 2019, but no data has been reported to date.

A second example is ABBV-8E12, a recombinant humanized anti-Tau antibody that recognizes and binds to abnormal Tau aggregates, blocking their spreading from neuron to neuron and thereby decreasing the severity of the disease[248]. Currently, two phase II clinical trials run to evaluate the efficacy and safety of multiple doses of ABBV-8E12 in AD patients (ClinicalTrials.gov Identifier: NCT02880956 and NCT03712787) and they are expected to end in 2026.

RO7105705 is another potential therapy based on an antibody that reacts against Tau slowing its spread in the brain[246]. A Phase II clinical trial (ClinicalTrials.gov Identifier: NCT03289143) started in 2017 and will be completed in 2022. Another

phase II study, which evaluates RO7105705 in patients with moderate AD, started at the beginning of 2019 and will be completed in September 2021 (ClinicalTrials.gov Identifier: NCT03828747).

Finally, LY3303560 is a humanized antibody engineered to bind and neutralize soluble Tau aggregates[249]. A phase II study evaluating the safety and efficacy of LY3303560 administered intravenously in AD patients has been designed, and the results are expected to be reported in October 2021 (ClinicalTrials.gov Identifier: NCT03518073).

4.3 Multi-target directed ligands

To date, most pharmacological research is driven to the discovery of highly selective drugs. Drugs with high selectivity, indeed, have been historically designed to target a single biological entity, usually a protein, in order to avoid any adverse side effects caused by mistargeting other biological targets. Thus the paradigm "one target, one drug" has been considered the dominant drug discovery hypothesis during the past few decades[250]. However, until now this strategy has failed to develop any drugs able to slow down or stop the progression of AD.

This philosophy started to change in the last 20 years due to the emergent growing awareness that drugs designed to act on individual molecular targets are usually inadequate for multigenic diseases such as cancer, neurodegenerative and infectious diseases. Nowadays the knowledge of the complex word underlying the pathogenesis of these multifactorial diseases is being enriched, suggesting the multi-target therapeutics as potentially more advantageous than mono-therapies[251] (Figure 26).
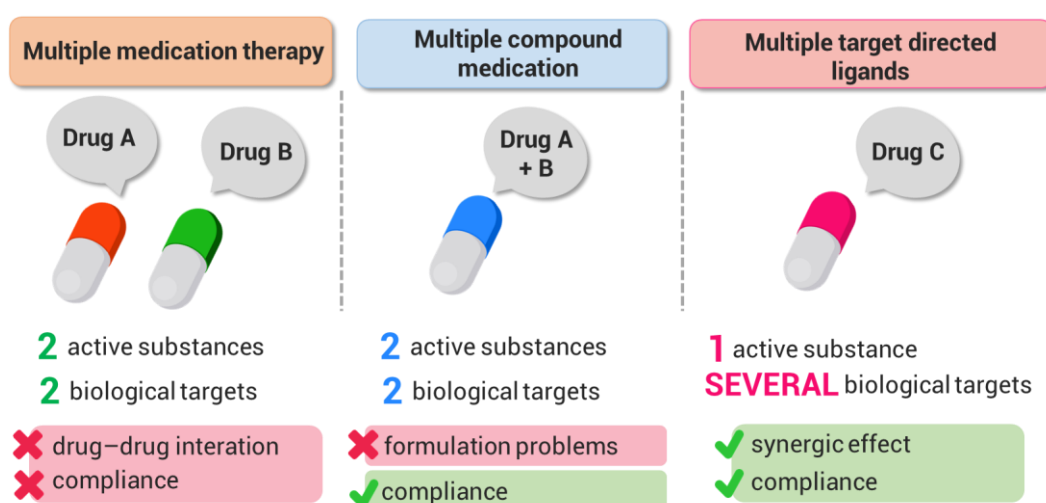
FIGURE 26| Advantages and disadvantages of different therapeutical approaches.

One logical alternative to multi-target modulation is combination therapy, in which different therapeutic agents that act independently on various components of the disease network are applied simultaneously to treat complex diseases like AD. The current standard treatment of Alzheimer's disease is the combination of an acetylcholinesterase inhibitor and the only NMDA receptor antagonist marketed memantine[252]. Though powerful, the combination therapy-based approach displays noteworthy disadvantages, including increased drug toxicity, treatment costs, drug-drug interactions as well as to patients' compliance. Another strategy is represented by the incorporation of different drugs into the same formulation; this simplifies dosing regiments and improves patient compliance with respect to combination therapies. In this sense, an example is Namzaric©, approved for the treatment of moderate to severe dementia of the Alzheimer's type in December 2014, that combines memantine and donepezil in a once-daily fixed-dose combination therapy[253] (Figure 27). However, this strategy does not allow to overcome the intrinsic conflict of drug combination, where positive outcomes deriving from combating the disease on multiple fronts coexist with drug-drug interaction concerns as two sides of the same coin[211]. All of this information enlighten it is appropriate and relevant to search for novel bioactive compounds able to combine in one molecule multi-target properties, since they may offer the interesting prospect of tackling intricate network effects with the benefits of a single-molecule therapy.
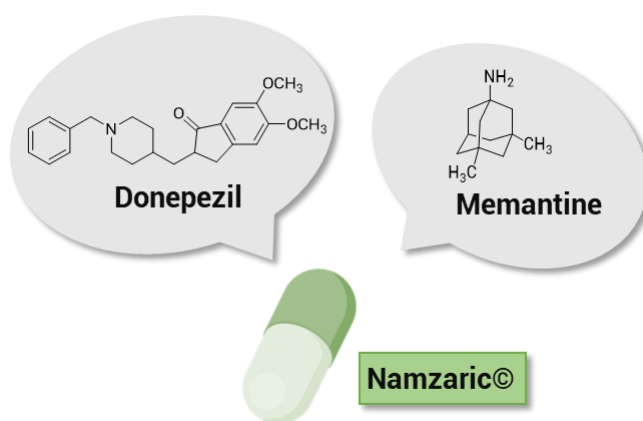
FIGURE 27| Schematic of Namzaric© and its active ingredients.

The greatest challenge to discover efficient multi-target leads for the treatment of complex diseases is to identify the best combination of biological targets. Thus, the key point is to find which and how many biological targets show the best results. Unfortunately, until now, all the efforts in this area have met with failure, confirming the challenge which is to face AD. Most efforts on the multi-target

strategy for AD treatment are focused on the development of compounds that have ChE inhibitor activity (tacrine and donepezil-related derivatives) plus one or more properties of: anti Aβ aggregation, -secretase inhibition, MAO inhibition, neuroprotection, anti-oxidation, metal-chelation, anti-inflammation and tau hyperphosphorylation inhibition.

At present, the development of multitarget drugs for AD is mostly based on rational molecular hybridization in which two or more pharmacophores with particular properties are combined in a single molecule, achieving the goal of polypharmacology. In addition, screening of natural products for the discovery of multi-target lead compounds has also regained the spotlight.

The cholinergic hypothesis and approved drugs make AChEIs a high profile in AD field and lead multi-target strategy to involve AChE in the drug design for the potential AD treatment. Tacrine and donepezil are still subjected to various modifications by research groups, and are often used as positive controls in *in vitro* and *in vivo* tests. In this context, phenserine (**Figure 28**), which belongs to the second generation of ChE inhibitors, not only is a selective, non-competitive AChE inhibitor, but it also reduces APP production *in vitro* and *in vivo*[254]. Moreover, it has a lower toxicity compared to tacrine and physostigmine[255]. Phenserine was observed to be a promising anti-AD agent due to its dual effect towards Aβ and AChE. It was clinically tested, but has shown only moderate success in initial phase II clinical trials. Subsequently, it proved to be uneffective in two curtailed phase III clinical trials[256] and failed also in phase III development. In 2016 it was demonstrated that phenserine exhibits non-cholinergic effects with clinical potential[257]. Therefore, investigations of its mechanism of action are currently under development[258]. Posiphen, one of the two follow-on compounds of phenserine, is currently evaluated in phase I/II clinical trial (ClinicalTrials.gov Identifier: NCT02925650 and NCT04524351).
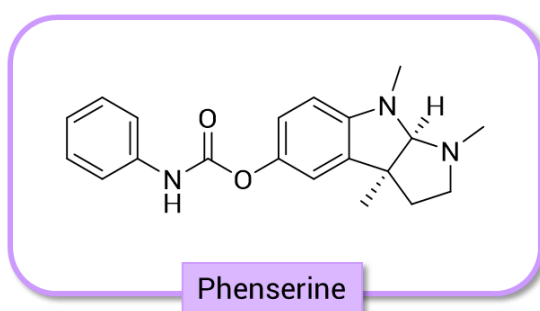

FIGURE 28| Structure of phenserine.

One example based on rational molecular hybridization is the AChE and NMDA receptor multi-target strategy that can affect both cholinergic and glutamatergic systems. The aim of this rational design was the obtainment of a single molecule endowed with anticholinesterase efficacy and NMDA receptor antagonism by integrating synergistic fragments into a single chemical identity[259]. The first

rationally designed hybrid carbacrine (**Figure 29**), formed by linking the AChEI tacrine with the carbazole moiety of carvediol, showed dual inhibitory activity against AChE and NMDA receptor (IC_{50} = 2.15 nM for AChE, IC_{50} = 0.74 mM for NR1/NR2A), 36.0% self-induced Aβ aggregation inhibition, 57.7% AChE-induced Aβ aggregation inhibition, and the ability to reduce oxidative stress[158].
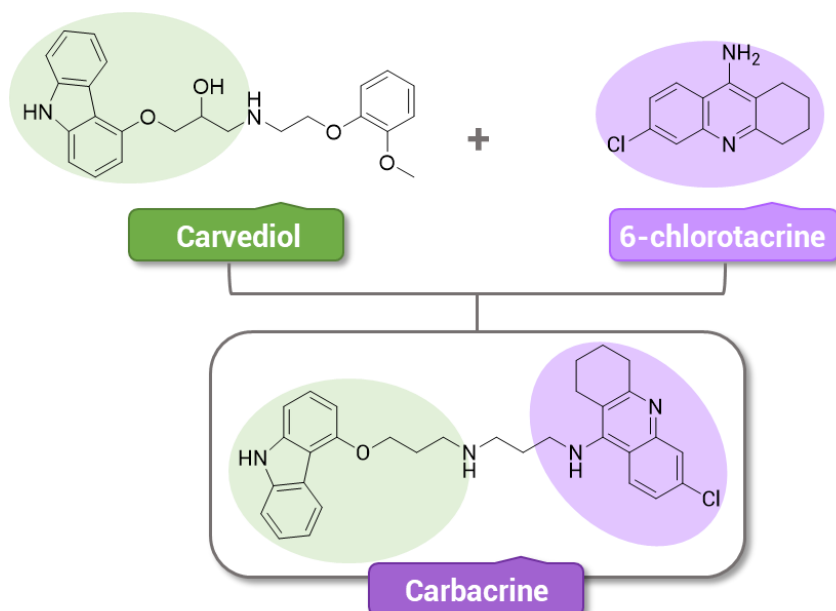

FIGURE 29| Design strategy for carbacrine.

Memagal (**Figure 30**) is a hybrid made by the structures of galantamine and memantine linked with a hexamethylene spacer. Memagal showed remarkably inhibitory potency against AChE (IC_{50} =1.16 nM), and NMDA receptor.
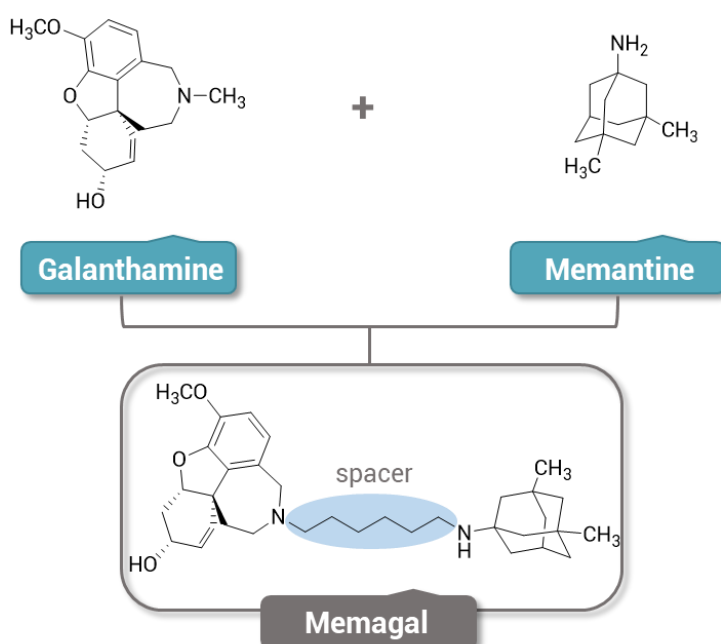
FIGURE 30| Design strategy for memagal.

In the framework of simultaneous AChE and NMDA receptor inhibition, it is worth mentioning the antihistamine drug dimebon. Dimebon is in a discontinued phase III clinical trial for AD treatment. Its mechanism of action for cognitive benefit has never been conclusively established; however, a broad spectrum of effects on neurologically relevant targets was proposed based on various *in vitro* and *in vivo* studies[260]. Particularly, dimebon has been variously reported to modulate the activity of channels and neurotransmitter systems, including L-type and voltage-gated calcium channels, AMPA and NMDA glutamate receptors, α-adrenergic receptors, and serotonergic or dopaminergic receptors. Based on computational studies, the γ-carboline moiety of dimebon was identified as the key fragment to explore in the search of an amplified drug activity profile. Therefore, a bivalent ligand approach led to dimebon congeners (**Figure 31**), which showed other satisfactory *in vitro* biological activities, including a remarkable increase of inhibitory potency against AChE combined with a greatly improved affinity towards NMDA receptor[261].
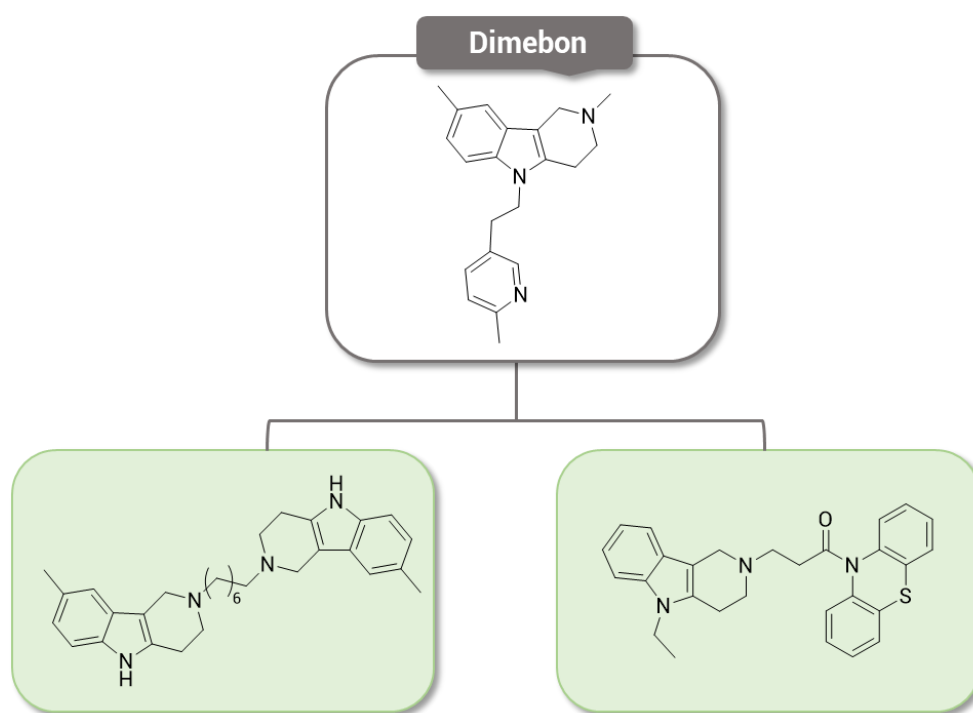
FIGURE 31| Design strategy for dimebon congeners.

Considering the structural analogy existing between RS67333 and donepezil, the pharmacophoric features of these two molecules were merged into a single chemical entity leading to the obtainment of donecopride (**Figure 32**)[262]. RS67333 is a partial 5-hydroxytryptamine 4 receptor (5-HT$_4$R) agonist which is well known for its procognitive effect. In addition to activate 5-HT$_4$R, it lowers Aβ levels by

directly inhibiting the activity of AChE with submicromolar activity (IC_{50} =1.16 nM)[263]. The rational of employing a 5-HT$_4$R agonist is that the serotonergic neurotransmitter system possesses a strong implication in cognitive function[264]. 5-HT$_4$R receptors, in particular, have been largely described to be involved in memory processes and thus they acquired interest in the development of new AD therapeutics. Interestingly, brain functions mediated by 5-HT$_4$R seem to require interaction with cholinergic neurotransmission[265]. Moreover, some authors hypothesize the up regulation of 5-HT$_4$R may contrast Aβ accumulation through the stimulation of the non-amyloidogenic APP processing[266]. Donecopride improves cholinergic transmission both through the inhibition of AChE and the 5-HT$_4$R-dependent release of ACh. In addition, it was observed that donecopride is able to interact with the PAS of AChE, thus acting as a dual binding site inhibitor able to limit Aβ accumulation. Finally, donecopride proved to be a druggable lead component, as it presents good bioavailability and features a nontoxic profile[267].
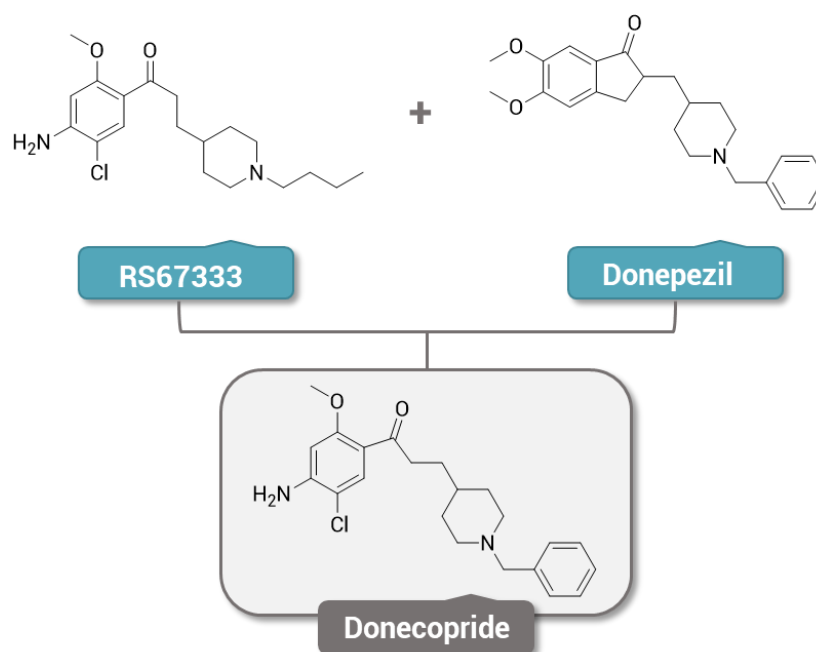
FIGURE 32| Design strategy for donecopride.

Since increasing attention has been paid to the therapeutic potential of MAO inhibitors in AD treatment, to meet the goal of MTDLs, AChE and MAO inhibitors structures were combined to produce hybrids endowed with multi-efficacy. Thus, ladostigil was obtained by combining the carbamate moiety of the ChEs inhibitor rivastigmine with the indolamine moiety of the MAO-B inhibitor rasagiline (**Figure 33**). This drug shows potent neuroprotective inhibitory activities against cholinesterase (both AChE and BChE) and MAO (both MAO-A and MAO-B)[268]. A

phase II clinical trials (ClinicalTrials.gov Identifier: NCT01354691) for the treatment of mild cognitive impairment (MCI) and Alzheimer's type dementia showed that low-dose ladostigil did not significantly affect progression from MCI to dementia, the treatment group had less brain shrinkage than the placebo group and, overall, ladostigil seemed well-tolerated[269].

On the track of these promising results, the multifunctional ligand ASS324 was designed and developed combining the 1-benzylpiperidine fragment of donepezil with a MAO-inhibiting indolyl propargylamine moiety. In addition to a potent MAO inhibitory effect, ASS234 also displays a dual binding site inhibition of AChE and thus the modulation of AChE-dependent Aβ aggregation[270].
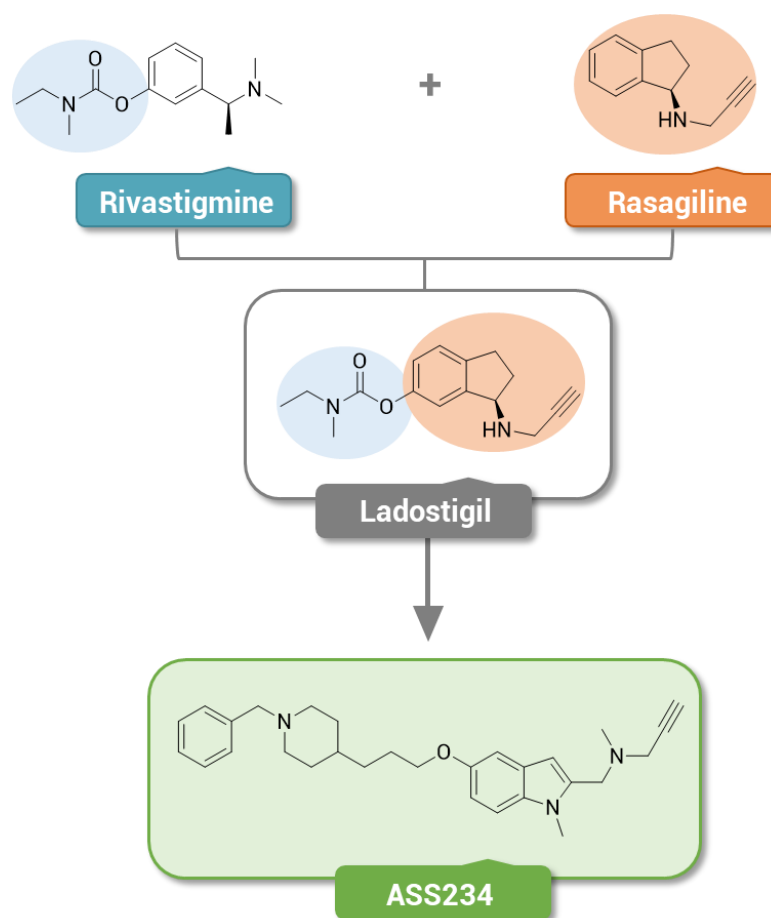
FIGURE 33| Design strategy for ladostigil and ASS234.

4.3.1 Quinone-based derivatives

Within the variety of molecules serving as scaffold for the design of multi-target directed ligands, a moiety that emerges for its anti-AD potential is the quinone one. Quinones are interesting chemical structures whose main features include a non-aromatic ring and two carbonyl functions at the 1,4 or the 1,2 positions to one another. The three most common quinone-based derivatives are benzoquinones, naphthoquinones (NQs) and anthraquinones (AQs) (**Figure 34**).
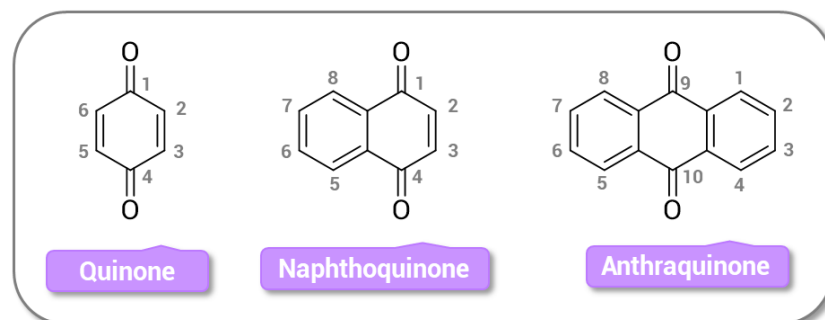
FIGURE 34| Structures of 1,4-quinone and related benzoquinones.

NQs are colored chemical compounds that in nature exist as secondary metabolites of plants and are used in many traditional medicines in Asian countries. They have gained considerable interest from researchers due to their antibacterial, antifungal, antitumor, and insecticidal properties[271–273]. Therefore, NQ can be considered a privileged structure since its derivatives have demonstrated the ability to interact with several and different biological/pharmacological targets exhibiting a wide range of activities. However, few studies investigated the effect of 1,4-NQs on neurodegenerative diseases. Only recently, natural and synthetic NQ derivatives have started to be explored as potential agents for the treatment of AD[274] (**Figure 35**).
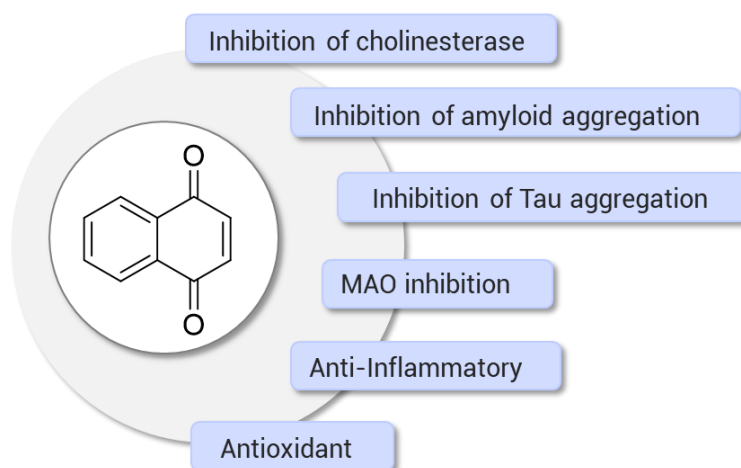

FIGURE 35| Biological profiles of 1,4-NQs in the treatment of Alzheimer's disease.

Naphthoquinones from natural sources are subject of a large number of studies. Plumbagin (**Figure 36**) presents potent biological activities, including antioxidant and anti-inflammatory, by selective inhibition of COX-2[275,276], which suggest the activation of adaptive cellular stress response pathways as plausible neuroprotective effects[277]. Moreover, plumbagin displays an anti-Alzheimer's effect associated with activation of Nrf2/ARE signaling with consequential suppression of astrogliosis and inhibition of BACE1.

Another interesting natural naphthoquinone is juglone, a phenolic compound produced by numerous species of walnut tree. Juglone (**Figure 36**) has antioxidant properties that make it useful in combating oxidative stress-linked disease as AD. Particularly, deprotonated juglone has demonstrated the ability to chelate Fe^{2+} [278] leading to the formation of stable complexes, thereby preventing this metal from participating in free radical generation[279]. In addition, juglone is an inhibitor of Pin1, a member of peptidyl-prolyl cis/trans isomerases[280], that can regulate protein phosphorylation and cell signaling and its activity has been connected to AD through the modulation of phosphorylation of Tau protein[281]. Finally, juglone has also been studied for its ability to inhibit both BACE1 (IC_{50}= 6.51 µM) and the aggregation of β-amyloid (IC_{50}= 11.10 µM) and for its ability to disaggregate preformed amyloid fibrils (IC_{50}= 15.49 µM)[282].
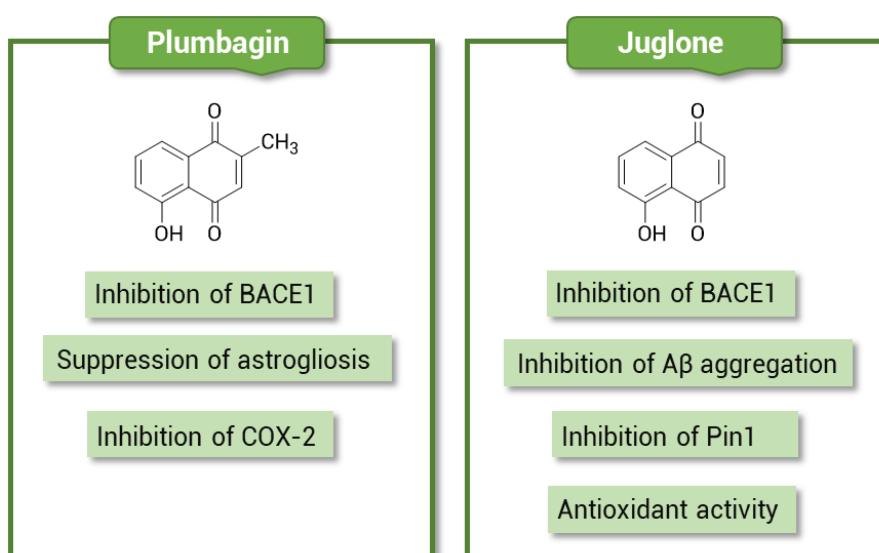

FIGURE 36| Representative NQs from natural sources as lead compounds for the development of new MTDLs.

Among the anthraquinone derivatives which have been and are currently being studied as potential anti-AD agents, most of them derive from natural sources. To date, more than 700 natural anthraquinones, derived from 9,10-anthracenedione

nucleus, have been isolate from plants, lichens and fungi. In the field of drug discovery, the AQ moiety is an important scaffold associated with a wide range of pharmacological properties, such as anti-inflammatory, anti-cancer, diuretic, laxative, antidepressant, antioxidant and anti-parasitic[283]. Different AQ-based molecules have recently shown to be capable of hit different molecular targets involved in AD[274]. In particular, AQs act as cholinesterase inhibitors[284], reduce the formation of protein aggregates, and act as antioxidants, thus impairing the increased ROS formation associated with the AD progression. Within the natural AQs, emodin[285–287], alaternin[285] and helmintosporin[284] proved to be promising chemotypes for the development of anti-AD drugs (**Figure 37**).

Emodin

ChE inhibition

IC_{50} (AChE) = 9.17 μM
IC_{50} (BChE) = 157 μM

BACE1 inhibition

IC_{50} (BACE1) = 4.48 μg/mL

Inhibition of tau polymerization

IC_{50} (PHF ass) = 1.26 μM
IC_{50} (PHF diass) = 2.8 μM

Alaternin

ChE inhibition

IC_{50} (AChE) = 6.3 μM
IC_{50} (BChE) = 113 μM

BACE1 inhibition

IC_{50} (BACE1) = 0.94 μg/mL

Helmintosporin

ChE inhibition

IC_{50} (AChE) = 2.63 μM
IC_{50} (BChE) = = 2.99 μM
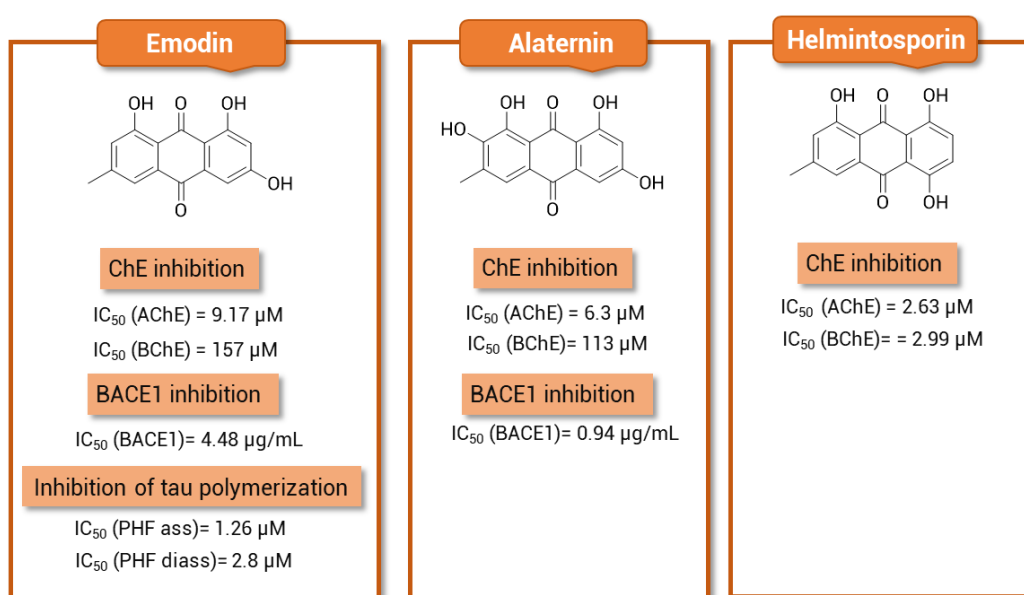
FIGURE 37| Representative AQs from natural sources as lead compounds for the development of new MTDLs.

Alongside the discovery of the several potential applications of natural NQ and AQ derivatives for AD treatment, synthetic analogues have also been developed with the aim to target diverse factors implicated in AD pathology[274]. The greatest results have been obtained by following a conjugation approach that allowed the yield of hybrid molecules composed of naphtho- or anthraquinone scaffold in combination with other structures, such as tryptophan[288,289], tacrine[290–292] and huprine[293,294], tethered through a linker of variable length and nature, in order to integrate their anti-AD properties.

# Discussion

5. BACKGROUND

The research group where I developed my PhD work, for some years has been dealing with the study of dual AChE and BChE inhibitors, as well as the design of multitarget ligands capable of inhibiting both cholinesterases and Aβ aggregation. This thesis represents the continuation of a previous work about a library of thioxanthen-9-one, xanthen-9-one, naphthoquinone (**I-VIII**) and anthraquinone derivatives (**IX-XIV**) decorated with a basic side chain (especially quinolizidinyl-alkyl chains), which displayed a multitarget behavior by inhibiting both AChE and BChE, and the spontaneous aggregation of β-amyloid with similar potencies[295] (**Figure 38**). The naphthoquinones demonstrated to be AChE-preferring inhibitors (IC$_{50}$= 0.011−5.8 μM) with respect to BChE, while the anthraquinones were equipotent towards both enzymes in the low micromolar range. Moreover, the tricyclic anthraquinone system resulted to be more suited to promote the inhibition of Aβ aggregation (mean IC$_{50}$ ~ 8 μM) than smaller naphthoquinones, which generally provided molecules endowed with less efficacy.
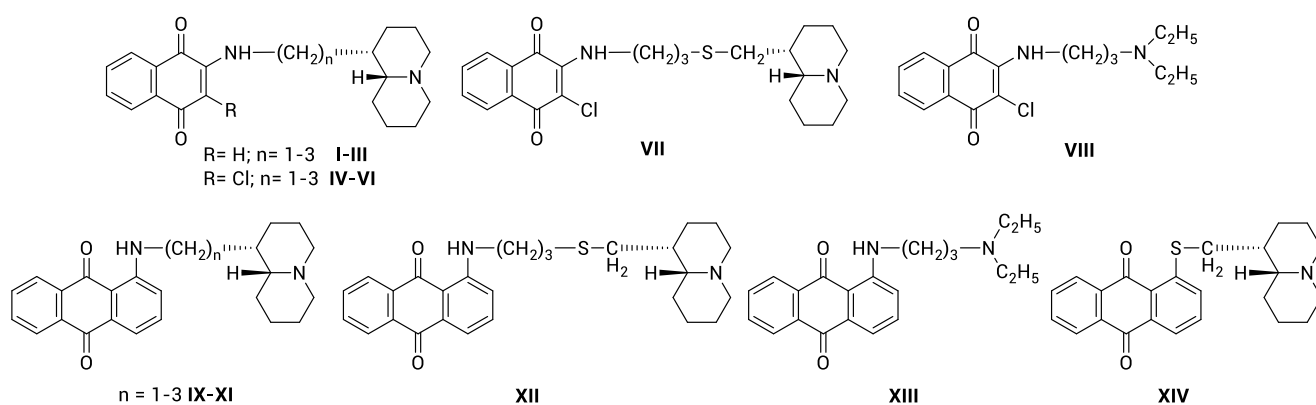
Target	NQs range IC$_{50}$ (μM)	AQs range IC$_{50}$ (μM)
AChE	0.011(**VI**) - 5.8 (**I**)	0.84 (**IX, X**) - 3.8 (**XIV**)
BChE	4.1 (**VII**) − 12 (**VI**)	1.1 (**XII**) - 3.4 (**XIV**)
Aβ$_{40}$	61 (**VII**)	6.4 (**IX**) − 61 (**XIII**)

FIGURE 38| Previous series of naphthoquinone and anthraquinone derivatives, bearing a dialkylaminoalkyl or a quinolizidinylalkyl chain as multitarget agents inhibiting cholinesterases and Aβ aggregation.

Since the above-mentioned compounds may represent interesting leads for the development of multi-target directed ligands of potential utility in the control of symptoms and/or progression of AD, the efforts of my PhD work have concerned the design and synthesis of novel libraries of naphthoquinone and anthraquinone derivatives connected through a polymethylene linker to unexplored functionalities such as a basic head or an aromatic or heteroaromatic ring (**Figure 39**).
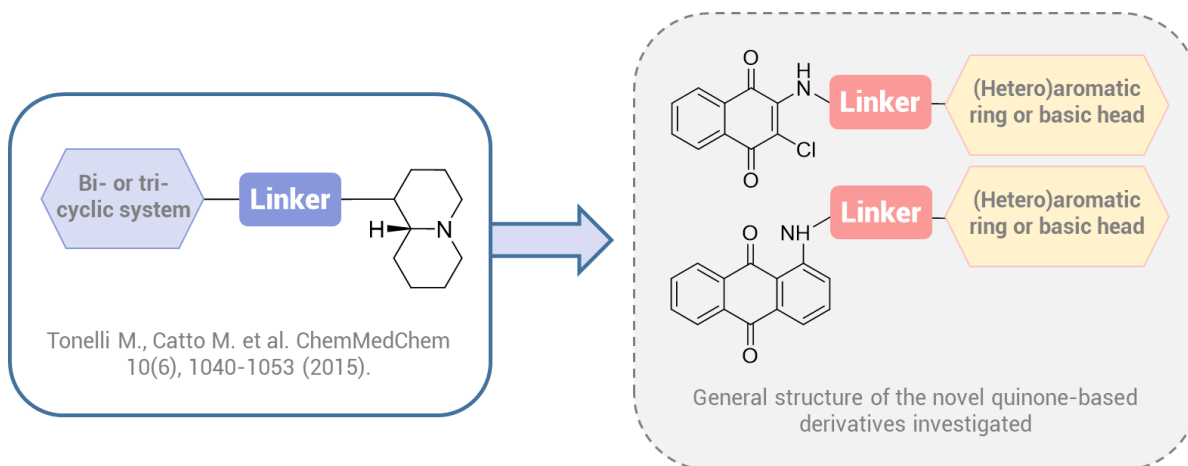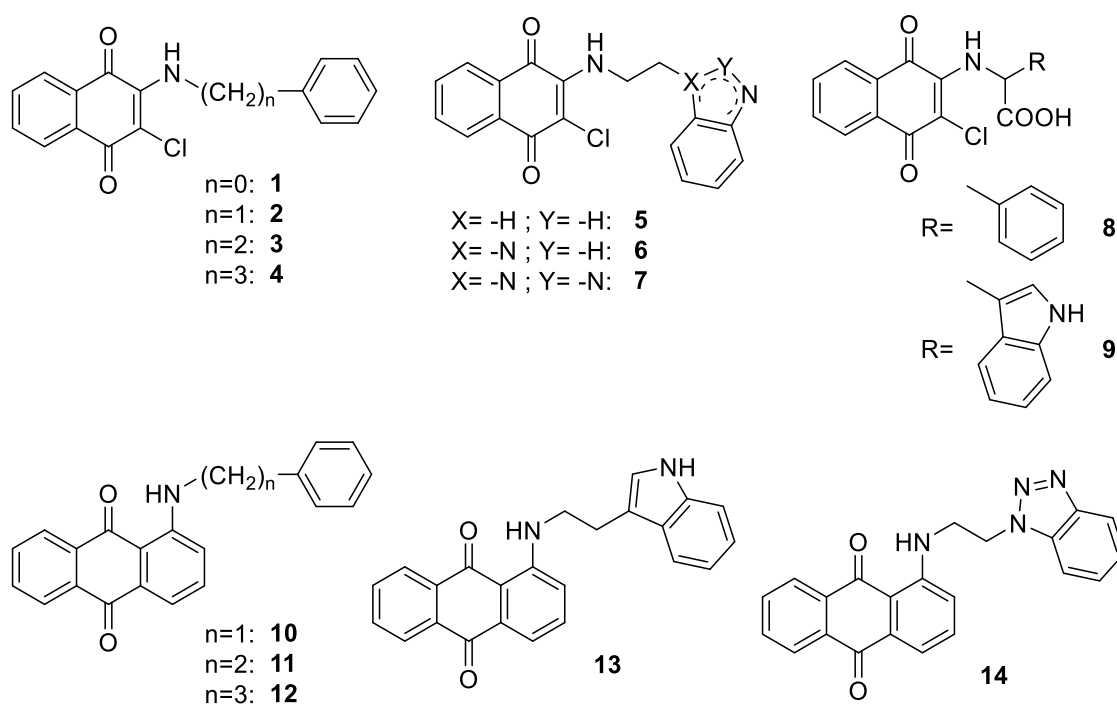

FIGURE 39| General structure of naphthoquinone and anthraquinone derivatives investigated in the present thesis.

6.   FIRST SET

6.1 Project

The first library probes the ability of an aromatic or heteroaromatic ring tethered to the quinone scaffolds through a polymethylene chain to exhibit a multitarget profile against key targets of AD[296] (**Figure 40**). These hydrophobic features have been selected with the aim to establish π-π stacking interactions with a sequence of aromatic amino acids (H14QKLVFF20) of Aβ, which plays an important role in the initial phases of molecular recognition and structural transition, leading to Aβ aggregation in soluble oligomers and fibrillary species[116].

FIGURE 40| Chemical structures of the first subgroup of naphthoquinone and anthraquinone investigated derivatives **1-14** as MTDLs for AD.

6.2 Chemistry

The novel naphthoquinones derivatives **1-4** were obtained by reacting the 2,3-dichloro-1,4-naphthoquinone, previously suspended in ethanol, with 2 equivalents of the proper amine (**Scheme 1**).
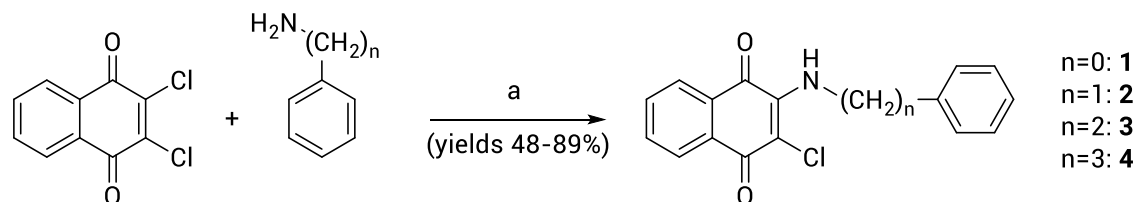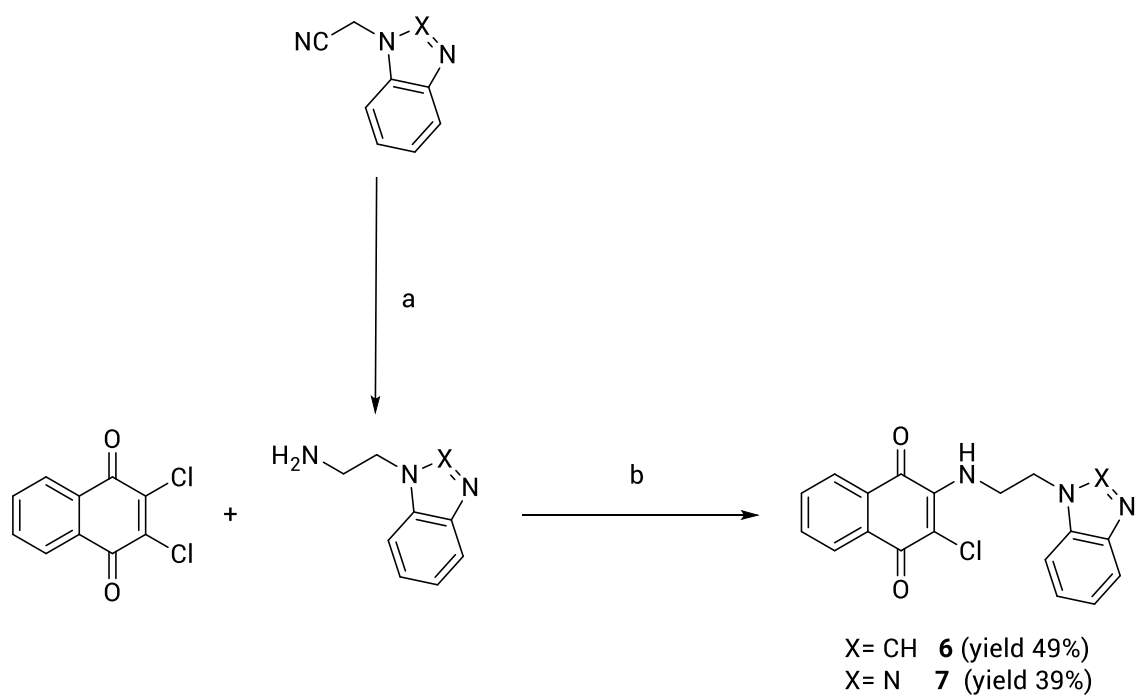

Scheme 1. Reagents and conditions: a) EtOH, Δ, 6 h.

To prepare derivatives **5-7**, it was first necessary to synthetize the appropriate intermediate (heteroaryl)ethylamines, by reducing with LiAlH$_4$ in anhydrous THF the 3-indolyl acetamide (**Scheme 2**) and the 1-benzimidazolyl and 1-benzotriazolyl acetonitriles, respectively (**Scheme 3**). The 1-(2-aminoethyl)-benzotriazole was also obtained with comparable yield from the acid catalyzed hydrolysis (HCl 6N) of the 2-[2-(1H-benzotriazol-1-yl)ethyl]phthalimide.

While 2-(3-indolyl)acetamide was commercially available, to synthesize 2-(benzimidazol-1-yl) and 2-(benzotriazol-1-yl) acetonitriles, benzimidazole and benzotriazole were condensed with 2-chloroacetonitrile in DMF in the presence of TEA according to the literature[297].
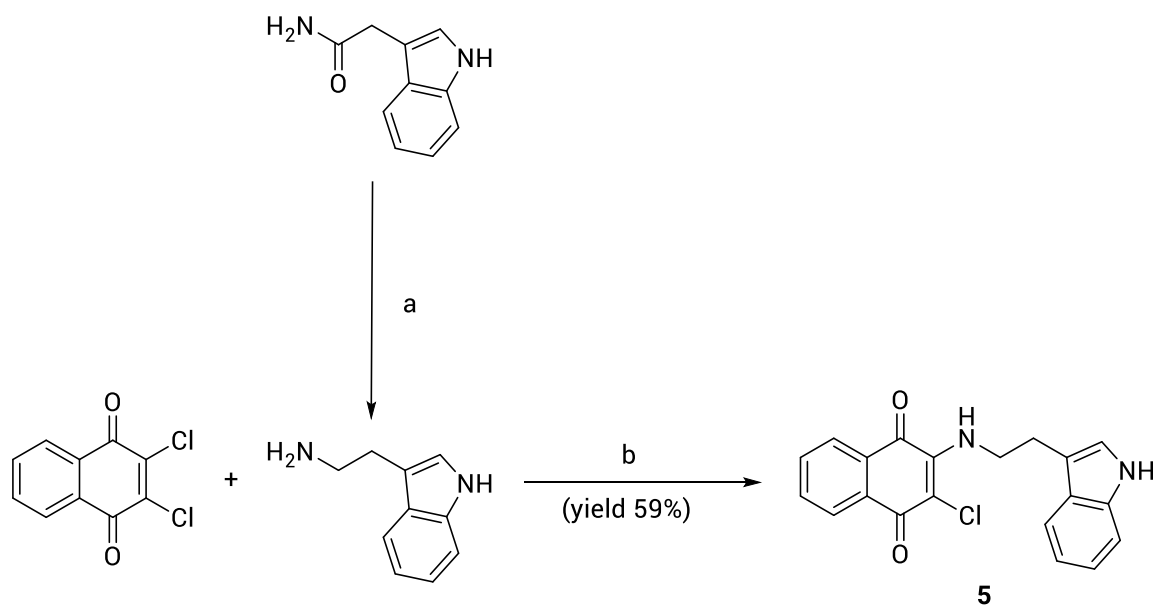

**Scheme 2.** Reagents and conditions: a) LiAlH$_4$ /anhydrous THF, 8 h; b) MeOH, r.t. 24 h.

Scheme 3. Reagents and conditions: a) LiAlH$_4$ /anhydrous THF, 10 h; b) MeOH, r.t. 24 h.

For the derivatives **8** and **9**, to a suspension of 2,3-dichloro-1,4-naphthoquinone in methanol, a solution of phenylalanine or tryptophan in NaOH 6N was added; the equimolar mixture was then stirred for 24 h at room temperature (**Scheme 4**).
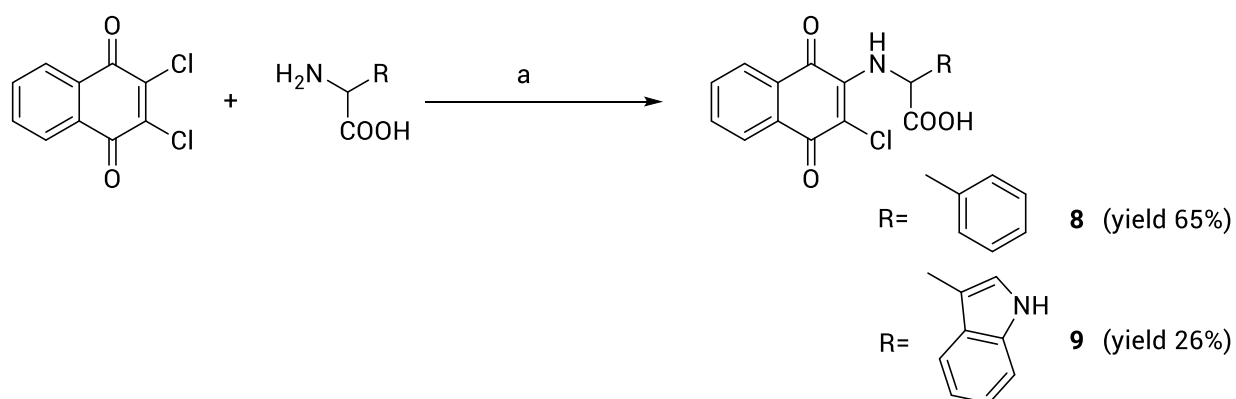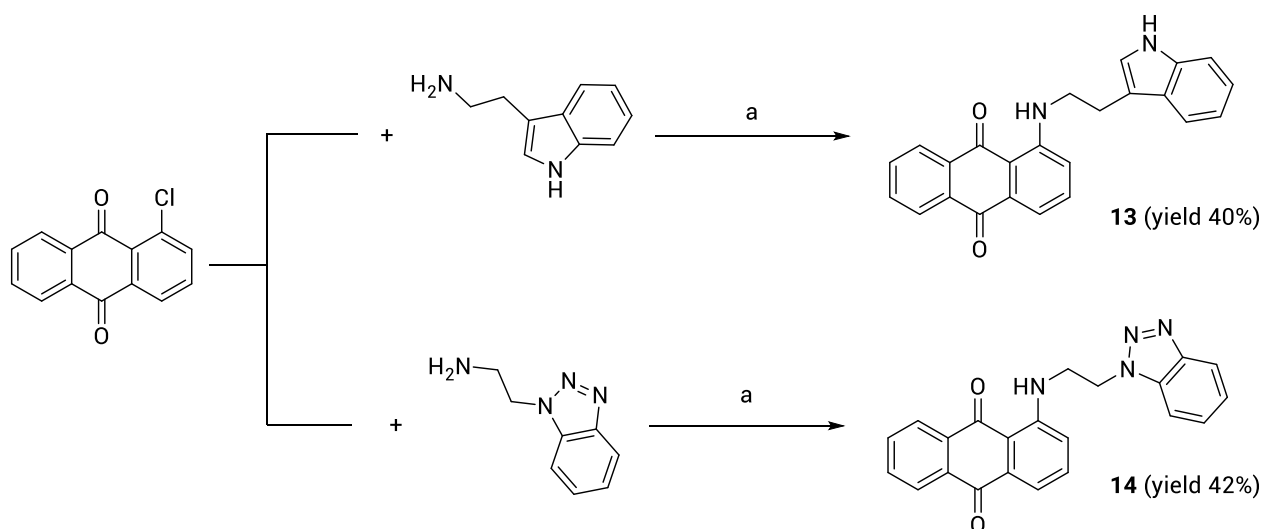

Scheme 4. Reagents and conditions: a) MeOH/NaOH 6N r.t. 24 h

The condensation at 160°C of a mixture of 1-chloroanthraquinone with the proper aryl/heteroaryl alkylamine afforded compounds **10-14** (**Schemes 5** and **6**).

n=1: **10** (yield 90%)
n=2: **11** (yield 71%)
n=3: **12** (yield 76%)
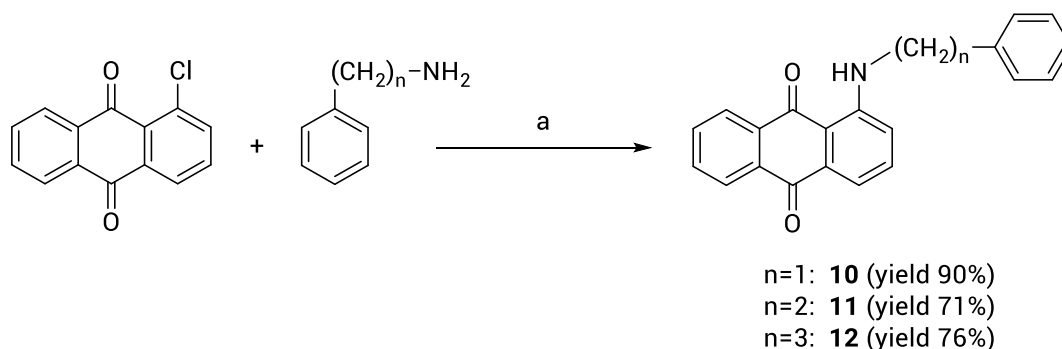
Scheme 5. Reagents and conditions: a) 160 °C, 7 h.

13 (yield 40%)

14 (yield 42%)

Scheme 6. Reagents and conditions: a) 160 °C, 8 h.

Several unsuccessful attempts to obtain the anthraquinone derivative of tryptophan were made, in sealed tube with DMF (or DMF and KI), rather than in BuOH at reflux and even applying microwaves-assisted synthesis.

Compounds **1**, **3**[298], **2**[299], **5**, **9**[300] and **8**[301] have been achieved according to the cited references; while for compound **10**[302] a different synthetic route with respect to the literature was applied, as above mentioned. The structures of compounds **1-14** have been confirmed using ^{1}H and ^{13}C NMR, and elemental analysis. The purity of compounds (checked by elemental analysis) has been in all cases >95%.
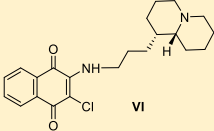
6.3 In vitro biological profiling

These quinone-based derivatives have been evaluated *in vitro* for their inhibitory activities against different targets with a view to explore their potential as single entity multitarget agents for the treatment of AD. The biological profiling of these derivatives included the *in vitro* evaluation of (i) self-induced Aβ and tau aggregation inhibition; (ii) the inhibitory activities against AChE and BChE; (iii) inhibition of MAO A and B isoforms, that have been all performed by Prof. Marco Catto – University of Bari. Moreover, to assess the ability of the best performing Aβ inhibitors (**2**, **5**, **11** and **12**) to inhibit Aβ$_{42}$ fibrillation, atomic force microscopy (AFM) was then employed, which revealed clear differences between Aβ$_{42}$ aggregate morphologies obtained in the presence or absence of the compounds. The same compounds have been assayed for their protective effect against Aβ$_{42}$-induced toxicity in primary cultures of cerebellar granule cells from postnatal rats (P7).

As fundamental prerequisite for AD therapy, drugs have to demonstrate the ability to enter the CNS. Accordingly, the propensity of these quinone-based compounds to cross the BBB by passive diffusion has been tested *in silico*, calculating their LogPS values[303] in comparison to the reference drugs donepezil, quercetin, safinamide and the quinolizidine-containing naphthoquinone **VI** (**Table 3**), whose BBB permeability profile was experimentally confirmed[295].

Table 3. *In silico* evaluation of quinone-based derivatives propensity to cross blood-brain barrier measured as LogPS analysis (ACD/Percepta platform 2015 v14.0.0, www.acdlabs.co).

The last two columns report the experimental permeability results from the PAMPA-BBB assay (P_e, 10^{-6} cm/s) and the corresponding predictive penetration in the CNS for compounds **2**, **5**, **8**, **11**, **12** and for donepezil and quercetin as positive (CNS+) and negative (CNS-) controls, respectively.

Cpd	LogPS[a]	P_e (10^{-6} cm/s)	CNS prediction[b]
1	-0.11		
2	-1.1	28.4 ± 2.1	CNS+
3	-1.1		
4	-1.1		
5	-1.2	14.3 ± 1.3	CNS+
6	-1.3		
7	-1.4		
8	-2.5	6.1 ± 0.4	CNS+
9	-2.8		
10	-1.1		
11	-1.1	24.7 ± 2.2	CNS+
12	-1.1	22.0 ± 1.9	CNS+
13	-1.1		
14	-1.2		
Donepezil	-1.3	23.2 ± 2.3	CNS+
Quercetin	-3.6	0.14 ± 0.06	CNS-
Safinamide	-2.0		
	-1.5		

[a]Rate of brain penetration, –3 (medium affinity) < LogPS < –1 (high affinity). PS represents Permeability-Surface area product and is derived from the kinetic equation of capillary transport. [b]CNS permeation prediction based on the PAMPA-BBB classification range from Di et al.[304]

The results listed in **Table 3**, predicted that all the compounds are able to permeate the BBB as the reference compounds, reaching pharmacologically relevant concentrations within the CNS. However, the capability of amino acids naphthoquinones **8** and **9** to penetrate the BBB was poor, as LogPS values fell close to the lower limit of the recommended ranges (-3 <LogPS< -1), even if they could presumably reach the CNS by carrier-mediated active transport. The *in vitro* permeability (P_e) of compounds **2**, **5**, **8**, **11** and **12** was also

determined using the PAMPA-BBB assays[304] (**Table 3**, 3rd column). Successful assay validation was performed by comparing the experimental permeability ($P_{e,exp}$) with the corresponding reported values ($P_{e,rep}$) for 20 commercial drugs ($P_{e,exp}$ = 0.9625 x $P_{e,rep}$ + 0.2836, R^2 = 0.9622, data not showed). Based on the P_e values obtained, all analyzed compounds should be endowed with good-to-high BBB passive permeability, with P_e values ranging from 6.1 to 28.4×10^{-6} cm/s (**Table 3**, last two columns).

6.3.1 Inhibition of self-induced Aβ aggregation and Cholinesterases.

The newly synthesized compounds **1-14** have been tested for the direct inhibition of $Aβ_{40}$ aggregation and for the inhibition of electric eel acetylcholinesterase (eeAChE) and equine serum butyrylcholinesterase (esBChE).

In vitro inhibition of $Aβ_{40}$ aggregation was assessed following a previously reported thioflavin T (ThT) fluorescence-based method which involves the use of hexafluoroisopropanol (HFIP) as aggregation enhancer. HFIP is a low-polar solvent that can stabilize the α-helix of Aβ and disrupt the interstrand hydrogen bonds of the β-sheet. For the most active compounds (≥ 80% Aβ aggregation inhibition) IC_{50} values were determined under the same assay conditions as previously described[305]. Inhibitory activities on eeAChE and esBChE were determined by the spectrophotometric method of Ellman[306] and are reported in **Table 4** as IC_{50} (μM) for the most active compounds, or as percentage of inhibition at 10 μM for the low active (i.e., <50%) compounds.

At 100 μM concentration, compounds **1-14** were proved to inhibit Aβ aggregation, with IC_{50} values in the range of 1.9-19 μM. Among them, eight (**2-9**) and three (**11**, **12** and **14**) were naphthoquinone and anthraquinone derivatives, respectively. Compounds **1**, **10** and **13** exhibited an Aβ inhibition rate of about 60% at a concentration of 100 μM instead.

Interestingly, the size of the aromatic bi- and tricyclic system seems to influence the biological effect, as the most potent compounds, **12** and **11**, sharing IC_{50} values equal to 1.9 and 2.1 μM, respectively, belongs to the anthraquinone series. As mentioned, previous studies demonstrated the capability of (hetero)aromatic tricyclic systems to establish strong hydrophobic and electrostatic interactions with the amino acid sequence H14QKLVFF20 of Aβ, which is prone to aggregating[307].

The length of the spacer between the quinone scaffolds and the (hetero)aromatic rings also proved to influence the biological activity with a

different trend in the two series. If one methylene unit was found the optimal distance for naphthoquinone-based derivatives (compare aryl derivatives **2-4**), for anthraquinones the increase of the carbon units from 1 to 3 (compare derivatives **10-12**) resulted in a proportional increase of the inhibition potency against Aβ aggregation. The effect of linker length on biological activity was already explored on the basis of previous experience gained, from studies of dual homo- and hetero-dimeric inhibitors of AChE binding sites, performed by both my Research Group and other authors[308−312].

Regarding the naphthoquinones linked to a heterocyclic system, the activities of the indole (**5**, IC_{50}= 6.6 μM) and benzotriazole (**7**, IC_{50}= 8.7 μM) derivatives were comparable and about 2-fold higher than that of benzimidazole derivative **6**. As a consequence, the presence of a hydrogen bond donor group, such as the NH group of indole ring, rather than a hydrogen bond acceptor feature as experienced by the N(2) atom of the benzotriazole ring were both permitted, allowing the yield of the same degree of activity. *In silico* studies previously highlighted the marginal role of NH indole in the tryptophan derivative **9**, since its N-methylation did not affect the binding affinity to amyloid oligomers, while its NH group on naphthoquinone C(2) and its CO group of carboxylic function were reported as essential features for the inhibition of Aβ aggregation[313]. However, these experimental results pointed out that compound **5**, lacking in the COOH function, was 2-fold more effective than the amino acid analogue **9** such as Aβ aggregation inhibitor. Analogues **3** and **8** showed the same potencies trend, whereas the presence of the polar carboxylic group in the phenylalanine derivative **8** negatively impaired the activity.

These results corroborate the suitability of naphthoquinone and anthraquinone scaffolds in providing Aβ peptide inhibition, even more when properly substituted with hydrophobic moieties able to target the aromatic interactions occurring in amyloid self-assembly process. Such behaviour was then confirmed by AFM studies, as showed below.

Table 4. Inhibitory activities (µM) of the investigated compounds **1-14** against Aβ aggregation and ChEs.

Cpd	IC_{50} (µM) or (% inhibition)[b]		
	Aβ$_{40}$ aggr.	eeAChE	esBChE
1	(63 ± 3)[c]	(39 ± 1)	(8 ± 3)
2	3.2 ± 0.8	9.2 ± 0.6	(26 ± 3)
3	4.4 ± 0.3	7.9 ± 0.8	(24 ± 1)
4	8.2 ± 0.3	3.5 ± 0.3	(35 ± 3)
5	6.6 ± 0.1	8.7 ± 0.8	(29 ± 4)
6	19 ± 4	6.8 ± 0.7	(24 ± 4)
7	8.7 ± 0.4	1.7 ± 0.1	(15 ± 3)
8	17 ± 2	13 ± 2	(14 ± 3)
9	14 ± 2	11 ± 1	(17 ± 1)
10	(62 ± 2)[c]	8.7 ± 0.5	(24 ± 3)
11	2.1 ± 0.2	7.3 ± 0.7	1.7 ± 0.3
12	1.9 ± 0.3	7.84 ± 0.03	8.2 ± 0.4
13	(57 ± 5)[c]	1.85 ± 0.04	(17 ± 1)
14	11 ± 2	8.1 ± 0.5	3.4 ± 0.2
Quercetin	0.82 ± 0.07	-	-
Donepezil	-	0.021 ± 0.002	2.3 ± 0.1

[a]Data are the means ± SEM of n=3 experiments; SEM <10%; [b]Data in parenthesis correspond to % of inhibition at 10 µM, or 100 µM[c]

Apart from the phenylamino naphthoquinone **1**, all the compounds **2-14** have been also proven to inhibit AChE reaching a low micromolar potency range. On the contrary, BChE has been found less sensitive to these series of compounds. The only exceptions are represented by the anthraquinone derivatives **11**, **12** and **14** whose IC_{50} ranged from 1.7 to 8.2 µM.

The most potent and selective AChE inhibitor were the benzotriazole-based naphthoquinone **7** (IC_{50} = 1.7 µM) and the indole-based anthraquinone **13** (IC_{50}= 1.85 µM). Two anthraquinone derivatives, **11** and **12**, behaved as dual cholinesterase inhibitors; compound **11** exhibited a comparable potency profile towards the two enzymes, whilst **12** resulted 2.5-fold more selective for BChE. Overall, the substitution pattern explored in the present series of quinone-based derivatives, from one hand positively ameliorated the inhibitory potency against Aβ aggregation, but from the other was responsible for a reduced efficacy against cholinesterases, especially BChE, in comparison to the previous series explored (**Figure 28**) which showed to be more potent dual inhibitors of both enzymes[295].

6.3.2 Inhibition of hMAOs

MAO inhibition was performed with a routine spectrophotometric assay, monitoring the fluorescence of 4-hydroxyquinoline produced in the MAO-catalyzed oxidation of kynuramine[314]. With few exceptions, all the compounds acted as selective MAO B inhibitors (**Table 5**), thus corroborating their potential as multitarget anti-AD agents, with IC_{50} values in the submicromolar range.

Table 5. Inhibitory activities (µM) of the investigated compounds **1-14** against MAO A and MAO B.

| Cpd	IC_{50} (µM) or (% inhibition)[b]	
	hMAO A	hMAO B
1	(<5)	(22 ± 4)
2	3.6 ± 0.3	0.0077 ± 0.0013
3	(41 ± 3)	0.031 ± 0.001
4	3.0 ± 0.2	0.054 ± 0.001
5	5.0 ± 0.2	0.11 ± 0.01
6	(23 ± 4)	(24 ± 6)
7	(21 ± 6)	0.48 ± 0.08
8	(26 ± 6)	2.7 ± 0.8
9	(22 ± 2)	(52 ± 3)
10	1.1 ± 0.3	(34 ± 3)
11	3.1 ± 0.3	0.57 ± 0.02
12	(50 ± 3)	0.24 ± 0.05
13	(25 ± 5)	(42 ± 1)
14	(53 ± 3)	0.98 ± 0.14
Safinamide	(18 ± 3)	0.031 ± 0.001

[a]Data are the means ± SEM of n=3 experiments; SEM <10%; [b]Data in parenthesis correspond to % of inhibition at 10 µM.

Noteworthy, the N-arylalkyl substituted naphthoquinones **2-4** displayed high potency with IC_{50} values laying in the nanomolar range. Benzylamine derivative **2**, with an IC_{50} = 7.7 nM, resulted in a potency higher than reference drug safinamide, whilst **11** and **12**, homologues of **3** and **4**, were the most potent MAO B inhibitors within the anthraquinone series. Compared with phenethyl derivative **3**, the substitution of phenyl with indole of compound **5** retained good potency, while the introduction of different heteroaromatic systems was somehow detrimental.

The very high potency of naphthoquinone **2** deserved further biochemical investigation, in order to clarify its inhibition mechanism. Firstly, it was confirmed that MAO B inhibition was not the consequence of a pan-assay interference of **2** in the fluorimetric assay[315], by performing the same

kynuramine-based assay in spectrophotometric mode, following the increase of absorbance of 4-hydroxyquinoline at 316 nm[316]. In agreement with that reported in **Table 5**, an IC_{50} equal to 18 nM was obtained. Then, in regard to the inhibition mechanism, it was detected a competitive inhibition (inhibition constant K_i = 22 nM) when the coincubation with enzyme was limited to 5 min (**Figure 41**).
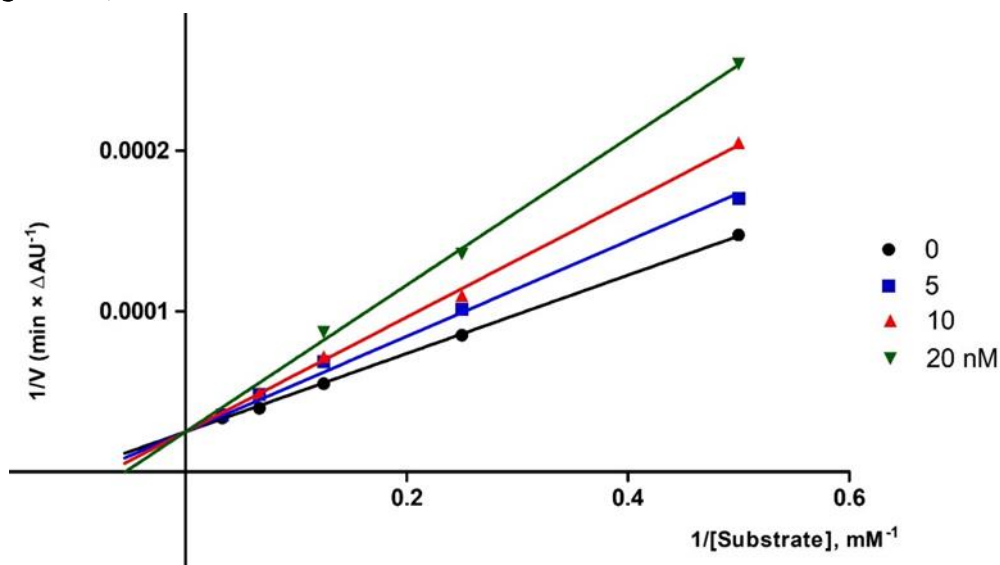
FIGURE 41| Lineweaver-Burk plot of inhibition kinetics of MAO B by compound **2** (0 to 20 nM), in the presence of five concentrations of substrate kynuramine (2 to 30 µM).

For higher coincubation times (up to 2 h) the mechanism apparently turned to noncompetitive, with the K_i increasing of about 20-fold. This change could be ascribed to the formation of a covalent complex with the N5 of flavin[317], due to the presence of the chlorine leaving group. Indeed, a time course of absorption of 4-hydroxyquinoline at 316 nm revealed that the enzymatic activity was still present even after 3 hours in the presence of 10 nM **2** (**Figure 42**). This activity profile was quite comparable to that of 10 nM safinamide, the reference drug used for reversible and selective MAO B inhibition, when the assay was performed without preincubation with the enzyme (**Figure 42**, left). With a preincubation of 1 h, the time course of MAO B activity was still comparable for **2** and safinamide, although **2** suffered a strong decrease of potency (**Figure 42**, right). When incubated with 100 nM pargyline, a known irreversible MAO B inhibitor, the MAO B kinetic profiles were clearly different, since the enzymatic activity in the presence of pargyline came to saturation in about 1 h (**Figure 42**, left) and was completely inhibited with the preincubation (**Figure 42**, right). Probably, the time-dependent change in potency of compound **2** may be due to its inactivation, either from chemical decomposition or from covalent reaction with nucleophilic residues of the enzyme, rather than to the formation of a

95

covalent adduct with the flavin of catalytic site of the enzyme[318], and by consequence, that the inhibition of **2** may be considered as reversible.
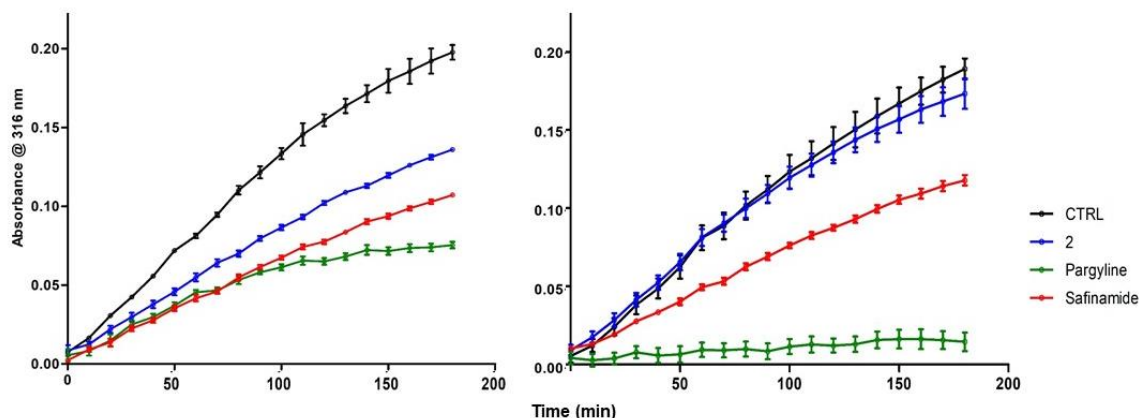
FIGURE 42| Time course of inhibition of MAO B by **2** (10 nM, blue line), safinamide (10 nM, red line), and pargyline (100 nM, green line). Left, no preincubation; right, 1 h preincubation with enzyme. Data points represent the absorbance of 4-hydroxyquinoline at 316 nm (n = 3; mean ± SD).

The results listed in **Table 5** so far highlighted the naphthoquinone **2** as the molecule endowed with the most effective inhibitory activity against MAO B (IC$_{50}$= 7.7 nM) and AChE (IC$_{50}$= 9.2 μM).

6.3.3 Molecular modeling studies

In order to investigate the molecular determinants for the potency and selectivity of **2** towards MAO B and AChE, molecular modeling studies were next performed by Prof. Sabrina Pricl Laboratory – University of Trieste. Accordingly, the putative binding sites and modes for **2** were first identified on both human enzymes (**Figure 43**) and then molecular dynamics (MD) simulations of the resulting inhibitor/protein complexes were carried out to evaluate the corresponding free energy of binding (ΔG_{bind}). The simulation results clearly show that **2** has a substantially higher affinity for MAO B (ΔG_{bind} = -10.98 ± 0.16 kcal/mol) than for AChE (ΔG_{bind} = -7.93 ± 0.13 kcal/mol), in agreement with the relevant experimental findings. The inspection of the relevant MD trajectories reveals that, when in complex with MAO B (**Figure 43A**), the two carbonyl groups of **2** are engaged in two stable hydrogen bonds (HBs) with the monoamine oxidase side chains of Y326 (3.21 ± 0.13 Å) and Y435 (2.87 ± 0.11 Å), respectively. Moreover, one of the -C=O groups of **2** is also permanently H-bonded with the -NH$_2$ moiety of MAO B Q206 (3.23 ± 0.13 Å), whilst the chlorine atom of **2** interacts via a halogen bond (HaB) with the SH group of MAO B C172 at an optimal distance of 2.95 ± 0.11 Å

96

(Figure 43A). In addition, the **2**/MAO B complex is further stabilized through an extended network of close Van der Waals/hydrophobic contact interactions (CIs) between the ligand and the side chains of MAO B residues F103, P104, W119, L164, L167, L171, I198, I199, K296, F343, and Y398.
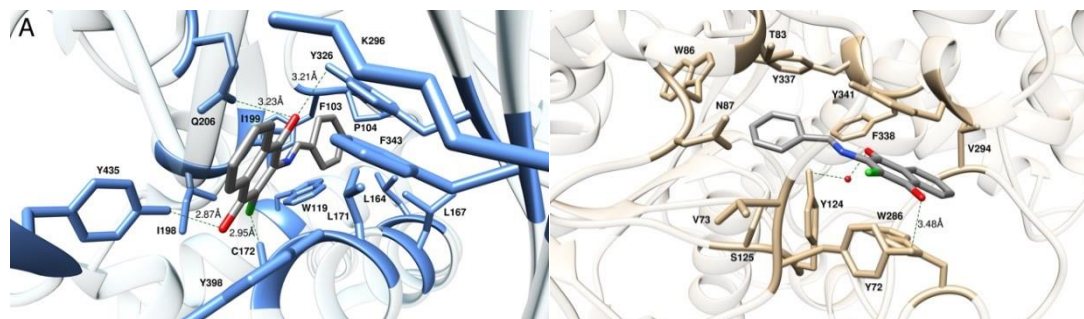

FIGURE 43| Details of compound **2** in the binding pocket of human MAO B (A) and human AChE (B). Compound **2** is shown as atom-coloured sticks (C, grey; O, red; N, blue, Cl, green), while the side chains of the protein residues mainly interacting with the compound are highlighted as coloured sticks and labelled. HBs/HaBs are shown as dark green broken lines and their length are indicated (Å). Hydrogen atoms, water molecules, ions and counterions are omitted for clarity.

On the other hand, within the putative binding site of AChE the naphthoquinone core of **2** is involved in a π-π interaction with AChE W286, and is further stabilized by weak van der Waals interactions with the side chains of the esterase residues V294, F338, and Y341. One of the two -C=O groups of **2** directly engages the side chain of Y72 in a long but stable HB (3.48 ± 0.22 Å), while the second CO moiety interacts with the -OH group of AChE Y124 via a water-mediated HB (2.40 ± 0.33 ($2…H_2O$), 2.38 ± 0.36 Å (Y124…H_2O)). Additionally, mildly favorable, unspecific contacts are detected between the phenyl moiety of **2** and AChE residues V73, T83, W86, N87, S125, and Y337. Accordingly, the interactions between **2** and AChE are definitely less optimized than those detected in the alternative **2**/MAO B complex, and provide a molecular-based rationale for the weaker (μM) and stronger (nM) affinity of **2** for the esterase and the monoamino oxidase, respectively.

6.3.4 Inhibition of PHF6 aggregation

Since new evidences have shifted the role of tau in AD pathogenesis, acting as crucial partner of Aβ[319], the high potency of compounds **1-14** in inhibiting Aβ aggregation prompted us to investigate the same feature in a smart *in vitro* model of tau aggregation, represented by the highly repeated sequence (306)VQIVYK(311) (PHF6) responsible for aggregation of tau in paired helical fragments (PHF)[320]. To this aim, a fast assay method based on ThT

fluorescence was performed[314]. Results listed in **Figure 44** account for a high potency profile of the entire set compounds in inhibiting PHF6 aggregation, with inhibition values often exceed 90% and are comparable to reference drug quercetin. Noteworthy, phenethyl derivatives **3** and **11** emerged as the most potent within their structural subsets (inhibition > 95%).
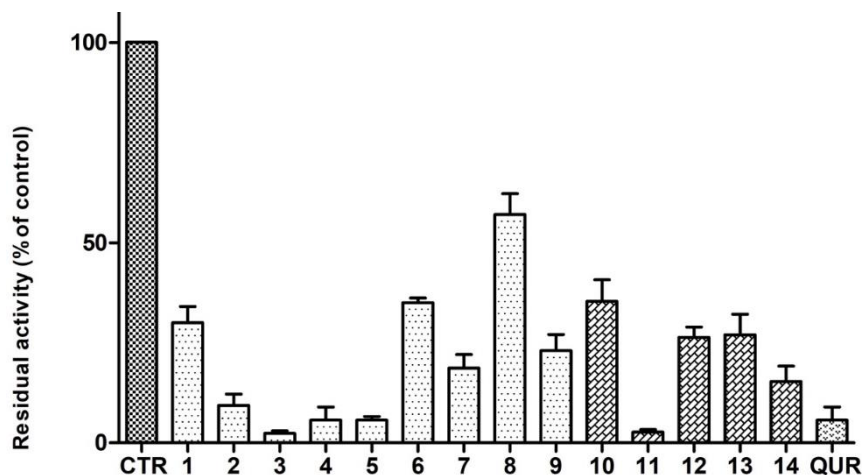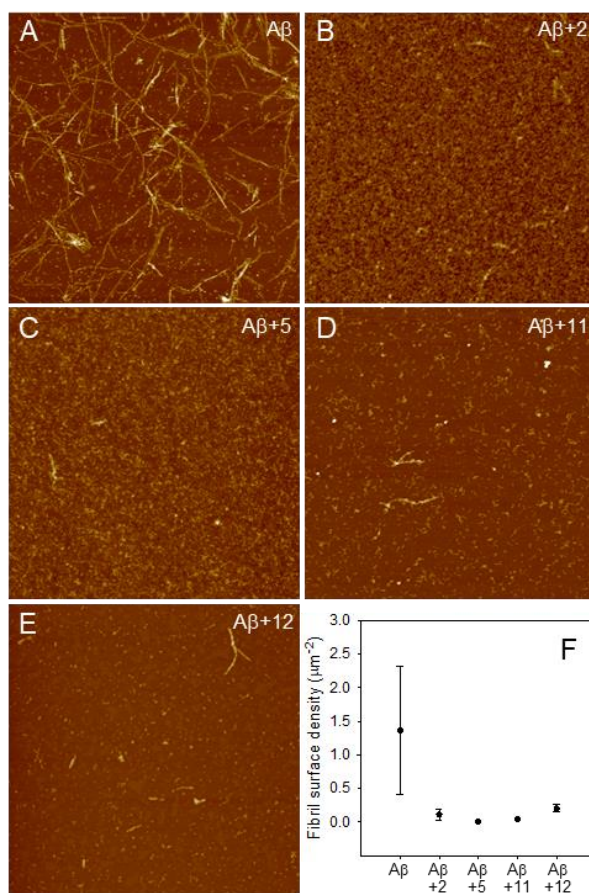

FIGURE 44| Inhibition of aggregation of PHF6 tau sequence (50 μM) by 10 μM test molecules. Quercetin (QUR) was used as reference compound. Bars represent mean ± SD of residual aggregation compared with control (CTR). Clear and dark filling patterns are for naphthoquinones and anthraquinones, respectively.

## 6.3.5 Inhibition of $A\beta_{42}$ fibrillation studied by AFM

Since the naphthoquinone derivatives **2** and **5**, and the anthraquinone derivatives **11** and **12** exhibited the highest efficiency against $A\beta_{40}$ aggregation, they were assayed by Prof. Annalisa Relini Laboratory - University of Genoa, for the ability to inhibit fibrillation of the highly amyloidogenic fragment $A\beta_{42}$, employing tapping mode atomic force microscopy (AFM).

$A\beta_{42}$ aggregated for 72 h in fibrillar morphology in the absence (**Figure 45A**) and in the presence (**Figures 45B-E**) of the compounds, in a molar ratio 1:2 peptide/compound. The AFM inspection allowed a quantitative evaluation of the number of fibrils per unit area at a fixed aggregation time, in the different conditions (**Figure 45F**). In the presence of all the investigated compounds, a significant decrease of the fibril surface density was observed compared with the control.

FIGURE 45| Inhibition of $A\beta_{42}$ fibrillation tested by AFM. Tapping mode AFM images of $A\beta_{42}$ after 72 h aggregation at room temperature in the absence (A) and in the presence of compounds **2** (B), **5** (C), **11** (D) and **12** (E). Scan size 5.0 µM, Z range 25 nm. (F) Quantitative evaluation of the fibril surface density (number of fibrils per unit area) in the absence and in the presence of the compounds. Mean values obtained on at least six different areas of 100 µm^2 are reported. Errors were calculated using Student's statistics, assuming a confidence level of 95%.

The inhibitory effect of the compounds was already observed after 24 h of aggregation. Although at this stage of aggregation the sample was mainly oligomeric with a low fibrils number, in the presence of the compounds there was still a decrease in the fibrils surface density (**Figure 46**).
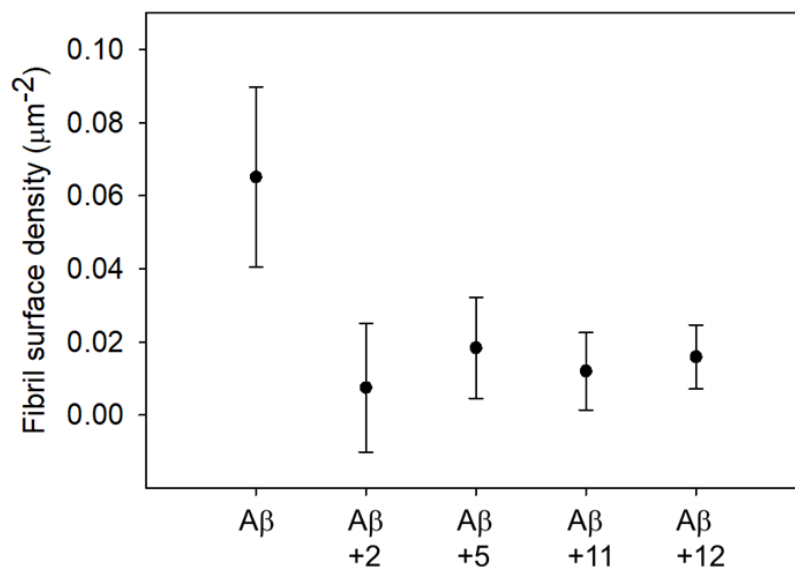
FIGURE 46| Evaluation of the fibril surface density (number of fibrils per unit area) after 24 h of $A\beta_{42}$ aggregation in the absence and in the presence of the compounds (**2**, **5**, **11** and **12**). Mean values obtained on at least four different areas of 100 μm^2 are reported. Errors were calculated using Student's statistics, assuming a confidence level of 95%.

6.3.6 Protection against $A\beta_{42}$-induced toxicity

The most promising MTDLs **2**, **5**, **11** and **12** were also tested by Dr. Elena Gatta - University of Genoa, for their ability to restore cell viability against the toxic effects exerted by $A\beta_{42}$. Cerebellar granule cells (CGCs) were exposed for 48 h to 5 μM $A\beta_{42}$ aggregated for 24 hours with and without the compounds (molar ratio peptide/compound 1:2). Then, after the exposure, cell viability was measured through MTT test (**Figure 47**). Viability of cells treated with $A\beta_{42}$ alone decreased to 51%, compared with the control. A partial recovery of the viability in the presence of the compounds was generally observed, with compound **2** as the best neuroprotective agents.

This behaviour is probably due to the fact that, although the compounds are effective in inhibiting aggregation of the peptide, they display some degree of intrinsic toxicity. Indeed, there was only a marginal toxic effect from any of the test compounds, since at 10 μM the cell viability remained as high as ≥80% compared to the untreated control cells (**Table 6**).

100
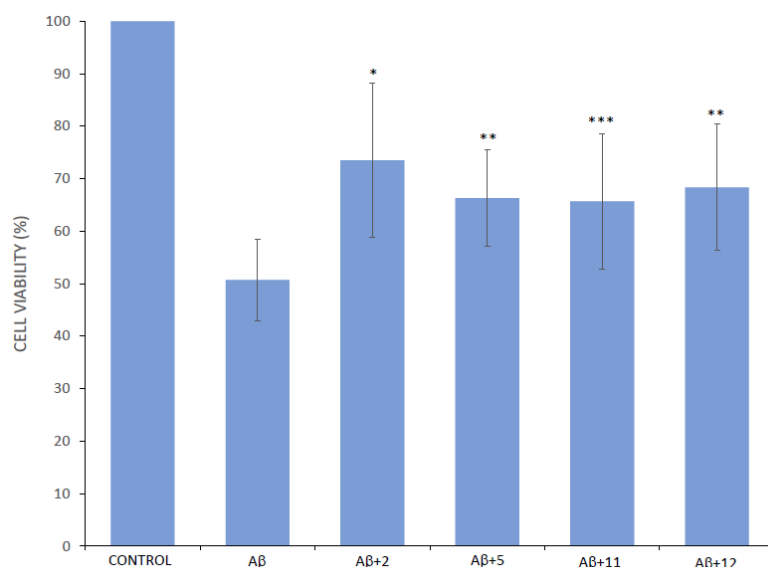
FIGURE 47| Protection against Aβ$_{42}$ toxicity in cerebellar granule cells. The CGCs were treated with vehicle (control) or with Aβ$_{42}$, with or without the tested compounds, for 48 h. Cell viability was measured by MTT reduction test and expressed as loss of viability in comparison with vehicle-treated controls. Values have been obtained from three experiments.
Compound + A vs A : * p < 0.01, ** p < 0.02, ***p < 0.05

Table 6. In vitro cytotoxicity of compounds 2, 5, 11, 12. The CGCs were treated with the compounds (10 μM) for 48 h. Cell viability was measured by MTT reduction test and expressed as loss of viability in comparison with vehicle-treated controls. Values have been obtained from at least three experiments. Data are expressed as mean ± SEM.

Compound	2	5	11	12
Cell viability vs control (%)	89 ± 14	85 ± 14	85 ± 15	77 ± 12

6.4 Conclusion

By comparing compounds **1**-**14** with the previous series of naphthoquinone and anthraquinones bearing a basic side chain[295] (**Figure 38**), in the case of naphthoquinones the activity improved with 8 out of 9 compounds able to target Aβ peptide, while the anthraquinones exhibited only a slight increase of the potency, but with a reduced number of active compounds. Therefore, the more apolar nature of the side chain (aromatic/heteroaromatic moiety), in place of polar basic groups, emerged as relevant factor in enhancing the intrinsic capability of naphthoquinone and anthraquinone scaffolds to target Aβ fibrillation. These molecules were purportedly designed to inhibit Aβ aggregation being properly decorated with hydrophobic moieties able to target the aromatic interactions implicated in amyloid self-assembly; in agreement with the design rationale the compounds significantly inhibited $Aβ_{40}$ aggregation. The most active derivatives (**2**, **5**, **11** and **12**) confirmed to disrupt fibrillation of the highly amyloidogenic fragment $Aβ_{42}$ and they were also found to ameliorate the cytotoxicity caused by $Aβ_{42}$ peptide.

All the compounds exhibited a preferential inhibition of AChE than BChE and, appeared to be efficient inhibitors of fast-aggregating tau peptide PHF6, displaying inhibition values exceeding 90%. Moreover, most of them turned out to be potent and selective MAO B inhibitors, being able to provide IC_{50} values in the nanomolar or sub-micromolar range with respect to the MAO A isoform.
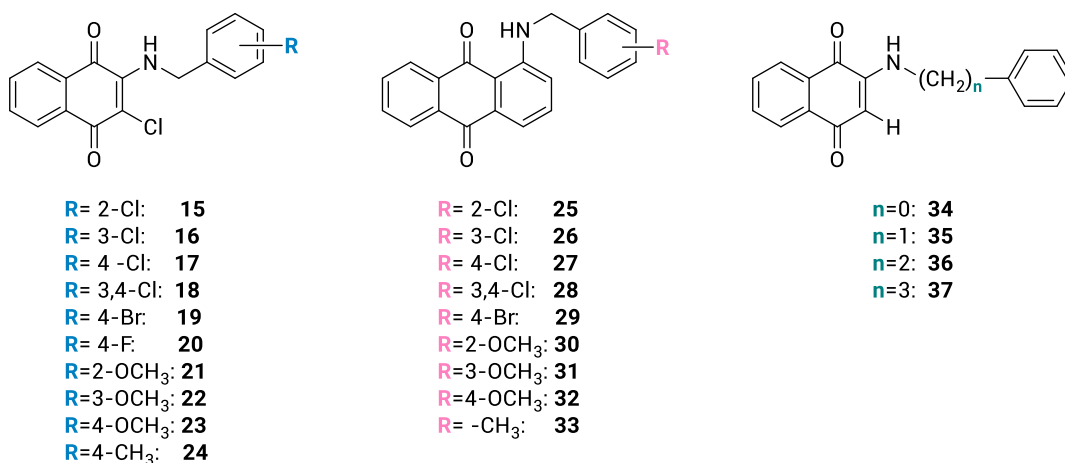
7. SECOND SET

7.1 Project

The second set of molecules (**15**-**37**) accounts for 23 quinone derivatives (**Figure 48**), that were designed assuming compound **2** as lead prototype in virtue of its high potency towards AChE and Aβ aggregation (the *in vitro* screening against PHF6 aggregation and MAO were completed only after this series was synthesized). Firstly, novel decorations on the phenyl ring, including both electron-withdrawing and electron-donors groups, were explored with the aim of investigate their contributions to the inhibitory activities against ChEs and Aβ aggregation. Secondarily, the electron-withdrawing chlorine atom in position 3 of the naphthoquinone scaffold was replaced with a hydrogen or the electron-donating group -OCH$_3$. The last idea regarded the isosteric replacement the NH on C(2) of the naphthoquinone ring with an oxygen atom in order to probe its role as essential feature for the activity.

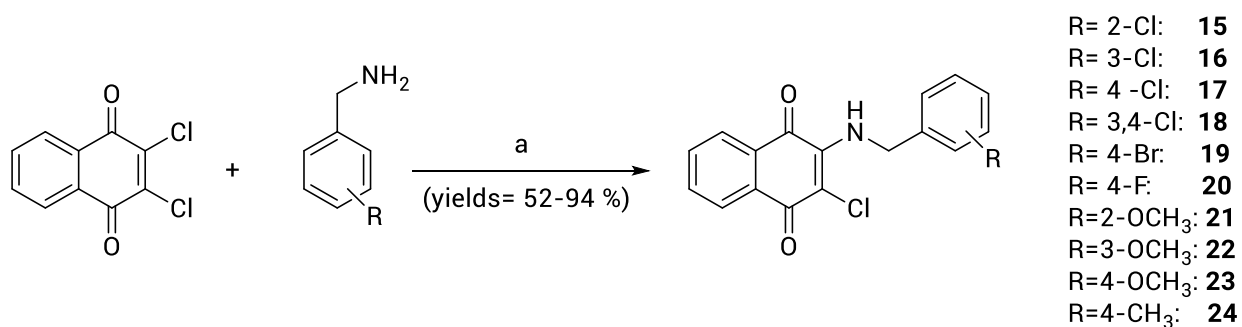The chemical structures of the entire set two are listed in **Figure 49**.
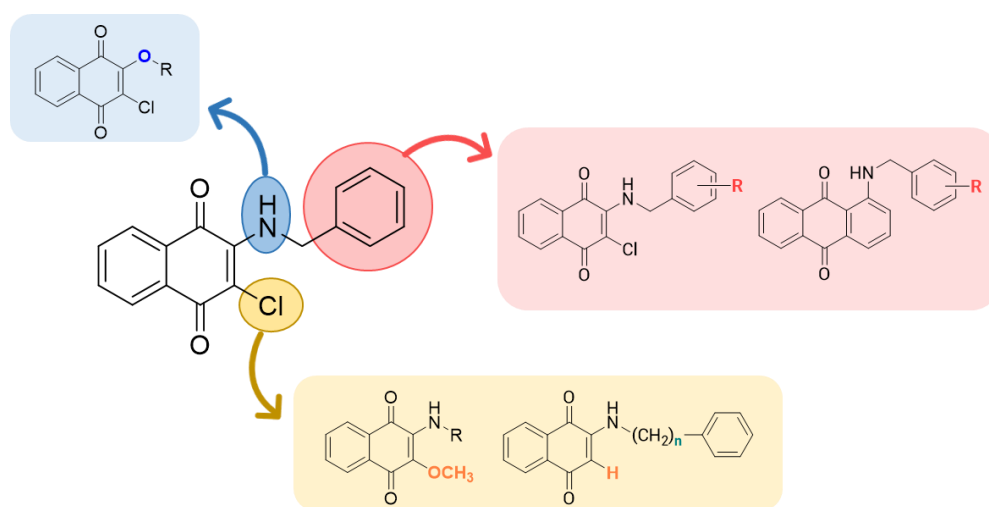
FIGURE 48| Design strategy of the second set of quinones based on the prototype **2** core structure.

R= 2-Cl: **15**
R= 3-Cl: **16**
R= 4 -Cl: **17**
R= 3,4-Cl: **18**
R= 4-Br: **19**
R= 4-F: **20**
R=2-OCH$_3$: **21**
R=3-OCH$_3$: **22**
R=4-OCH$_3$: **23**
R=4-CH$_3$: **24**

R= 2-Cl: **25**
R= 3-Cl: **26**
R= 4-Cl: **27**
R= 3,4-Cl: **28**
R= 4-Br: **29**
R=2-OCH$_3$: **30**
R=3-OCH$_3$: **31**
R=4-OCH$_3$: **32**
R= -CH$_3$: **33**

n=0: **34**
n=1: **35**
n=2: **36**
n=3: **37**

FIGURE 49| Structures of the second set of quinone-based derivatives **15**-**37**.
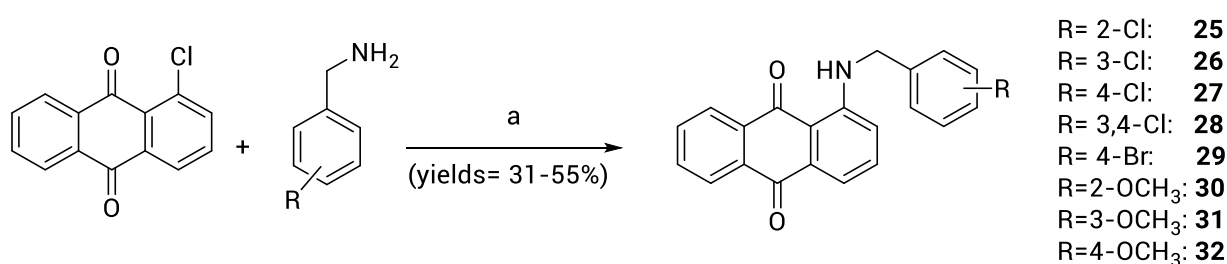
7.2 Chemistry

Naphthoquinone derivatives **15**-**24** were obtained by reacting the 2,3-dichloro-1,4-naphthoquinone, previously suspended in ethanol, with the proper amine in a molar ratio 1:2 (**Scheme 7**).

R= 2-Cl: **15**
R= 3-Cl: **16**
R= 4 -Cl: **17**
R= 3,4-Cl: **18**
R= 4-Br: **19**
R= 4-F: **20**
R=2-OCH$_3$: **21**
R=3-OCH$_3$: **22**
R=4-OCH$_3$: **23**
R=4-CH$_3$: **24**

Scheme 7. Reagents and conditions: a) EtOH, 80°C, 4 h.

The melted mixture at 160°C of 1-chloroanthraquinone with the proper benzylamine has given compounds **25**-**32** (**Scheme 8**).

R= 2-Cl: **25**
R= 3-Cl: **26**
R= 4-Cl: **27**
R= 3,4-Cl: **28**
R= 4-Br: **29**
R=2-OCH$_3$: **30**
R=3-OCH$_3$: **31**
R=4-OCH$_3$: **32**

Scheme 8. Reagents and conditions: a) direct fusion 160 °C 7 h.

The yields of the anthraquinone reactions are generally lower than that of the naphthoquinone analogues, probably due to the drastic reaction conditions that are necessary to yield the expected products. Some reactions were also repeated in *n*-BuOH at reflux for 7-8 h, or in DMF in sealed tube at 130 °C for 10 h, but the yields still remained unvaried.

In the case of compound **33** the best reaction yield was obtained by adding the 4-methylbenzylamine to a suspension of 1-chloroanthraquinone in n-BuOH, and stirring the mixture at reflux for 8 h (**Scheme 9**).
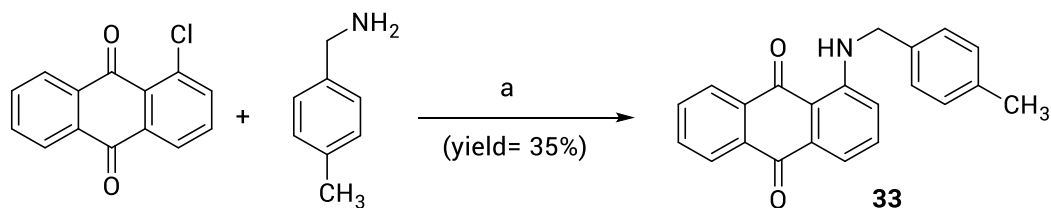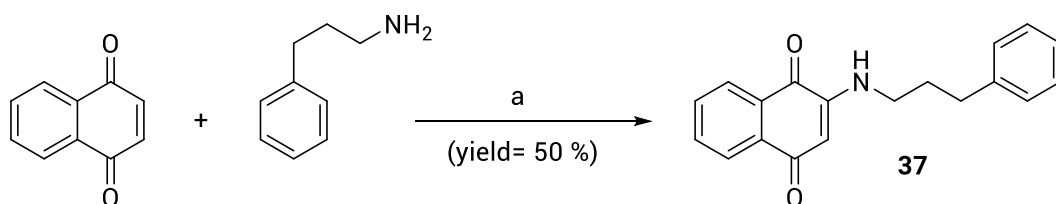

Scheme 9. Reagents and conditions: a) BuOH at reflux 8 h.

To prepare derivatives **34**-**36** the 2-bromo-1,4-naphthoquinone suspended in ethanol was reacted with the proper amine in a molar ratio 1:2 (**Scheme 10**).
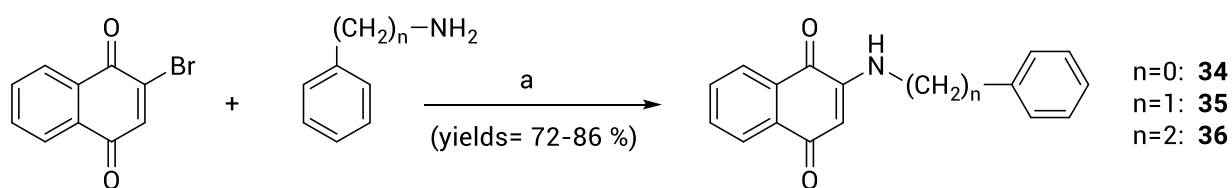

Scheme 10. Reagents and conditions: a) EtOH at reflux 4 h.

In the case of **37**, 2-Br-naphthoquinone did not adequately react with 3-phenylpropylamine, that instead formed the desired product via Michael addition to 1,4-naphthoquinone (molar ratio 2:1) (**Scheme 11**).
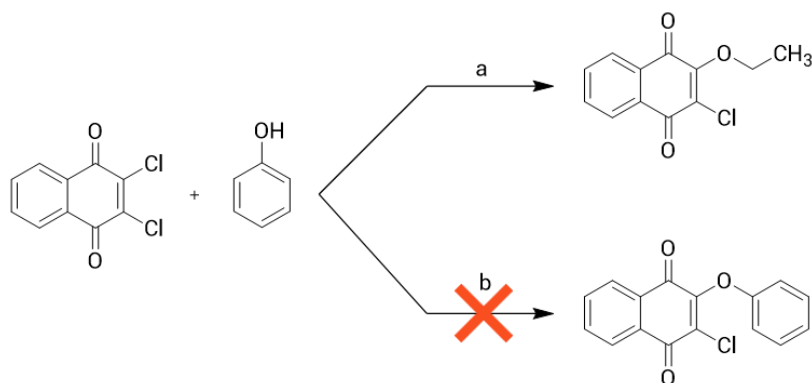

Scheme 11. Reagents and conditions: a) EtOH at reflux 4 h.

As shown below, the synthetic methods carried out for the 3-OMe substituted naphthoquinones did not allow the yield of the expected products (**Scheme 12**); the only derivative isolated and characterized was the 2-chloro-3-methoxynaphthoquinone, obtained with a synthetic route similar to the literature[321].
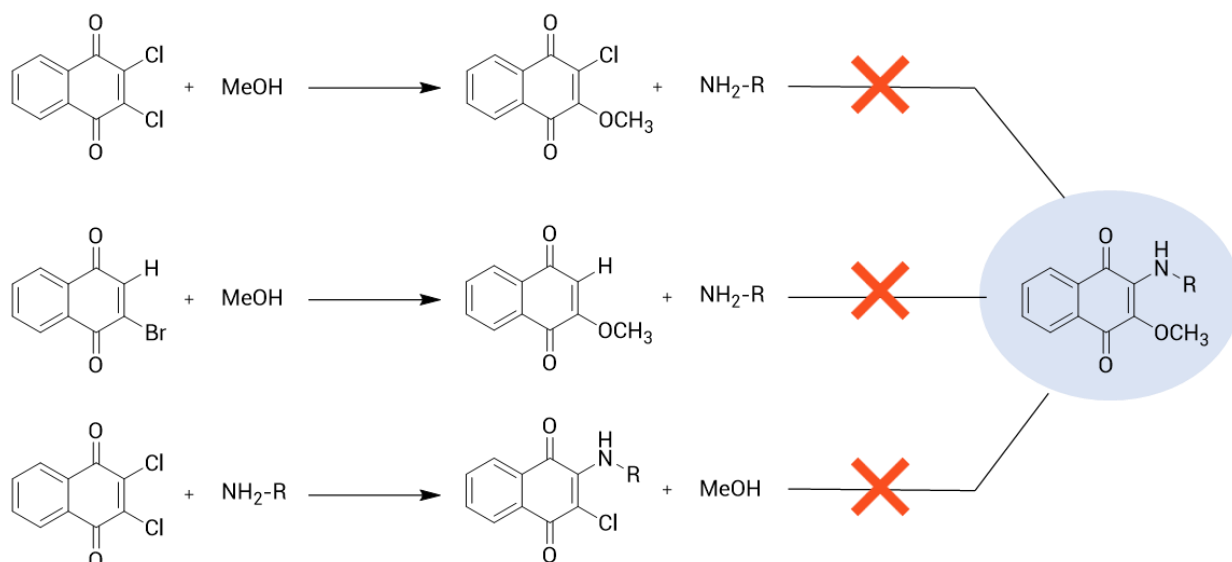
Scheme 12. Synthetic routes explored in an effort to prepare the 3-methoxynaphthoquinone derivatives.

Schemes 13 and **14** depict the failed attempts to obtain the phenolic derivatives of naphtho- and anthraquinones, despite the formation of sodium phenolate was exploited as more reactive nucleophile than phenol itself.

Scheme 13. Reagents and conditions: a) EtOH, NaOH, 80°C, 4 h; b) Cs_2CO_3, an. THF, R.T. 24 h.
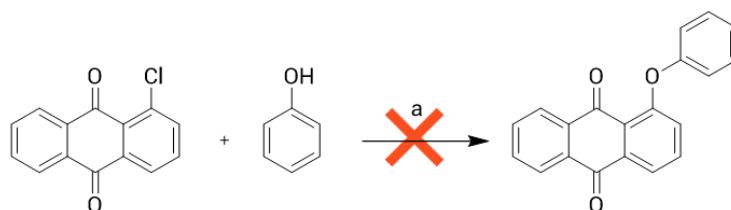
Scheme 14. Reagents and conditions: a) NaH, anhydrous THF, 60°C, 4 h.

Compounds **34**[322] and **37**[323] have been achieved according to the cited references; while for compounds **20**[324], **35**[325], **36**[325] a different synthetic route with respect to the literature was applied. The structures of the compounds have been confirmed using ^{1}H NMR and elemental analysis. The purity of compounds (checked by elemental analysis) has been in all cases >95%.

7.3 In vitro biological profiling

7.3.1 Inhibition of self-induced Aβ aggregation and Cholinesterases

The newly synthesized compounds **15**-**37** (with the exception of **30** and **31** which are still under investigation) have been tested for the direct inhibition of $A\beta_{40}$ aggregation and for the inhibition of electric eel acetylcholinesterase (eeAChE) and equine serum butyrylcholinesterase (esBChE). Inhibitory activities on AChE and BChE were determined by the spectrophotometric method of Ellman[306] and are reported in **Table 7** as IC_{50} values for the most active compounds or as percent inhibition at 10 μM for less active (i.e., <50%) compounds. In vitro inhibition of $A\beta_{40}$ aggregation was assessed following the already mentioned thioflavin T (ThT) fluorescence-based method involving the use of hexafluoroisopropanol (HFIP) as aggregation enhancer[305]. Results are listed in **Table 7** as IC_{50} values for the most active compounds or as percent inhibition at 100 μM for less active (i.e., <80%) compounds.

Table 7. Inhibitory activities (µM) of compounds **15–37** against Aβ aggregation, eeAChE and esBChE[a].

Cpd	IC_{50} (µM) or (% inhibition)[b]		
	$A\beta_{40}$ aggr.	eeAChE	esBChE
15	(56 ± 3)	10.2 ± 1.3	-
16	(58 ± 3)	6.99 ± 0.47.	(38 ± 6)
17	(67 ± 5)	**5.57 ± 0.62**	(31 ± 5)
18	(16 ± 3)	12.2 ± 1.2	(8 ± 2)
19	(62 ± 4)	6.36 ± 0.7	(26 ± 4)
20	(57 ± 5)	12.2 ± 1.8	(11 ± 3)
21	(54 ± 4)	16.4 ± 1.7	(20 ± 4)
22	**7.13 ± 0.64**	6.93 ± 0.57	(23 ± 2)
23	**9.70 ± 0.27**	6.94 ± 0.75	(23 ± 5)
24	(74 ± 1)	8.52 ± 0.69	-
25	(68 ± 3)	**4.35 ± 0.51**	(47 ± 3)
26	(36 ± 4)	7.63 ± 0.48	(12 ± 3)
27	(21 ± 4)	7.31 ± 0.23	(10 ± 2)
28	(60 ± 4)	12.4 ± 2.6	(8 ± 2)
29	(47 ± 2)	11.2 ± 0.6	(7 ± 2)
30	-	-	-
31	-	-	-
32	(8 ± 2)	7.67 ± 0.66	(11 ± 3)
33	(32 ± 2)	8.41 ± 0.97	(15 ± 3)
34	(65 ± 1)	7.16 ± 0.61	(17 ± 1)
35	**26.9 ± 2.5**	6.86 ± 0.78	(7 ± 3)
36	**16.4 ± 3.2**	5.74 ± 0.68	(11 ± 2)
37	**13.9 ± 1.5**	**5.02 ±0.69**	(19 ± 1)
Quercetin	0.82 ± 0.07	-	-
Donepezil	-	0.021 ± 0.002	2.3 ± 0.1

[a]Values represent the mean of two/three independent experiments; SEM <10%; [b]Data in parenthesis correspond to % of inhibition at 10 µM (eeAChE and hsBChE), or 100 µM (Aβ aggregation)[c].

The biological results confirm a moderate inhibitory activity against acetylcholinesterase for all new molecules, whose IC_{50} values fell in the range 4.35 - 16.4 µM.

In six out of ten 3-Cl-2-aminobenzyl-naphthoquinones, the substitution in position 4 and 3 of the phenyl ring is responsible for an improved inhibitory potency on AChE with respect to the prototype **2**, with about a 2-fold increase

of the activity for the 4-Cl benzyl derivative **17** (IC_{50}= 5.57 μM). Indeed, also the 3-Cl isomer (**16**), and 3/4-OCH$_3$ analogues (**22** and **23**) proved to be comparable AChE inhibitors, suggesting that both lipophilic and electron-withdrawing (Cl, Br, F) and polar and electron-donor groups (OCH$_3$) were permitted. The double substitution in position 3 and 4 (**18**) worsens the activity as well as the mono-substitution in position 2 (**15**, **21**), probably causing a greater steric hindrance.

Again, good activity may be observed for 4-Br (**19**) and 4-F (**20**) derivatives, although the 4-Cl analogue (**17**) remains unsurpassed.

Regarding the derivatives **34**-**37**, devoid of the chlorine atom in position 3 of the naphthoquinone scaffold, the AChE inhibitory potency proportionally increases with the length of the alkyl spacer, with 3-phenylpropyl derivative **37** as the most active compound (IC_{50}= 5.02 μM).

All naphthoquinone derivatives demonstrate no activity against BChE, confirming to be AChE-selective inhibitors as prototype **2**. Finally, it worth noting the good inhibitory activity on self-induced Aβ aggregation of only 3-methoxy (**22**) and 4-methoxy substituted compounds (**23**) showing IC_{50} values equal to 7.13 and 9.70 μM, respectively, however with a lesser extent than the unsubstituted prototype **2** (IC_{50} = 3.2 μM).

The four derivatives without the chlorine atom in position 3 on the naphthoquinone nucleus (**34**-**37**) displayed a micromolar inhibitory activity towards Aβ, thus ranking second to 3/4-methoxybenzyl naphthoquinones **22** and **23**.

In the anthraquinone series (**25**-**33**), the presence of a substituent on the benzyl ring always provides a good and selective activity against AChE (mean IC_{50}= 7 μM) over BChE, with the 2-Cl benzyl anthraquinone **25** as the most potent, reaching an IC_{50} value of 4.35 μM against acetylcholinesterase enzyme. These tricyclic derivatives resulted to be less interesting multitarget ligands than smaller naphthoquinones, lacking an adequate inhibition potency against Aβ aggregation.
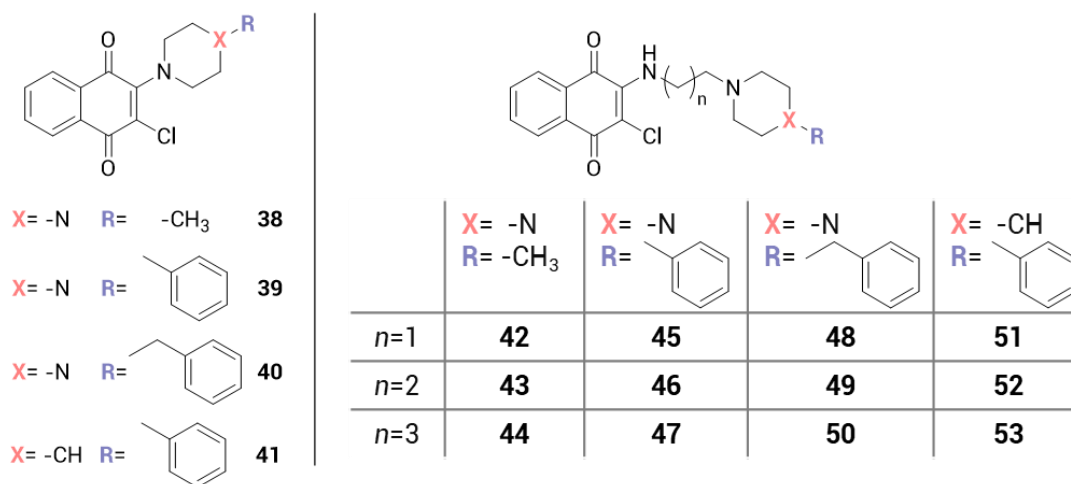
7.4 Conclusion

The introduction of a substituent on the phenyl ring does not seem to entail significant amelioration of the individual biological activities compared to those experienced by the starting compounds (**2** and **10**). Indeed, this type of functionalities have generally moved the biological behavior from a multitarget profile (first set) to a more selective one, towards AChE. Indeed, further studies are deserved to evaluate the potential of these molecules also against other targets with more credential for a disease-modifying effect, as tau and MAO, as recently demonstrated for the first set of naphtho- and anthraquinones (**1**-**14**). The new SAR insights gathered from this study have provided crucial information around the chemical space of prototypes **2** and **10** and will guide the successive development of an improved generation of anti-AD agents.
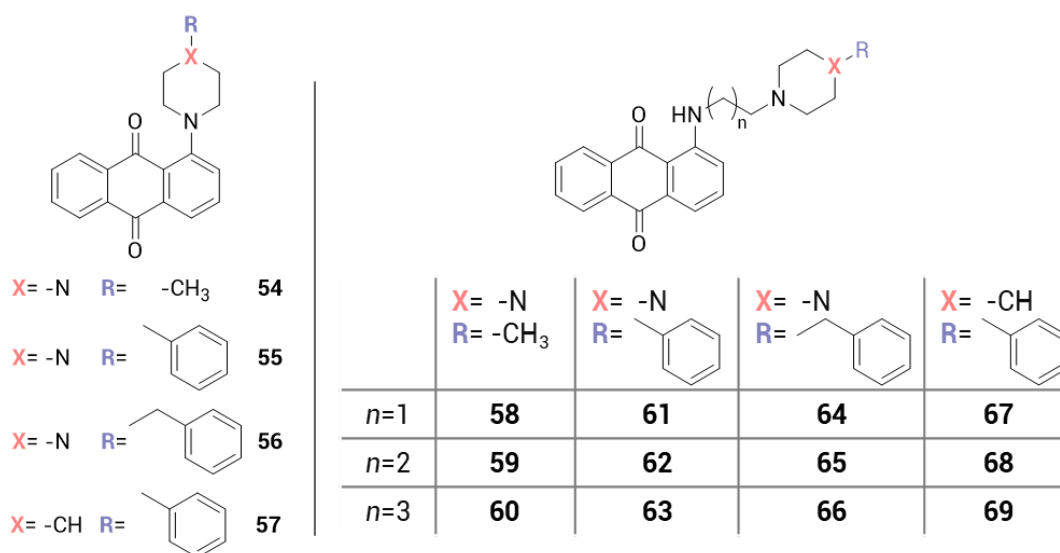
8. THIRD SET

8.1 Project

The third subgroup is represented by a different library of quinone-based derivatives that were decorated with a basic framework, which has been selected in order to reduce the high hydrophobicity of the quinolizidine moiety recurring in the naphthoquinone (I-VIII) and anthraquinone derivatives (IX-XIV), previously investigated by my Research Group. To this aim I synthesized two novel series of aryl naphtho- and anthraquinone derivatives, introducing a piperazine or a piperidine ring as a basic and rigid spacer between the two main units. Meanwhile the basic feature, resembling the lateral chain of Donepezil, should maintain an efficient inhibition of both ChEs, by means of a suited bond with anionic site (PAS) of AChE, the aromatic ring should guarantee the direct inhibition of Aβ aggregation by interacting with its aromatic amino acids sequence[295].

As the elongation of the linker chain was favorable for anthraquinones activity of first set, in this series it was also explored the importance of the distance between the quinone scaffold and the basic nucleus including a polymethylene chain of variable length up to 4 carbon units (**Figures 50** and **51**).

	X= -N R= -CH$_3$	X= -N R=	X= -N R=	X= -CH R=
n=1	42	45	48	51
n=2	43	46	49	52
n=3	44	47	50	53

X= -N   R=   -CH$_3$ **38**

X= -N   R=   **39**

X= -N   R=   **40**

X= -CH   R=   **41**

FIGURE 50| Chemical structure of the investigated naphthoquinone derivatives 38-53 of the second set.

	X= -N R= -CH$_3$	X= -N R=	X= -N R=	X= -CH R=
n=1	58	61	64	67
n=2	59	62	65	68
n=3	60	63	66	69

X= -N	R= -CH$_3$	54
X= -N	R=	55
X= -N	R=	56
X= -CH	R=	57

FIGURE 51| Chemical structure of the investigated anthraquinone derivatives 54-69 of the second set.

In the wake of the encouraging results from a preliminary screening, this third set of compounds **38**-**69** was then expanded with other derivatives (**70**-**83**, **Figure 52**), for which biological studies are still ongoing. The changes made were to lengthen the polymethylene chain up to 6 carbon atoms for the naphthoquinone derivatives, and to explore the benzyl-piperidine moiety in the lateral chain.
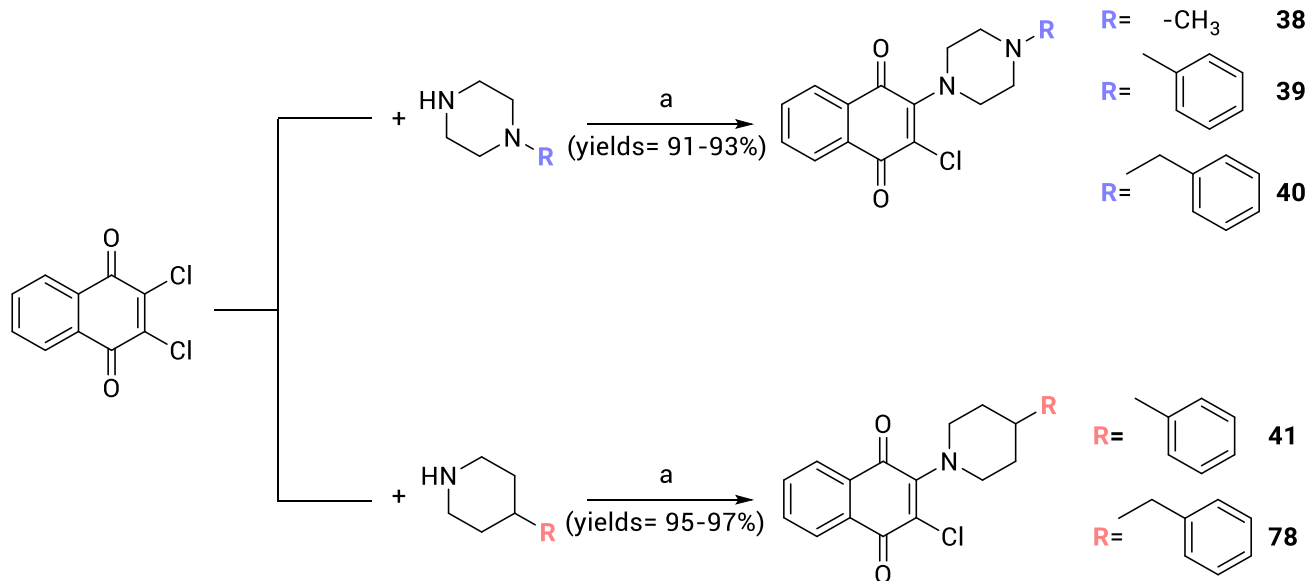

	X= -N R= -CH$_3$	X= -N R=	X= -N R=	X= -CH R=
n=4	70	72	74	76
n=5	71	73	75	77

n=1	79
n=2	80
n=3	81
n=4	82
n=5	83
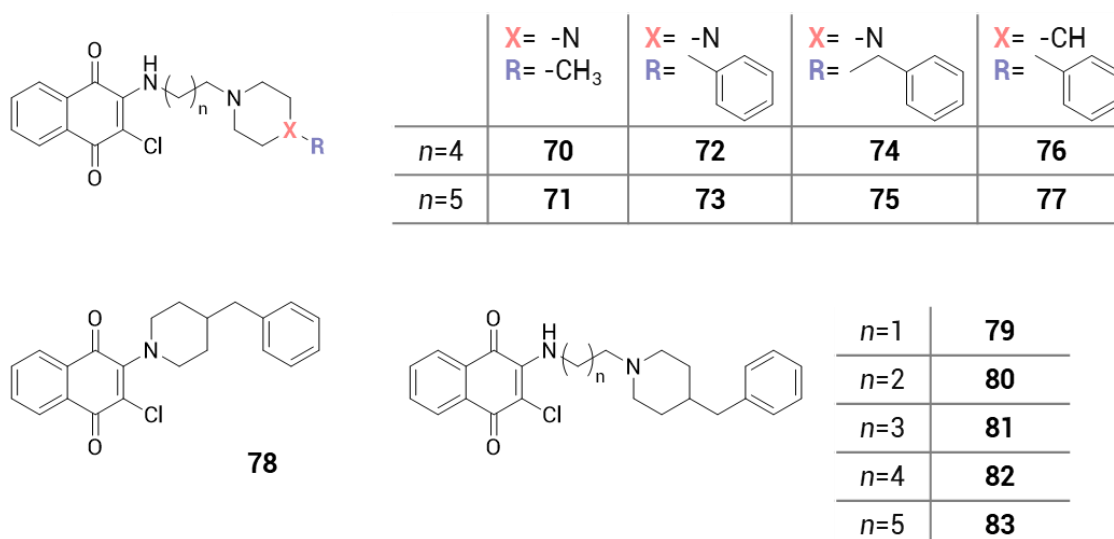
FIGURE 52| Chemical structure of the derivatives 70-83 of the second set.

8.2 Chemistry

The novel naphthoquinone derivatives **38-41** and **78** were obtained by reacting the 2,3-dichloro-1,4-naphthoquinone, previously suspended in CH_3CN, with the proper amine in a molar ratio 1:2 (**Scheme 15**).
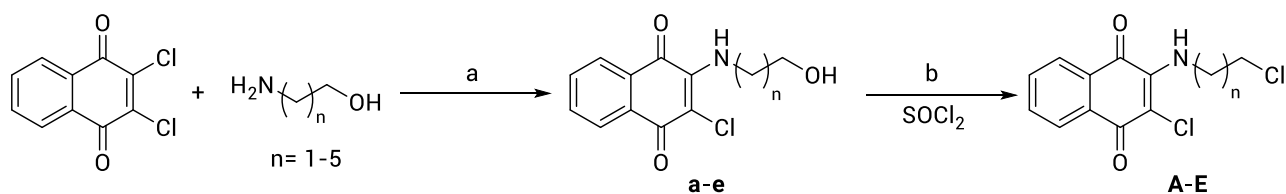

Scheme 15. Reagents and conditions: a) CH_3CN 100 °C 24 h.

Anthraquinone derivatives **54-57** were synthesized by reacting the 1-chloroanthraquinone and the proper amine (in a molar ratio 1:2) in CH_3CN in a sealed tube at 100 °C for 24 h (**Scheme 16**).
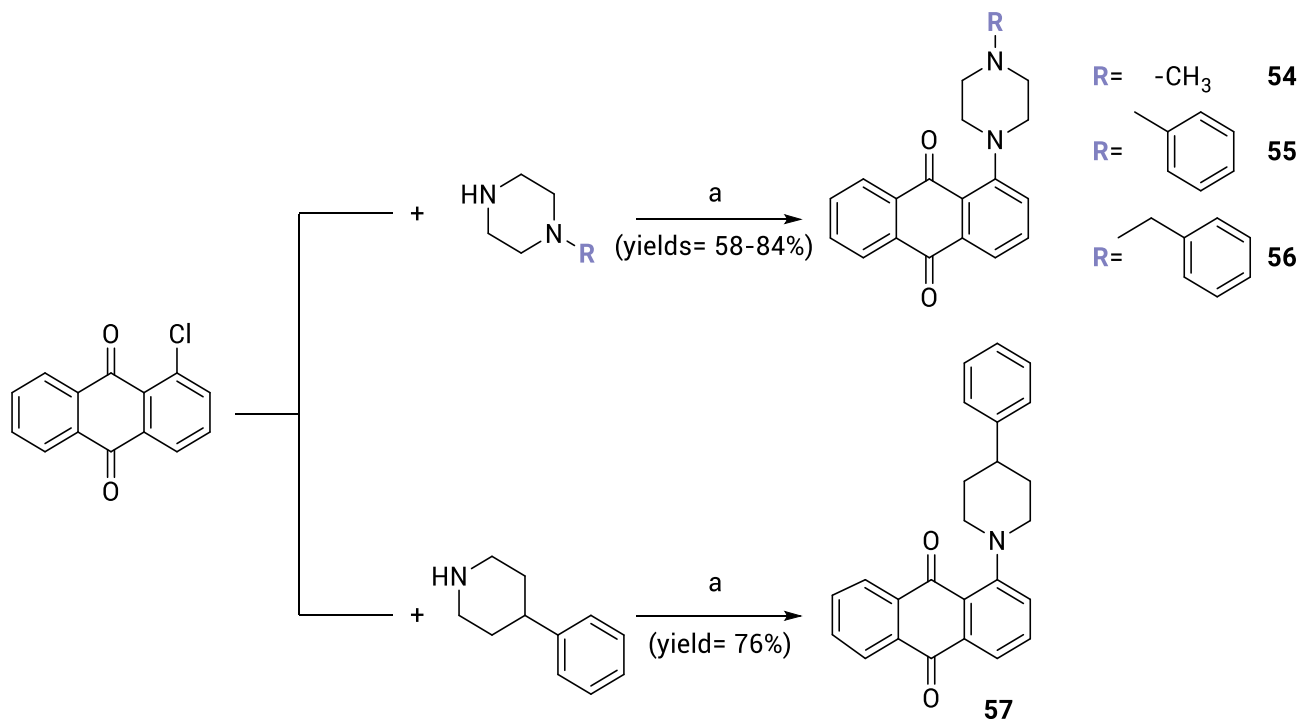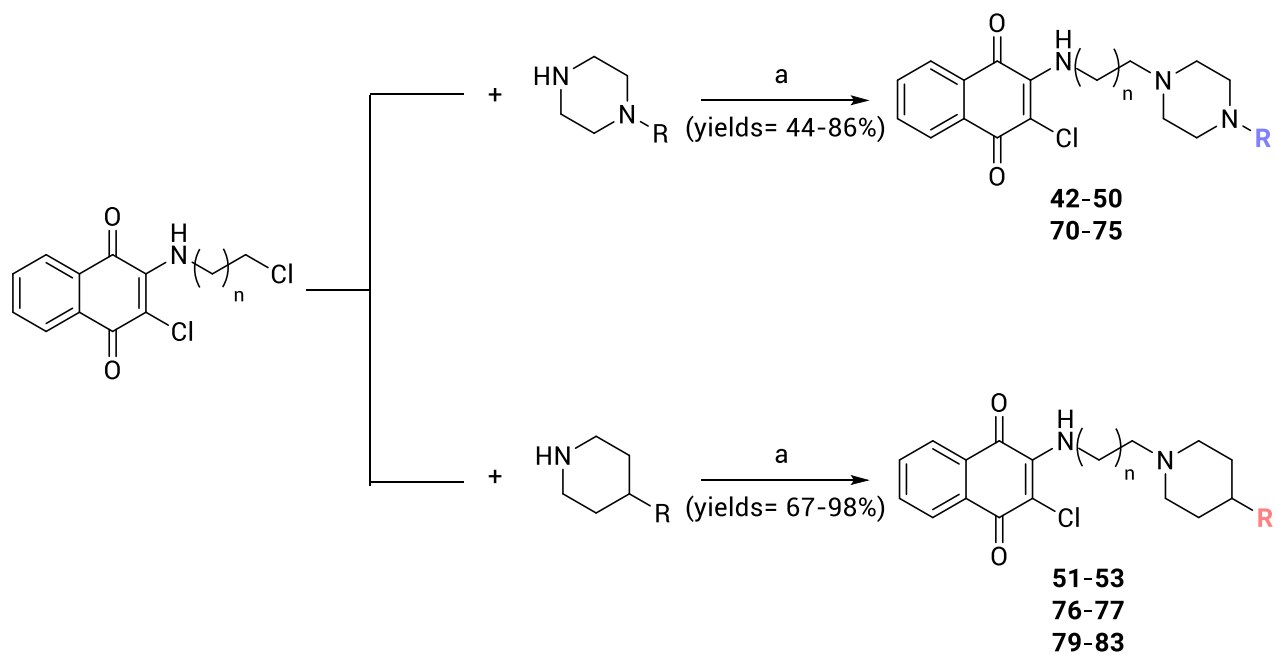

Scheme 16. Reagents and conditions: a) CH_3CN 100 °C 24 h.

113

The intermediate chloro-alkylamino naphthoquinones (A-E) required for the synthesis of 42-53, 70-77 and 79-83, were prepared by reacting at reflux an ethanolic solution of the 2,3-dichloro-1,4-naphthoquinone and the proper aminoalchool, in a molar ratio 1:2, and then converting the alcoholic group into the corresponding alkyl chloride with an excess of SOCl$_2$ (1:4) in anhydrous CHCl$_3$ (**Scheme 17**).

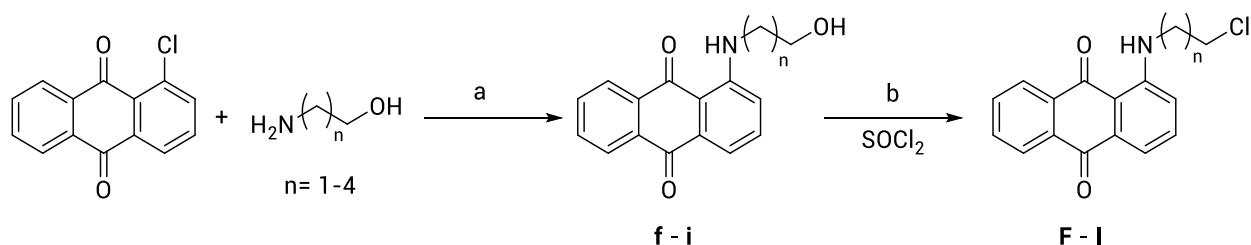**Scheme 17.** Reagents and conditions: a) EtOH at reflux 20 h; b) anhydrous CHCl$_3$, 60°C, 5 h.

Finally intermediates **A-E** were added to the proper piperazine derivative dissolved in CH$_3$CN (molar ratio 1:2), thus affording derivatives **42-53**, **70-77** and **79-83** (**Scheme 18**).

	R= -CH$_3$	R=	R=		R=	R=
n=1	42	45	48	n=1	51	79
n=2	43	46	49	n=2	52	80
n=3	44	47	50	n=3	53	81
n=4	70	72	74	n=4	76	82
n=5	71	73	75	n=5	77	83

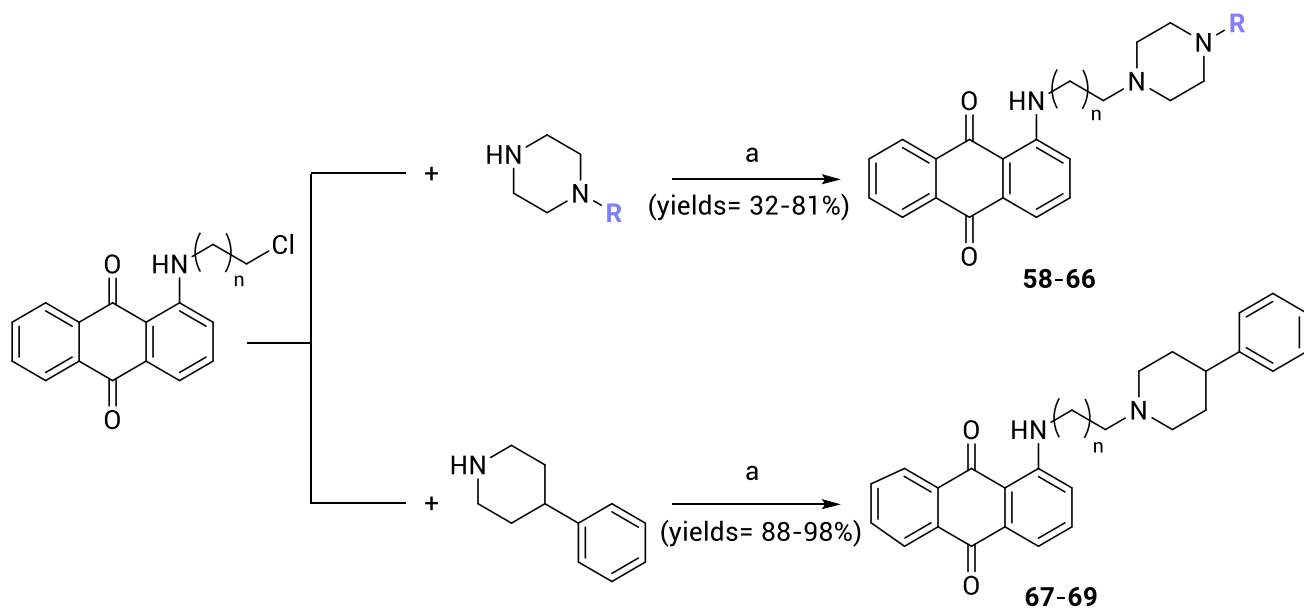**Scheme 18.** Reagents and conditions: a) CH$_3$CN 100 °C 24 h.

The same synthetic method was applied to obtain the anthraquinone analogues **58-69**: the reaction between the 1-chloroanthraquinone and the proper aminoalchool was followed by the chlorination with $SOCl_2$ of corresponding product (**f-I**), yielding the intermediates **F-I** (**Scheme 19**).

Scheme 19. Reagents and conditions: a) two different methods with comparable yields were carried out: BuOH at reflux, 20 h in a molar ratio 1:2 or fusion in sealed tube 140 °C, 8h in a molar ratio 1:3; b) anhydrous $CHCl_3$, 60°C, 5 h.

In the final step, a mixture of an intermediate **F-I** and of a proper piperazine or piperidine derivative was heated in a sealed tube for 24 h at 100°C, leading to derivatives **58-69** (**Scheme 20**).

Scheme 20. Reagents and conditions: a) CH_3CN 100 °C 24 h.

Intermediate **e**[326] has been achieved according to the cited reference, while the intermediates **a**[327], **b**[327] and compound **38**[328], has been achieved applying different reaction condition with respect to the literature as above mentioned. The structures of the novel compounds have been confirmed using ^{1}H and ^{13}C NMR, and elemental analysis. The purity of compounds (checked by elemental analysis) has been in all cases >95%.

8.3 In vitro biological profiling

These quinone-based derivatives have been evaluated in vitro for their inhibitory activities against different targets playing a significant role in AD pathology. The biological profiling included the in vitro evaluation of (i) self-induced Aβ aggregation inhibition; (ii) inhibitory activities against AChE and BChE; (iii) safety profile and neuroprotection activity against hydrogen peroxide; (iv) inhibitory activity against γ-secretase.

Firstly, the inhibition of self-induced Aβ aggregation and ChEs, were performed by Prof. Marco Catto, as for the others set of derivatives. During my last year of PhD (from October 2019 to February 2020) I performed the remaining biological studies, in the laboratory of Dr. Robert Williams - University of Bath (UK). Particularly, the safety profile of these molecules was tested in cell-based assays, through two different methods, namely, the 3-(4,5-dimethylthiazol-2-yl)-2,5-diphenyltetrazolium bromide (MTT) and the lactate dehydrogenase (LDH) assays; the six most promising derivatives were then tested for their ability to protect cortical neurons against an insult as hydrogen peroxide (H_2O_2) in different concentration, in order to investigate their potential as neuroprotective and antioxidant agents. Meantime, the four compounds with the best activities against Aβ aggregation and ChEs, underwent another *in vitro* test: a reporter gene assay, with a view to defining them as modulators of APP processing and particularly, γ-secretase inhibitors.

8.3.1 Inhibition of self-induced Aβ aggregation and Cholinesterases

The newly synthesized compounds **38-69** have been tested for the direct inhibition of $A\beta_{40}$ aggregation and for the inhibition of electric eel acetylcholinesterase (eeAChE) and equine serum butyrylcholinesterase (esBChE). Inhibitory activities on AChE and BChE are reported in **Table 8** as IC_{50} values for the most active compounds or as percent inhibition at 10 µM for less active (i.e., <50%) compounds. *In vitro* inhibition of $A\beta_{40}$ aggregation data are listed in **Table 8** as percent inhibition at 100 µM.

Table 8. Inhibitory activities of compounds **38**-**69** against Aβ aggregation, eeAChE and esBChE[a].

Cpd	IC$_{50}$ (µM) or (% inhibition)[b]		
	Aβ$_{40}$ aggr.	eeAChE	esBChE
Naphthoquinones			
38	52	4.21±0.21	(24±3)
39	96.00	3.60±0.52	(29±2)
40	93.00	5.71±0.51	(28±4)
41	97.00	5.00±0.98	(19±4)
42	41	**0.494±0.013**	(25±1)
43	61	**0.449±0.056**	(18±2)
44	69	**0.891±0.014**	(30±4)
45	95.00	6.23±0.07	(31±3)
46	93.00	5.71±0.51	(28±4)
47	96.00	3.45±0.31	(36±1)
48	86.00	**0.046±0.010**	(44±2)
49	95.00	**0.366±0.024**	**4.52±0.25**
50	86.00	**0.086±0.002**	**1.20±0.13**
51	96.00	**1.76±0.35**	**1.65±0.06**
52	93.00	2.78±0.35	(13±1)
53	98.00	**1.24±0.04**	**4.83±0.22**
Anthraquinones			
54	29	8.43±1.03	(40±5)
55	91.00	6.10±0.61	(36±1)
56	98.00	5.50±0.19	**2.82±0.17**
57	91.00	5.76±1.03	(48±4)
58	88.00	3.25±0.41	**5.02±0.18**
59	94.00	**1.79±0.11**	**4.94±0.25**
60	-	-	-
61	96.00	6.10±0.75	(31±5)
62	97.00	8.50±0.64	(39±4)
63	99.00	3.86±0.04	(27±2)
64	100.00	**0.093±0.011**	**0.883±0.032**
65	100.00	**0.195±0.025**	**1.62±0.17**
66	101.00	**1.10±0.02**	**1.56±0.35**
67	99.00	3.48±0.33	16±2
68	101.00	2.43±0.37	**2.12±0.27**
69	104.00	**0.87±0.07**	**1.76±0.29**
Quercetin	0.82 ± 0.07	-	-
Donepezil	-	0.021 ± 0.002	2.3 ± 0.1

[a]Values represent the mean of two/three independent experiments; SEM <10%. [b] % Inhibition at 10 µM (eeAChE and esBChE) or 100 µM (Aβ aggregation).

The results relative to the direct inhibition of Aβ experienced by naphthoquinone **38**-**53** show that all compounds exert an inhibitory activity. The 1-methyl-piperazine series proved to be the less efficient, while the other series display a percentage inhibition in the range 86-98% at 10 μM. This finding further supports the importance of the presence of lipophilic substitutions, like an aromatic moiety, as decoration of the side chain of these compounds, thus providing an appropriate interaction with Aβ and preventing its aggregation. As regards the length of the polymethylene chain, a greater inhibitory activity has been exhibited either by derivatives without a linker (**39**-**41**) or by those endowed with a spacer of 3-4 carbon atoms. Therefore, this information prompted me to expand this set of compounds including also some homologues characterized by linkers of 5 and 6 carbon atoms.

Interestingly, all compounds have shown to inhibit the AChE activity in an IC_{50} range of 0.046-6.23 μM. Also for this set, the activity profile is generally preferential for AChE over BChE; indeed, only a few number of compounds (**49**, **50**, **51**, **53**) behave as dual ChEs inhibitors.

The benzyl-piperazine naphthoquinones provided the greatest potency against AChE, with compounds **48** and **50** displaying, respectively, nanomolar IC_{50} values equal to 46 and 86 nM. Concerning the role played by the polymethylene spacer, a peak of activity may be observed when its length is of 2 and 4 carbonaceous units. For the BChE inhibitory activity, the two best performing series are the benzyl-piperazine derivatives, see compounds **49** and **50** (IC_{50} 4.52 and 1.20 μM), and the phenyl-piperidine ones, see compounds **51** and **53**, (IC_{50} 1.65 and 4.83 μM).

As for naphthoquinone derivatives, also anthraquinone derivatives **54**-**69** (with the exception of **60** which is still under investigation) are able to inhibit Aβ aggregation. With the only exception of **54** (%$_{inhib.}$= 29), these derivatives displayed a strong inhibition of Aβ aggregation, in the range 88-104%. The activity increases proportional to the increase of the length of the polymethylene linker, although the main feature, crucial for the activity, seems to be the overall lipophilic nature of these derivatives.

All the anthraquinones have shown to inhibit the acetylcholinesterase activity, with an IC_{50} value in the range 0.093-8.53 μM, and interestingly, 8 compounds out of 15 have proven also to inhibit BChE, in the range 0.883-5.02 μM; thus, anthraquinones may be considered as dual ChEs inhibitors. The benzyl-piperazine series has shown to be the most active against both enzymes, with the best results showed by compounds **64** (IC_{50} AChE= 0.093 μM, IC_{50} BChE=

0.883 µM) and **65** (IC$_{50}$ AChE= 0.195 µM, IC$_{50}$ BChE= 1.62 µM), whereas compounds **59** (IC$_{50}$ AChE= 1.79 µM, IC$_{50}$ BChE= 4.94 µM) and **69** (IC$_{50}$ AChE= 0.87 µM, IC$_{50}$ BChE= 1.76 µM) displayed the highest potency among methyl-piperazine and phenyl-piperidine series, respectively. Except for the benzyl-piperazine series, for the other derivatives the trend of activity improves with the increase of the carbon units of the linker tethering the quinone moiety to the basic core.

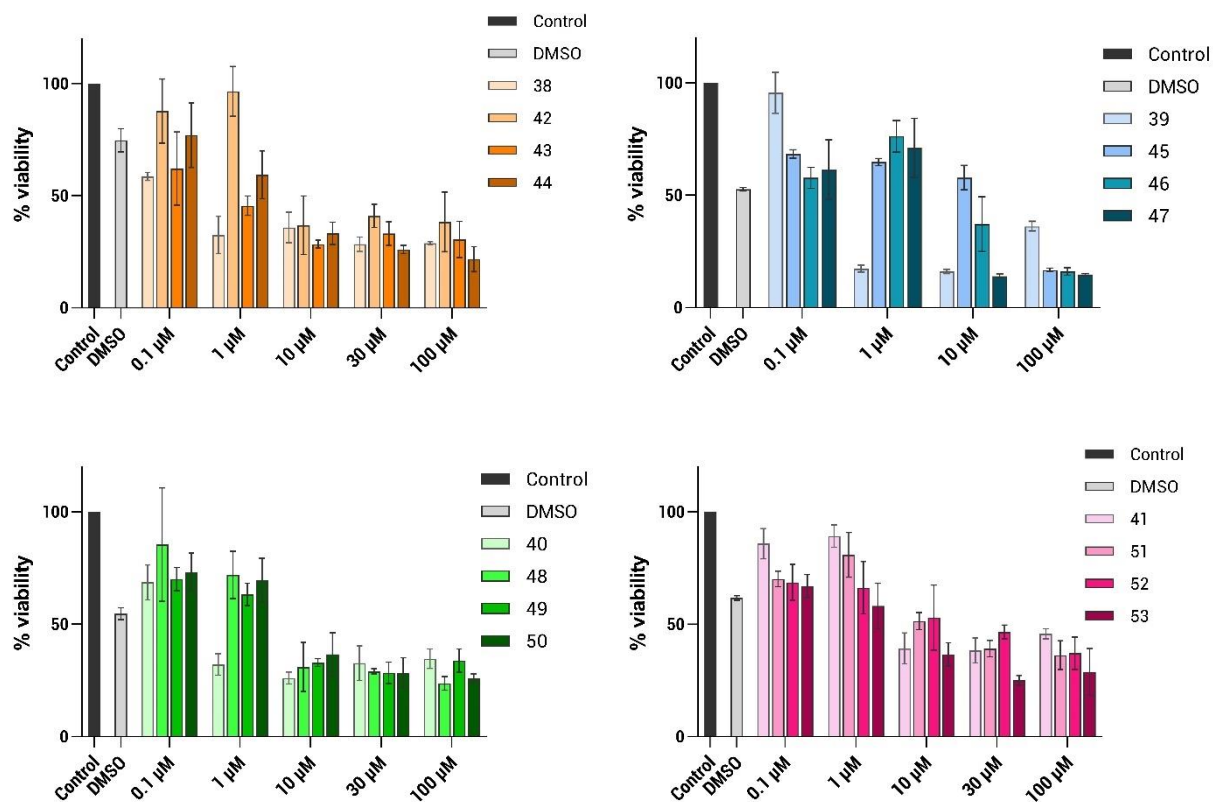## 8.3.2 Determination of cell viability

8.3.2.1 MTT assay

MTT test is a standard colorimetric assay for assessing cell metabolic activity[329]. The yellow MTT is reduced by succinate dehydrogenase to purple insoluble formazan (**Figure 53**) in the mitochondria of living cells, and the level of reduction activity is a measure of cells viability.
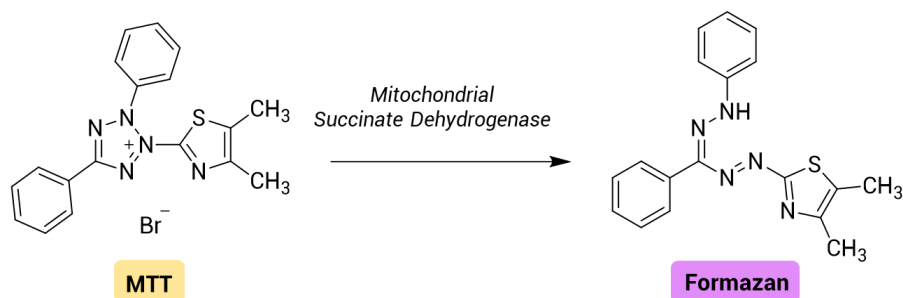
FIGURE 53| Metabolism of MTT to a formazan salt by viable cells as shown in the chemical reaction.

The mitochondrial-dependent reduction of MTT to formazan was used to exclude a cytotoxic effect of the compounds in primary neurons prepared from CD1 mouse embryos, and, for some compounds also in SHSY-5Y neuroblastoma cells. Each compound was dissolved in DMSO and tested in a concentration range between 0.1 µM and 100 µM for 24 h (**Figures 54-56**).

Data are presented as a percentage by comparison with the respective vehicle control. All data from MTT measurements are expressed as Formazan blue % production of control, considered as maximum formazan blue formation (100%).

FIGURE 54| Determination of cell viability after exposure to different concentration (0.1,1,10,30,100 μM) of naphthoquinone compounds for 24 h of primary cultures of mouse cortical neurons. (orange: methyl-piperazine series; blue: phenyl-piperazine series; green: benzyl-piperazine series; pink: phenyl-piperidine series) Data are presented as percentage relative to their vehicle controls, considered as 100%, obtained from the mean ± SD of three experiment.
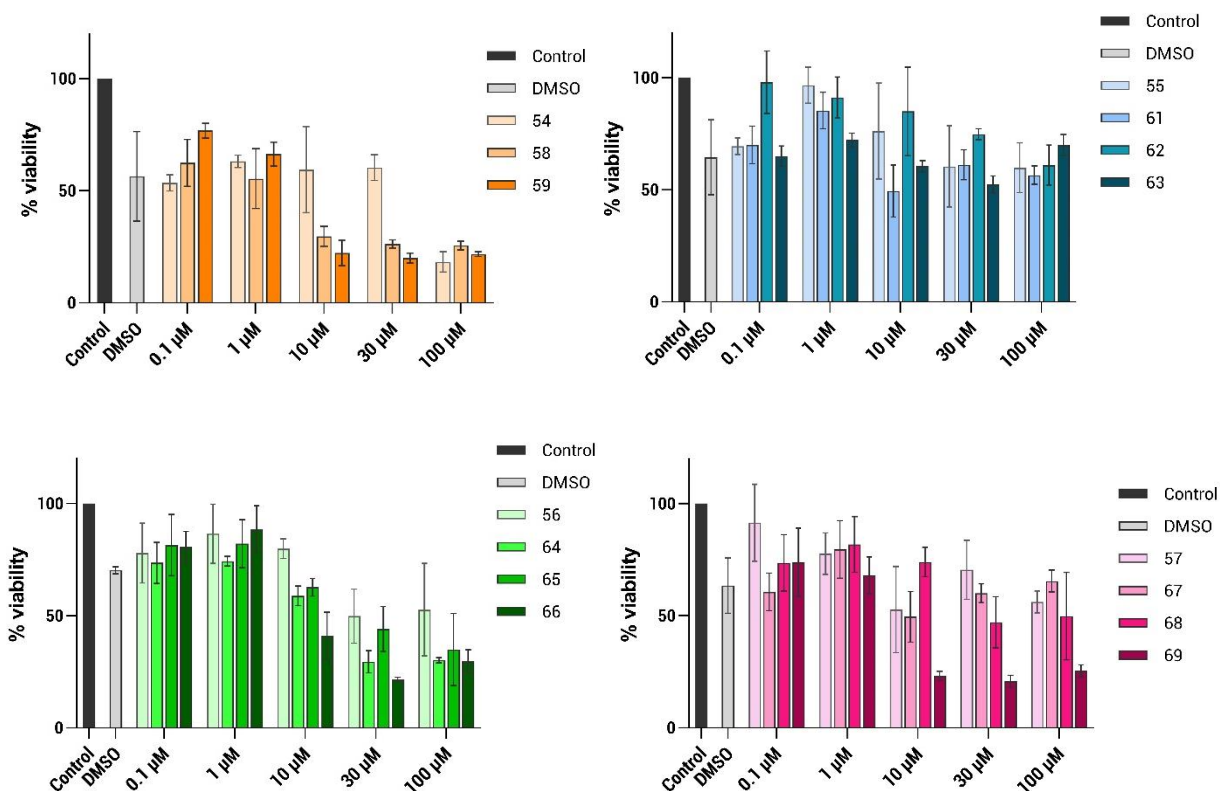
FIGURE 55| Determination of cell viability after exposure to different concentration (0.1,1,10,30,100 μM) of anthraquinone compounds for 24 h of primary cultures of mouse cortical neurons. (orange: methyl-piperazine series; blue: phenyl-piperazine series; green: benzyl-piperazine series; pink: phenyl-piperidine series) Data are presented as percentage relative to their vehicle controls, considered as 100%, obtained from the mean ± SD of three experiment.

In general, the compounds demonstrated to have a progressive toxicity in the concentration range 0.1-100 μM. Whereas for some anthraquinones, see compounds **63**, **66**, **67**, **68** and **69**, the 100 μM concentration allows to display a safer profile than the 30 μM one, and this fact may be explained by their low and irregular solubility at high concentrations in DMSO.

Comparing the two scaffolds, the anthraquinone derivatives appear to be less toxic for the neurons than naphthoquinones.

In regard to the lateral chain some considerations can be made. First, the methyl-piperazine substituent results to exert the most cytotoxic effect; whereas the phenyl-piperidine and phenyl-piperazine moieties proved to be the safest among naphthoquinones and anthraquinones, respectively. In general, the increase of the length of the linker, even though from one hand it is associated with a gain of the activity, from the other hand it is responsible for an increase of toxicity.

Finally, it is worthy of note that the compounds, in the concentration range 0.1-10 µM, showed to be safer than the DMSO alone, suggesting they may exert some protective behavior for the cells towards the intrinsic toxicity of DMSO (around 50-60%).

SHSY-5Y neuroblastoma cells were found less sensitive than primary neurons (Figure 56). Moreover, in this cell line, the derivatives displayed to be less toxic than DMSO alone even at the highest concentration tested (100 µM). Concerning the experimental conditions, cells were cultured using two different types of medium, that differ one from the other for the presence/absence of bovine foetal serum. If the toxicity experienced by DMSO alone appeared to be similar in the two types of medium, all the compounds proved to be safer in the serum free medium.

Interestingly, in these experiments the toxicity profile does not increase with the compound's concentration contrary to what observed in primary neurons. Both compounds **55** and **66** were found to be safer at 10 µM concentration since cell viability exceeded the 90%.
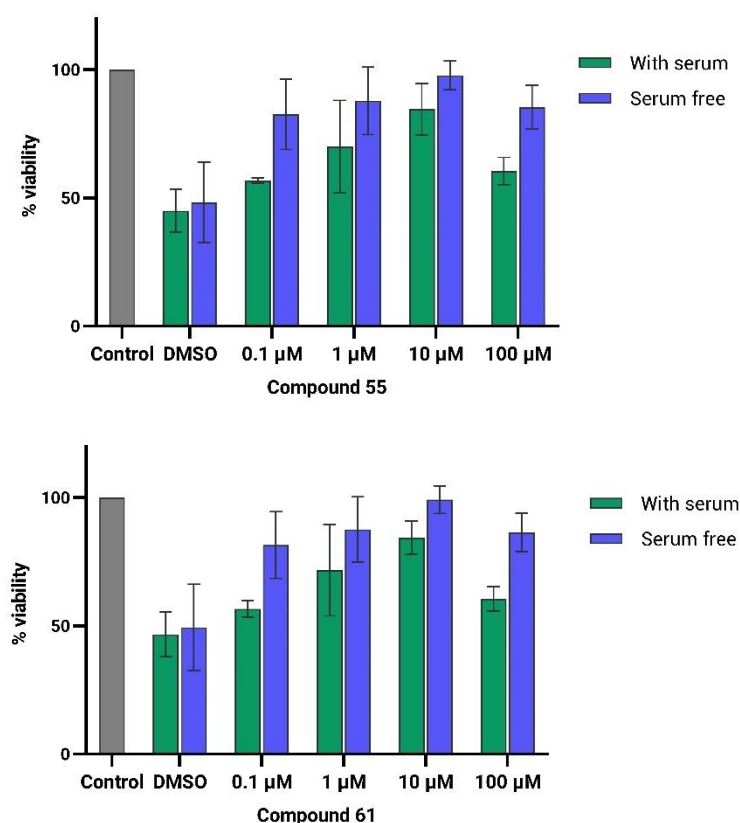
FIGURE 56| Determination of cell viability after exposure to different concentration (0.1,1,10,100 µM) of compounds **55** and **61** for 24 h of SHSY-5Y neuroblastoma cell lines. Cells were cultured using two different types of medium (with and without foetal bovine serum) to explore the different behaviour. Data are presented as percentage relative to their vehicle controls, considered as 100%, obtained from the mean ± SD of three experiment.

8.3.2.2 LDH assay

Lactate dehydrogenase (LDH) assay is a colorimetric method to quantify cellular cytotoxicity by measuring extracellular LDH. LDH is a cytosolic enzyme present in different cell types and released into the surrounding cell culture medium after a damage to the plasma membrane. This enzyme can be quantified by a coupled enzymatic reaction in which LDH catalyzes the conversion of lactate to pyruvate via NAD+ reduction to NADH. The oxidation of NADH leads to the reduction of tetrazolium salt (INT) to a red formazan (**Figure 19**). The level of formazan formation is directly proportional to the amount of LDH released in the medium, which is considered as a measure of cytotoxicity.
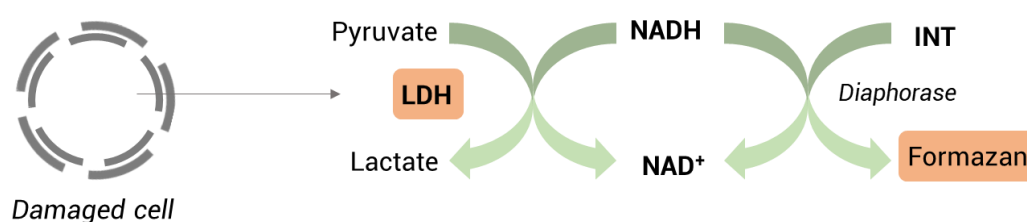
FIGURE 57| Schematic of LDH cytotoxicity assay mechanism.

LDH assay was performed on some selected compounds among derivatives **38**-**69** in order to validate the results gathered from MTT test (**Figures 58**-**59**).

As observed with the MTT test, anthraquinone derivatives have proven to be endowed with a better safety profile with respect to naphthoquinone ones; however, in this experiment, problems with their solubility at high concentrations might cause interferences with the absorbance measurements, as some compounds at 100 µM crystalized among the cells.
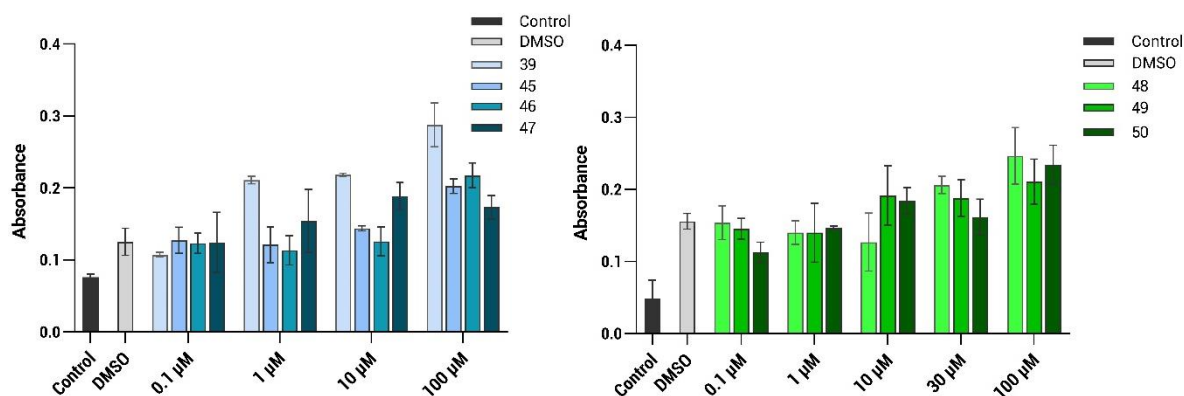
FIGURE 58| Cytotoxicity determination after exposure to different concentration (0.1,1,10,30,100 μM) of naphthoquinone compounds for 24 h of primary cultures of mouse cortical neurons. (blue: phenyl-piperazine series; green: benzyl-piperazine series) Data are presented as the absorbances calculated from the difference in measurements at 490 nm and 655 nm, obtained from the mean ± SD three experiment.
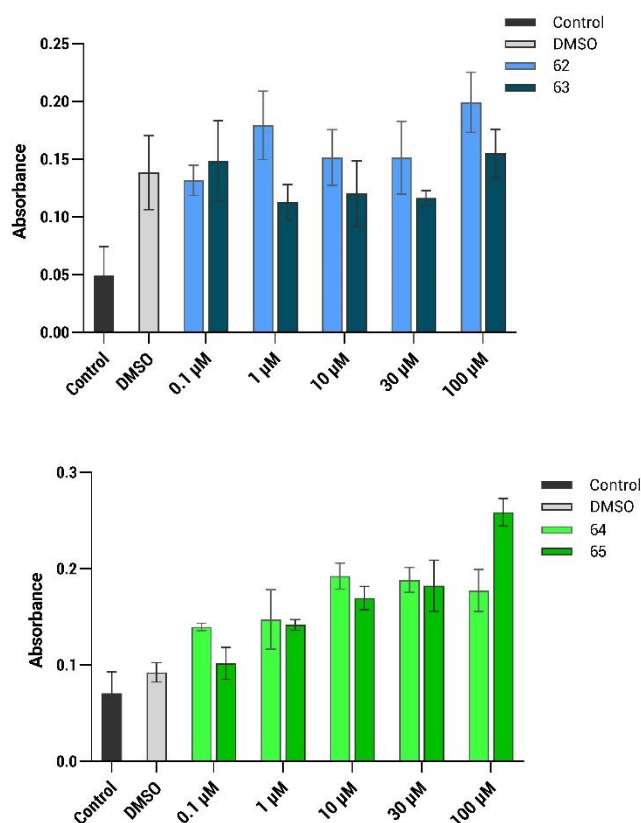
FIGURE 59| Cytotoxicity determination after exposure to different concentration (0.1,1,10,30,100 μM) of anthraquinone compounds for 24 h of primary cultures of mouse cortical neurons. (blue: phenyl-piperazine series; green: benzyl-piperazine series) Data are presented as absorbances calculated from the difference in measurements at 490 nm and 655 nm, obtained from the mean ± SD of three experiment.

124

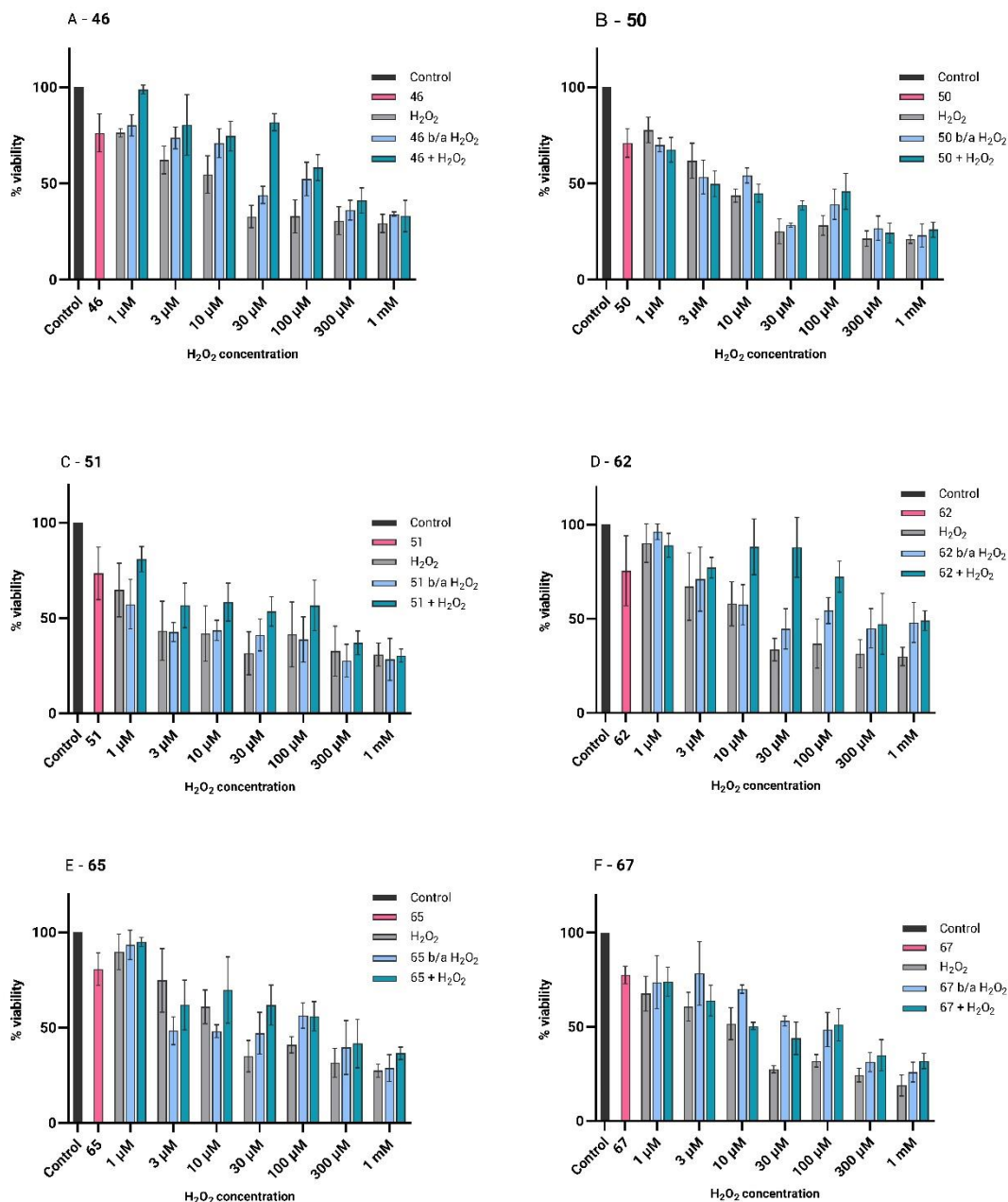### 8.3.3 Neuroprotection against hydrogen peroxide

The neuroprotective effect of the derivatives against hydrogen peroxide (H_2O_2) was evaluated by MTT assay on cortical neurons exposed for 30 min to different concentration of H_2O_2 (1 µM – 1 mM). The neuroprotective potential of compounds **46**, **50**, **51**, **62**, **65**, **67** was evaluated through two methods (i) exposing primary neurons to each compound (1 µM concentration) for 18 h before the treatment with H_2O_2 and for further 6 h after the treatment; (ii) exposing primary neurons to each compound (1 µM concentration) for 18 h before the treatment with H_2O_2, during the exposition to H_2O_2, and for further 6 h after the treatment.

Cell viability after the exposure was then measured with MTT test (**Figures 60-61**). The viability of cells treated with H_2O_2 (1 µM – 1 mM) decreased to a range of 30–70 % compared to the untreated cells (considered as 100%). In the presence of the compounds, a partial viability recovery was generally observed, with compounds **46** and **62** as the best neuroprotective agents.

Despite quinone nucleus is a well know scaffold for its redox potential, the compounds did not show a relevant neuroprotective activity; this is probably due to the intrinsic toxicity of the compounds combined with that of DMSO used as solvent. Homogeneous results were met in the concentration range of 10-300 µM, while at lower concentration of H_2O_2 a certain discrepancy has been observed.

Definitely, with very few exceptions, the exposure of the cells to H_2O_2 in the presence compounds proved to ameliorate the neuroprotective activity with respect to the exposure to H_2O_2 alone.

The same experimental conditions were carried out for compounds **50** and **65** in SHSY-5Y neuroblastoma cells (data not showed). However, data obtained exposing this cell line to hydrogen peroxide were not proportional to the concentration used, and most importantly, they were not reproducible.

FIGURE 60| Schematic of neuroprotection results. The neuroprotective activity of compounds **46**, **50**, **51**, **62**, **65**, **67** (1 µM) was evaluated in cortical neurons exposed hydrogen peroxide (1, 3, 10, 30, 100, 300 µM; t= 30 min). Untreated cells (black bars) were considered as 100%. Compounds treated cells (pink bars). Cell treated with increasing concentration of H_2O_2 (grey bars). Compounds were applied to the cells 18 h before the exposure and immediately following the removal of H_2O_2 and toxicity assessed by MTT test (light blue bars). Compounds were applied to the cells 18 h before the exposure, together with, and immediately following the removal of H_2O_2 and toxicity assessed by MTT test (blue bars). Data are presented as percentage relative to their vehicle controls, considered as 100%, obtained from the mean ± SD of three experiment.

.
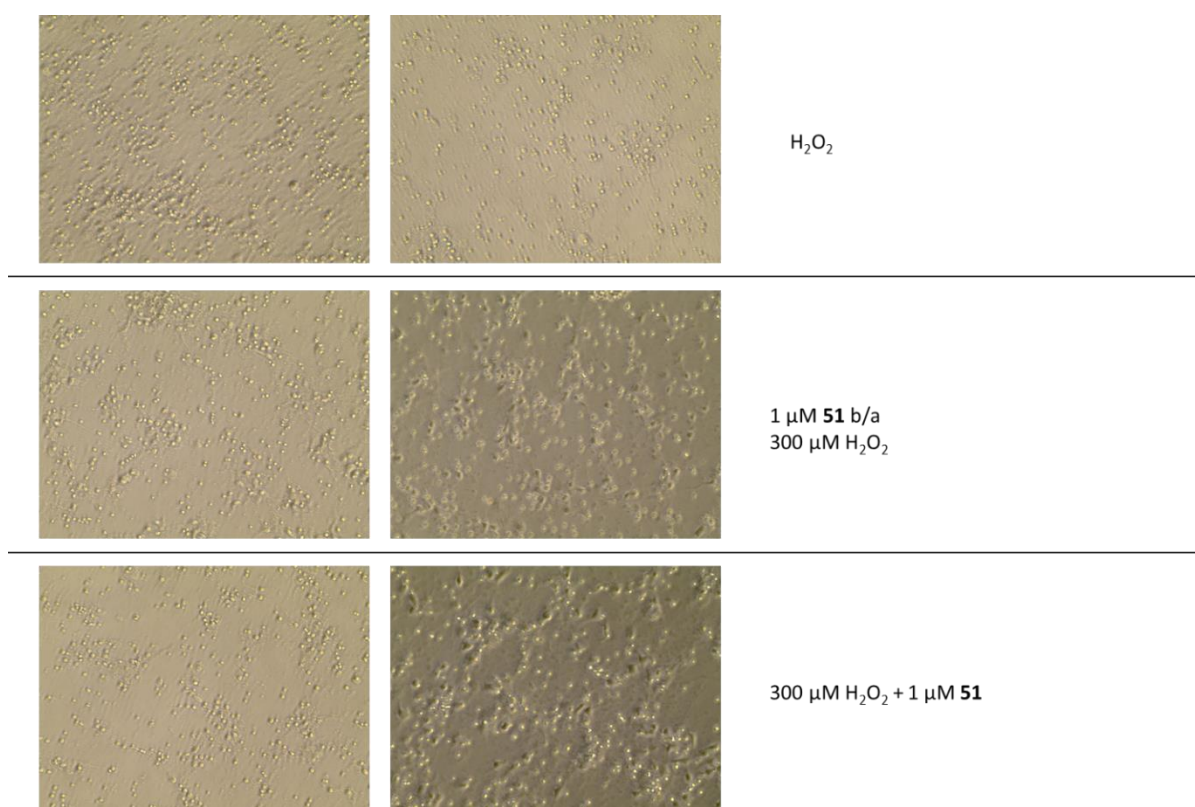
FIGURE 61| Images obtained after exposure of primary neurons to (A) 300 µM of hydrogen peroxide for 30 minutes; (B) 1 µM of compound **51** for 18 h before the application of 300 µM of hydrogen peroxide for 30 minutes and for 6 h after; (C) 1 µM of compounds **51** for 18 h before, 6 h after and during the application of 300 µM of hydrogen peroxide for 30 minutes.

8.3.4 Dual-Glo luciferase gene reporter assay

Four promising MTDLs, namely compounds **46**, **51**, **65** and **67**, were also tested with a cell based reporter gene assay, established in primary neurons, that allows the identification of γ−secretase mediated APP processing modulators[330].

The APP-Gal4 assay utilizes the well-known Gal4-UAS system and takes advantage of the fact that APP is a type I transmembrane protein, meaning the holoprotein is retained at cell membranes. The assay measures level of transfected APP_{695} processing in primary neurons by coupling this processing, via Gal4-UAS system, to transcription of a luciferase gene. To enable this to occurs, a number of plasmids must be chemically transfected into the primary neurons. The plasmid pRC-APP_{695}-Gal4, encodes full length human APP_{695} with the yeast transcription factor Gal4 inserted in frame at its C terminus via a glycine linker, allowing expression of the fusion protein APP-Gal4[331]. Following γ-secretase mediated APP cleavage, an AICD-Gal4 fragment is released, which, unlike the full-length protein, is free to translocate and binds to the synthetic,

127

Gal4 specific, UAS promoter of a second plasmid pFR-luciferase, which encodes the Firefly luciferase gene (**Figure 62**). Firefly luciferase expression can be quantified through a standard luminescence assay. A third plasmid, TK-Renilla is also transfected, which constitutively expresses the *Renilla* luciferase gene, acting as an internal control to which the Firefly luminescence values can be standardized.
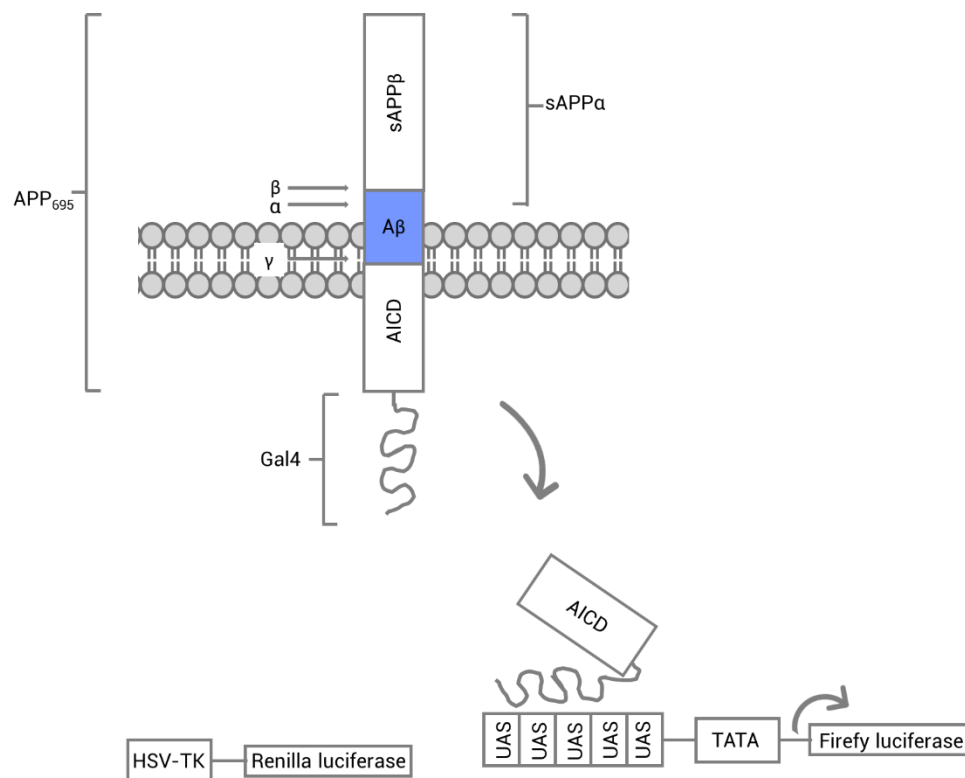
FIGURE 62| Schematic representation of APP-Gal4 gene reporter assay which measures γ-secretase mediated APP processing. Cleavage by γ-secretase of human APP$_{695}$ fused to the yeast transcription factor Gal4 (APP-Gal4) allows the release of AICD-Gal4. Free AICD-Gal4 then binds to the synthetic promoter of Firefly luciferase plasmid (consisting of 5 UAS repeats and a TATA box), driving the expression of reporter gene Firefly luciferase. Resultant Firefly luciferase expression changes are measured relative to an independent *Renilla* luciferase signal.

Transfected neurons were treated with compounds at 1 µM concentration and processed 24 h post-transfection for quantification of firefly luciferase and *Renilla* luciferase expression (**Figure 63**).

All the four derivatives were able to exert a strong inhibitory effect toward γ-secretase activity. Compound **51**, in particular, was found to be the best inhibitor, even better than the DAPT used as positive control. These encouraging results might be due to the ability of these derivatives to interact with a sequence of aromatic amino acids of APP which is retained in Aβ

128

structure. The ability of these quinone-derivatives to modulate APP processing and γ-secretase activity will deserve further investigations.
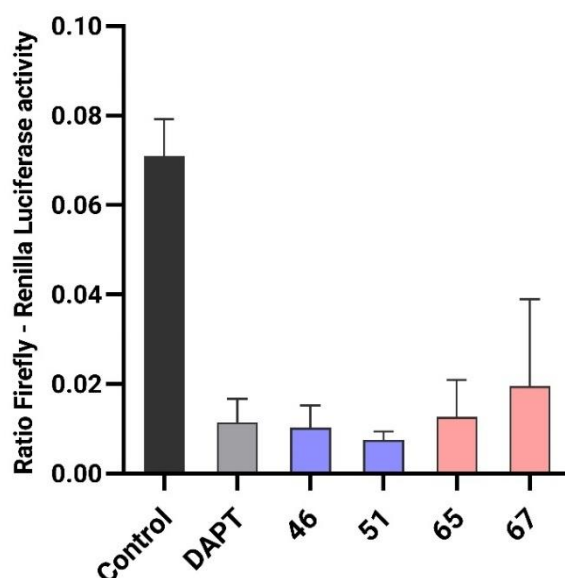
FIGURE 63| Schematic of dual-Glo luciferase gene reporter assay results. APP-Gal4 driven luciferase gene reporter activity reports amyloidogenic processing in primary cortical neurons. Five DIV primary mouse cortical neurons chemically transfected with 0.1 μg APP-Gal4, pFR-Luciferase and TK-Renilla plasmids using 1μL/well Lipofectamine 2000. Data are obtained from the ratio between the firefly and Renilla luminescence measurements, respectively, and gather from the mean of quadruplicate experiment. Blue and pink filling colours are for naphthoquinones and anthraquinones, respectively.

8.4 Conclusion

Compounds of the third set were able to display an inhibitory activity against both AChE and BChE and on the spontaneous aggregation of Aβ. These satisfying results prompt us to perform more in-depth analysis of their biological activity, investigating them in other pathways involved in AD, such as oxidative stress and APP processing.

Even though quinone scaffold is known for its redox potential, not all the compounds tested were capable of preventing H_2O_2 toxicity. In particular, compounds **46** and **62** displayed the best neuroprotective activity. In order to strengthen the link between their protective effect and their redox potential, additional tests should be performed.

Surprisingly, the four compounds tested by means of the dual-Glo luciferase gene reporter assay were found to be strong inhibitors of γ−secretase, being comparable to DAPT used as control (which reduced luciferase expression by approximately 80%). In case of compound **51** the inhibitory activity was even higher than that of DAPT. All together, these results show that these derivatives may provide different potential benefit to AD as non-toxic agents.

9. FOURTH SET

9.1 Project

On the base of promising results gathered from previous studies on the third set of quinones **38**-**69** as MTDLs, I focused my research activity on the functionalization of the benzyl-piperazine motif in the lateral chain of the naphthoquinone scaffold. In particular, the substitution of the aromatic ring was explored, including the electron-withdrawing chlorine atom and the electro-donating methoxy group, with a view to investigating their influence for the inhibition of ChEs and Aβ aggregation (**Figure 64**).


o-Cl	84
m-Cl	85
p-Cl	86
o-OCH$_3$	87
m-OCH$_3$	88
p-OCH$_3$	89

	o-Cl	*m*-Cl	*p*-Cl	*o*-OCH$_3$	*m*-OCH$_3$	*p*-OCH$_3$
n=1	90	94	98	102	106	110
n=2	91	95	99	103	107	111
n=3	92	96	100	104	108	112
n=4	93	97	101	105	109	113
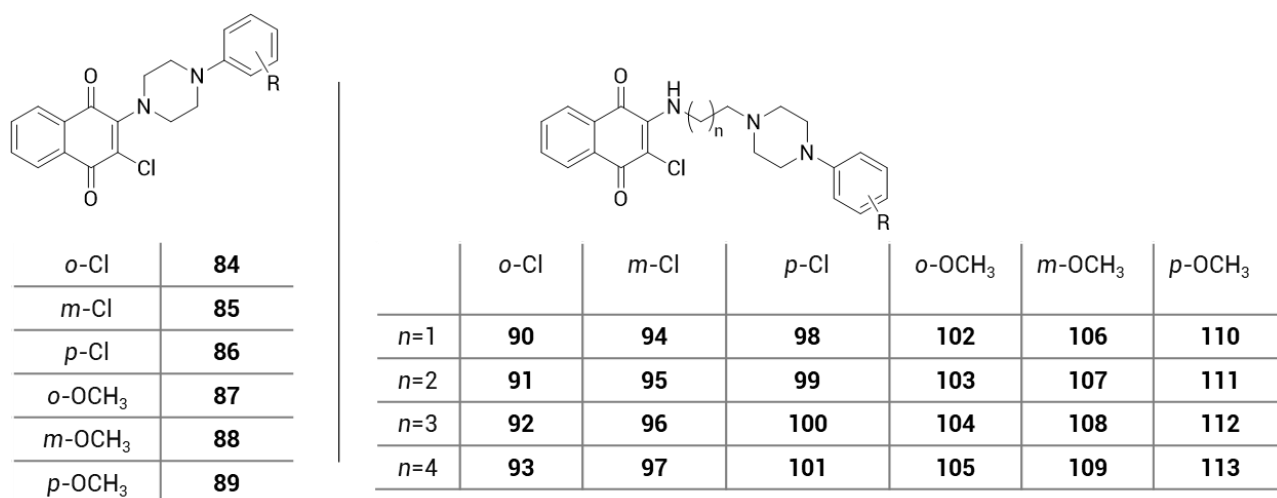
FIGURE 64| Structure of the investigated naphthoquinone derivatives **84**-**113**.

9.2 Chemistry

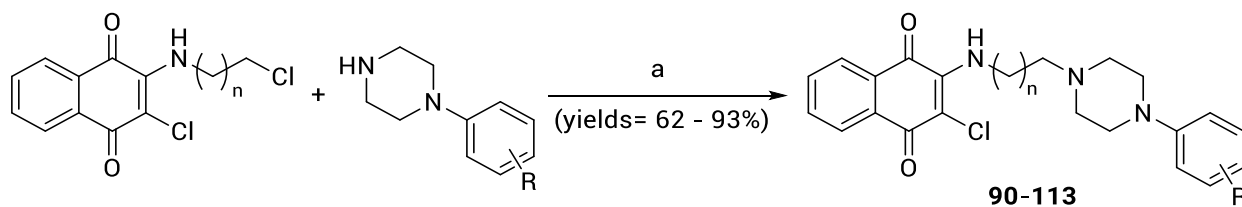Concerning the fourth of compounds, derivatives **84-89** were obtained by reacting the 2,3-dichloro-1,4-naphthoquinone, previously suspended in CH$_3$CN, with the proper amine in a molar ratio 1:2 (**Scheme 21**).
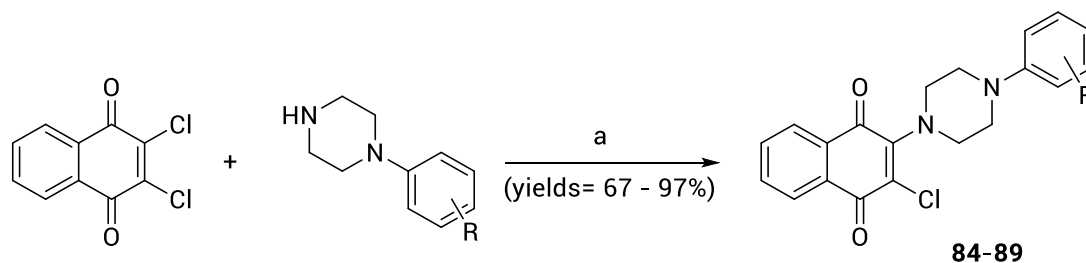
R=	*o*-Cl	*m*-Cl	*p*-Cl	*o*-OCH$_3$	*m*-OCH$_3$	*p*-OCH$_3$
	84	85	86	87	88	89

Scheme 21. Reagents and conditions: a) CH$_3$CN 100 °C 24 h.

Finally, for derivatives **90-113** it was necessary to first prepare the appropriate chloro-alkylamino reagents using the same two synthetic steps depicted in **Scheme 16**; then the reaction of the intermediates in a molar ratio 1:2 with the proper N-aryl piperazine in sealed tube afforded the desired products (**Scheme 22**).

R=	o-Cl	m-Cl	p-Cl	o-OCH$_3$	m-OCH$_3$	p-OCH$_3$
n=1	90	94	98	102	106	110
n=2	91	95	99	103	107	111
n=3	92	96	100	104	108	112
n=4	93	97	101	105	109	113

Scheme 22. Reagents and conditions: a) CH$_3$CN 100 °C 24 h.

The structures of the novel compounds have been confirmed using ^{1}H and ^{13}C NMR, and elemental analysis. The purity of compounds (checked by elemental analysis) has been in all cases >95%.

9.3 In vitro biological profiling

9.3.1 Inhibition of self-induced Aβ aggregation and Cholinesterases

As for the aforementioned quinone-based derivatives, the novel compounds **84-113** have been evaluated for their inhibitory activity against eeAChE, esBChE, and the spontaneous aggregation of Aβ$_{40}$, performed by Prof. Marco Catto – University of Bari. The inhibitory activities on AChE and BChE are listed in **Table 9** as IC$_{50}$ values for the most active compounds or as percent inhibition at 10 µM for less active compounds. *In vitro* inhibition of Aβ$_{40}$ aggregation data are listed in **Table 9** as IC$_{50}$ values for the most active compounds or as percent inhibition at 100 µM for less active (i.e., <80%) compounds.

Table 9. Inhibitory activities of compounds against $A\beta_{40}$ aggregation, eeAChE and esBChE [a].

	Cpd	IC_{50} (μM) or (% inhibition)[b]		
		$A\beta_{40}$ aggr.	*ee*AChE	*es*BChE
o - Cl	**84**	*85.00*	*(58±2)*	*(14±1)*
	90	89.00	*(61±5)*	*(21±3)*
	91	97.00	*(60±1)*	*(39±4)*
	92	95.00	**2.99±0.42**	*(49±3)*
	93	98.00	*(62±1)*	(53±2)
m - Cl	**85**	91.00	*(55±2)*	*(13±3)*
	94	86.00	*(56±3)*	(12±3)
	95	101.00	*(61±2)*	(16±4)
	96	97.00	*(60±2)*	(22±2)
	97	99.00	*(60±3)*	(23±4)
p - Cl	**86**	90.00	*(52±3)*	(20±3)
	98	95.00	*(54±4)*	(15±4)
	99	96.00	*(56±1)*	(17±4)
	100	86.00	*(51±1)*	(51±3)
	101	100.00	*(69±2)*	(20±3)
o − OCH₃	**87**	98.00	*(54±2)*	(11±3)
	102	98.00	*(59±1)*	*(15±3)*
	103	95.00	*(60±2)*	*(19±2)*
	104	97.00	*(68±1)*	*(37±2)*
	105	98.00	*(67±1)*	(46±1)
m − OCH₃	**88**	95.00	*(59±4)*	*(15±4)*
	106	97.00	*(60±2)*	(12±3)
	107	98.00	*(66±1)*	(19±3)
	108	98.00	**7.27±0.14**	(27±1)
	109	99.00	*(69±1)*	(34±3)
p − OCH₃	**89**	97.00	*(62±2)*	(12±1)
	110	95.00	*(66±4)*	(14±3)
	111	97.00	*(65±2)*	(16±3)
	112	95.00	**6.99±0.54**	(17±2)
	113	98.00	**4.16±0.29**	(19±3)
	Quercetin	*0.82 ± 0.07*	*-*	*-*
	Donepezil	*-*	*0.021 ± 0.002*	*2.3 ± 0.1*

[a] Values represent the mean of two/three independent experiments; SEM <10%. [b] % Inhibition at 10 μM (eeAChE and esBChE) or 100 μM ($A\beta$ aggregation).

Compounds **84**-**113** have proven to inhibit Aβ$_{40}$ aggregation in the range 85-101% at 100 μM. The best compounds resulted to be the *m*-Cl derivative with a propylene linker (**95**), and the *p*-Cl derivative with a pentylene chain (**101**), which displayed an inhibition percentage of 101 and 100%, respectively. However, either the different substitution of the aromatic ring nor the length of the linker seem to influence the inhibitory behavior on Aβ aggregation, that does not significantly vary, suggesting for the naphthoquinone scaffold and the aromatic ring in the lateral chain as the main features able to assure the activity.

In regard to the inhibition of ChEs, the derivatives displayed inhibitory activity at 10 μM in the range of 51-69% against AChE and 11-53% against BChE. The best AChE inhibitor compounds resulted to be the *o*-Cl derivative with a butylene chain **92** (IC$_{50}$ = 2.99 μM), followed by the *p*-OCH$_3$ derivative with a five carbon atoms chain **113** which shows an IC$_{50}$ equal to 4.16 μM.

Once again, these compounds proved to be more selective toward AChE with respect to BChE. Whereas, compounds **100** and **105** demonstrated a similar inhibitory activity against the two enzymes. The compounds most active against AChE (**92**, **108**, **112**) present a polymethylene chain of four carbon units; however, as for the inhibition of Aβ aggregation, also for AChE the different substitutions and the length of the polymethylene chain somehow do not influence the inhibitory activity. Conversely, the inhibitory activity against BChE seems to improve with the increase of the carbon unit number of the linker.

9.4 Conclusion

The newly obtained derivatives demonstrated to be promising dual targeting inhibitors of Aβ aggregation and ChEs. The most active compounds against Aβ aggregation resulted to be **95** and **101**, with an inhibition percentage of 101 and 100%, respectively. The best performing AChE inhibitor were **92** with an IC$_{50}$ value equal to 2.99 μM, and **113** with an IC$_{50}$ value of 4.16 μM. In general, either the substitution of the aromatic ring nor the number of carbon atoms of the linker, significantly influenced the inhibitory profile against Aβ aggregation or AChE. Regarding BChE inhibition, the increase of the length of the linker seems to be beneficial for the activity.

This last study has allowed to deepen the SAR around the benzylpiperazine motif linked to the naphthoquinone scaffold, even if the structural changes introduced do not favor the improvement of the inhibitory activity against the investigated targets in comparison to the previous set which show a better MTDL profile.

Experimental Section

10. CHEMISTRY

Chemicals and solvents were purchased from Sigma-Aldrich (Milan, Italy). Mps: Büchi apparatus, uncorrected. ^{1}H NMR spectra and ^{13}C NMR spectra were recorded on a Varian Gemini-200 instrument at 200 and 50 MHz, respectively; CDCl$_3$ or DMSO-d6; δ in ppm rel. to Me$_4$Si as internal standard. J in Hz. Elemental analyses were performed on a Flash 2000 CHNS (Thermo Scientific) instrument in the Microanalysis Laboratory of the Department of Pharmacy, University of Genova. Results of elemental analyses and NMR spectra indicated that the purity of all compounds was ≥95%.

General method for the synthesis of naphthoquinone-derivatives (**1**-**4**)

A mixture of appropriate amine (2 mmol) and 2,3-dichloronaphthoquinone 1 (1 mmol) in absolute ethanol (20 mL) was stirred under reflux for 6 h. During the progress of the reaction, monitored by TLC, a change in the colour from yellow to red was observed. After evaporation of the solvent, the residue was purified by CC (SiO$_2$, CHCl$_3$+ 2%MeOH) or crystallized from EtOH.

2-Chloro-3-(phenylamino)-1,4-naphthoquinone (1)

Yield: 89%; M.p. 216-217°C
Elemental analysis for C$_{21}$H$_{14}$ClNO$_2$:

found:	C% 67.46	H% 3.56	N% 4.96
calcd.:	C% 67.74	H% 3.55	N% 4.94

^{1}H-NMR (200 MHz, CDCl$_3$) δ: 8.38-8.10 (m, 2H, arom); 7.98-7.65 (m, 2H, arom); 7.58-7.20 (m, 5H, arom); 6.27 (s, 1H, NH).

^{13}C NMR (200 MHz, CDCl$_3$) δ: 179.5, 176.5, 140.4, 136.3, 134.0, 131.9, 131.5, 128.8, 127.4, 126.1, 126.0, 124.6, 123.2, 113.9

2-(Benzylamino)-3-chloro-1,4-naphthoquinone (2)

Yield: 84%; M.p. 112-113°C
Elemental analysis for $C_{17}H_{12}ClNO_2$:

found:	C% 68.83	H% 4.19	N% 4.71
calcd.:	C% 68.58	H% 4.06	N% 4.70

^{1}H-NMR (200 MHz, CDCl$_3$) δ: 8.22-7.98 (m, 2H, arom); 7.82-7.59 (m, 2H, arom); 7.50-7.20 (m, 5H, arom); 6.26 (s, 1H, NH); 5.08 (d, J = 6 Hz, 2H, CH$_2$).

^{13}C NMR (50 MHz, CDCl$_3$) δ: 179.4, 175.9, 143.0, 136.8, 133.9, 131.5, 128.7, 128.0, 127.0, 126.6, 125.8, 47.9

2-Chloro-3-(phenethylamino)-1,4-naphthoquinone (3)

Yield: 48 %; M.p. 115-116°C
Elemental analysis for $C_{18}H_{14}ClNO_2$:

found:	C% 69.18	H% 4.84	N% 4.38
calcd.:	C% 69.35	H% 4.53	N% 4.49

^{1}H-NMR (200 MHz, CDCl$_3$) δ: 8.21-7.90 (m, 2H, arom); 7.80-7.54 (m, 2H, arom); 7.41-7.15 (m, 5H, arom); 6.11 (s, 1H, NH); 4.11 (q, J = 7 Hz, 2H, NHCH$_2$CH$_2$CH); 2.99 (d, J = 7.2 Hz, 2H, NHCH$_2$CH$_2$CH).

^{13}C NMR (50 MHz, CDCl$_3$) δ: 179.3, 175.8, 142.9, 136.7, 133.8, 131.5, 131.4, 128.6, 127.7, 125.7, 44.9, 36.2

2-Chloro-3-(phenylpropylamino)-1,4-naphthoquinone (4)

Yield: 75 %; M.p. 94-96°C
Elemental analysis for $C_{19}H_{16}ClNO_2$:

found:	C% 70.30	H% 5.17	N% 4.17
calcd.:	C% 70.05	H% 4.95	N% 4.30

^{1}H-NMR (200 MHz, CDCl$_3$) δ: 7.82-7.60 (m, 2H, arom); 7.41-7.18 (m, 5H, arom); 6.15 (s, 1H, NH); 3.90 (q, J = 7 Hz, 2H, NHCH$_2$CH$_2$CH$_2$Ar); 2.77 (t, J = 7.6 Hz, 2H, NHCH$_2$CH$_2$CH$_2$Ar); 2.07 (quint, J = 6.8 Hz, 2H, NHCH$_2$CH$_2$CH$_2$Ar).

^{13}C NMR (50 MHz, CDCl$_3$) δ: 179.4, 175.8, 143.0, 139.7, 133.9, 131.7, 131.4, 128.6, 127.5, 127.3, 125.8, 125.2, 43.2, 31.8, 31.5.

General method for the synthesis of intermediates: tryptamine, 2-(benzimidazol-1-yl)ethylamine and 2-(benzotriazol-1-yl)ethylamine

To a suspension of $LiAlH_4$ (40 mmol) in 20 mL of anhydrous THF cooled at 0-5°C, a solution of 3-indolylacetamide or 2-(benzimidazol-1-yl)acetonitrile or 2-(benzotriazol-1-yl)acetonitrile (10 mmol) in anhydrous THF (5 mL) was added drop by drop in 20 min. Then the mixture was refluxed for 8-10 h. At r.t. 5 mL of H_2O, 5 mL of 2N NaOH and 5 mL of H_2O were carefully added to the mixture to decompose the excess of $LiAlH_4$, filtering and washing the inorganic residue with Et_2O. The solution was dried with Na_2SO_4, filtered and evaporated to dryness, yielding an orange oil corresponding to the title ethylamino derivative that was cromatographed on SiO_2 eluting with Et_2O.

2-(Benzotriazol-1-yl)ethylamine was also prepared from the 2-[2-(1H-benzotriazol-1-yl)ethyl]phthalimide (2 mmol) dissolved in 10.5 mL of HCl refluxed for 17 h. The crystals of phthalic acid were removed by filtering and washing with H_2O; the aqueous solution was treated with NaOH 6N and extracted with CH_2CH_2. The organic solution was then dried with Na_2SO_4, filtered and evaporated to dryness, yielding a yellow oil corresponding to the expected product.

These intermediates were already prepared through different procedures, thus they were characterized as follows.

Tryptamine

Yield: 81 %;
Elemental analysis for $C_{10}H_{12}N_2$:

found:	C% 74.81	H% 7.95	N% 17.23
calcd.:	C% 74.97	H% 7.55	N% 17.48

^{1}H-NMR (200 MHz, $CDCl_3$) δ: 10.11 (s, NH of Indole), 7.71−7.52 (m, 2H, arom.), 7.39−7.20 (m, 2H, arom.), 7.16-7.03 (m, 1H, arom.), 4.88 (broad s, NH_2), 3.09-2.95 (m, 4H, CH_2CH_2-NH_2).

2-(Benzimidazol-1-yl)ethylamine

Yield: 76 %;
Elemental analysis for $C_9H_{11}N_3$:

found:	C% 66.91	H% 6.79	N% 26.31
calcd.:	C% 67.06	H% 6.88	N% 26.07

^{1}H-NMR (200 MHz, CDCl$_3$) δ: 8.21 (s, 1H, arom.), 7.65−7.49 (m, 2H, arom.), 7.35−7.21 (m, 2H, arom.), 4.97 (broad s, NH$_2$), 4.19−4.01 (m, 2H, N-CH$_2$), 3.16-3.07 (m, 2H, CH$_2$-NH$_2$).

2-(Benzotriazol-1-yl)ethylamine

Yield: 76 %;
Elemental analysis for C$_8$H$_{10}$N$_4$:

	found:	C% 59.01	H% 6.56	N% 34.16
	calcd.:	C% 59.24	H% 6.21	N% 34.54

^{1}H-NMR (200 MHz, CDCl$_3$) δ: 8.11-7.71 (m, 2H, arom.), 7.52-7.31 (m, 2H, arom.), 5.01 (broad s, NH$_2$), 4.22 (pseudo s, 2H, N-CH$_2$), 3.45 (pseudo s, 2H, CH$_2$-NH$_2$).

General method for the synthesis of naphthoquinone-derivatives (**5-7**)

A mixture of appropriate amine (5 mmol) and 2,3-dichloronaphthoquinone 1 (2.5 mmol) in methanol (20 mL) was stirred at room temperature for 20-24 h. During the progress of the reaction, monitored by TLC, a change in the colour from yellow to red was observed. After evaporation of the solvent, the residue was treated with a solution of 2N NaOH and CHCl$_3$. The layers were separated, and the chloroform solution was dried (Na$_2$SO$_4$), filtered and evaporated, affording a residue that was purified by CC (SiO$_2$, CHCl$_3$+ 2%MeOH).

2-[2-(1*H*-indol-3-yl)ethylamino]-3-chloro-1,4-naphthoquinone (5)

Yield: 59 %; M.p. 140°C
Elemental analysis for C$_{20}$H$_{15}$ClN$_2$O$_2$:

	found:	C% 66.45	H% 4.46	N% 7.45
	calcd.:	C% 66.70	H% 4.16	N% 7.78

^{1}H-NMR (200 MHz, CDCl$_3$) δ: 10.84 (s, 1H, NH indolic); 8.28-7.40 (m, 6H, 1H NH + 5H arom); 7.38-6.79 (m, 4H, arom); 4.17-3.79 (m, 2H, NH<u>CH$_2$</u>CH$_2$CH); 3.18-2.80 (m, 2H, NHCH$_2$<u>CH$_2$</u>CH).

^{13}C NMR (50 MHz, CDCl$_3$) δ: 179.7, 175.5, 141.9, 135.8, 134.4, 134.2, 132.1, 131.5, 130.5, 129.5, 126.6, 126.0, 125.3, 122.7, 120.6, 117.9, 110.9, 110.3, 44.2, 26.5

2-[2-(1*H*-Benzimidazol-1-yl)ethylamino]-3-chloro-1,4-naphthoquinone (6)

Yield: 49 %; M.p. 205-207°C
Elemental analysis for $C_{19}H_{14}ClN_3O_2$:

found: C% 64.63   H% 4.28   N% 12.06

calcd.: C% 64.87   H% 4.01   N% 11.94

^{1}H-NMR (200 MHz, CDCl$_3$) δ: 8.17 (s, 1H, NH); 7.87 (s, 1H, CH); 7.58-7.18 (m, 2H, arom); 7.00-6.42 (m, 4H, arom); 6.39-6.10 (m, 2H, arom); 3.42-2.99 (m, 2H, NHCH$_2$CH$_2$CH); 2.22-1.91 (m, 2H, NHCH$_2$CH$_2$CH).

^{13}C NMR (50 MHz, CDCl$_3$) δ: 172.9, 153.6, 142.7, 140.0, 137.6, 131.4, 129.6, 128.5, 124.5, 124.0, 121.9, 118.5, 112.0, 105.6, 48.5, 27.3

2-{[2-(1H-Benzotriazol-1-yl)ethy]amino}-3-chloro-1,4-naphthoquinone (7)

Yield: 39 %; M.p. 193-194°C
Elemental analysis for $C_{18}H_{13}ClN_4O_2$:

found: C% 61.17   H% 3.77   N% 15.98

calcd.: C% 61.28   H% 3.71   N% 15.88

^{1}H-NMR (200 MHz, DMSO) δ: .05-7.65 (m, 5H, arom); 7.62-7.41 (m, 2H, arom); 7.39-7.23 (m, 1H, arom); 6.29 (s, 1H, NH); 4.98 (t, J = 5.8 Hz, 2H, NHCH$_2$CH$_2$-N(1)Bzt); 4.24 (q, J = 6.2 Hz, 2H, NHCH$_2$CH$_2$-N(1)Bzt).

^{13}C NMR (50 MHz, DMSO) δ: 179.6, 174.9, 145.2, 144.7, 134.4, 134.2, 132.7, 132.3, 131.1, 129.6, 126.8, 126.0, 125.3, 123.5, 118.6, 110.1, 47.8, 43.0.

General method for the synthesis of naphthoquinone-derivatives (**8**-**9**)

A mixture of the appropriate amino acid in NaOH 6N and 2,3-dichloronaphthoquinone (5 mmol) in methanol (100 mL) was stirred at room temperature for 20-24 h. The solution was treated with HCl 6N until the precipitation of a residue, that was then filtered, washed with H$_2$O and purified by CC (SiO$_2$, CHCl$_3$+ 2%MeOH).

N-[(3-Chloro-1,4-naphthoquinon-2-yl)]phenylalanine (8)

Yield: 65%; M.p. 150°C
Elemental analysis for $C_{19}H_{14}ClNO_4$:

found: C% 64.39   H% 4.11   N% 3.87

calcd.: C% 64.14   H% 3.97   N% 3.94

^{1}H-NMR (200 MHz, DMSO) δ: 10.90 (s, 1H, COOH); 8.02-7.65 (m, 4H, arom); 7.38-7.10 (m, 5H, arom); 6.65 (s, 1H, NH); 5.42-5.20 (m, 1H, NH<u>CH</u>); 3.26 (d, J = 5 Hz, 2H, CH$_2$).

^{13}C NMR (50 MHz, DMSO) δ: 179.3, 178.9, 172.5, 146.6, 135.7, 134.4, 132.4, 131.1, 126.8, 126.0, 125.1, 124.1, 120.6, 110.9, 64.5, 14.7

N-[(3-Chloro-1,4-naphthoquinon-2-yl)]tryptophan (9)

Yield: 26%; M.p. 130°C dec.
Elemental analysis for $C_{21}H_{15}ClN_2O_4$:

found: C% 63.93   H% 4.14   N% 7.18

calcd.: C% 63.89   H% 3.83   N% 7.10

^{1}H-NMR (200 MHz, CDCl$_3$) δ: 10.91 (s, 1H, COOH); 8.35-8.10 (m, 2H, arom); 8.01-7.58 (m, 3H, arom); 7.42-7.10 (m, 4H, arom); 6.32 (s, 1H, NH); 5.61 (s, 1H, NH); 3.62-3.44 (m, 2H, CH$_2$); 1.38-1.10 (m, 1H, NH<u>CH</u>).

^{13}C NMR (50 MHz, DMSO) δ: 191.6, 172.5, 169.9, 135.7, 134.5, 132.4, 129.4, 126.8, 126.1, 125.4, 124.1, 120.6, 117.8, 115.2, 110.9, 107.9, 64.5, 28.4

General method for the synthesis of anthraquinone derivatives (**10-14**)

A mixture of 1-chloroanthraquinone (1.5 mmol) with the suitable amino compound (3 mmol) was heated at 160°C in a sealed tube for 7-8 h. After cooling, the mixture was treated with 2 M NaOH till alkalinity and extracted with CHCl$_3$. After removing the solvent, the residue was purified by CC (SiO$_2$/CHCl$_3$+2%MeOH).

1-(Benzylamino)-9,10-anthraquinone (10)

Yield: 90 %; M.p. 171-173°C
Elemental analysis for $C_{21}H_{15}NO_2$:

found:	C% 80.11	H% 5.20	N% 4.17
calcd.:	C% 80.49	H% 4.82	N% 4.47

^{1}H-NMR (200 MHz, CDCl$_3$) δ: 10.15 (s, 1H, NH); 8.43-8.19 (m, 2H, arom); 7.96-7.61 (m, 4H, arom); 7.58-7.20 (m, 4H, arom); 7.17-6.98 (m, 2H, arom); 4.62 (s, 2H, NH<u>CH$_2$</u>Ar).

^{13}C NMR (50 MHz, CDCl$_3$) δ: 184.2, 182.7, 150.4, 136.9, 136.7, 134.3, 133.9, 133.6, 133.5, 132.9, 132.6, 132.0, 127.8, 126.5, 126.4, 126.0, 125.7, 117.3, 115.1,112.4, 46.0

1-(Phenethylamino)-9,10-anthraquinone (11)

Yield: 71 %; M.p. 100-103°C
Elemental analysis for $C_{22}H_{17}NO_2$:

found:	C% 80.62	H% 5.04	N% 3.98
calcd.:	C% 80.71	H% 5.23	N% 4.28

^{1}H-NMR (200 MHz, CDCl$_3$) δ: 10.00 (s, 1H, NH); 8.42-8.20 (m, 2H, arom); 7.90-7.70 (m, 4H, arom); 7.66-7.52 (m, 3H, arom); 7.45-7.22 (m, 2H, arom); 7.11 (dd, 1H, J = 1.6, 6.6 Hz, arom); 3.63 (t, J = 7.2 Hz, 2H, NH<u>CH$_2$</u>CH$_2$Ar); 3.10 (t, J = 7.8 Hz, 2H, NHCH$_2$<u>CH$_2$</u>Ar).

^{13}C NMR (50 MHz, CDCl$_3$) δ: 184.0, 182.8, 150.4, 137.7, 134.3, 134.0, 133.7, 131.9, 127.7, 127.6, 126.5, 125.7, 116.7, 114.7, 112.1, 43.6, 34.6

1-[(3-Phenylpropryl)amino]-9,10-anthraquinone (12)

Yield: 76 %; M.p. 115-116°C
Elemental analysis for $C_{23}H_{19}NO_2$:

found:	C% 80.73	H% 5.98	N% 3.93
calcd.:	C% 80.92	H% 5.61	N% 4.10

^{1}H-NMR (200 MHz, CDCl$_3$) δ: 10.02 (s, 1H, NH); 8.42-8.21 (m, 2H, arom); 7.90-7.70 (m, 4H, arom); 7.65-7.48 (m, 3H, arom); 7.43-7.18 (m, 2H, arom); 7.06 (dd,

1H, J = 1.6, 8.2 Hz, arom); 3.38 (t, J = 7.0 Hz, 2H, NH$\underline{CH_2}$CH$_2$CH$_2$Ar); 2.86 (t, J = 7.4 Hz, 2H, NHCH$_2$CH$_2$$\underline{CH_2}$Ar); 2.15 (quint, J = 7.2 Hz, 2H, NHCH$_2$$\underline{CH_2}CH_2$Ar).

^{13}C NMR (200 MHz, CDCl$_3$) δ: 183.9, 182.8, 150.6, 140.1, 134.2, 133.9, 133.5, 132.9, 131.9, 128.3, 127.5, 127.4, 125.7, 125.6, 125.1, 116.8, 114.6, 111.8, 41.0, 32.1, 29.5.

1-{[2-(1H-Indol-3-yl)ethyl]amino}-9,10-anthraquinone (13)

Yield: 40 %; M.p. 240-241°C
Elemental analysis for C$_{24}$H$_{18}$N$_2$O$_2$:

found: C% 78.81   H% 4.95   N% 7.43

calcd.: C% 78.67   H% 4.95   N% 7.65

^{1}H-NMR (200 MHz, CDCl$_3$) δ:10.84 (s, 1H, NH of indole); 8.18-7.41 (m, 7H, arom); 7.39-6.82 (m, 5H, arom); 6.60 (s, 1H, NH); 3.98 (pseudo s, 2H, NH$\underline{CH_2}$CH$_2$Ind); 2.99 (pseudo s, 2H, NHCH$_2$$\underline{CH_2}$Ind).

^{13}C NMR (50 MHz, CDCl$_3$) δ: 184.6, 182.6, 150.0, 135.8, 134.4, 134.2, 132.1, 131.5, 130.5, 129.5, 126.6, 126.0, 125.3, 122.7, 120.6, 117.9, 110.9, 110.3, 44.2, 33.0.

1-{[2-(1H-Benzotriazol-1-yl)ethyl]amino}-9,10-anthraquinone (14)

Yield: 42 %; M.p. 176-177°C
Elemental analysis for C$_{22}$H$_{16}$N$_4$O$_2$:

found: C% 71.59   H% 4.31   N% 15.20

calcd.: C% 71.73   H% 4.38   N% 15.21

^{1}H-NMR (200 MHz, CDCl$_3$) δ: 8.36-8.15 (m, 3H, arom); 7.86-7.69 (m, 3H, arom); 7.63-7.57 (m, 2H, arom); 7.49-7.22 (m, 3H, arom); 6.82 (s, 1H, NH); 4.57 (t, J = 7.0 Hz, 2H, NHCH$_2$$\underline{CH_2}$-N(1)Bzt); 3.03 (t, J = 7.0 Hz, 2H, NH$\underline{CH_2}$CH$_2$-N(1)Bzt).

^{13}C NMR (50 MHz, DMSO) δ: 184.5, 183.7, 146.2, 144.0, 135.9, 133.9, 133.4, 132.9, 132.0, 127.8, 126.9, 125.8, 125.0, 121.9, 119.0, 48.5, 44.2.

General method for the synthesis of naphthoquinone-derivatives (**15-24**)

A mixture of appropriate amine (3 mmol) and 2,3-dichloronaphthoquinone 1 (1,5 mmol) in absolute ethanol (10 mL) was stirred under reflux for 4 h. During

the progress of the reaction, monitored by TLC, a change in the colour from yellow to red was observed. After evaporation of the solvent, the residue was treated with an acid aqueous solution and $CHCl_3$. The layers were separated, and the chloroform solution was dried (Na_2SO_4), filtered and evaporated, affording a residue that was crystallized from ethanol.

2-Chloro-3-(2-chlorobenzylamino)-1,4-naphthoquinone (15)

Yield: 86 %; M.p. 162-163 °C
Elemental analysis for $C_{17}H_{11}Cl_2NO_2$:

found:	C% 61.46	H% 3.69	N% 4.61
calcd.:	C% 61.47	H% 3.34	N% 4.22

^{1}H-NMR ($CDCl_3$) δ: 8.25-8.05 (m, 2H, arom); 7.85-7.60 (m, 2H, arom); 7.55-7.24 (m, 4H, arom); 6.38 (s, 1H, NH); 5.18 (d, 2H, J = 6.6, NH<u>CH</u>$_2$Ar).

2-Chloro-3-(3-chlorobenzylamino)-1,4-naphthoquinone (16)

Yield: 94 %; M.p. 135-136 °C
Elemental analysis for $C_{17}H_{11}Cl_2NO_2$:

found:	C% 61.56	H% 3.74	N% 4.02
calcd.:	C% 61.47	H% 3.34	N% 4.22

^{1}H-NMR ($CDCl_3$) δ: 8.23-8.05 (m, 2H, arom); 7.84-7.61 (m, 2H, arom); 7.42-7.18 (m, 4H, arom); 6.28 (s, 1H, NH); 5.07 (d, 2H, J = 6.4, NH<u>CH</u>$_2$Ar).

2-Chloro-3-(4-chlorobenzylamino)-1,4-naphthoquinone (17)

Yield: 92 %; M.p. 167-169 °C
Elemental analysis for $C_{17}H_{11}Cl_2NO_2$:

found:	C% 61.54	H% 3.71	N% 4.56
calcd.:	C% 61.47	H% 3.34	N% 4.22

^{1}H-NMR ($CDCl_3$) δ: 8.26-8.03 (m, 2H, arom); 7.83-7.61 (m, 2H, arom); 7.44-7.22 (m, 4H, arom); 6.25 (s, 1H, NH); 5.05 (d, 2H, J = 6.4 Hz, NH<u>CH</u>$_2$Ar).

^{13}C NMR (200 MHz, $CDCl_3$) δ: 179.3, 175.9, 142.8, 135.5, 134.0, 132.9, 131.6, 131.5, 128.7, 128.1, 127.9, 125.9, 47.1

2-Chloro-3-(3,4-*di*chlorobenzylamino)-1,4-naphthoquinone (18)

Yield: 91 %; M.p. 179-181 °C
Elemental analysis for $C_{17}H_{10}Cl_3NO_2$:

found: C% 55.54   H% 2.58   N% 4.10

calcd.: C% 55.69   H% 2.75   N% 3.82

^{1}H-NMR (CDCl₃) *δ*: 8.24-8.04 (m, 2H, arom); 7.85-7.60 (m, 2H, arom); 7.46 (s, 1H, arom); 7.39-7.21 (m, 2H, arom); 6.36 (s, 1H, NH); 5.13 (d, 2H, *J* = 6.6 Hz, NHCH₂Ar).

2-(4-Bromobenzylamino)-3-chloro-1,4-naphthoquinone (19)

Yield: 74 %; M.p. 183-185 °C
Elemental analysis for $C_{17}H_{10}BrClNO_2$:

found: C% 54.19   H% 2.71   N% 4.03

calcd.: C% 54.21   H% 2.94   N% 3.72

^{1}H-NMR (CDCl₃) *δ*: 8.26-8.00 (m, 2H, arom); 7.82-7.41 (m, 4H, arom); 7.32-7.15 (m, 2H, arom); 6.25 (s, 1H, NH); 5.04 (d, 2H, *J* = 6.4 Hz, NHCH₂Ar).

2-Chloro-3-(4-fluorobenzylamino)-1,4-naphthoquinone (20)

Yield: 84 %; M.p. 154-155 °C
Elemental analysis for $C_{17}H_{10}ClFNO_2$:

found: C% 64.40   H% 3.38   N% 4.45

calcd.: C% 64.67   H% 3.51   N% 4.44

^{1}H-NMR (CDCl₃) *δ*: 8.25-8.03 (m, 2H, arom); 7.84-7.59 (m, 2H, arom); 7.43-7.28 (m, 2H, arom); 7.18-7.02 (m, 2H, arom); 6.22 (s, 1H, NH); 5.05 (d, 2H, *J* = 6.2 Hz, NHCH₂Ar).

2-Chloro-3-(2-methoxybenzylamino)-1,4-naphthoquinone (21)

Yield: 88 %; M.p. 155-157 °C
Elemental analysis for $C_{18}H_{14}ClNO_3$:

found: C% 65.79   H% 4.27   N% 4.06

calcd.: C% 65.96   H% 4.31   N% 4.27

^{1}H-NMR (CDCl$_3$) δ: 8.22-8.02 (m, 2H, arom); 7.80-7.58 (m, 2H, arom); 7.43-7.24 (m, 2H, arom); 7.06-6.92 (m, 2H, arom); 6.57 (s, 1H, NH); 5.10 (d, 2H, J = 6.4 Hz, NHC$\underline{H}_2$Ar); 3.93 (s, 3H, OCH$_3$).

2-Chloro-3-(3-methoxybenzylamino)-1,4-naphthoquinone (22)

Yield: 52 %; M.p. 122-123 °C
Elemental analysis for C$_{18}$H$_{14}$ClNO$_3$:

found:	C% 66.04	H% 4.48	N% 3.97
calcd.:	C% 65.96	H% 4.31	N% 4.27

^{1}H-NMR (CDCl$_3$) δ: 8.23-8.04 (m, 2H, arom); 7.82-7.61 (m, 2H, arom); 7.41-7.24 (m, 2H, arom); 7.02-6.90 (m, 2H, arom); 6.26 (s, 1H, NH); 5.06 (d, 2H, J = 5.8 Hz, NHC$\underline{H}_2$Ar); 3.84 (s, 3H, OCH$_3$).

2-Chloro-3-(4-methoxybenzylamino)-1,4-naphthoquinone (23)

Yield: 88 %; M.p. 124-126 °C
Elemental analysis for C$_{18}$H$_{14}$ClNO$_3$:

found:	C% 65.90	H% 4.32	N% 4.55
calcd.:	C% 65.96	H% 4.31	N% 4.27

^{1}H-NMR (CDCl$_3$) δ: 8.30-8.01 (m, 2H, arom); 7.83-7.60 (m, 2H, arom); 7.40-7.22 (m, 2H, arom); 7.02-6.88 (m, 2H, arom); 6.17 (s, 1H, NH); 5.02 (d, 2H, J = 6.0 Hz, NHC$\underline{H}_2$Ar); 3.85 (s, 3H, OCH$_3$).

2-Chloro-3-(4-methylbenzylamino)-1,4-naphthoquinone (24)

Yield: 68 %; M.p. 134-135 °C
Elemental analysis for C$_{18}$H$_{14}$ClNO$_2$:

found:	C% 69.43	H% 4.43	N% 4.25
calcd.:	C% 69.35	H% 4.53	N% 4.49

^{1}H-NMR (CDCl$_3$) δ: 8.26-8.01 (m, 2H, arom); 7.84-7.60 (m, 2H, arom); 7.42-7.16 (m, 4H, arom); 6.22 (s, 1H, NH); 5.04 (d, 2H, J = 6.0 Hz, NHC$\underline{H}_2$Ar); 2.39 (s, 3H, CH$_3$).

General method for the synthesis of anthraquinone-derivatives (**25**-**32**)

A mixture of 1-chloroanthraquinone (1.5 mmol) with the appropriate amino compound (3 mmol) was heated at 160°C in a sealed tube for 7 h. After cooling, the mixture was solubilized with $CHCl_3$ and washed with 10 mL HCl 2N for three times (in most of the cases it was necessary to extract the aqueous solution with other $CHCl_3$). The layers were separated, and the chloroform solution was dried (Na_2SO_4), filtered and evaporated. The residue was then crystallized from toluene or purified by CC ($SiO_2/CHCl_3$).

1-(2-Chlorobenzylamino)-9,10-anthraquinone (25)

Yield: 35 %; M.p. 119-121 °C.
Elemental analysis for $C_{21}H_{14}ClNO_2$:

	C%	H%	N%
found:	72.51	3.98	4.40
calcd.:	72.52	4.06	4.03

^{1}H-NMR ($CDCl_3$) δ: 10.22 (s, 1H, NH); 8.43-8.21 (m, 2H, arom); 7.97-7.61 (m, 4H, arom); 7.59-7.22 (m, 4H, arom); 7.02-6.88 (m, 2H, arom); 6.97 (d, 1H, J = 7.6 H, arom); 4.72 (s, 2H, NH$\underline{CH_2}$Ar).

1-(3-Chlorobenzylamino)-9,10-anthraquinone (26)

Yield: 31%; M.p. 216-217 °C
Elemental analysis for $C_{21}H_{14}ClNO_2$:

	C%	H%	N%
found:	72.49	4.30	4.23
calcd.:	72.52	4.06	4.03

^{1}H-NMR (200 MHz, $CDCl_3$) δ: 10.19 (s, 1H, NH); 8.42-8.23 (m, 2H, arom); 7.98-7.59 (m, 4H, arom); 7.58-7.25 (m, 3H, arom); 7.05-6.91 (m, 2H, arom); 6.96 (d, 1H, J = 7.6, arom); 4.63 (s, 2H, NH$\underline{CH_2}$Ar).

1-(4-Chlorobenzylamino)-9,10-anthraquinone (27)

Yield: 47%; M.p. 204-206 °C
Elemental analysis for $C_{21}H_{14}ClNO_2$:

	C%	H%	N%
found:	72.51	4.18	4.08
calcd.:	72.52	4.06	4.03

^{1}H-NMR (200 MHz, CDCl$_3$) δ: 10.17 (s, 1H, NH); 8.41-8.20 (m, 2H, arom); 7.97-7.61 (m, 3H, arom); 7.60-7.21 (m, 5H, arom); 6.98 (d, 1H, J = 8.2 Hz, arom); 4.60 (d, 2H, J = 5.2 Hz, NHCH$_2$Ar).

1-(3,4-*Di*chlorobenzylamino)-9,10-anthraquinone (28)

Yield: 47%; M.p. 190-193 °C
Elemental analysis for C$_{21}$H$_{13}$Cl$_2$NO$_2$:

found:	C% 65.92	H% 3.57	N% 3.75
calcd.:	C% 65.99	H% 3.43	N% 3.66

^{1}H-NMR (200 MHz, CDCl$_3$) δ: 10.18 (s, 1H, NH); 8.42-8.22 (m, 2H, arom); 7.97-7.62 (m, 3H, arom); 7.60-7.40 (m, 2H, arom); 7.38-7.19 (m, 2H, arom); 6.94 (d, 1H, J = 8.4 Hz, arom); 4.59 (d, 2H, J = 6.0 Hz, NHCH$_2$Ar).

^{13}C NMR (200 MHz, CDCl$_3$) δ: 184.6, 182.6, 150.0, 137.4, 134.5, 133.8, 133.0, 132.2, 131.9, 130.5, 129.8, 127.9, 125.8, 125.2, 116.9, 115.5, 112.8, 44.9

1-(4-Bromobenzylamino)-9,10-anthraquinone (29)

Yield: 43%; M.p. 220-223 °C
Elemental analysis for C$_{21}$H$_{14}$BrNO$_2$:

found:	C% 64.32	H% 3.79	N% 3.87
calcd.:	C% 64.30	H% 3.60	N% 3.57

^{1}H-NMR (200 MHz, CDCl$_3$) δ: 10.16 (s, 1H, NH); 8.44-8.23 (m, 2H, arom); 7.96-7.62 (m, 3H, arom); 7.56-7.15 (m, 4H, arom); 6.98 (d, 1H, J = 8.2 Hz, arom); 4.63 (d, 2H, J = 6.4 Hz, NHCH$_2$Ar).

1-(2-Methoxybenzylamino)-9,10-anthraquinone (30)

Yield: 55 %; M.p. 177-179 °C
Elemental analysis for C$_{22}$H$_{17}$NO$_3$:

found.:	C% 76.27	H% 5.04	N% 4.21
calcd.:	C% 76.95	H% 4.99	N% 4.08

^{1}H-NMR (CDCl$_3$) δ: 10.16 (s, 1H, NH); 8.39-8.19 (m, 2H, arom); 7.88-7.43 (m, 4H, arom); 7.41-7.20 (m, 2H, arom); 7.16-6.84 (m, 3H, arom); 4.63 (d, 2H, J = 6.0 Hz, NHCH$_2$Ar); 3.94 (s, 3H, OCH$_3$).

1-(3-Methoxybenzylamino)-9,10-anthraquinone (31)

Yield: 41%; M.p. 112-113 °C
Elemental analysis for $C_{22}H_{17}NO_3$:

found:	C% 76.93	H% 5.33	N% 4.41
calcd.:	C% 76.95	H% 4.99	N% 4.08

^{1}H-NMR (CDCl$_3$) δ: 10.10 (s, 1H, NH); 8.40-8.22 (m, 2H, arom); 7.95-7.47 (m, 4H, arom); 7.45-6.84 (m, 5H, arom); 4.60 (s, 2H, NH$\underline{CH_2}$Ar); 3.83 (s, 3H, OCH$_3$).

1-(4-Methoxybenzylamino)-9,10-anthraquinone (32)

Yield: 49%; M.p. 150-152 °C
Elemental analysis for $C_{22}H_{17}NO_3$:

found:	C% 76.57	H% 5.08	N% 4.33
calcd.:	C% 76.95	H% 4.99	N% 4.08

^{1}H-NMR (CDCl$_3$) δ: 10.14 (s, 1H, NH); 8.40-8.21 (m, 2H, arom); 7.90-7.47 (m, 4H, arom); 7.30-6.85 (m, 5H, arom); 4.35 (d, 2H, J = 5.6 Hz, NH$\underline{CH_2}$Ar); 3.82 (s, 3H, OCH$_3$).

Method for the synthesis of 1-(4-methylbenzylamino)-9,10-anthraquinone (**33**)

A mixture of 1-chloroanthraquinone (1.5 mmol) with 4-methylbenzylamine (3 mmol) in 10 mL of butanol was heated at 120°C and stirred for 8 h. After cooling, the mixture was solubilized with CHCl$_3$ and washed with 10 mL HCl 2N for three times. The layers were separated, and the chloroform solution was dried (Na$_2$SO$_4$), filtered and evaporated. The dark residue was then crystallized from toluene.

1-(4-Methylbenzylamino)-9,10-anthraquinone (33)

Yield: 35 %; M.p. 132-135 °C
Elemental analysis for $C_{22}H_{17}NO_2$:

found:	C% 80.87	H% 4.81	N% 3.93
calcd.:	C% 80.71	H% 5.23	N% 4.28

^{1}H-NMR (CDCl$_3$) δ: 10.16 (s, 1H, NH); 8.42-8.21 (m, 3H, arom); 7.95-7.61 (m, 4H, arom); 7.38-7.12 (m, 4H, arom); 4.59 (s, 2H, NH$\underline{CH_2}$Ar); 2.38 (s, 3H, CH$_3$).

General method for the synthesis of naphthoquinone-derivatives (**34**-**37**)

A mixture of appropriate amine (3 mmol) and 2-bromonaphthoquinone (or 1,4-naphthoquinone in case of compound **37**) (1,5 mmol) in absolute ethanol (10 mL) was stirred at 80°C for 4 h. During the progress of the reaction, monitored by TLC, a change in the colour from yellow to red was observed. After evaporation of the solvent, the residue was treated with an acid aqueous solution and CHCl$_3$. The layers were separated, and the chloroform solution was dried (Na$_2$SO$_4$), filtered and evaporated, affording a residue that crystallized from ethanol.

2-(Phenylamino)-1,4-naphthoquinone (34)

Yield: 86 %; M.p. 180-185 °C
Elemental analysis for C$_{16}$H$_{11}$NO$_2$:

found:	C% 77.08	H% 4.25	N% 5.47
calcd.:	C% 77.10	H% 4.45	N% 5.62

^{1}H-NMR (CDCl$_3$) δ: 8.55-8.10 (m, 2H, arom); 7.95-7.62 (m, 3H, arom); 7.50-7.05 (m, 5H, arom); 6.48 (s, 1H, NH).

2-(Benzylamino)-1,4-naphthoquinone (35)

Yield: 72 %; M.p. 157-159 °C
Elemental analysis for C$_{17}$H$_{13}$NO$_2$:

found:	C% 77.74	H% 5.02	N% 5.26
calcd.:	C% 77.55	H% 4.98	N% 5.32

^{1}H-NMR (CDCl$_3$) δ: 8.22-8.01 (m, 2H, arom); 7.89-7.60 (m, 2H, arom); 7.55-7.22 (m, 5H, arom); 6.28 (s, 1H, NH); 5.85 (s, 1H, CH); 4.42 (d, 2H, *J* = 5.4 Hz, NHC̲H̲$_2$Ar).

2-(Phenethylamino)-1,4-naphthoquinone (36)

Yield: 73 %; M.p. 140-142 °C
Elemental analysis for C$_{18}$H$_{15}$NO$_2$:

found:	C% 78.16	H% 5.49	N% 5.38
calcd.:	C% 77.96	H% 5.45	N% 5.05

^{1}H-NMR (CDCl$_3$) δ: 8.20-8.00 (m, 2H, arom); 7.82-7.60 (m, 2H, arom); 7.45-7.17 (m, 5H, arom); 6.00 (s, 1H, NH); 5.84 (s, 1H, CH); 3.50 (q, 2H, J = 6.6 Hz, NHC$\underline{H}_2$CH$_2$Ar); 3.02 (t, 2H, J = 7.0 Hz, NHCH$_2$C$\underline{H}_2$Ar).

2-[(3-Phenylpropyl)amino]-1,4-naphthoquinone (37)

Yield: 50 %; M.p. 113-115°C
Elemental analysis for C$_{19}$H$_{17}$NO$_2$:

	C%	H%	N%
found:	78.33	5.75	5.31
calcd.:	78.33	5.88	4.81

^{1}H-NMR (CDCl$_3$) δ: 8.21-8.02 (m, 2H, arom); 7.86-7.58 (m, 2H, arom); 7.42-7.17 (m, 5H, arom); 5.94 (s, 1H, NH); 5.74 (s, 1H, CH); 3.24 (q, 2H, J = 6.6 Hz, NHC$\underline{H}_2$CH$_2$CH$_2$Ar); 2.78 (t, 2H, J = 7.6 Hz, NHCH$_2$CH$_2$C$\underline{H}_2$Ar); 2.07 (quint, 2H, J = 7.2 Hz, NHCH$_2$C$\underline{H}_2$CH$_2$Ar).

2-Chloro-3-methoxynaphthoquinone

Yield: 80 %; M.p. 147-148°C
Elemental analysis for C$_{12}$H$_9$ClO$_3$:

	C%	H%	N%
found:	61.11	3.95	0.00
calcd.:	60.90	3.83	0.00

^{1}H-NMR (CDCl$_3$) δ: 8.30-8.10 (m, 2H, arom); 7.90-7.70 (m, 2H, arom); 4.67 (q, 2H, J = 7.0 Hz, OC$\underline{H}_2$CH$_3$); 1.50 (t, 3H, J = 6.0 Hz, OCH$_2$C$\underline{H}_3$).

General method for the synthesis of naphthoquinone-derivatives (**38-41**)

A mixture of 2,3-*di*chloro-naphthoquinone (1.5 mmol) with the appropriate amino compound (3 mmol) with 5 mL of CH$_3$CN was heated at 100°C in a sealed tube for 24 h. After cooling, the mixture was solubilized with CHCl$_3$ and evaporated. The residue was then purified by CC (SiO$_2$/CHCl$_3$).

2-Chloro-3-(4-methylpiperazin-1-yl)-1,4-naphthoquinone (38)

Yield: 93 %; M.p. 115-117 °C
Elemental analysis for C$_{15}$H$_{15}$ClN$_2$O$_2$:

	C%	H%	N%
found:	61.87	4.97	9.85
calcd.:	61.97	5.20	9.64

^{1}H-NMR (CDCl$_3$) δ: 8.23-7.94 (m, 2H, arom); 7.82-7.61 (m, 2H, arom); 3.82-3.58 (m, 4H, N(CH$_2$CH$_2$)$_2$N); 2.82-2.58 (m, 4H, N(CH$_2$CH$_2$)$_2$N); 2.4 (s, 3H, NCH$_3$).

3-Chloro-2-(4-phenylpiperazin-1-yl)-1,4-naphthoquinone (39)

Yield: 91 %; M.p. 123–125 °C
Elemental analysis for C$_{20}$H$_{17}$ClN$_2$O$_2$:

	found: C% 68.07	H% 4.87	N% 8.17
	calcd.: C% 68.09	H% 4.86	N% 7.94

^{1}H-NMR (CDCl$_3$) δ: 8.23-8.03 (m, 2H, arom); 7.83-7.68 (m, 2H, arom); 7.42-7.26 (m, 2H, arom); 7.10-6.90 (m, 3H, arom); 3.92-3.73 (m, 4H, N(CH$_2$CH$_2$)$_2$N); 3.50-3.32 (m, 4H, N(CH$_2$CH$_2$)$_2$N).

^{13}C NMR (200 MHz, CDCl$_3$) δ: 180.8, 177.0, 150.1, 148.8, 133.1, 132.1, 130.6, 130.4, 128.2, 125.9, 125.6, 122.3, 119.3, 115.5, 50.6, 49.3

2-(4-Benzylpiperazin-1-yl)-3-chloro-1,4-naphthoquinone (40)

Yield: 92 %; M.p. 92-94 °C
Elemental analysis for C$_{21}$H$_{19}$ClN$_2$O$_2$:

	found: C% 68.49	H% 5.25	N% 7.84
	calcd.: C% 68.76	H% 5.22	N% 7.64

^{1}H-NMR (CDCl$_3$) δ: 8.20-7.99 (m, 2H, arom); 7.77-7.67 (m, 2H, arom); 7.47-7.27 (m, 5H, arom); 3.75-3.59 (m, 6H, 4H, N(CH$_2$CH$_2$)$_2$N, + s, 2H, NCH$_2$Ar); 2.78-2.63 (m, 4H, N(CH$_2$CH$_2$)$_2$N).

2-Chloro-3-(4-phenylpiperidin-1-yl)-1,4-naphthoquinone (41)

Yield: 97 %; M.p. 117-118 °C
Elemental analysis for C$_{21}$H$_{18}$ClNO$_2$:

	found: C% 71.53	H% 5.03	N% 3.93
	calcd.: C% 71.69	H% 5.16	N% 3.98

^{1}H-NMR (CDCl$_3$) δ: 8.23-8.03 (m, 2H, arom); 7.83-7.65 (m, 2H, arom); 7.45-7.10 (m, 5H, arom); 4.08-3.90 (m, 2H, N(CH$_2$CH$_2$)$_2$CH); 3.58-3.38 (m, 2H, N(CH$_2$CH$_2$)$_2$CH); 2.85 (s, 1H, N(CH$_2$CH$_2$)$_2$CH); 2.18-1.92 (m, 4H, N(CH$_2$CH$_2$)$_2$CH).

General method for the synthesis of hydroxyalkylamino-naphthoquinone-derivatives (a-e)

A mixture of 2,3-*di*chloro-naphthoquinone (5 mmol) with the appropriate hydroxy-alkyl-amino compound (10 mmol) with 20 mL of EtOH was heated at reflux for 6 h. During the progress of the reaction, monitored by TLC, a change in the colour from yellow to red was observed. After evaporation of the solvent, the residue was treated with an acid aqueous solution and $CHCl_3$. The layers were separated, and the chloroform solution was dried (Na_2SO_4), filtered and evaporated, affording a residue that crystallized from toluene.

2-Chloro-3-(2-hydroxyethylamino)-1,4-naphthoquinone (a)

Yield: 92 %; M.p. 143-144 °C
Elemental analysis for $C_{12}H_{10}ClNO_3$:

found:	C% 57.05	H% 4.07	N% 5.25
calcd.:	C% 57.27	H% 4.01	N% 5.57

^{1}H-NMR ($CDCl_3$) δ: 8.23-7.94 (m, 2H, arom); 7.82-7.55 (m, 2H, arom); 6.21 (s, 1H, NH); 4.18-4.02 (m, 2H, CH_2O); 4.00-3.83 (m, 2H, NCH_2); 1.88 (s, 1H, broad, OH).

2-Chloro-3-(3-hydroxypropylamino)-1,4-naphthoquinone (b)

Yield: 96 %; M.p. 112-113 °C
Elemental analysis for $C_{13}H_{12}ClNO_3$:

found:	C% 58.92	H% 4.54	N% 5.05
calcd.:	C% 58.77	H% 4.55	N% 5.27

^{1}H-NMR ($CDCl_3$) δ: 8.24-7.94 (m, 2H, arom); 7.81-7.56 (m, 2H, arom); 6.28 (s, 1H, NH); 4.06 (t, 2H, J= 6.6 Hz, OCH_2); 3.89 (t, 2H, J= 5.8 Hz, NCH_2); 1.99 (quint, 2H, $CH_2\underline{CH_2}CH_2$ + s broad, 1H, OH).

2-Chloro-3-(4-hydroxybutylamino)-1,4-naphthoquinone (c)

Yield: 80 %; M.p. 99-100 °C
Elemental analysis for $C_{14}H_{14}ClN_2O_3$:

found:	C% 60.12	H% 4.94	N% 4.83
calcd.:	C% 60.11	H% 5.04	N% 5.01

^{1}H-NMR (CDCl$_3$) δ: 8.25-7.99 (m, 2H, arom); 7.84-7.58 (m, 2H, arom); 6.23 (s, broad, 1H, NH); 3.94 (t, 2H, $J=$ 6.8 Hz, OCH$_2$); 3.76 (t, 2H, $J=$ 6.2 Hz, NCH$_2$); 1.94-1.62 (m, 4H, CH$_2$CH$_2$CH$_2$CH$_2$ + s broad, 1H, OH).

2-Chloro-3-(5-hydroxypentylamino)-1,4-naphthoquinone (d)

Yield: 85 %; M.p. 93-95 °C
Elemental analysis for C$_{15}$H$_{16}$ClNO$_3$:

	found: C% 61.65	H% 5.71	N% 4.89
	calcd.: C% 61.33	H% 5.49	N% 4.77

^{1}H-NMR (CDCl$_3$) δ: 8.21-7.99 (m, 2H, arom); 7.80-7.57 (m, 2H, arom); 6.13 (s, broad, 1H, NH); 3.89 (q, 2H, $J=$ 6.6 Hz, OCH$_2$); 3.71 (t, 2H, $J=$ 6.4 Hz, NCH$_2$); 1.98-1.39 (m, 6H, CH$_2$CH$_2$CH$_2$CH$_2$CH$_2$ + s broad, 1H, OH).

2-Chloro-3-(5-hydroxyhexylamino)-1,4-naphthoquinone (e)

Yield: 86 %; M.p. 90-92 °C
Elemental analysis for C$_{16}$H$_{18}$ClNO$_3$:

	found: C% 62.71	H% 5.85	N% 5.03
	calcd.: C% 62.44	H% 5.90	N% 4.55

^{1}H-NMR (CDCl$_3$) δ: 8.25-7.95 (m, 2H, arom); 7.82-7.58 (m, 2H, arom); 6.11 (s, 1H, NH); 3.83 (q, 2H, $J=$ 7.0 Hz, NHCH$_2$); 3.68 (t, 2H, $J=$ 5.8 Hz, CH$_2$OH); 1.86-1.00 (m, 8H, CH$_2$CH$_2$CH$_2$CH$_2$CH$_2$CH$_2$ + s broad, 1H, OH).

^{13}C NMR (200 MHz, CDCl$_3$) δ: 179.5, 175.8, 143.1, 133.9, 131.7, 131.4, 128.6, 125.8, 61.7, 43.8, 31.5, 29.9, 25.4, 24.4.

General method for the synthesis of chloroalkylamino-naphthoquinone derivatives (A-E)

To a suspension of the proper chloroalkylamino-naphthoquinone (a-e) (4 mmol) in 15 mL of anhydrous CHCl$_3$, a solution of thionyl-chloride (16 mmol) in anhydrous CHCl$_3$ (5 mL) was added drop by drop. Then the mixture was refluxed for 4 h. During the reaction progress, monitored by TLC, a change in the colour from red to a darker red was observed. After cooling, the mixture was treated with 10 mL of a cool solution of NaHCO3 10% v/v. The layers were separated, and the chloroform solution was dried (Na$_2$SO$_4$),

filtered and evaporated, affording a residue that was then purified by CC (SiO$_2$/CHCl$_3$).

2-Chloro-3-(2-chloroethylamino)-1,4-naphthoquinone (A)

Yield: 88 %; M.p. 166-168 °C

Elemental analysis for C$_{12}$H$_9$Cl$_2$NO$_2$:

found:	C% 53.62	H% 3.73	N% 4.88
calcd.:	C% 53.36	H% 3.36	N% 5.19

^{1}H-NMR (CDCl$_3$) δ: 8.25-7.98 (m, 2H, arom); 7.83-7.56 (m, 2H, arom); 6.24 (s, broad, 1H, NH); 4.04 (q, 2H, J= 6.6, ClCH$_2$); 3.67 (t, 2H, J= 6.2, NCH$_2$).

2-Chloro-3-(3-chloropropylamino)-1,4-naphthoquinone (B)

Yield: 92 %; M.p. 134-135 °C
Elemental analysis for C$_{13}$H$_{11}$Cl$_2$NO$_2$:

found:	C% 55.06	H% 3.70	N% 4.90
calcd.:	C% 54.95	H% 3.90	N% 4.93

^{1}H-NMR (CDCl$_3$) δ: 8.26-7.98 (m, 2H, arom); 7.84-7.58 (m, 2H, arom); 6.19 (s, broad, 1H, NH); 4.06 (q, 2H, J= 6.8 Hz, ClCH$_2$); 3.68 (t, 2H, J= 6.2 Hz, NCH$_2$); 2.30-2.08 (m, 2H, CH$_2$CH$_2$CH$_2$).

2-Cloro-3-(4-chlorobutylamino)-1,4-naphthoquinone (C)

Yield: 83 %; M.p. 125-126 °C
Elemental analysis for C$_{14}$H$_{13}$Cl$_2$NO$_2$:

found:	C% 56.44	H% 4.18	N% 4.40
calcd.:	C% 56.40	H% 4.39	N% 4.70

^{1}H-NMR (CDCl$_3$) δ: 8.25-7.98 (m, 2H, arom); 7.82-7.58 (m, 2H, arom); 6.11 (s, broad, 1H, NH); 3.92 (q, 2H, J= 6.8 Hz, ClCH$_2$); 3.62 (t, 2H, J= 6.0 Hz, NCH$_2$); 2.04-1.78 (m, 4H, CH$_2$CH$_2$CH$_2$CH$_2$).

2-Chloro-3-(5-chloropentylamino)-1,4-naphthoquinone (D)

Yield: 84 %; M.p. 101-103 °C
Elemental analysis for C$_{15}$H$_{15}$Cl$_2$NO$_2$:

found: C% 57.91   H% 5.03   N% 4.35

calcd.: C% 57.71   H% 4.84   N% 4.49

^{1}H-NMR (CDCl$_3$) δ: 8.23-7.97 (m, 2H, arom); 7.82-7.58 (m, 2H, arom); 6.12 (s, broad, 1H, NH); 3.89 (q, 2H, J = 6.6 Hz, ClCH$_2$); 3.59 (t, 2H, J = 6.6 Hz, NCH$_2$); 2.05-1.46 (m, 6H, CH$_2$CH$_2$CH$_2$CH$_2$CH$_2$).

2-Chloro-3-(5-chlorohexylamino)-1,4-naphthoquinone (E)

Yield: 66 %; M.p. 81-82 °C
Elemental analysis for C$_{16}$H$_{17}$Cl$_2$NO$_2$:

found: C% 59.18   H% 5.12   N% 4.31

calcd.: C% 58.91   H% 5.25   N% 4.29

^{1}H-NMR (CDCl$_3$) δ: 8.23-7.97 (m, 2H, arom); 7.82-7.58 (m, 2H, arom); 6.10 (s, broad, 1H, NH); 3.87 (q, 2H, J = 7.0 Hz, ClCH$_2$); 3.57 (t, 2H, J = 6.4 Hz, NCH$_2$); 1.90-1.05 (m, 8H, CH$_2$CH$_2$CH$_2$CH$_2$CH$_2$CH$_2$).

^{13}C NMR (200 MHz, CDCl$_3$) δ: 179.5, 175.8, 143.0, 134.0, 131.7, 131.4, 128.6, 125.8, 43.9, 43.7, 31.3, 29.9, 25.5, 24.9

General method for the synthesis of naphthoquinone-derivatives (**42-53**)

A mixture of the proper chloroalkylamino-naphthoquinone (**A-E**) (1.5 mmol) with the appropriate amino compound (3 mmol) in 5 mL of CH$_3$CN was heated at 100°C in a sealed tube for 24 h. After cooling, the mixture was solubilized with CHCl$_3$ and evaporated. The residue was then purified by CC (SiO$_2$/CHCl$_3$).

2-Chloro-3-[2-(4-methylpiperazin-1-yl)ethylamino]-1,4-naphthoquinone (42)

Yield: 75 %; M.p. 94-96 °C
Elemental analysis for C$_{17}$H$_{20}$ClN$_3$O$_2$:

found: C% 61.10   H% 6.21   N% 12.80

calcd.: C% 61.17   H% 6.04   N% 12.59

^{1}H-NMR (CDCl$_3$) δ: 8.23-7.96 (m, 2H, arom); 7.81-7.56 (m, 2H, arom); 6.95 (s, 1H, NH); 3.97 (q, J = 5.6 Hz, 2H, HNCH$_2$); 2.69 (t, 2H, J = 6.0 Hz, CH$_2$N); 2.65-2.42 (m, 8H, 3 N(CH$_2$CH$_2$)$_2$N); 2.33 (s, 3H, NCH$_3$).

2-Chloro-3-[3-(4-methylpiperazin-1-yl)propylamino]-1,4-naphthoquinone (43)

Yield: 83 %; M.p. 84-87 °C
Elemental analysis for C$_{18}$H$_{22}$ClN$_3$O$_2$:

trov.:	C% 62.10	H% 6.57	N% 11.80
calcd.:	C% 62.15	H% 6.38	N% 12.08

^{1}H-NMR (CDCl$_3$) δ: 8.24-8.01 (m, 2H, arom); 7.91-7.78 (m, 2H, arom); 7.54 (s, 1H, NH); 4.03 (q, J = 6.2 Hz, 2H, HNCH$_2$); 2.81-2.39 (m, 10H, 2H, CH$_2$N + 8H, N(CH$_2$CH$_2$)$_2$N); 2.38 (s, 3H, NCH$_3$); 1.87 (quint, 2H, J = 6.2 Hz, CH$_2$CH$_2$CH$_2$).

2-Chloro-3-[4-(4-methylpiperazin-1-yl)butylamino]-1,4-naphthoquinone (44)

Yield: 69 %; M.p. 76-80 °C
Elemental analysis for C$_{19}$H$_{24}$ClN$_3$O$_2$:

found:	C% 62.91	H% 6.58	N% 11.89
calcd.:	C% 63.06	H% 6.69	N% 11.61

^{1}H-NMR (CDCl$_3$) δ: 8.22-7.97 (m, 2H, arom); 7.82-7.57 (m, 2H, arom); 6.22 (s, 1H, NH); 3.90 (q, J = 6.6 Hz, 2H, HNCH$_2$); 2.83-2.34 (m, 10H, 2H, CH$_2$N + 8H, N(CH$_2$CH$_2$)$_2$N); 2.31 (s, 3H, NCH$_3$); 1.84-1.56 (m, 4H, J = 6.2 Hz, CH$_2$CH$_2$CH$_2$CH$_2$).

2-Chloro-3-[2-(4-phenylpiperazin-1-yl)ethylamino]-1,4-naphthoquinone (45)

Yield: 63 %; M.p. 120-123 °C
Elemental analysis for C$_{22}$H$_{22}$ClN$_3$O$_2$:

found:	C% 66.65	H% 5.73	N% 10.97
calcd.:	C% 66.75	H% 5.60	N% 10.61

^{1}H-NMR (CDCl$_3$) δ: 8.23-8.00 (m, 2H, arom); 7.82-7.59 (m, 2H, arom); 7.39-7.23 (m, 2H, arom); 7.10-6.84 (m, 3H, arom); 6.94 (s, 1H, NH); 4.03 (q, 2H, J=5.4 Hz,

HNCH$_2$); 3.40-3.20 (m, 4H, N(CH$_2$CH$_2$)$_2$N); 2.90-2.65 (m, 6H, 2H of CH$_2$N, 4H of N(CH$_2$CH$_2$)$_2$N).

^{13}C NMR (200 MHz, CDCl$_3$) δ: 179.6, 150.2, 143.6, 133.7, 131.7, 131.3, 128.1, 125.7, 118.9, 115.1, 55.3, 51.5, 48.3, 40.0

2-Chloro-3-[3-(4-phenylpiperazin-1-yl)propylamino]-1,4-naphthoquinone (46)

Yield: 85 %; M.p. 119-120 °C
Elemental analysis for C$_{23}$H$_{24}$ClN$_3$O$_2$:

found:	C% 67.40	H% 5.99	N% 10.05
calcd.:	C% 67.39	H% 5.90	N% 10.25

^{1}H-NMR (CDCl$_3$) δ: 8.22-7.99 (m, 2H, arom); 7.80-7.54 (m, 2H, arom); 7.40-7.26 (m, 2H, arom); 7.05-6.85 (m, 3H, arom); 6.94 (s, 1H, NH); 4.07 (q, 2H, J = 6 Hz, HNCH$_2$); 3.44-3.30 (m, 4H, N(CH$_2$CH$_2$)$_2$N); 2.80-2.55 (m, 6H, 2H, CH$_2$N, 4H, N(CH$_2$CH$_2$)$_2$N); 2.00-1.84 (m, 2H, CH$_2$CH$_2$CH$_2$).

^{13}C NMR (200 MHz, CDCl$_3$) δ: 179.6, 150.2, 143.9, 133.7, 131.8, 131.2, 128.9, 128.1, 125.7, 125.6, 118.6, 115.1, 56.2, 52.5, 47.8, 44.4, 25.0

2-Chloro-3-[4-(4-phenylpiperazin-1-yl)butylamino]-1,4-naphthoquinone (47)

Yield: 64 %; M.p. 206-208 °C
Elemental analysis for C$_{24}$H$_{26}$ClN$_3$O$_2$:

found:	C% 68.11	H% 6.41	N% 10.11
calcd.:	C% 68.00	H% 6.18	N% 9.91

^{1}H-NMR (CDCl$_3$) δ: 8.23-8.00 (m, 2H, arom); 7.83-7.59 (m, 2H, arom); 7.40-7.20 (m, 2H, arom); 7.13-6.81 (m, 3H, arom); 6.24 (s, 1H, NH); 3.93 (q, 2H, J = 6.4 Hz, HNCH$_2$); 3.35-3.10 (m, 4H, N(CH$_2$CH$_2$)$_2$N); 2.77-2.40 (m, 6H, 2H, CH$_2$N, 4H, N(CH$_2$CH$_2$)$_2$N); 1.90-1.60 (m, 4H, CH$_2$CH$_2$CH$_2$CH$_2$).

^{13}C NMR (200 MHz, CDCl$_3$) δ: 179.5, 175.8, 150.3, 143.2, 133.9, 131.8, 131.3, 128.7, 128.1, 125.8, 125.7, 118.6, 115.0, 56.9, 52.3, 48.1, 43.7, 28.0, 22.9

2-[2-(4-Benzylpiperazin-1-yl)ethylamino]-3-chloro-1,4-naphthoquinone (48)

Yield: 76 %; M.p. 103-106 °C
Elemental analysis for $C_{23}H_{24}ClN_3O_2$:

	found:	C% 67.58	H% 5.90	N% 10.58
	calcd.:	C% 67.39	H% 5.90	N% 10.25

^{1}H-NMR (CDCl$_3$) δ: 8.23-8.03 (m, 2H, arom); 7.82-7.60 (m, 2H, arom); 7.50-7.24 (m, 5H, arom); 6.98 (s, 1H, NH); 3.96 (q, 2H, J = 5.6, HNCH$_2$); 3.55 (s, 2H, NCH$_2$); 2.78-2.67 (m, 2H, CH$_2$N); 2.67-2.40 (m, 8H, N(CH$_2$CH$_2$)$_2$N).

^{13}C NMR (200 MHz, CDCl$_3$) δ: 179.6, 143.7, 137.1, 133.7, 131.7, 131.2, 128.9, 128.1, 128.0, 127.3, 127.2, 126.3, 126.0, 125.6, 61.9, 55.3, 52.1, 51.5, 40.1

2-[3-(4-Benzylpiperazin-1-yl)propylamino]-3-chloro-1,4-naphthoquinone (49)

Yield: 81 %; M.p. 95-98 °C
Elemental analysis for $C_{24}H_{26}ClN_3O_2$:

	found:	C% 67.93	H% 6.14	N% 10.24
	calcd.:	C% 68.00	H% 6.18	N% 9.91

^{1}H-NMR (CDCl$_3$) δ: 8.23-8.02 (m, 2H, arom); 7.80-7.62 (m, 2H, arom); 7.55 (s, 1H, NH); 7.45-7.23 (m, 5H, arom); 4.02 (q, 2H, J = 6 Hz, HNCH$_2$); 3.59 (s, 2H, NCH$_2$Ar); 2.72-2.40 (m, 8H, N(CH$_2$CH$_2$)$_2$N); 1.96-1.70 (m, 4H, 2H, CH$_2$N, 2H, CH$_2$CH$_2$CH$_2$).

2-[4-(4-Benzylpiperazin-1-yl)butylamino]-3-chloro-1,4-naphthoquinone (50)

Yield: 44 %; oil
Elemental analysis for $C_{25}H_{28}ClN_3O_2$:

	found:	C% 68.40	H% 6.21	N% 9.80
	calcd.:	C% 68.56	H% 6.44	N% 9.59

^{1}H-NMR (CDCl$_3$) δ: 8.22-8.00 (m, 2H, arom); 7.82-7.58 (m, 2H, arom); 7.50-7.18 (m, 5H, arom); 6.23 (s, 1H, NH); 3.89 (q, 2H, J = 6.6 Hz, HNCH$_2$); 3.54 (s, 2H, NCH$_2$Ar); 2.72-2.25 (m, 10H, 8H of N(CH$_2$CH$_2$)$_2$N, 2H di CH$_2$N); 1.84-1.53 (m, 4H, CH$_2$CH$_2$CH$_2$CH$_2$).

2-Chloro-3-[2-(4-phenylpiperidin-1-yl)ethylamino]-1,4-naphthoquinone (51)

Yield: 67 %; M.p. 80-82 °C
Elemental analysis for $C_{23}H_{23}ClN_2O_2$:

$$\text{found: C\% 69.81} \quad \text{H\% 5.80} \quad \text{N\% 6.96}$$

$$\text{calcd.: C\% 69.96} \quad \text{H\% 5.87} \quad \text{N\% 7.09}$$

^{1}H-NMR (CDCl$_3$) δ: 8.24-8.05 (m, 2H, arom); 7.83-7.60 (m, 2H, arom); 7.42-7.20 (m, 5H, arom); 7.09 (s, 1H, NH); 4.18-4.01 (m, 2H, HNCH$_2$); 3.30-3.10 (m, 2H, N(CH$_2$CH$_2$)$_2$CH); 2.96-2.78 (m, 2H, N(CH$_2$CH$_2$)$_2$CH); 2.72-2.52 (m, 1H, N(CH$_2$CH$_2$)$_2$CH); 2.50-2.25 (m, 2H, CH$_2$N); 2.10-1.86 (m, 4H, N(CH$_2$CH$_2$)$_2$CH).

2-Chloro-3-[3-(4-phenylpiperidin-1-yl)propylamino]-1,4-naphthoquinone (52)

Yield: 88 %; M.p. 118-120 °C
Elemental analysis for $C_{24}H_{25}ClN_2O_2$:

$$\text{found: C\% 70.49} \quad \text{H\% 6.16} \quad \text{N\% 6.85}$$

$$\text{calcd.: C\% 70.41} \quad \text{H\% 5.90} \quad \text{N\% 7.02}$$

^{1}H-NMR (CDCl$_3$) δ: 8.28-8.04 (m, 2H, arom); 7.99 (s, 1H, NH); 7.84-7.59 (m, 2H, arom); 7.50-7.20 (m, 5H, arom); 4.08 (q, 2H, J= 6 Hz, HNCH$_2$); 3.30-3.10 (m, 2H, N(CH$_2$CH$_2$)$_2$CH); 2.63 (t, 3H, 2H, J=6 Hz, N(CH$_2$CH$_2$)$_2$CH, 1H, N(CH$_2$CH$_2$)$_2$CH); 2.30-2.05 (m, 4H, 2H, N(CH$_2$CH$_2$)$_2$CH, 2H, CH$_2$N); 2.05-1.80 (m, 4H, 2H, N(CH$_2$CH$_2$)$_2$CH, 2H di CH$_2$CH$_2$CH$_2$).

2-Chloro-3-[4-(4-phenylpiperidin-1-yl)butylamino]-1,4-naphthoquinone (53)

Yield: 81 %; M.p. 94-95 °C
Elemental analysis for $C_{25}H_{27}ClN_2O_2$:

$$\text{found: C\% 70.85} \quad \text{H\% 6.27} \quad \text{N\% 6.46}$$

calcd.: C% 70.99   H% 6.43   N% 6.62

^{1}H-NMR (CDCl$_3$) δ: 8.25-8.00 (m, 2H, arom); 7.83-7.59 (m, 2H, arom); 7.43-7.18 (m, 5H, arom); 6.29 (s, 1H, NH); 3.92 (q, J = 6.2 Hz, 2H, HNCH$_2$); 3.23-3.05 (m, 2H, N(CH$_2$CH$_2$)$_2$CH); 2.65-2.40 (m, 3H, 2H, N(CH$_2$CH$_2$)$_2$CH, 1H, N(CH$_2$CH$_2$)$_2$CH);

2.13-2.04 (m, 2H, N(CH$_2$CH$_2$)$_2$CH); 1.99-1.84 (m, 4H, 2H di N(CH$_2$CH$_2$)$_2$CH, 2H di CH$_2$N); 1.82-1.63 (m, 4H, CH$_2$<u>CH$_2$CH$_2$</u>CH$_2$).

General method for the synthesis of anthraquinone-derivatives (**54-57**)

A mixture of 1-chloro-anthraquinone (1.5 mmol) with the appropriate amino compound (3 mmol) in 5 mL of CH$_3$CN was heated at 100°C in a sealed tube for 24 h. After cooling, the mixture was solubilized with CHCl$_3$ and evaporated. The residue was then purified by CC (SiO$_2$/CHCl$_3$).

1-(4-Methylpiperazin-1-yl)-9,10-anthraquinone (54)

Yield: 77 %; M.p. 157-160 °C
Elemental analysis for C$_{19}$H$_{18}$N$_2$O$_2$:

	found:	C% 74.60	H% 5.90	N% 9.18
	calcd.:	C% 74.49	H% 5.92	N% 9.14

^{1}H-NMR (CDCl$_3$) *δ*: 8.38-8.19 (m, 2H, arom); 7.99 (d, 1H, *J* = 7.4 Hz, arom); 7.83-7.61 (m, 3H, arom); 7.44 (d, 1H, *J* = 8.4 Hz, arom); 3.43-3.18 (m, 4H, N(CH$_2$CH$_2$)$_2$N); 2.92-2.70 (m, 4H, N(CH$_2$CH$_2$)$_2$N); 2.47 (s, 3H, NCH$_3$).

1-(4-Phenylpiperazin-1-yl)-9,10-anthraquinone (55)

Yield: 84 %; M.p. 217-218 °C
Elemental analysis for C$_{24}$H$_{20}$N$_2$O$_2$:

	found:	C% 78.23	H% 5.61	N% 7.35
	calcd.:	C% 78.24	H% 5.47	N% 7.60

^{1}H-NMR (CDCl$_3$) *δ*: 8.38-8.21 (m, 2H, arom); 8.02 (dd, 1H, *J* = 0.8 Hz, *J* = 0.7 Hz, arom); 7.87-7.63 (m, 3H, arom); 7.49 (d, 1H, *J* = 8.2 Hz; arom); 7.40-7.25 (m, 2H, arom); 7.00-7.15 (m, 2H, arom); 6.94 (t, 1H, *J* = 6.8 Hz, arom) 3.62-3.50 (m, 4H, N(CH$_2$CH$_2$)$_2$N); 3.48-3.35 (m, 4H, N(CH$_2$CH$_2$)$_2$N).

^{13}C NMR (200 MHz, CDCl$_3$) δ: 183.1, 180.8, 152.2, 150.3, 135.6, 134.3, 133.3, 133.1, 132.0, 131.3, 128.1, 126.3, 125.4, 123.8, 121.9, 120.0, 118.9, 115.3, 51.3, 48.4

1-(4-Benzylpiperazin-1-yl)-9,10-anthraquinone (56)

Yield: 58 %; M.p. 128-131 °C
Elemental analysis for $C_{25}H_{22}N_2O_2$:

	found: C% 78.75	H% 5.69	N% 7.34
	calcd.: C% 78.51	H% 5.80	N% 7.32

^{1}H-NMR (CDCl$_3$) δ: 8.38-8.19 (m, 2H, arom); 7.99 (d, 1H, J = 7.4 Hz, arom); 7.85-7.60 (m, 3H, arom); 7.50-7.25 (m, 6H, arom); 3.71 (s, 2H, NCH$_2$); 3.37-3.20 (m, 4H, N(CH$_2$CH$_2$)$_2$N); 2.78-2.98 (m, 4H, N(CH$_2$CH$_2$)$_2$N).

1-(4-Phenylpiperidin-1-yl)-9,10-anthraquinone (57)

Yield: 76 %; M.p. 201-203 °C
Elemental analysis for $C_{25}H_{21}NO_2$:

	found: C% 81.83	H% 5.44	N% 3.80
	calcd.: C% 81.72	H% 5.76	N% 3.81

^{1}H-NMR (CDCl$_3$) δ: 8.38-8.19 (m, 2H, arom); 7.99 (d, 1H, J = 7.6 Hz, arom); 7.86-7.61 (m, 3H, arom); 7.59 (s, 1H, arom); 7.48-7.18 (m, 5H, arom); 3.62 (d, 2H, J = 12.2 Hz, N(<u>CH$_2$</u>CH$_2$)$_2$CH); 3.37-3.08 (m, 2H, N(CH$_2$CH$_2$)$_2$CH); 2.92-2.71 (m, 1H, N(CH$_2$CH$_2$)$_2$<u>CH</u>); 2.40-2.13 (m, 2H, N(CH$_2$<u>CH$_2$</u>)$_2$CH); 2.04 (d, 2H, J = 12.2 Hz, N(CH$_2$<u>CH$_2$</u>)$_2$CH).

General method for the synthesis of hydroxyalkylamino-anthraquinone-derivatives (**f-i**)

A mixture of 1-chloro-anthraquinone (5 mmol) with the appropriate hydroxy-alkyl-amino compound (10 mmol) in 20 mL of BuOH was heated at reflux for 20 h. During the progress of the reaction, monitored by TLC, a change in the colour from yellow to red was observed. After evaporation of the solvent, the residue was treated with an acid aqueous solution and CHCl$_3$. The layers were separated, and the chloroform solution was dried (Na$_2$SO$_4$), filtered and evaporated, affording a residue that crystallized from toluene or purified by CC (SiO$_2$/CHCl$_3$).
A second method carried out was stirred the mixture of 1-chloro-anthraquinone (5 mmol) with the appropriate hydroxy-alkyl-amino compound (15 mmol) in sealed tube at 140 °C for 8 h; the residue was then purified as described above for the first method.

1-(2-Hydroxyethylamino)-9,10-anthraquinone (f)

Yield: 68 %; M.p. 168-170 °C
Elemental analysis for $C_{16}H_{13}NO_3$:

found:	C% 71.71	H% 5.08	N% 5.38
calcd.:	C% 71.90	H% 4.90	N% 5.24

^{1}H-NMR (CDCl$_3$) δ: 9.67 (s, 1H, NH); 8.38-8.16 (m, 2H, arom); 7.85-7.49 (m, 4H, arom); 7.44 (dd, 1H, J = 8.0, 1.8 Hz, arom); 4.02 (t, 2H, J= 5.2 Hz, OCH$_2$); 3.59 (t, 2H, J= 5.4 Hz, NCH$_2$).

1-(3-Hydroxypropylamino)-9,10-anthraquinone (g)

Yield: 74 %; M.p. 178-179 °C
Elemental analysis for $C_{17}H_{15}NO_3$:

found:	C% 72.55	H% 5.73	N% 4.69
calcd.:	C% 72.58	H% 5.37	N% 4.98

^{1}H-NMR (CDCl$_3$) δ: 9.72 (s, 1H, NH); 8.39-8.21 (m, 2H, arom); 7.94-7.52 (m, 4H, arom); 7.31 (dd, J = 8.0, 1.8 Hz, 1H, arom); 3.91 (t, 2H, J= 6.0 Hz, OCH$_2$); 3.55 (t, 2H, J = 6.6 Hz, NCH$_2$); 2.06 (quint, 2H, J = 6.0 Hz, CH$_2$CH$_2$CH$_2$).

1-(4-Hydroxyibutylamino)-9,10-anthraquinone (h)

Yield: 68 %; M.p. 130-131 °C
Elemental analysis for $C_{18}H_{17}NO_3$:

found:	C% 73.00	H% 5.95	N% 4.60
calcd.:	C% 73.20	H% 5.80	N% 4.74

^{1}H-NMR (CDCl$_3$) δ: 9.69 (s, 1H, NH); 8.38-8.20 (m, 2H, arom); 7.91-7.53 (m, 4H, arom); 7.18 (d, J = 8.0 Hz, 1H, arom); 3.79 (t, 2H, J = 6.2 Hz, OCH$_2$); 3.42 (t, 2H, J = 6.6 Hz, NCH$_2$); 2.08-1.74 (m, 4H, CH$_2$CH$_2$CH$_2$CH$_2$).

1-(5-Hydroxypentylamino)-9,10-anthraquinone (i)

Yield: 55 %; M.p. 107-111 °C
Elemental analysis for $C_{19}H_{19}NO_3$:

found:	C% 73.53	H% 6.35	N% 4.72

calcd.: C% 73.77   H% 6.19   N% 4.53

^{1}H-NMR (CDCl$_3$) δ: 9.98 (s, 1H, NH); 8.39-8.19 (m, 2H, arom); 7.85-7.46 (m, 4H, arom); 7.18-7.03 (m, 1H, arom); 3.74 (t, 2H, J = 5.2 Hz, HNCH$_2$); 3.38 (t, 2H, J = 5.4 Hz, CH$_2$O); 2.01-1.44 (m, 6H, CH$_2$CH$_2$CH$_2$CH$_2$CH$_2$ + 1H, OH).

General method for the synthesis of chloroalkylamino-anthraquinone-derivatives (**F-I**)

To a suspension of the proper chloroalkylamino-anthraquinone (**f-i**) (4 mmol) in 20 mL of anhydrous CHCl$_3$, a solution of thionyl-chloride (16 mmol) in anhydrous CHCl$_3$ (5 mL) was added drop by drop. Then the mixture was refluxed for 4 h. During the reaction progress, monitored by TLC, a change in the colour from red to a darker red was observed. After cooling, the mixture was treated with 10 mL of a cool solution of NaHCO3 10% v/v. The layers were separated, and the chloroform solution was dried (Na$_2$SO$_4$), filtered and evaporated, affording a residue that was then purified by CC (SiO$_2$/CHCl$_3$).

1-(2-Chloroethylamino)-9,10-anthraquinone (F)

Yield: 86 %; M.p. 174-176 °C
Elemental analysis for C$_{16}$H$_{12}$ClNO$_2$:

found: C% 67.09   H% 4.58   N% 4.66

calcd.: C% 67.26   H% 4.23   N% 4.90

^{1}H-NMR (CDCl$_3$) δ: 10.02 (s, 1H, NH); 8.40-8.12 (m, 2H, arom); 7.92-7.57 (m, 4H, arom); 7.10 (dd, 1H, J = 8.2, 1.4 Hz, arom); 3.94-3.68 (m, 4H, NCH$_2$ e CH$_2$Cl).

1-(3-Chloropropylamino)-9,10-anthraquinone (G)

Yield: 91 %; M.p. 125-127 °C
Elemental analysis for C$_{17}$H$_{14}$ClNO$_2$:

found: C% 67.99   H% 4.58   N% 4.66

calcd.: C% 68.12   H% 4.71   N% 4.67

^{1}H-NMR (CDCl$_3$) δ: 9.81 (s, 1H, NH); 8.41-8.17 (m, 2H, arom); 7.96-7.51 (m, 4H, arom); 7.12 (dd, J = 8.0, 1,8 Hz, 1H, arom); 3.75 (t, J = 6.2 Hz, 2H, CH$_2$Cl); 3.59 (t, J = 6.2 Hz, 2H, NCH$_2$); 2.38-2.16 (quintetto, J = 6.4 Hz, 2H, CH$_2$CH$_2$CH$_2$).

1-(4-Chlorobutylamino)-9,10-anthraquinone (H)

Yield: 83 %; M.p. 89-90 °C
Elemental analysis for $C_{18}H_{16}ClNO_2$:

	found: C% 68.73	H% 4.97	N% 4.29
	calcd.: C% 68.90	H% 5.14	N% 4.46

^{1}H-NMR (CDCl$_3$) δ: 9.80 (s, 1H, NH); 8.38-8.21 (m, 2H, arom); 7.88-7.54 (m, 4H, arom); 7.08 (dd, J = 8.0, 2.0 Hz, 1H, arom); 3.66 (t, J = 6.2 Hz, 2H, CH$_2$Cl); 3.42 (t, J = 6.4 Hz, 2H, NCH$_2$); 2.15-1.86 (m, 4H, CH$_2$C̲H̲$_2$C̲H̲$_2$CH$_2$)

1-(5-Chloropentylamino)-9,10-anthraquinone (I)

Yield: 55 %; M.p. 96-97 °C
Elemental analysis for $C_{19}H_{18}ClNO_2$:

	found: C% 69.93	H% 5.29	N% 4.55
	calcd.: C% 69.62	H% 5.53	N% 4.27

^{1}H-NMR (CDCl$_3$) δ: 10.02 (s, 1H, NH); 8.37-8.21 (m, 2H, arom); 7.84-7.45 (m, 4H, arom); 7.08 (d, 1H, J = 7.8 Hz, arom); 3.62 (t, 2H, J = 6.4 Hz, HNCH$_2$); 3.38 (t, 2H, J = 6.8 Hz, CH$_2$Cl); 2.04-1.61 (m, 6H, CH$_2$C̲H̲$_2$C̲H̲$_2$C̲H̲$_2$CH$_2$).

General method for the synthesis of anthraquinone-derivatives (**58-69**)

A mixture of the proper chloroalkylamino-anthraquinone (**F-I**) (1.5 mmol) with the appropriate amino compound (3 mmol) in 5 mL of CH$_3$CN was heated at 100°C in a sealed tube for 24 h. After cooling, the mixture was solubilized with CHCl$_3$ and evaporated. The residue was then purified by CC (SiO$_2$/CHCl$_3$).

1-[2-(4-Methylpiperazin-1-yl)ethylamino]-9,10-anthraquinone (58)

Yield: 60 %; M.p. 93-94 °C
Elemental analysis for $C_{21}H_{23}N_3O_2$:

	found: C% 72.15	H% 6.85	N% 11.82
	calcd.: C% 72.12	H% 6.63	N% 12.03

^{1}H-NMR (CDCl$_3$) δ: 9.87 (s, 1H, NH); 8.41-8.20 (m, 2H, arom); 7.93-7.45 (m, 4H, arom); 7.08 (d, 1H, J = 9.2 Hz, arom); 3.48 (q, 2H, J = 6.2 Hz; HNCH$_2$); 2.80 (t, 2H, J = 6.4 Hz, CH$_2$N); 2.79-2.42 (m, 8H, N(CH$_2$CH$_2$)$_2$N); 2.48 (s, 3H, NCH$_3$).

^{13}C NMR (200 MHz, CDCl$_3$) δ: 183.8, 182.9, 150.4, 134.2, 134.0, 133.6, 132.9, 132.0, 131.8, 125.7, 125.6, 116.9, 114.6, 112.2, 55.4, 54.0, 51.2, 44.8, 39.2

1-[3-(4-Methylpiperazin-1-yl)propylamino]-9,10-anthraquinone (59)

Yield: 39 %; M.p. 104-106 °C
Elemental analysis for C$_{22}$H$_{25}$N$_3$O$_2$:

	found: C% 72.88	H% 6.67	N% 11.40
	calcd.: C% 72.70	H% 6.93	N% 11.56

^{1}H-NMR (CDCl$_3$) δ: 9.82 (s, 1H, NH); 8.38-8.18 (m, 2H, arom); 7.84-7.51 (m, 4H, arom); 7.14 (dd, 1H, J = 8.0 Hz, 1.8, arom); 3.44 (q, 2H, J = 6.8 Hz, HNCH$_2$); 2.83-2.36 (m, 10H, 8H, 2H, CH$_2$N + 8H, N(CH$_2$CH$_2$)$_2$N); 2.36 (s, 3H, NCH$_3$); 1.96 (quint, 2H, J = 7.0 Hz, CH$_2$<u>CH$_2$</u>CH$_2$).

1-[4-(4-Methylpiperazin-1-yl)butylamino]-9,10-anthraquinone (60)

Yield: 32 %; M.p. 126-127 °C
Elemental analysis for C$_{23}$H$_{27}$N$_3$O$_2$:

	found: C% 73.43	H% 7.37	N% 10.84
	calcd.: C% 73.18	H% 7.21	N% 11.13

^{1}H-NMR (CDCl$_3$) δ: 9.95 (s, 1H, NH); 8.41-8.22 (m, 2H, arom); 7.87-7.48 (m, 4H, arom); 7.16 (dd, 1H, J = 8.4 Hz, 1.8, arom); 3.45 (q, 2H, J = 6.8 Hz, HNCH$_2$); 2.88-2.32 (m, 10H, 8H, 2H, CH$_2$N + 8H, N(CH$_2$CH$_2$)$_2$N); 2.39 (s, 3H, NCH$_3$); 2-01-1.60 (m, 4H, J = 7.0 Hz, CH$_2$<u>CH$_2$CH$_2$</u>CH$_2$).

1-[2-(4-Phenylpiperazin-1-yl)ethylamino]-9,10-anthraquinone (61)

Yield: 75 %; M.p. 138-140 °C
Elemental analysis for C$_{26}$H$_{25}$N$_3$O$_2$:

	found: C% 75.89	H% 6.09	N% 10.56
	calcd.: C% 75.89	H% 6.12	N% 10.21

^{1}H-NMR (CDCl$_3$) δ: 9.91 (s, 1H, NH); 8.38-8.20 (m, 2H, arom); 7.82-7.45 (m, 4H, arom); 7.39-7.22 (m, 2H, arom); 7.10-6.82 (m, 4H, arom); 3.49 (q, 2H, J = 5.2 Hz; HNCH$_2$); 3.40-3.21 (m, 4H, N(CH$_2$CH$_2$)$_2$N); 2.92-2.63 (m, 6H, 2H, CH$_2$N, 4H, N(CH$_2$CH$_2$)$_2$N).

^{13}C NMR (200 MHz, CDCl$_3$) δ: 183.7, 182.8, 150.3, 134.1, 134.0, 133.7, 132.8, 131.9, 131.8, 128.1, 125.8, 125.6, 118.7, 116.8, 115.0, 114.6, 112.2, 55.4, 52.1, 48.2, 39.2

1-[3-(4-Phenylpiperazin-1-yl)propylamino]-9,10-anthraquinone (62)

Yield: 43 %; M.p. 143-145 °C
Elemental analysis for C$_{27}$H$_{27}$N$_3$O$_2$:

	found:	C% 76.20	H% 6.38	N% 9.69
	calcd.:	C% 76.21	H% 6.41	N% 9.87

^{1}H-NMR (CDCl$_3$) δ: 9.83 (s, 1H, NH); 8.36-8.19 (m, 2H, arom); 7.82-7.45 (m, 4H, arom); 7.40-7.20 (m, 2H, arom); 7.13 (dd, 1H, *J* = 1.6, 8.0 Hz, arom); 7.03-6.82 (m, 3H, arom); 3.46 (q, 2H, *J* = 5.6 Hz, HNCH$_2$); 3.34-3.20 (m, 4H, 2H, CH$_2$N, 2H, N(CH$_2$CH$_2$)$_2$N); 2.80-2.50 (m, 6H, N(CH$_2$CH$_2$)$_2$N); 2.18-1.90 (m, 2H, CH$_2$<u>CH$_2$</u>CH$_2$).

^{13}C NMR (200 MHz, CDCl$_3$) δ: 183.9, 182.8, 150.7, 150.3, 134.2, 134.0, 133.6, 132.9, 132.0, 131.8, 128.1, 125.6, 118.6, 116.8, 115.0, 114.6, 111.9, 54.9, 52.3, 48.1, 40.1, 25.5

1-[4-(4-Phenylpiperazin-1-yl)butylamino]-9,10-anthraquinone (63)

Yield: 59 %; M.p. 123-125 °C
Elemental analysis for C$_{28}$H$_{29}$N$_3$O$_2$:

	found:	C% 76.73	H% 6.95	N% 9.86
	calcd.:	C% 76.51	H% 6.65	N% 9.56

^{1}H-NMR (CDCl$_3$) δ: 9.81 (s, 1H, NH); 8.38-8.21 (m, 2H, arom); 7.83-7.51 (m, 4H, arom); 7.39-7.20 (m, 2H, arom); 7.11 (dd, 1H, *J* = 1.6, 7.8 Hz, arom); 7.00-6.81 (m, 3H, arom); 3.42 (q, 2H, *J* = 5.4 Hz, HNCH$_2$); 3.25-3.12 (m, 4H, N(CH$_2$CH$_2$)$_2$N); 2.77-2.60 (m, 4H, N(CH$_2$CH$_2$)$_2$N); 2.52 (t, 2H, *J* = 7.0 Hz, CH$_2$N); 1.91-1.60 (m, 4H, CH$_2$<u>CH$_2$CH$_2$</u>CH$_2$).

^{13}C NMR (200 MHz, CDCl$_3$) δ: 183.9, 182.8, 150.7, 150.3, 134.2, 134.0, 133.7, 133.0, 132.0, 131.9, 128.4, 128.0, 125.7, 125.6, 118.6, 116.8, 116.1, 115.0, 114.6, 111.9, 57.1, 52.3, 48.1, 41.8, 40.1, 26.1, 26.0, 23.4, 23.3

1-[2-(4-Benzylpiperazin-1-yl)ethylamino]-9,10-anthraquinone (64)

Yield: 81 %; M.p. 93-97 °C
Elemental analysis for $C_{27}H_{27}N_3O_2$:

found:	C% 76.06	H% 6.53	N% 10.07
calcd.:	C% 76.21	H% 6.40	N% 9.87

^{1}H-NMR (CDCl$_3$) δ: 9.85 (s, 1H, NH); 8.39-8.20 (m, 2H, arom); 7.87-7.67 (m, 2H, arom); 7.67-7.49 (m, 2H, arom); 7.42-7.20 (m, 5H, arom); 7.10 (t, 1H, J = 11.6 Hz, arom); 3.58 (s, 2H, NCH$_2$Ar); 3.51-3.37 (m, 2H, NHCH$_2$) 2.79 (t, 2H, J = 6.6 Hz, CH$_2$N); 2.76-2.38 (m, 8H, N(CH$_2$CH$_2$)$_2$N).

^{13}C NMR (200 MHz, CDCl$_3$) δ: 183.8, 182.9, 150.4, 137.1, 134.2, 134.0, 133.7, 132.9, 132.0, 131.9, 128.2, 128.0, 127.3, 127.2, 126.3, 126.0, 125.7, 116.9, 114.6, 112.2, 62.0, 55.5, 54.8, 52.2, 52.1, 40.1

1-[3-(4-Benzylpiperazin-1-yl)propylamino]-9,10-anthraquinone (65)

Yield: 55 %; oil
Elemental analysis for $C_{28}H_{29}N_3O_2$:

found:	C% 76.51	H% 6.88	N% 9.59
calcd.:	C% 76.51	H% 6.65	N% 9.56

^{1}H-NMR (CDCl$_3$) δ: 9.85 (s, 1H, NH); 8.38-8.19 (m, 2H, arom); 7.83-7.65 (m, 2H, arom); 7.65-7.48 (m, 2H, arom); 7.48-7.20 (m, 5H, arom); 7.19-7.03 (m, 1H, arom); 3.56 (s, 2H, NCH$_2$Ar); 3.50-3.35 (m, 2H, J = 6.8 Hz; NHCH$_2$); 2.78 (t, 2H, J = 6.0 Hz, CH$_2$N); 2.65- 2.32 (m, 8H, N(CH$_2$CH$_2$)$_2$N); 2.08-1.79 (m, 2H, CH$_2$CH$_2$CH$_2$).

^{13}C NMR (200 MHz, CDCl$_3$) δ: 183.9, 182.8, 150.8, 137.1, 134.2, 134.0, 133.6, 132.9, 132.0, 131.8, 128.1, 127.2, 126.0, 116.9, 114.6, 111.9, 62.0, 55.6, 54.8, 52.3, 52.1, 52.0, 40.0, 25.5

1-[4-(4-benzylpiperazin-1-yl)butylamino]-9,10-anthraquinone (66)

Yield: 66 %; oil
Elemental analysis for $C_{29}H_{31}N_3O_2$:

found:	C% 76.30	H% 6.70	N% 9.90
calcd.:	C% 76.79	H% 6.89	N% 9.26

^{1}H-NMR (CDCl$_3$) δ: 9.80 (s, 1H, NH); 8.38-8.21 (m, 2H, arom); 7.83-7.45 (m, 4H, arom); 7.41-7.20 (m, 4H, arom); 7.12-7.03 (m, 2H, arom); 3.54 (s, 2H, CH$_2$Ar); 3.62-3.31 (m, 4H, NHCH$_2$, CH$_2$N); 2.65-2.37 (m, 8H, N(CH$_2$CH$_2$)$_2$N); 1.91-1.60 (m, 4H, CH$_2$<u>CH$_2$CH$_2$</u>CH$_2$).

1-[2-(4-Phenylpiperidin-1-yl)ethylamino]-9,10-anthraquinone (67)

Yield: 88 %; M.p. 120-124 °C
Elemental analysis for C$_{27}$H$_{26}$N$_2$O$_2$:

	found: C% 79.28	H% 6.30	N% 6.88
	calcd.: C% 79.00	H% 6.38	N% 6.82

^{1}H-NMR (CDCl$_3$) δ: 9.92 (s, 1H, NH); 8.41-8.20 (m, 2H, arom); 7.85-7.68 (m, 2H, arom); 7.68-7.53 (m, 2H, arom); 7.53-7.19 (m, 5H, arom); 7.13 (dd, 1H, J = 1.8, 8 Hz, arom); 3.56 (q, 2H, J = 5.2 Hz; HNCH$_2$); 3.20 (m, 2H, CH$_2$N); 2.85 (t, 2H, J = 6.6 Hz, CH$_2$N); 2.61 (quint, 1H, J = 6.6, N(CH$_2$CH$_2$)$_2$<u>CH</u>); 2.39-2.18 (m, 3H, N(CH$_2$CH$_2$)$_2$CH); 2.10-1.82 (m, 3H, N(CH$_2$CH$_2$)$_2$CH).

^{13}C NMR (200 MHz, CDCl$_3$) δ: 183.8, 182.9, 150.5, 145.2, 134.2, 134.0, 133.7, 132.9, 132.0, 131.8, 127.4, 125.9, 125.7, 125.6, 125.2, 116.9, 114.6, 112.2, 55.9, 53.4, 41.5, 39.4, 32.3

1-[3-(4-Phenylpiperidin-1-yl)propylamino]-9,10-anthraquinone (68)

Yield: 98 %; M.p. 117-118 °C
Elemental analysis for C$_{28}$H$_{28}$N$_2$O$_2$:

	found: C% 79.16	H% 6.61	N% 6.61
	calcd.: C% 79.22	H% 6.65	N% 6.60

^{1}H-NMR (CDCl$_3$) δ: 9.85 (s, 1H, NH); 8.38-8.17 (m, 2H, arom); 7.86-7.42 (m, 4H, arom); 7.40-7.05 (m, 6H, arom); 3.47 (q, 2H, J = 5.4 Hz, NHCH$_2$); 3.14 (m, CH$_2$N); 2.65-2.41 (m, 3H, 2H NCH$_2$, 1H, N(CH$_2$CH$_2$)$_2$<u>CH</u>); 2.20-1.95 (m, 4H, N(CH$_2$CH$_2$)$_2$CH); 1.95-1.73 (m, 4H, N(CH$_2$CH$_2$)$_2$CH).

1-[4-(4-Phenylpiperidin-1-yl)butylamino]-9,10-anthraquinone (69)

Yield: 89 %; M.p. 82-87 °C
Elemental analysis for C$_{29}$H$_{30}$N$_2$O$_2$:

	found: C% 79.58	H% 6.67	N% 6.39

^{1}H-NMR (CDCl$_3$) δ: 9.82 (s, 1H, NH); 8.37-8.20 (m, 2H, arom); 7.82-7.50 (m, 4H, arom); 7.40-7.05 (m, 6H, arom); 3.50-3.36 (m, 2H, NHCH$_2$); 3.25-3.03 (m, 2H, CH$_2$N); 2.63-2.42 (m, 3H, 2H NCH$_2$, 1H, N(CH$_2$CH$_2$)$_2$C$\underline{H}$); 2.23-2.03 (m, 2H, NCH$_2$); 2.03-1.64 (m, 8H, 4H, N(CH$_2$C$\underline{H_2}$)$_2$CH, 4H, CH$_2$C$\underline{H_2}$C$\underline{H_2}$CH$_2$).

General method for the synthesis of naphthoquinone-derivatives (**70-113**)

A mixture of the proper chloroalkylamino-naphthoquinone (**A-E**) (1.5 mmol) with the appropriate amino compound (3 mmol) in 5 mL of CH$_3$CN was heated at 100°C in a sealed tube for 24 h. After cooling, the mixture was solubilized with CHCl$_3$ and evaporated. The residue was then purified by CC (SiO$_2$/CHCl$_3$ + 2% MeOH).

2-Chloro-3-[5-(4-methylpiperazin-1-yl)pentylamino]-1,4-naphthoquinone (**70**)

Yield: 64 %; M.p. 93-96 °C
Elemental analysis for C$_{20}$H$_{26}$ClN$_3$O$_2$:

found:	C% 64.05	H% 6.79	N% 11.02
calcd.:	C% 63.91	H% 6.97	N% 11.18

^{1}H-NMR (CDCl$_3$) δ: 8.24-8.01 (m, 2H, arom); 7.83-7.59 (m, 2H, arom); 6.12 (s, 1H, NH); 3.87 (q, 2H, J = 6.6 Hz, HNC$\underline{H_2}$); 2.82-2.33 (m, 10H, 2H, CH$_2$N + 8H, N(CH$_2$CH$_2$)$_2$N); 2.33 (s, 3H, NCH$_3$); 1.82-1.41 (m, 6H, CH$_2$C$\underline{H_2}$C$\underline{H_2}$C$\underline{H_2}$CH$_2$).
^{13}C NMR (200 MHz, CDCl$_3$) δ: 179.5, 143.1, 133.9, 131.8, 131.4, 128.7, 125.8, 125.7, 57.2, 53.9, 52.0, 44.9, 43.8, 29.9, 25.4, 23.5

2-Chloro-3-[5-(4-methylpiperazin-1-yl)hexylamino]-1,4-naphthoquinone (**71**)

Yield: 56 %; M.p. 75-77 °C
Elemental analysis for C$_{21}$H$_{28}$ClN$_3$O$_2$:

found:	C% 64.33	H% 6.98	N% 10.82
calcd.:	C% 64.69	H% 7.24	N% 10.78

^{1}H-NMR (CDCl$_3$) δ: 8.22-8.00 (m, 2H, arom); 7.85-7.58 (m, 2H, arom); 6.11 (s, 1H, NH); 3.84 (q, 2H, J = 6.8 Hz, HNC$\underline{H_2}$); 2.80-2.32 (m, 10H, 2H, CH$_2$N + 8H, N(CH$_2$CH$_2$)$_2$N); 2.31 (s, 3H, NCH$_3$); 1.82-1.25 (m, 8H, CH$_2$C$\underline{H_2}$C$\underline{H_2}$C$\underline{H_2}$C$\underline{H_2}$CH$_2$).

2-Chloro-3-[5-(4-phenylperazin-1-yl)pentylamino]-1,4-naphthoquinone (72)

Yield: 86 %; M.p. 147-149 °C
Elemental analysis for $C_{25}H_{28}ClN_3O_2$:

	found: C% 68.29	H% 6.77	N% 9.48
	calcd.: C% 68.56	H% 6.44	N% 9.59

^{1}H-NMR (CDCl$_3$) δ: 8.23-8.00 (m, 2H, arom); 7.84-7.60 (m, 2H, arom); 7.40-7.20 (m, 2H, arom); 7.14-6.82 (m, 3H, arom); 6.22 (s, 1H, NH); 3.89 (q, 2H, J = 6.4 Hz, HNCH$_2$); 3.36-3.11 (m, 4H, N(CH$_2$CH$_2$)$_2$N); 2.75-2.40 (m, 6H, 2H, CH$_2$N, 4H, N(CH$_2$CH$_2$)$_2$N); 1.85-1.40 (m, 6H, CH$_2$<u>CH$_2$CH$_2$CH$_2$</u>CH$_2$).

2-Chloro-3-[5-(4-phenylpiperazin-1-yl)hexylamino]-1,4-naphthoquinone (73)

Yield: 84 %; M.p. 107-108 °C
Elemental analysis for $C_{26}H_{30}ClN_3O_2$:

	found: C% 68.83	H% 6.67	N% 9.88
	calcd.: C% 69.09	H% 6.69	N% 9.30

^{1}H-NMR (CDCl$_3$) δ: 8.21-7.99 (m, 2H, arom); 7.83-7.59 (m, 2H, arom); 7.42-7.22 (m, 2H, arom); 7.15-6.83 (m, 3H, arom); 6.15 (s, 1H, NH); 3.86 (q, 2H, J = 7.0 Hz, HN<u>CH$_2$</u>); 2.85-2.30 (m, 10H, 2H, CH$_2$N + 8H, N(CH$_2$CH$_2$)$_2$N); 1.81-1.25 (m, 8H, CH$_2$<u>CH$_2$CH$_2$CH$_2$CH$_2$</u>CH$_2$).

2-[3-(4-Benzylpiperazin-1-yl)pentylamino]-3-chloro-1,4-naphthoquinone (74)

Yield: 66 %; M.p. 94-96 °C
Elemental analysis for $C_{26}H_{30}ClN_3O_2$:

	found: C% 68.88	H% 6.76	N% 9.47
	calcd.: C% 69.09	H% 6.69	N% 9.30

^{1}H-NMR (CDCl$_3$) δ: 8.20-8.00 (m, 2H, arom); 7.83-7.60 (m, 2H, arom); 7.45-7.22 (m, 5H, arom); 6.22 (s, 1H, NH); 3.93 (q, 2H, J = 6.6 Hz, HNCH$_2$); 3.55 (s, 2H, NCH$_2$Ar); 2.76-2.24 (m, 10H, 8H di N(CH$_2$CH$_2$)$_2$N, 2H di CH$_2$N); 1.85-1.42 (m, 6H, CH$_2$<u>CH$_2$CH$_2$CH$_2$</u>CH$_2$).

2-[3-(4-Benzylpiperazin-1-yl)hexylamino]-3-chloro -1,4-naphthoquinone (75)

Yield: 64 %; M.p. 91-93 °C

Elemental analysis for $C_{27}H_{32}ClN_3O_2$:

	found:	C% 69.42	H% 6.79	N% 9.34
	calcd.:	C% 69.59	H% 6.92	N% 9.02

^{1}H-NMR (CDCl$_3$) δ: 8.21-7.99 (m, 2H, arom); 7.81-7.59 (m, 2H, arom); 7.41-7.18 (m, 5H, arom); 6.21 (s, 1H, NH); 3.87 (q, 2H, J = 7.0 Hz, HN$\underline{CH_2}$); 3.58 (s, 2H, NCH$_2$Ar); 2.82-2.30 (m, 10H, 2H, CH$_2$N + 8H, N(CH$_2$CH$_2$)$_2$N); 1.80-1.25 (m, 8H, CH$_2$$\underline{CH_2CH_2CH_2CH_2}CH_2$).

2-Chloro-3-[3-(4-phenylpiperidin-1-yl)pentylamino]-1,4-naphthoquinone (76)

Yield: 85 %; M.p. 92-94 °C

Elemental analysis for $C_{26}H_{29}ClN_2O_2$:

	found:	C% 71.87	H% 6.77	N% 6.54
	calcd.:	C% 71.46	H% 6.69	N% 6.41

^{1}H-NMR (CDCl$_3$) δ: 8.24-8.00 (m, 2H, arom); 7.83-7.58 (m, 2H, arom); 7.45-7.17 (m, 5H, arom); 6.24 (s, 1H, NH); 3.91 (q, 2H, J = 6.2 Hz, HNCH$_2$); 3.25-3.00 (m, 2H, N(CH$_2$CH$_2$)$_2$CH); 2.67-2.42 (m, 3H, 2H, N(CH$_2$CH$_2$)$_2$CH, 1H, N(CH$_2$CH$_2$)$_2$$\underline{CH}$); 2.12-2.02 (m, 2H, N(CH$_2$CH$_2$)$_2$CH); 1.97-1.82 (m, 4H, 2H di N(CH$_2$CH$_2$)$_2$CH, 2H di CH$_2$N); 1.75-1.40 (m, 6H, CH$_2$$\underline{CH_2CH_2CH_2}CH_2$).

2-Chloro-3-[3-(4-phenylpiperidin-1-yl)hexylamino]-1,4-naphthoquinone (77)

Yield: 82 %; M.p. 85-90 °C

Elemental analysis for $C_{27}H_{31}ClN_2O_2$:

	found:	C% 71.53	H% 6.64	N% 6.89
	calcd.:	C% 71.91	H% 6.93	N% 6.21

^{1}H-NMR (CDCl$_3$) δ: 8.20-7.99 (m, 2H, arom); 7.84-7.58 (m, 2H, arom); 7.47-7.15 (m, 5H, arom); 6.22 (s, 1H, NH); 3.92 (q, 2H, J = 6.2 Hz, HNCH$_2$); 3.26-2.99 (m, 2H, N(CH$_2$CH$_2$)$_2$CH); 2.65-2.40 (m, 3H, 2H, N(CH$_2$CH$_2$)$_2$CH, 1H, N(CH$_2$CH$_2$)$_2$$\underline{CH}$);

2.14-2.03 (m, 2H, N(CH$_2$CH$_2$)$_2$CH); 1.96-1.80 (m, 4H, 2H of N(CH$_2$CH$_2$)$_2$CH, 2H of CH$_2$N); 1.70-1.25 (m, 8H, CH$_2$<u>CH$_2$CH$_2$CH$_2$CH$_2$</u>CH$_2$).

2-(4-Benzylpiperidin-1-yl)-3-chloro-1,4-naphthoquinone (78)

Yield: 95 %; M.p. 104-106 °C
Elemental analysis for C$_{22}$H$_{20}$ClNO$_2$:

	found:	C% 71.98	H% 5.35	N% 3.77
	calcd.:	C% 72.23	H% 5.51	N% 3.83

^{1}H-NMR (CDCl$_3$) δ: 8.20-7.99 (m, 2H, arom); 7.78-7.68 (m, 2H, arom); 7.42-6.98 (m, 5H, arom); 2.78-2.40 (m, 4H, N(CH$_2$CH$_2$)$_2$N); 2.11 (s, 2H, NCH$_2$Ar); 1.80-1.20 (m, 5H, 1H of N(CH$_2$CH$_2$)$_2$<u>CH</u>, 4H of N(CH$_2$CH$_2$)$_2$N).

2-[3-(4-Benzylpiperazin-1-yl)ethylamino]-3-chloro   -1,4-naphthoquinone (79)

Yield: 98 %; M.p. 91-92 °C
Elemental analysis for C$_{24}$H$_{25}$ClN$_2$O$_2$:

	found:	C% 69.99	H% 6.00	N% 7.12
	calcd.:	C% 70.49	H% 6.16	N% 6.85

^{1}H-NMR (CDCl$_3$) *δ*: 8.23-7.97 (m, 2H, arom); 7.82-7.61 (m, 2H, arom); 7.42-6.90 (m, 6H, 5H arom, 1H, NH); 3.96 (q, 2H, *J* = 6.8 Hz, HN<u>CH$_2$</u>); 3.05-2.82 (m, 2H, <u>CH2</u>N(CH$_2$CH$_2$)$_2$N); 2.78-2.41 (m, 4H, N(CH$_2$CH$_2$)$_2$N); 2.19-1.89 (m, 2H, NCH$_2$Ar); 1.82-1.20 (m, 5H, 1H of N(CH$_2$CH$_2$)$_2$<u>CH</u>, 4H of N(CH$_2$CH$_2$)$_2$N).

2-[3-(4-Benzylpiperazin-1-yl)propylamino]-3-chloro   -1,4-naphthoquinone (80)

Yield: 70 %; M.p. 85-86 °C
Elemental analysis for C$_{25}$H$_{27}$ClN$_2$O$_2$:

	found:	C% 70.28	H% 6.45	N% 6.77
	calcd.:	C% 70.99	H% 6.43	N% 6.62

^{1}H-NMR (CDCl$_3$) *δ*: 8.21-7.95 (m, 2H, arom); 7.80-7.60 (m, 2H, arom); 7.40-6.86 (m, 6H, 5H arom, 1H, NH); 3.95 (q, 2H, *J* = 6.6 Hz, HN<u>CH$_2$</u>); 3.02-2.80 (m, 2H, <u>CH2</u>N(CH$_2$CH$_2$)$_2$N); 2.75-2.39 (m, 4H, N(CH$_2$CH$_2$)$_2$N); 2.20-1.95 (m, 2H, NCH$_2$Ar);

1.80-1.20 (m, 7H, 1H of N(CH$_2$CH$_2$)$_2$CH, 4H of N(CH$_2$CH$_2$)$_2$N, 2H of NHCH$_2$CH$_2$CH$_2$).

2-[3-(4-Benzylpiperazin-1-yl)buthylamino]-3-chloro   -1,4-naphthoquinone (**81**)

Yield: 80 %; M.p. 80-82 °C
Elemental analysis for C$_{26}$H$_{29}$ClN$_2$O$_2$:

	found: C% 71.42	H% 6.40	N% 6.10
	calcd.: C% 71.46	H% 6.69	N% 6.41

^{1}H-NMR (CDCl$_3$) δ: 8.23-7.97 (m, 2H, arom); 7.81-7.62 (m, 2H, arom); 7.38-6.88 (m, 6H, 5H arom, 1H, NH); 3.94 (q, 2H, J = 6.8 Hz, HNCH$_2$); 3.01-2.79 (m, 2H, CH2N(CH$_2$CH$_2$)$_2$N); 2.73-2.43 (m, 4H, N(CH$_2$CH$_2$)$_2$N); 2.18-1.96 (m, 2H, NCH$_2$Ar); 1.78-1.20 (m, 9H, 1H of N(CH$_2$CH$_2$)$_2$CH, 4H of N(CH$_2$CH$_2$)$_2$N, 4H of NHCH$_2$ CH$_2$CH$_2$CH$_2$).

2-[3-(4-Benzylpiperazin-1-yl)pentylamino]-3-chloro   -1,4-naphthoquinone (**82**)

Yield: 75 %; M.p. 78-79 °C
Elemental analysis for C$_{27}$H$_{31}$ClN$_2$O$_2$:

	found: C% 71.53	H% 6.24	N% 6.15
	calcd.: C% 71.91	H% 6.93	N% 6.21

^{1}H-NMR (CDCl$_3$) δ: 8.20-7.94 (m, 2H, arom); 7.79-7.55 (m, 2H, arom); 7.38-6.87 (m, 6H, 5H arom, 1H, NH); 3.95 (q, 2H, J = 6.6 Hz, HNCH$_2$); 3.02-2.82 (m, 2H, CH2N(CH$_2$CH$_2$)$_2$N); 2.77-2.37 (m, 4H, N(CH$_2$CH$_2$)$_2$N); 2.18-1.94 (m, 2H, NCH$_2$Ar); 1.80-1.64 (m, 5H, 1H of N(CH$_2$CH$_2$)$_2$CH, 4H of N(CH$_2$CH$_2$)$_2$N); 1.59-1.18 (m, 6H, CH$_2$CH$_2$CH$_2$CH$_2$CH$_2$CH$_2$).

2-[3-(4-Benzylpiperazin-1-yl)hexylamino]-3-chloro   -1,4-naphthoquinone (**83**)

Yield: 69 %; M.p. 75-76 °C
Elemental analysis for C$_{28}$H$_{33}$ClN$_2$O$_2$:

	found: C% 71.99	H% 6.89	N% 6.41
	calcd.: C% 72.32	H% 7.15	N% 6.02

^{1}H-NMR (CDCl$_3$) δ: 8.20-7.95 (m, 2H, arom); 7.83-7.57 (m, 2H, arom); 7.42-6.88 (m, 6H, 5H arom, 1H, NH); 3.93 (q, 2H, J = 6.8 Hz, HNCH$_2$); 3.10-2.83 (m, 2H, CH2N(CH$_2$CH$_2$)$_2$N); 2.78-2.42 (m, 4H, N(CH$_2$CH$_2$)$_2$N); 2.20-1.98 (m, 2H, NCH$_2$Ar); 1.85-1.55 (m, 5H, 1H of N(CH$_2$CH$_2$)$_2$CH, 4H of N(CH$_2$CH$_2$)$_2$N); 1.48-1.23 (m, 8H, CH$_2$CH$_2$CH$_2$CH$_2$CH$_2$CH$_2$).

2-Chloro-3-[4-(2-chlorophenyl)piperazin-1-yl]-1,4-naphthoquinone (84)

Yield: 67 %; M.p. 145-148 °C
Elemental analysis for C$_{20}$H$_{16}$Cl$_2$N$_2$O$_2$:

	found: C% 61.53	H% 4.17	N% 7.23
	calcd.: C% 62.03	H% 4.16	N% 7.23

^{1}H-NMR (CDCl$_3$) δ: 8.22-8.02 (m, 2H, arom); 7.81-7.66 (m, 2H, arom); 7.45-7.39 (m, 1H, arom); 7.36-7.22 (m, 1H, arom); 7.20-6.99 (m, 2H, arom); 3.91-3.78 (m, 4H, N(CH$_2$CH$_2$)$_2$N); 3.98-3.20 (m, 4H, N(CH$_2$CH$_2$)$_2$N).

2-Chloro-3-[4-(3-chlorophenyl)piperazin-1-yl]-1,4-naphthoquinone (85)

Yield: 79 %; M.p. 69-70 °C
Elemental analysis for C$_{20}$H$_{16}$Cl$_2$N$_2$O$_2$:

	found: C% 62.08	H% 4.45	N% 6.79
	calcd.: C% 62.03	H% 4.16	N% 7.23

^{1}H-NMR (CDCl$_3$) δ: 8.21-8.04 (m, 2H, arom); 7.81-7.68 (m, 2H, arom); 7.31-7.19 (m, 1H, arom); 7.00-6.84 (m, 3H, arom); 3.88-3.74 (m, 4H, N(CH$_2$CH$_2$)$_2$N); 3.98-3.37 (m, 4H, N(CH$_2$CH$_2$)$_2$N).

2-Chloro-3-[4-(4-chlorophenyl)piperazin-1-yl]-1,4-naphthoquinone (86)

Yield: 95 %; M.p. 151-154 °C
Elemental analysis for C$_{20}$H$_{16}$Cl$_2$N$_2$O$_2$:

	found: C% 62.59	H% 4.09	N% 7.49
	calcd.: C% 62.03	H% 4.16	N% 7.23

^{1}H-NMR (CDCl$_3$) δ: 8.21-8.01 (m, 2H, arom); 7.81-7.65 (m, 2H, arom); 7.35-7.20 (m, 2H, arom); 7.02-6.88 (m, 2H, arom); 3.92-3.72 (m, 4H, N(CH$_2$CH$_2$)$_2$N); 3.90-3.28 (m, 4H, N(CH$_2$CH$_2$)$_2$N).

2-Chloro-3-[4-(2-methoxyphenyl)piperazin-1-yl]-1,4-naphthoquinone (87)

Yield: 97 %; M.p. 157-159 °C
Elemental analysis for $C_{21}H_{19}ClN_2O_3$:

	found: C% 65.08	H% 4.85	N% 7.38
	calcd.: C% 65.88	H% 5.00	N% 7.32

^{1}H-NMR (CDCl$_3$) δ: 8.22-8.01 (m, 2H, arom); 7.82-7.64 (m, 2H, arom); 7.18-6.89 (m, 4H, arom); 3.94 (s, 3H, OCH$_3$) 3.91-3.79 (m, 4H, N(CH$_2$CH$_2$)$_2$N); 3.40-3.20 (m, 4H, N(CH$_2$CH$_2$)$_2$N).

2-Chloro-3-[4-(3-methoxyphenyl)piperazin-1-yl]-1,4-naphthoquinone (88)

Yield: 84 %; M.p. 74-78 °C
Elemental analysis for $C_{21}H_{19}ClN_2O_3$:

	found: C% 65.44	H% 4.90	N% 7.20
	calcd.: C% 65.88	H% 5.00	N% 7.32

^{1}H-NMR (CDCl$_3$) δ: 8.22-8.01 (m, 2H, arom); 7.83-7.64 (m, 2H, arom); 7.37-7.18 (m, 2H, arom); 6.70-6.43 (m, 2H, arom); 3.97-3.70 (m, 7H, 4H of N(CH$_2$CH$_2$)$_2$N, 3H of OCH$_3$); 3.50-3.32 (m, 4H, N(CH$_2$CH$_2$)$_2$N).

2-Chloro-3-[4-(4-methoxyphenyl)piperazin-1-yl]-1,4-naphthoquinone (89)

Yield: 87 %; M.p. 134-138 °C
Elemental analysis for $C_{21}H_{19}ClN_2O_3$:

	found: C% 65.64	H% 4.95	N% 7.31
	calcd.: C% 65.88	H% 5.00	N% 7.32

^{1}H-NMR (CDCl$_3$) δ: 8.21-8.00 (m, 2H, arom); 7.81-7.64 (m, 2H, arom); 7.08-6.82 (m, 4H, arom); 3.90-3.70 (m, 7H, 4H of N(CH$_2$CH$_2$)$_2$N, 3H of OCH$_3$); 3.37-3.20 (m, 4H, N(CH$_2$CH$_2$)$_2$N).

2-Chloro-3-{2-[4-(2-chlorophenyl)piperazin-1-yl]ethylamino}-1,4-naphthoquinone (90)

Yield: 70 %; M.p. 166-168 °C
Elemental analysis for $C_{22}H_{21}Cl_2N_3O_2$:

	found: C% 61.13	H% 4.56	N% 9.59

calcd.: C% 61.69   H% 4.77   N% 9.29

^{1}H-NMR (CDCl$_3$) δ: 8.23-7.98 (m, 2H, arom); 7.82-7.58 (m, 2H, arom); 7.44-7.35 (m, 1H, arom); 7.34-7.20 (m, 2H, arom); 7.18-6.97 (m, 2H, arom); (s, 1H, NH); 4.03 (q, 2H, J=5.4 Hz, HNCH$_2$); 3.24-3.02 (m, 4H, N(CH$_2$CH$_2$)$_2$N); 2.86-2.67 (m, 6H, 2H of CH$_2$N, 4H of N(CH$_2$CH$_2$)$_2$N).

2-Chloro-3-{2-[4-(2-chlorophenyl)piperazin-1-yl]propylamino}-1,4-naphthoquinone (91)

Yield: 75 %; M.p. 109-111 °C
Elemental analysis for C$_{23}$H$_{23}$Cl$_2$N$_3$O$_2$:

found: C% 62.18   H% 5.20   N% 9.53

calcd.: C% 62.17   H% 5.22   N% 9.46

^{1}H-NMR (CDCl$_3$) δ: 8.21-8.00 (m, 2H, arom); 7.81-7.58 (m, 3H, 2H arom, 1H, NH); 7.46-7.37 (m, 1H, arom); 7.35-7.22 (m, 1H, arom); 7.21-7.12 (m, 1H, arom); 7.10-6.98 (m, 1H, arom); 4.08 (q, 2H, J = 6.0 Hz, HNCH$_2$); 3.23 (t, 4H, J = 4.6 Hz, N(CH$_2$CH$_2$)$_2$N); 2.82-2.58 (m, 6H, 2H, CH$_2$N, 4H, N(CH$_2$CH$_2$)$_2$N); 1.92 (quint, 2H, J = 6.0 Hz, CH$_2$C̲H̲$_2$CH$_2$).

2-Chloro-3-{2-[4-(2-chlorophenyl)piperazin-1-yl]butylamino}-1,4-naphthoquinone (92)

Yield: 74 %; M.p. 103-104 °C
Elemental analysis for C$_{24}$H$_{25}$Cl$_2$N$_3$O$_2$:

found: C% 62.83   H% 5.20   N% 9.49

calcd.: C% 62.89   H% 5.50   N% 9.17

^{1}H-NMR (CDCl$_3$) δ: 8.22-7.99 (m, 2H, arom); 7.81-7.49 (m, 3H, 2H arom, 1H, NH); 7.37-7.16 (m, 2H, arom); 7.01-6.78 (m, 2H, arom); 4.07 (q, 2H, J = 6.0 Hz, HNCH$_2$); 3.46-3.20 (m, 4H, N(CH$_2$CH$_2$)$_2$N); 2.82-2.37 (m, 6H, 2H, CH$_2$N, 4H, N(CH$_2$CH$_2$)$_2$N); 1.94 (quint, 4H, J = 5.8 Hz, CH$_2$C̲H̲$_2$C̲H̲$_2$CH$_2$).

2-Chloro-3-{2-[4-(2-chlorophenyl)piperazin-1-yl]pentylamino}-1,4-naphthoquinone (93)

Yield: 66 %; M.p. 78-80 °C
Elemental analysis for C$_{25}$H$_{27}$Cl$_2$N$_3$O$_2$:

found: C% 63.05   H% 5.62   N% 8.94

calcd.: C% 63.56 H% 5.76 N% 8.90

^{1}H-NMR (CDCl$_3$) δ: 8.22-7.99 (m, 2H, arom); 7.82-7.58 (m, 2H, arom); 7.43-7.33 (m, 1H, arom); 7.30-6.18 (m, 1H, arom); 6.11-6.92 (m, 2H, arom); 6.13 (s, 1H, NH); 3.89 (q, 2H, J = 7.0 Hz, HNCH$_2$); 3.24-2.99 (m, 4H, N(CH$_2$CH$_2$)$_2$N); 2.88-2.60 (m, 4H, N(CH$_2$CH$_2$)$_2$N); 2.48 (t, 2H, J = 7.8 Hz, CH$_2$N); 1.88-1.38 (m, 6H, CH$_2$<u>CH$_2$CH$_2$CH$_2$</u>CH$_2$).

2-Chloro-3-{2-[4-(3-chlorophenyl)piperazin-1-yl]ethylamino}-1,4-naphthoquinone (94)

Yield: 70 %; M.p. 111-113 °C
Elemental analysis for C$_{22}$H$_{21}$Cl$_2$N$_3$O$_2$:

    found: C% 61.13 H% 4.56 N% 9.59

    calcd.: C% 61.40 H% 4.92 N% 9.76

^{1}H-NMR (CDCl$_3$) δ: 8.23-8.12 (m, 2H, arom); 8.10-7.93 (m, 2H, arom); 7.82-7.48 (m, 2H, arom); 7.36-7.17 (m, 1H, arom); 6.98-6.79 (m, 2H, arom); (s, 1H, NH); 4.03 (q, 2H, J= 5.8 Hz, HNCH$_2$); 3.40-3.20 (m, 4H, N(CH$_2$CH$_2$)$_2$N); 2.88-2.63 (m, 6H, 2H of CH$_2$N, 4H of N(CH$_2$CH$_2$)$_2$N).

2-Chloro-3-{2-[4-(3-chlorophenyl)piperazin-1-yl]propylamino}-1,4-naphthoquinone (95)

Yield: 75 %; M.p. 123-124 °C
Elemental analysis for C$_{23}$H$_{23}$Cl$_2$N$_3$O$_2$:

    found: C% 62.48 H% 5.28 N% 9.05

    calcd.: C% 62.17 H% 5.22 N% 9.46

^{1}H-NMR (CDCl$_3$) δ: 8.23-8.00 (m, 2H, arom); 7.82-7.39 (m, 2H, arom); 7.44-7.19 (m, 2H, arom); 7.16-6.96 (m, 2H, arom); 6.28 (s, 1H, NH); 3.93 (q, 2H, J = 6.4 Hz, HNCH$_2$); 3.28-3.08 (m, 4H, N(CH$_2$CH$_2$)$_2$N); 2.89-2.67 (m, 4H, N(CH$_2$CH$_2$)$_2$N); 2.58 (t, 2H, J = 6.8 Hz, CH$_2$N); 1.77 (quint, 2H, J = 3.2 Hz, CH$_2$<u>CH$_2$</u>CH$_2$).

2-Chloro-3-{2-[4-(3-chlorophenyl)piperazin-1-yl]butylamino}-1,4-naphthoquinone (96)

Yield: 74 %; M.p. 118-119 °C
Elemental analysis for C$_{24}$H$_{25}$Cl$_2$N$_3$O$_2$:

    found: C% 62.98 H% 5.30 N% 8.96

calcd.: C% 62.89   H% 5.50   N% 9.17

^{1}H-NMR (CDCl$_3$) δ: 8.23-8.00 (m, 2H, arom); 7.83-7.60 (m, 2H, arom); 7.35-7.12 (m, 2H, arom); 6.97-6.78 (m, 2H, arom); 6.27 (s, 1H, NH); 3.93 (q, 2H, J = 6.8 Hz, HNCH$_2$); 3.37-3.17 (m, 4H, N(CH$_2$CH$_2$)$_2$N); 2.75-2.57 (m, 4H, N(CH$_2$CH$_2$)$_2$N); 2.48 (t, 2H, J = 6.8 Hz, CH$_2$N); 1.91-1.58 (m, 4H, CH$_2$CH$_2$CH$_2$CH$_2$).

2-Chloro-3-{2-[4-(3-chlorophenyl)piperazin-1-yl]pentylamino}-1,4-naphthoquinone (97)

Yield: 83 %; M.p. 69-72 °C
Elemental analysis for C$_{25}$H$_{27}$Cl$_2$N$_3$O$_2$:

found: C% 63.67   H% 5.64   N% 9.19

calcd.: C% 63.56   H% 5.76   N% 8.90

^{1}H-NMR (CDCl$_3$) δ: 8.24-8.00 (m, 2H, arom); 7.82-7.58 (m, 2H, arom); 7.35-7.10 (m, 2H, arom); 6.95-6.75 (m, 2H, arom); 6.14 (s, 1H, NH); 3.89 (q, 2H, J = 6.8 Hz, HNCH$_2$); 3.34-3.15 (m, 4H, N(CH$_2$CH$_2$)$_2$N); 2.70-2.55 (m, 4H, N(CH$_2$CH$_2$)$_2$N); 2.45 (t, 2H, J = 7.8 Hz, CH$_2$N); 1.87-1.39 (m, 6H, CH$_2$CH$_2$CH$_2$CH$_2$CH$_2$).

2-Chloro-3-{2-[4-(4-chlorophenyl)piperazin-1-yl]ethylamino}-1,4-naphthoquinone (98)

Yield: 70 %; M.p. 130-132 °C
Elemental analysis for C$_{22}$H$_{21}$Cl$_2$N$_3$O$_2$:

found: C% 60.53   H% 4.86   N% 9.99

calcd.: C% 61.40   H% 4.92   N% 9.76

^{1}H-NMR (CDCl$_3$) δ: 8.21-8.00 (m, 2H, arom); 7.81-7.59 (m, 2H, arom); 7.32-7.19 (m, 2H, arom); 7.00-6.81 (m, 3H, 2H arom, 1H, NH); 4.02 (q, 2H, J =5.8 Hz, HNCH$_2$); 3.37-3.15 (m, 4H, N(CH$_2$CH$_2$)$_2$N); 2.83-2.60 (m, 6H, 2H of CH$_2$N, 4H of N(CH$_2$CH$_2$)$_2$N).

2-Chloro-3-{2-[4-(4-chlorophenyl)piperazin-1-yl]propylamino}-1,4-naphthoquinone (99)

Yield: 75 %; M.p. 137-139 °C
Elemental analysis for C$_{23}$H$_{23}$Cl$_2$N$_3$O$_2$:

found: C% 62.51   H% 5.28   N% 9.47

^{1}H-NMR (CDCl$_3$) δ: 8.21-7.98 (m, 2H, arom); 7.80-7.48 (m, 3H, 2H arom, 1H, NH); 7.37-7.19 (m, 2H, arom); 6.99-6.82 (m, 2H, arom); 4.07 (q, 2H, J = 6.0 Hz, HNCH$_2$); 3.32 (t, 4H, J = 5.0 Hz, N(CH$_2$CH$_2$)$_2$N); 2.79-2.54 (m, 6H, 2H, CH$_2$N, 4H, N(CH$_2$CH$_2$)$_2$N); 1.92 (quint, 2H, J = 6.2 Hz, CH$_2$<u>CH$_2$</u>CH$_2$).

2-Chloro-3-{2-[4-(4-chlorophenyl)piperazin-1-yl]butylamino}-1,4-naphthoquinone (100)

Yield: 67 %; M.p. 128-131 °C
Elemental analysis for C$_{24}$H$_{25}$Cl$_2$N$_3$O$_2$:

found: C% 62.48   H% 5.32   N% 9.39

calcd.: C% 62.89   H% 5.50   N% 9.17

^{1}H-NMR (CDCl$_3$) δ: 8.23-7.99 (m, 2H, arom); 7.81-7.59 (m, 2H, arom); 7.33-7.17 (m, 2H, arom); 6.95-6.79 (m, 2H, arom); 6.25 (s, 1H, NH); 3.91 (q, 2H, J = 6.6 Hz, HNCH$_2$); 3.30-3.08 (m, 4H, N(CH$_2$CH$_2$)$_2$N); 2.73-2.55 (m, 4H, N(CH$_2$CH$_2$)$_2$N); 2.47 (t, 2H, J = 6.0 Hz, CH$_2$N); 1.97-1.59 (m, 4H, CH$_2$<u>CH$_2$</u><u>CH$_2$</u>CH$_2$).

2-Chloro-3-{2-[4-(4-chlorophenyl)piperazin-1-yl]pentylamino}-1,4-naphthoquinone (101)

Yield: 53 %; M.p. 142-145 °C
Elemental analysis for C$_{25}$H$_{27}$Cl$_2$N$_3$O$_2$:

found: C% 63.05   H% 5.70   N% 8.19

calcd.: C% 63.56   H% 5.76   N% 8.90

^{1}H-NMR (CDCl$_3$) δ: 8.26-8.01 (m, 2H, arom); 7.83-7.59 (m, 2H, arom); 7.37-7.18 (m, 2H, arom); 6.95-6.81 (m, 2H, arom); 6.13 (s, 1H, NH); 3.90 (q, 2H, J = 7.0 Hz, HNCH$_2$); 3.27-3.11 (m, 4H, N(CH$_2$CH$_2$)$_2$N); 2.74-2.56 (m, 4H, N(CH$_2$CH$_2$)$_2$N); 2.44 (t, 2H, J = 7.6 Hz, CH$_2$N); 1.86-1.39 (m, 6H, CH$_2$<u>CH$_2$</u><u>CH$_2$</u><u>CH$_2$</u>CH$_2$).

2-Chloro-3-{2-[4-(2-methoxyphenyl)piperazin-1-yl]ethylamino}-1,4-naphthoquinone (102)

Yield: 74 %; M.p. 164-165 °C
Elemental analysis for C$_{22}$H$_{21}$Cl$_2$N$_3$O$_2$:

found: C% 64.99   H% 5.61   N% 9.80

calcd.: C% 64.86   H% 5.68   N% 9.87

^{1}H-NMR (CDCl$_3$) δ: 8.21-7.99 (m, 2H, arom); 7.82-7.58 (m, 2H, arom); 7.10-6.82 (m, 5H, 4H arom, 1H NH); 4.03 (q, 2H, J= 2.8 Hz, HNCH$_2$); 3.90 (s, 3H, OCH$_3$); 3.28-3.07 (m, 4H, N(CH$_2$CH$_2$)$_2$N); 2.90-2.70 (m, 6H, 2H di CH$_2$N, 4H di N(CH$_2$CH$_2$)$_2$N).

2-Chloro-3-{2-[4-(2-methoxyphenyl)piperazin-1-yl]propylamino}-1,4-naphthoquinone (103)

Yield: 73 %; M.p. 120-124 °C
Elemental analysis for C$_{24}$H$_{26}$ClN$_3$O$_3$:

found: C% 65.27   H% 5.55   N% 9.89

calcd.: C% 65.52   H% 5.96   N% 9.55

^{1}H-NMR (CDCl$_3$) δ: 8.21-7.98 (m, 2H, arom); 7.79-7.57 (m, 2H, arom); 7.14-6.83 (m, 5H, 4H arom, 1H NH); 4.07 (q, 2H, J = 6.0 Hz, HNCH$_2$); 3.90 (s, 3H, OCH$_3$); 3.38-3.17 (m, 4H, N(CH$_2$CH$_2$)$_2$N); 2.89-2.72 (m, 4H, N(CH$_2$CH$_2$)$_2$N); 2.64 (t, 2H, J = 6.0 Hz, CH$_2$N); 1.92 (quint, 2H, J = 5.8 Hz, CH$_2$CH$_2$CH$_2$).

2-Chloro-3-{2-[4-(2-methoxyphenyl)piperazin-1-yl]butylamino}-1,4-naphthoquinone (104)

Yield: 62 %; M.p. 125-128 °C
Elemental analysis for C$_{25}$H$_{28}$ClN$_3$O$_3$:

found: C% 66.00   H% 6.04   N% 9.31

calcd.: C% 66.14   H% 6.22   N% 9.26

^{1}H-NMR (CDCl$_3$) δ: 8.22-8.00 (m, 2H, arom); 7.81-7.59 (m, 2H, arom); 7.08-6.83 (m, 4H, arom); 6.26 (s, 1H, NH); 4.01-3.80 (m, 5H, 2H HNCH$_2$, 3H OCH$_3$); 3.24-3.04 (m, 4H, N(CH$_2$CH$_2$)$_2$N); 2.79-2.61 (m, 4H, N(CH$_2$CH$_2$)$_2$N); 2.50 (t, 2H, J = 6.6 Hz, CH$_2$N); 1.98-1.59 (m, 4H, CH$_2$CH$_2$CH$_2$CH$_2$).

2-Chloro-3-{2-[4-(2-methoxyphenyl)piperazin-1-yl]pentylamino}-1,4-naphthoquinone (105)

Yield: 71 %; M.p. 90-93 °C
Elemental analysis for C$_{26}$H$_{30}$ClN$_3$O$_3$:

found: C% 66.43   H% 6.40   N% 9.36

calcd.: C% 66.73   H% 6.46   N% 8.98

^{1}H-NMR (CDCl$_3$) δ: 8.23-8.00 (m, 2H, arom); 7.81-7.59 (m, 2H, arom); 7.10-6.82 (m, 4H, arom); 6.13 (s, 1H, NH); 4.00-3.78 (m, 5H, 2H HNCH$_2$, 3H OCH$_3$); 3.28-2.99 (m, 4H, N(CH$_2$CH$_2$)$_2$N); 2.82-2.59 (m, 4H, N(CH$_2$CH$_2$)$_2$N); 2.46 (t, 2H, J = 7.8 Hz, CH$_2$N); 1.90-1.39 (m, 6H, CH$_2$CH$_2$CH$_2$CH$_2$CH$_2$).

2-Chloro-3-{2-[4-(3-methoxyphenyl)piperazin-1-yl]ethylamino}-1,4-naphthoquinone (106)

Yield: 91 %; M.p. 139-141 °C
Elemental analysis for C$_{22}$H$_{21}$Cl$_2$N$_3$O$_2$:

found: C% 64.18   H% 5.60   N% 9.58

calcd.: C% 64.86   H% 5.68   N% 9.87

^{1}H-NMR (CDCl$_3$) δ: 8.22-8.02 (m, 2H, arom); 7.80-7.60 (m, 2H, arom); 6.98 (s, 1H, NH); 6.63-6.41 (m, 4H, arom); 4.03 (q, 2H, J= 5.4 Hz, HNCH$_2$); 3.83 (s, 3H, OCH$_3$); 3.38-3.21 (m, 4H, N(CH$_2$CH$_2$)$_2$N); 2.81-2.64 (m, 6H, 2H of CH$_2$N, 4H of N(CH$_2$CH$_2$)$_2$N).

2-Chloro-3-{2-[4-(3-methoxyphenyl)piperazin-1-yl]propylamino}-1,4-naphthoquinone (107)

Yield: 93 %; M.p. 90-91 °C
Elemental analysis for C$_{24}$H$_{26}$ClN$_3$O$_3$:

found: C% 65.75   H% 5.91   N% 9.45

calcd.: C% 65.52   H% 5.96   N% 9.55

^{1}H-NMR (CDCl$_3$) δ: 8.22-7.99 (m, 2H, arom); 7.80-7.50 (m, 3H, 2H arom, 1H NH); 7.35-7.17 (m, 2H, arom); 6.64-6.42 (m, 2H, arom); 4.07 (q, 2H, J = 6.2 Hz, HNCH$_2$); 3.84 (s, 3H, OCH$_3$); 3.43-3.26 (m, 4H, N(CH$_2$CH$_2$)$_2$N); 2.75-2.43 (m, 6H, 4H N(CH$_2$CH$_2$)$_2$N, 2H CH$_2$N); 1.91 (quint, 2H, J = 6.2 Hz, CH$_2$CH$_2$CH$_2$).

2-Chloro-3-{2-[4-(3-methoxyphenyl)piperazin-1-yl]butylamino}-1,4-naphthoquinone (108)

Yield: 76 %; M.p. 96-98 °C

Elemental analysis for C$_{25}$H$_{28}$ClN$_3$O$_3$:

found: C% 65.89   H% 6.11   N% 9.14

calcd.: C% 66.14   H% 6.22   N% 9.26

^{1}H-NMR (CDCl$_3$) δ: 8.22-8.00 (m, 2H, arom); 7.81-7.59 (m, 2H, arom); 7.32-7.12 (m, 2H, arom); 6.62-6.38 (m, 2H, arom); 6.26 (s, 1H, NH); 3.92 (q, 2H, J = 6.6 Hz, HNCH$_2$); 3.82 (s, 3H, OCH$_3$); 3.39-3.17 (m, 4H, N(CH$_2$CH$_2$)$_2$N); 2.78-2.56 (m, 4H, N(CH$_2$CH$_2$)$_2$N); 2.48 (t, 2H, J = 7.0 Hz, CH$_2$N); 1.93-1.59 (m, 4H, CH$_2$CH$_2$CH$_2$CH$_2$).

2-Chloro-3-{2-[4-(3-methoxyphenyl)piperazin-1-yl]pentylamino}-1,4-naphthoquinone (109)

Yield: 85 %; M.p. 70-73 °C
Elemental analysis for C$_{26}$H$_{30}$ClN$_3$O$_3$:

found: C% 66.45   H% 6.45   N% 8.82

calcd.: C% 66.73   H% 6.46   N% 8.98

^{1}H-NMR (CDCl$_3$) δ: 8.23-7.99 (m, 2H, arom); 7.82-7.59 (m, 2H, arom); 7.26-7.13 (m, 1H, arom); 6.63-6.38 (m, 3H, arom); 6.14 (s, 1H, NH); 4.01-3.74 (m, 5H, 2H HNCH$_2$, 3H OCH$_3$); 3.38-3.14 (m, 4H, N(CH$_2$CH$_2$)$_2$N); 2.77-2.56 (m, 4H, N(CH$_2$CH$_2$)$_2$N); 2.44 (t, 2H, J = 7.6 Hz, CH$_2$N); 1.96-1.38 (m, 6H, CH$_2$CH$_2$CH$_2$CH$_2$CH$_2$).

2-Chloro-3-{2-[4-(4-methoxyphenyl)piperazin-1-yl]ethylamino}-1,4-naphthoquinone (110)

Yield: 72 %; M.p. 113-115 °C
Elemental analysis for C$_{22}$H$_{21}$Cl$_2$N$_3$O$_2$:

found: C% 64.54   H% 5.45   N% 9.63

calcd.: C% 64.86   H% 5.68   N% 9.87

^{1}H-NMR (CDCl$_3$) δ: 8.22-7.95 (m, 2H, arom); 7.80-7.56 (m, 2H, arom); 7.17-6.80 (m, 5H, 4H arom, 1H NH); 4.03 (q, 2H, J= 5.6 Hz, HNCH$_2$); 3.83 (s, 3H, OCH$_3$); 3.27-3.04 (m, 4H, N(CH$_2$CH$_2$)$_2$N); 2.87-2.64 (m, 6H, 2H of CH$_2$N, 4H of N(CH$_2$CH$_2$)$_2$N).

2-Chloro-3-{2-[4-(4-methoxyphenyl)piperazin-1-yl]propylamino}-1,4-naphthoquinone (111)

Yield: 73 %; M.p. 131-134 °C
Elemental analysis for C$_{24}$H$_{26}$ClN$_3$O$_3$:

found: C% 65.03   H% 5.96   N% 9.45

calcd.: C% 65.52   H% 5.96   N% 9.55

^{1}H-NMR (CDCl$_3$) δ: 8.22-7.97 (m, 2H, arom); 7.80-7.48 (m, 3H, 2H arom, 1H NH); 7.04-6.81 (m, 4H, arom); 4.06 (q, 2H, J = 5.8 Hz, HNCH$_2$); 3.81 (s, 3H, OCH$_3$); 3.35-3.14 (m, 4H, N(CH$_2$CH$_2$)$_2$N); 2.82-2.49 (m, 6H, 4H N(CH$_2$CH$_2$)$_2$N, 2H CH$_2$N); 1.92 (quint, 2H, J = 6.0 Hz, CH$_2$CH$_2$CH$_2$).

^{13}C NMR (200 MHz, CDCl$_3$) δ: 179.5, 175.7, 152.8, 144.6, 143.9, 133.7, 131.7, 131.2, 128.9, 125.7, 125.6, 117.3, 113.4, 56.1, 54.5, 52.6, 49.2, 44.3, 25.0

2-Chloro-3-{2-[4-(4-methoxyphenyl)piperazin-1-yl]butylamino}-1,4-naphthoquinone (112)

Yield: 71 %; M.p. 113-115 °C
Elemental analysis for C$_{25}$H$_{28}$ClN$_3$O$_3$:

found: C% 65.95   H% 5.85   N% 9.36

calcd.: C% 66.14   H% 6.22   N% 9.26

^{1}H-NMR (CDCl$_3$) δ: 8.23-8.00 (m, 2H, arom); 7.81-7.59 (m, 2H, arom); 7.03-6.80 (m, 4H, arom); 6.27 (s, 1H, NH); 3.93 (q, 2H, J = 6.4 Hz, HNCH$_2$); 3.80 (s, 3H, OCH$_3$); 3.28-3.04 (m, 4H, N(CH$_2$CH$_2$)$_2$N); 2.80-2.60 (m, 4H, N(CH$_2$CH$_2$)$_2$N); 2.52 (t, 2H, J = 6.0 Hz, CH$_2$N); 1.90-1.60 (m, 4H, CH$_2$CH$_2$CH$_2$CH$_2$).

2-Chloro-3-{2-[4-(4-methoxyphenyl)piperazin-1-yl]pentylamino}-1,4-naphthoquinone (113)

Yield: 72 %; M.p. 95-96 °C
Elemental analysis for C$_{26}$H$_{30}$ClN$_3$O$_3$:

found: C% 66.46   H% 6.52   N% 8.77

calcd.: C% 66.73   H% 6.46   N% 8.98

^{1}H-NMR (CDCl$_3$) δ: 8.23-8.00 (m, 2H, arom); 7.81-7.59 (m, 2H, arom); 7.00-6.80 (m, 4H, arom); 6.13 (s, 1H, NH); 3.90 (q, 2H, J = 7.0 Hz, HNCH$_2$); 3.80 (s, 3H, OCH$_3$); 3.22-3.05 (m, 4H, N(CH$_2$CH$_2$)$_2$N); 2.75-2.56 (m, 4H, N(CH$_2$CH$_2$)$_2$N); 2.45 (t, 2H, J = 7.8 Hz, CH$_2$N); 1.87-1.40 (m, 6H, CH$_2$CH$_2$CH$_2$CH$_2$CH$_2$).

11. Biology

Primary neuronal cell cultures

Primary cultures of mouse cortical neurons were prepared from CD1 mouse embryos. Animal procedures were in accordance with UK Home Office Guidelines as stated in the Animals Scientific Procedures Act (1986, UK) using Schedule 1 procedures approved by the University of Bath Animal Welfare and Ethical Review Body. Primary neurons were prepared essentially as described previously[332]. Briefly, the cortex was dissected from 15 days old CD1 mouse embryos, and mechanically separated in PBS supplemented with 33 mM glucose, using a firepolished glass Pasteur pipet. Cells were plated into 24-wells Nunc tissue culture plates, previously coated with 20 µg/mL poly-D-lysine (Sigma). Neurons were cultured in Neurobasal medium (phenol red free) (500 mL) supplemented with 5 mL L-glutamine, 5 mL penicillin/streptomycin, and 10 mL B27 (all from Invitrogen), and incubated at 37 °C, in high humidity with 5% CO2.

SHSY-5Y cell line

Human neuroblastoma catecholaminergic SHSY-5Y cells were seeded onto 24-well plates in DMEM/F-12 medium (435 mL) supplemented with 50 mL foetal bovine serum, 5 mL L-glutamine, 5 mL penicillin/streptomycin, and 5 mL nonessential amino acids at 37°C in a humidified atmosphere of 5% CO_2 and 95% air. Human neuroblastoma catecholaminergic SHSY-5Y cells were also seeded in the same conditions without the supplementation of foetal bovine serum.

MTT assay

Compounds **38**-**69** were dissolved in DMSO at concentrations ranging from 0.1 µM to 100 µM. Cells were plated in 24-well plates with 20 000 cells per well and incubated at 37 °C for 24 h to allow cells to attach. Each plate was then incubated with each compound in a concentration range of 0.1−100 µM for an additional 24 h. Afterwards, the medium was removed (keeping it aside for performing LDH assay) and cell viability was determined by additioning 50 µL of 1 mg/mL MTT to each well. After incubation for 1 h at 37 °C, the medium was aspirated and 50µL of isopropanol was added to each well to dissolve the formazan crystals, helping the dissolution by pipetting up and down. The

absorbance was read at 595 nm using a Bio-Rad iMark Microplate Absorbance Reader. The optical density of the formazan formed in the control cells (untreated) was taken as 100% viability. The survival rates of viable cells were calculated by comparing the optical absorbance of treated samples with that of the untreated controls using Prism software (GraphPad Prism version 9.00 for Windows, GraphPad Software, San Diego, CA, USA). All experiments were repeated three times, and data are expressed as mean ± SD.

LDH assay

The assay was performed according to the product information sheet of CyQUANT™ LDH Cytotoxicity Assay Kit from Invitrogen™. To perform this assay, 50μL of each sample medium, obtained from MTT assay as stated above, were transferred to a 96-wells plate. Then 50μL of Reaction Mixture was added to each sample well and the plate was incubated at r.t. for 30 minutes protected from light. Subsequently, 50μL of Stop Solution was added to each well and mixed by gentle tapping. Finally, the absorbance was read at 655 nm and 490 nm using a Bio-Rad iMark Microplate Absorbance Reader, and determined LDH activity by subtracting the 655 nm absorbance value (background) from the 490 nm absorbance. The survival rates of viable cells were calculated by comparing the optical absorbance of treated samples with that of the untreated controls using Prism software. Experiments were run in triplicate, and data are expressed as mean ± SD.

Neuroprotection against hydrogen peroxide

Primary neurons were cultured in an anti-oxidant free neurobasal medium (48 mL NBM, 1 mL anti-oxidant free B27, 5 mL L-glutamine, 5 mL penicillin/streptomycin) in order to not interfere with the experiment's results. To perform this study, three 24-well plates were used for each compound to test. One 24-well plate was treated with H_2O_2 in the absence of the compound, and the others two in the presence of the compound. On the first day of experiment 5μL of a solution of 1μM compound concentration was added onto each well of two 24-wells plates, and the plates were incubated at 37°C for 18 h. On the second day the medium was removed in both of the two 24-well plates, and cells were treated with H_2O_2 in a concentration range of 1μM- 1mM (H_2O_2 was prepared immediately before use as a 100mM stock solution in sterile tissue culture quality H_2O (Invitrogen)). In one of the two 24-well plates the exposure to H_2O_2 was chaperoned with the compound in a concentration of 1μM. The third 24-well plate was used instead as control, exposing the cells only to H_2O_2 insult. After 30 min of incubation at 37°C, in all plates the medium

was replaced with their original conditioned one and the neurons were incubated for a further 6h at 37°C. In this way the putative neuroprotective effect of each compound was evaluated before, during and after the insult made by H_2O_2. Afterwards the cultures were washed with sterile phosphate-buffered saline before the addition of MTT (1 mg/ 1 mL). Following incubation for 1 h at 37°C, MTT solutions were removed, the formazan product was solubilized in isopropanol, and the absorbance read at 595 nm using a Bio-Rad iMark Microplate Absorbance Reader. Data are presented as a percentage relative to the vehicle control (untreated neurons), considered as 100%.

Dual-Glo luciferase gene reporter assay

Primary cortical neurons cultured in a 24-well plate were transfected with APP-Gal4, pFR-Luciferase and TK-Renilla (0.1 µg per plasmid) using Lipofectamine 2000 (1 µL/well) (Invitrogen). pFR-Luciferase reporter vector with firefly (*Photinus pyralis*) luciferase gene under the control of a synthetic promoter containing 5 tandem repeats of the yeast Gal4 upstream activation sequence upstream of a minimal TATA box and phRL thymidine kinase (TK) vector containing sea pansy (*Renilla reniformis*) luciferase gene under control of the herpes simplex virus TK-promoter, from Promega. Transfection mixes containing lipid and DNA were prepared separately in OptiMEM reduced serum medium (Invitrogen) by vortexing and incubating for 30 min. Neuronal cultures were removed from the incubator, and transfection mixes (150 µL/well) were added dropwise onto the neuronal culture medium, after which, neuronal cultures were placed back in the incubator. Cell treatment started 30 min after transfection. Due to high intrinsic variability of this assay, quadruplicates for each condition were done, so 4 different compounds at 1µM were assayed together with vehicle (control condition) and (2S)-N-[(3,5-difluorophenyl)acetyl]-L-alanyl-2-phenyl]glycine 1,1-dimethylethyl ester (DAPT) (10µM, positive control)[333]. After processing 24 hours, firefly luciferase and Renilla luciferase expression were quantified. Neurons were lysed with Glo lysis buffer (60µL/well) (Promega), and the Dual-Glo luciferase activity assay was performed accordingly to manufacturer's instructions (Promega). Luciferase signals were captured using a microplate luminometer (Glomax Plate reader). Firefly luciferase reporters activity was normalized using the Renilla luciferase activity, which helps to differentiate between specific and nonspecific cellular responses and control for transfection efficiencies across experiments. Data are expressed as mean ± SD of quadruplicate measurements.

References

1.	World Health Organization. *Global action plan on the public health response to dementia 2017 - 2025. World Health Organization, Geneva* (2017).

2.	Prince, M. *et al. World Alzheimer Report 2015 - The Global Impact of Dementia: an analysis of prevalence, incidence, cost and trends*. (2015).

3.	O'Brien, J. T. & Thomas, A. Vascular dementia. *Lancet* **386**, 1698–1706 (2015).

4.	McKeith, I. *et al.* Dementia with Lewy bodies. *Lancet Neurol.* **3**, 19–28 (2004).

5.	Neary, D., Snowden, J. & Mann, D. Frontotemporal dementia. *Lancet Neurol.* **4**, 771–780 (2005).

6.	Langa, K. M., Foster, N. L. & Larson, E. B. Mixed Dementia. *JAMA* **292**, 2901 (2004).

7.	Raz, L., Knoefel, J. & Bhaskar, K. The neuropathology and cerebrovascular mechanisms of dementia. *J. Cereb. Blood Flow Metab.* **36**, 172–186 (2016).

8.	Alzheimer, A., Stelzmann, R. A., Schnitzlein, H. N. & Murtagh, F. R. An English translation of Alzheimer's 1907 paper, 'Uber eine eigenartige Erkankung der Hirnrinde'. *Clin. Anat.* **8**, 429–31 (1995).

9.	Storandt, M. Cognitive Deficits in the Early Stages of Alzheimer's Disease. *Curr. Dir. Psychol. Sci.* **17**, 198–202 (2008).

10.	Perl, D. P. Neuropathology of Alzheimer's Disease. *Mt. Sinai J. Med. A J. Transl. Pers. Med.* **77**, 32–42 (2010).

11.	Selkoe, D. J. Alzheimer's disease. *Cold Spring Harb. Perspect. Biol.* **3**, (2011).

12.	Braak, H. & Braak, E. Evolution of neuronal changes in the course of Alzheimer's disease. *J. Neural Transm. Suppl.* **53**, 127–140 (1998).

13.	Ballard, C. *et al.* Alzheimer's disease. *Lancet* **377**, 1019–1031 (2011).

14.	Reitz, C., Brayne, C. & Mayeux, R. Epidemiology of Alzheimer disease. *Nat. Rev. Neurol.* **7**, 137–152 (2011).

15.	Bagyinszky, E., Youn, Y. C., An, S. S. A. & Kim, S. The genetics of Alzheimer's disease. *Clin. Interv. Aging* **9**, 535–51 (2014).

16.	Wu, L. *et al.* Early-Onset Familial Alzheimer's Disease (EOFAD). *Can. J. Neurol. Sci. / J. Can. des Sci. Neurol.* **39**, 436–445 (2012).

17.	Bertram, L. The genetic epidemiology of neurodegenerative disease. *J. Clin. Invest.* **115**, 1449–1457 (2005).

18.	Tanzi, R. E. *et al.* Assessment of amyloid beta-protein precursor gene mutations in a large set of familial and sporadic Alzheimer disease cases. *Am. J. Hum. Genet.* **51**, 273–82 (1992).

19.	Prasher, V. P. *et al.* Molecular mapping of alzheimer-type dementia in Down's syndrome. *Ann. Neurol.* **43**, 380–383 (1998).

20.	De Jonghe, C. Pathogenic APP mutations near the gamma-secretase cleavage site differentially affect Abeta secretion and APP C-terminal fragment stability. *Hum. Mol. Genet.* **10**, 1665–1671 (2001).

21.	Cruts, M., Hendriks, L. & Van Broeckhoven, C. The presenilin genes: a new gene family involved in Alzheimer disease pathology. *Hum. Mol. Genet.* **5**, 1449–1455 (1996).

22.	Wolfe, M. S. *et al.* Two transmembrane aspartates in presenilin-1 required for presenilin endoproteolysis and γ-secretase activity. *Nature* **398**, 513–517 (1999).

23. Scheuner, D. *et al.* Secreted amyloid β–protein similar to that in the senile plaques of Alzheimer's disease is increased in vivo by the presenilin 1 and 2 and APP mutations linked to familial Alzheimer's disease. *Nat. Med.* **2**, 864–870 (1996).

24. Jayadev, S. *et al.* Alzheimer's disease phenotypes and genotypes associated with mutations in presenilin 2. *Brain* **133**, 1143–1154 (2010).

25. To, M. D. *et al.* Functional characterization of novel presenilin-2 variants identified in human breast cancers. *Oncogene* **25**, 3557–3564 (2006).

26. Bu, G. Apolipoprotein E and its receptors in Alzheimer's disease: pathways, pathogenesis and therapy. *Nat. Rev. Neurosci.* **10**, 333–344 (2009).

27. Green, R. C. *et al.* Disclosure of APOE Genotype for Risk of Alzheimer's Disease. *N. Engl. J. Med.* **361**, 245–254 (2009).

28. Myers, R. H. *et al.* Apolipoprotein E epsilon4 association with dementia in a population-based study: The Framingham study. *Neurology* **46**, 673–7 (1996).

29. Liu, C.-C., Kanekiyo, T., Xu, H. & Bu, G. Apolipoprotein E and Alzheimer disease: risk, mechanisms and therapy. *Nat. Rev. Neurol.* **9**, 106–118 (2013).

30. Mahley, R. W. & Huang, Y. Apolipoprotein (apo) E4 and Alzheimer's disease: unique conformational and biophysical properties of apoE4 can modulate neuropathology. *Acta Neurol. Scand.* **114**, 8–14 (2006).

31. Calero, M. *et al.* Apolipoprotein J (clusterin) and Alzheimer's disease. *Microsc. Res. Tech.* **50**, 305–315 (2000).

32. Crehan, H. *et al.* Complement receptor 1 (CR1) and Alzheimer's disease. *Immunobiology* **217**, 244–250 (2012).

33. Xiao, Q. *et al.* Role of Phosphatidylinositol Clathrin Assembly Lymphoid-Myeloid Leukemia (PICALM) in Intracellular Amyloid Precursor Protein (APP) Processing and Amyloid Plaque Pathogenesis. *J. Biol. Chem.* **287**, 21279–21289 (2012).

34. Rogaeva, E. *et al.* The neuronal sortilin-related receptor SORL1 is genetically associated with Alzheimer disease. *Nat. Genet.* **39**, 168–177 (2007).

35. Jonsson, T. *et al.* Variant of TREM2 Associated with the Risk of Alzheimer's Disease. *N. Engl. J. Med.* **368**, 107–116 (2013).

36. Guerreiro, R. *et al.* TREM2 Variants in Alzheimer's Disease. *N. Engl. J. Med.* **368**, 117–127 (2013).

37. Bradshaw, E. M. *et al.* CD33 Alzheimer's disease locus: altered monocyte function and amyloid biology. *Nat. Neurosci.* **16**, 848–850 (2013).

38. Weishaupt, J. Inhibition of CDK5 is protective in necrotic and apoptotic paradigms of neuronal cell death and prevents mitochondrial dysfunction. *Mol. Cell. Neurosci.* **24**, 489–502 (2003).

39. Wen, Y. *et al.* Cdk5 is involved in NFT-like tauopathy induced by transient cerebral ischemia in female rats. *Biochim. Biophys. Acta - Mol. Basis Dis.* **1772**, 473–483 (2007).

40. Gupta, A. *et al.* Mid-life Cardiovascular Risk Impacts Memory Function: The Framingham Offspring Study. *Alzheimer Dis. Assoc. Disord.* **29**, 117–23 (2014).

41. Kalaria, R. N. Vascular basis for brain degeneration: faltering controls and risk factors for dementia. *Nutr. Rev.* **68**, S74–S87 (2010).

42. Deane, R., Wu, Z. & Zlokovic, B. V. RAGE (yin) versus LRP (yang) balance regulates alzheimer amyloid beta-peptide clearance through transport across the blood-brain barrier. *Stroke* **35**, 2628–2631 (2004).

43. Luchsinger, J. A. Diabetes Mellitus and Risk of Alzheimer's Disease and Dementia with

Stroke in a Multiethnic Cohort. *Am. J. Epidemiol.* **154**, 635–641 (2001).

44. Craft, S. Insulin Resistance and Alzheimers Disease Pathogenesis: Potential Mechanisms and Implications for Treatment. *Curr. Alzheimer Res.* **4**, 147–152 (2007).

45. Yan, S. Du *et al.* RAGE and amyloid-β peptide neurotoxicity in Alzheimer's disease. *Nature* **382**, 685–691 (1996).

46. Kuo, Y.-M. *et al.* Elevated Low-Density Lipoprotein in Alzheimer's Disease Correlates with Brain Aβ 1–42 Levels. *Biochem. Biophys. Res. Commun.* **252**, 711–715 (1998).

47. Nelson, R. H. Hyperlipidemia as a Risk Factor for Cardiovascular Disease. *Prim. Care Clin. Off. Pract.* **40**, 195–211 (2013).

48. Traber, M. G., van der Vliet, A., Reznick, A. Z. & Cross, C. E. Tobacco-Related Diseases. *Clin. Chest Med.* **21**, 173–187 (2000).

49. Jones, G. M. M. Nicotine psychopharmacology: Molecular, cellular and behavioural aspects. *Int. J. Geriatr. Psychiatry* **6**, 683–684 (1991).

50. Jorm, A. F. History of Depression as a Risk Factor for Dementia: An Updated Review. *Aust. New Zeal. J. Psychiatry* **35**, 776–781 (2001).

51. Barnes, D. E., Alexopoulos, G. S., Lopez, O. L., Williamson, J. D. & Yaffe, K. Depressive Symptoms, Vascular Disease, and Mild Cognitive Impairment. *Arch. Gen. Psychiatry* **63**, 273 (2006).

52. Becker, J. T. *et al.* Depressed mood is not a risk factor for incident dementia in a community-based cohort. *Am. J. Geriatr. Psychiatry* **17**, 653–63 (2009).

53. Hughes, T. & Ganguli, M. Modifiable Midlife Risk Factors for Late-Life Cognitive Impairment and Dementia. *Curr. Psychiatry Rev.* **5**, 73–92 (2009).

54. Fratiglioni, L., Paillard-Borg, S. & Winblad, B. An active and socially integrated lifestyle in late life might protect against dementia. *Lancet Neurol.* **3**, 343–353 (2004).

55. Scarmeas, N., Levy, G., Tang, M.-X., Manly, J. & Stern, Y. Influence of leisure activity on the incidence of Alzheimer's Disease. *Neurology* **57**, 2236–2242 (2001).

56. Brayne, C. *et al.* Education, the brain and dementia: neuroprotection or compensation? *Brain* **133**, 2210–2216 (2010).

57. Farfel, J. M. *et al.* Very low levels of education and cognitive reserve: A clinicopathologic study. *Neurology* **81**, 650–657 (2013).

58. Roe, C. M., Xiong, C., Miller, J. P., Cairns, N. J. & Morris, J. C. Interaction of Neuritic Plaques and Education Predicts Dementia. *Alzheimer Dis. Assoc. Disord.* **22**, 188–193 (2008).

59. Bennett, D. A. *et al.* Education modifies the relation of AD pathology to level of cognitive function in older persons. *Neurology* **60**, 1909–1915 (2003).

60. Reed, B. R. *et al.* Cognitive Activities During Adulthood Are More Important than Education in Building Reserve. *J. Int. Neuropsychol. Soc.* **17**, 615–624 (2011).

61. Bennett, D. A., Schneider, J. A., Tang, Y., Arnold, S. E. & Wilson, R. S. The effect of social networks on the relation between Alzheimer's disease pathology and level of cognitive function in old people: a longitudinal cohort study. *Lancet Neurol.* **5**, 406–412 (2006).

62. Rovio, S. *et al.* Leisure-time physical activity at midlife and the risk of dementia and Alzheimer's disease. *Lancet Neurol.* **4**, 705–711 (2005).

63. Colcombe, S. & Kramer, A. F. Fitness Effects on the Cognitive Function of Older Adults. *Psychol. Sci.* **14**, 125–130 (2003).

64. Dishman, R. K. *et al.* Neurobiology of Exercise. *Obesity* **14**, 345–356 (2006).

65. Prince, M., Bryce, R. & Ferri, C. *World Alzheimer Report 2011 - The benefits of early diagnosis and intervention. Alzheimer's Disease International (ADI)* (2011).

66. Bond, J. *et al.* Inequalities in dementia care across Europe: key findings of the Facing Dementia Survey. *Int. J. Clin. Pract.* **59**, 8–14 (2005).

67. Hrubešová, K. *et al.* Search for biomarkers of Alzheimer's disease: Recent insights, current challenges and future prospects. *Clin. Biochem.* **72**, 39–51 (2019).

68. Manzine, P. R. *et al.* Blood-based Biomarkers of Alzheimer's Disease: The Long and Winding Road. *Curr. Pharm. Des.* **26**, 1300–1315 (2020).

69. McKhann, G. *et al.* Clinical diagnosis of Alzheimer's disease: Report of the NINCDS-ADRDA Work Group∗ under the auspices of Department of Health and Human Services Task Force on Alzheimer's Disease. *Neurology* **34**, 939–939 (1984).

70. Folstein, M. F., Folstein, S. E. & McHugh, P. R. "Mini-mental state". *J. Psychiatr. Res.* **12**, 189–198 (1975).

71. dos Santos Picanco, L. C. *et al.* Alzheimer's Disease: A Review from the Pathophysiology to Diagnosis, New Perspectives for Pharmacological Treatment. *Curr. Med. Chem.* **25**, 3141–3159 (2018).

72. von Arnim, C. A. F. *et al.* Diagnosis and treatment of cognitive impairment. *Z. Gerontol. Geriatr.* **52**, 309–315 (2019).

73. Jagust, W. Imaging the evolution and pathophysiology of Alzheimer disease. *Nat. Rev. Neurosci.* **19**, 687–700 (2018).

74. Bouwman, F. H. *et al.* CSF biomarkers and medial temporal lobe atrophy predict dementia in mild cognitive impairment. *Neurobiol. Aging* **28**, 1070–1074 (2007).

75. Unzeta, M. *et al.* Multi-Target Directed Donepezil-Like Ligands for Alzheimer's Disease. *Front. Neurosci.* **10**, 205 (2016).

76. Davies, P. & Maloney, A. J. Selective loss of central cholinergic neurons in Alzheimer's disease. *Lancet* **2**, 1403 (1976).

77. Picciotto, M. R., Higley, M. J. & Mineur, Y. S. Acetylcholine as a Neuromodulator: Cholinergic Signaling Shapes Nervous System Function and Behavior. *Neuron* **76**, 116–129 (2012).

78. Francis, P. T., Palmer, A. M., Snape, M. & Wilcock, G. K. The cholinergic hypothesis of Alzheimer's disease: A review of progress. *J. Neurol. Neurosurg. Psychiatry* **66**, 137–147 (1999).

79. David, L. *et al.* The α/β hydrolase fold. *Protein Eng. Des. Sel.* **5**, 197–211 (1992).

80. Nicolet, Y., Lockridge, O., Masson, P., Fontecilla-Camps, J. C. & Nachon, F. Crystal Structure of Human Butyrylcholinesterase and of Its Complexes with Substrate and Products. *J. Biol. Chem.* **278**, 41141–41147 (2003).

81. Mehta, M., Adem, A. & Sabbagh, M. New Acetylcholinesterase Inhibitors for Alzheimer's Disease. *Int. J. Alzheimers. Dis.* **2012**, 1–8 (2012).

82. Darvesh, S., Hopkins, D. A. & Geula, C. Neurobiology of butyrylcholinesterase. *Nat. Rev. Neurosci.* **4**, 131–138 (2003).

83. Giacobini, E. Cholinesterase inhibitors: new roles and therapeutic alternatives. *Pharmacol. Res.* **50**, 433–40 (2004).

84. Venneri, A., McGeown, W. J. & Shanks, M. F. Empirical evidence of neuroprotection by dual cholinesterase inhibition in Alzheimer's disease. *Neuroreport* **16**, 107–110 (2005).

85. Giacobini, E. Cholinesterases: New roles in brain function and in Alzheimer's disease. *Neurochem. Res.* **28**, 515–522 (2003).

86. Sussman, J. *et al.* Atomic structure of acetylcholinesterase from Torpedo californica: a prototypic acetylcholine-binding protein. *Science.* **253**, 872–879 (1991).

87. Kryger, G., Silman, I. & Sussman, J. L. Three-dimensional structure of a complex of E2020 with acetylcholinesterase from Torpedo californica. *J. Physiol.* **92**, 191–194 (1998).

88. Inestrosa, N. C., Dinamarca, M. C. & Alvarez, A. Amyloid-cholinesterase interactions. *FEBS J.* **275**, 625–632 (2008).

89. Inestrosa, N. C. *et al.* Acetylcholinesterase Accelerates Assembly of Amyloid-β-Peptides into Alzheimer's Fibrils: Possible Role of the Peripheral Site of the Enzyme. *Neuron* **16**, 881–891 (1996).

90. Rees, T. M. & Brimijoin, S. The role of acetylcholinesterase in the pathogenesis of Alzheimer's disease. *Drugs of Today* **39**, 75–83 (2003).

91. Castro, A. & Martinez, A. Peripheral and Dual Binding Site Acetylcholinesterase Inhibitors: Implications in treatment of Alzheimers Disease. *Mini-Reviews Med. Chem.* **1**, 267–272 (2001).

92. Zhang, Y., Kua, J. & McCammon, J. A. Role of the Catalytic Triad and Oxyanion Hole in Acetylcholinesterase Catalysis: An ab initio QM/MM Study. *J. Am. Chem. Soc.* **124**, 10572–10577 (2002).

93. Talesa, V. N. Acetylcholinesterase in Alzheimer's disease. *Mech. Ageing Dev.* **122**, 1961–1969 (2001).

94. Stanciu, G. D. *et al.* Alzheimer's Disease Pharmacotherapy in Relation to Cholinergic System Involvement. *Biomolecules* **10**, 40 (2019).

95. Darvesh, S. *et al.* Inhibition of Human Cholinesterases by Drugs Used to Treat Alzheimer Disease. *Alzheimer Dis. Assoc. Disord.* **17**, 117–126 (2003).

96. Macdonald, I. R., Rockwood, K., Martin, E. & Darvesh, S. Cholinesterase Inhibition in Alzheimer's Disease: Is Specificity the Answer? *J. Alzheimer's Dis.* **42**, 379–384 (2014).

97. Lahiri, D. K., Lewis, S. & Farlow, M. R. Tacrine alters the secretion of the beta-amyloid precursor protein in cell lines. *J. Neurosci. Res.* **37**, 777–787 (1994).

98. Bailey, J. A. & Lahiri, D. K. A novel effect of rivastigmine on pre-synaptic proteins and neuronal viability in a neurodegeneration model of fetal rat primary cortical cultures and its implication in Alzheimer's disease. *J. Neurochem.* **112**, 843–853 (2010).

99. Darvesh, S., Reid, G. A. & Martin, E. Biochemical and Histochemical Comparison of Cholinesterases in Normal and Alzheimer Brain Tissues. *Curr. Alzheimer Res.* **7**, 386–400 (2010).

100. Greig, N. H. *et al.* Selective butyrylcholinesterase inhibition elevates brain acetylcholine, augments learning and lowers Alzheimer -amyloid peptide in rodent. *Proc. Natl. Acad. Sci.* **102**, 17213–17218 (2005).

101. Hardy, J. & Higgins, G. Alzheimer's disease: the amyloid cascade hypothesis. *Science.* **256**, 184–185 (1992).

102. Karran, E., Mercken, M. & Strooper, B. De. The amyloid cascade hypothesis for Alzheimer's disease: an appraisal for the development of therapeutics. *Nat. Rev. Drug Discov.* **10**, 698–712 (2011).

103. Selkoe, D. Normal and Abnormal Biology of the Beta-Amyloid Precursor Protein. *Annu. Rev. Neurosci.* **17**, 489–517 (1994).

104. Buxbaum, J. D. *et al.* Evidence That Tumor Necrosis Factor α Converting Enzyme Is Involved in Regulated α-Secretase Cleavage of the Alzheimer Amyloid Protein Precursor. *J. Biol. Chem.* **273**, 27765–27767 (1998).

105. Hampel, H. *et al.* The β-Secretase BACE1 in Alzheimer's Disease. *Biol. Psychiatry* (2020) doi:10.1016/j.biopsych.2020.02.001.

106. Esler, W. P. A Portrait of Alzheimer Secretases--New Features and Familiar Faces. *Science (80-.).* **293**, 1449–1454 (2001).

107. Bergström, P. *et al.* Amyloid precursor protein expression and processing are differentially regulated during cortical neuron differentiation. *Sci. Rep.* **6**, 29200 (2016).

108. Glenner, G. G. & Wong, C. W. Alzheimer's disease: Initial report of the purification and characterization of a novel cerebrovascular amyloid protein. *Biochem. Biophys. Res. Commun.* **120**, 885–890 (1984).

109. Yoshiike, Y., Chui, D.-H., Akagi, T., Tanaka, N. & Takashima, A. Specific Compositions of Amyloid-β Peptides as the Determinant of Toxic β-Aggregation. *J. Biol. Chem.* **278**, 23648–23655 (2003).

110. Levine, H. Soluble multimeric Alzheimer β(1–40) pre-amyloid complexes in dilute solution. *Neurobiol. Aging* **16**, 755–764 (1995).

111. Lambert, M. P. *et al.* Diffusible, nonfibrillar ligands derived from A 1-42 are potent central nervous system neurotoxins. *Proc. Natl. Acad. Sci.* **95**, 6448–6453 (1998).

112. Yong, W. *et al.* Structure determination of micelle-like intermediates in amyloid -protein fibril assembly by using small angle neutron scattering. *Proc. Natl. Acad. Sci.* **99**, 150–154 (2002).

113. Marina, G. B. *et al.* Amyloid β-protein (Aβ) assembly: Aβ40 and Aβ42 oligomerize through distinct pathways. *Proc. Natl. Acad. Sci. U. S. A.* **100**, 330–335 (2003).

114. Kirkitadze, M. D., Condron, M. M. & Teplow, D. B. Identification and characterization of key kinetic intermediates in amyloid β-protein fibrillogenesis. *J. Mol. Biol.* **312**, 1103–1119 (2001).

115. Walsh, D. M., Lomakin, A., Benedek, G. B., Condron, M. M. & Teplow, D. B. Amyloid β-Protein Fibrillogenesis. *J. Biol. Chem.* **272**, 22364–22372 (1997).

116. Kirkitadze, M. D. & Kowalska, A. Molecular mechanisms initiating amyloid β-fibril formation in Alzheimer's disease. *Acta Biochim. Pol.* **52**, 417–423 (2005).

117. Necula, M., Kayed, R., Milton, S. & Glabe, C. G. Small Molecule Inhibitors of Aggregation Indicate That Amyloid β Oligomerization and Fibrillization Pathways Are Independent and Distinct. *J. Biol. Chem.* **282**, 10311–10324 (2007).

118. Lin, H., Bhatia, R. & Lal, R. Amyloid beta protein forms ion channels: implications for Alzheimer's disease pathophysiology. *FASEB J.* **15**, 2433–44 (2001).

119. Stefani, M. & Dobson, C. M. Protein aggregation and aggregate toxicity: new insights into protein folding, misfolding diseases and biological evolution. *J. Mol. Med.* **81**, 678–699 (2003).

120. Roher, A. E. *et al.* Oligomerization and fibril assembly of the amyloid-β protein. *Biochim. Biophys. Acta* **1502**, 31–43 (2000).

121. Borchelt, D. R. *et al.* Familial Alzheimer's Disease–Linked Presenilin 1 Variants Elevate Aβ1–42/1–40 Ratio In Vitro and In Vivo. *Neuron* **17**, 1005–1013 (1996).

122. Nalivaeva, N. N. & Turner, A. J. Targeting amyloid clearance in Alzheimer's disease as a therapeutic strategy. *Br. J. Pharmacol.* **176**, 3447–3463 (2019).

123. Cai, Z. *et al.* Role of RAGE in Alzheimer's Disease. *Cell. Mol. Neurobiol.* **36**, 483–495 (2016).

124. Ghiso, J. *et al.* Systemic Catabolism of Alzheimer's Aβ40 and Aβ42. *J. Biol. Chem.* **279**, 45897–45908 (2004).

125. Walsh, D. M. & Selkoe, D. J. Amyloid β-protein and beyond: the path forward in Alzheimer's disease. *Curr. Opin. Neurobiol.* **61**, 116–124 (2020).

126. Folch, J. *et al.* Review of the advances in treatment for Alzheimer disease: strategies for combating β-amyloid protein. *Neurología* **33**, 47–58 (2018).

127. Moussa-Pacha, N. M., Abdin, S. M., Omar, H. A., Alniss, H. & Al-Tel, T. H. BACE1 inhibitors: Current status and future directions in treating Alzheimer's disease. *Med. Res. Rev.* **40**, 339–384 (2020).

128. Buée, L., Bussière, T., Buée-Scherrer, V., Delacourte, A. & Hof, P. R. Tau protein isoforms, phosphorylation and role in neurodegenerative disorders. *Brain Res. Rev.* **33**, 95–130 (2000).

129. Arriagada, P. V., Growdon, J. H., Hedley-Whyte, E. T. & Hyman, B. T. Neurofibrillary tangles but not senile plaques parallel duration and severity of Alzheimer's disease. *Neurology* **42**, 631–631 (1992).

130. Maccioni, R. *et al.* Anomalously phosphorylated tau and Aβ fragments in the CSF correlates with cognitive impairment in MCI subjects. *Neurobiol. Aging* **27**, 237–244 (2006).

131. Crespo-Biel, N., Theunis, C. & Van Leuven, F. Protein Tau: Prime Cause of Synaptic and Neuronal Degeneration in Alzheimer's Disease. *Int. J. Alzheimers. Dis.* **2012**, 1–13 (2012).

132. Naseri, N. N., Wang, H., Guo, J., Sharma, M. & Luo, W. The complexity of tau in Alzheimer's disease. *Neurosci. Lett.* **705**, 183–194 (2019).

133. Trinczek, B., Biernat, J., Baumann, K., Mandelkow, E. M. & Mandelkow, E. Domains of tau protein, differential phosphorylation, and dynamic instability of microtubules. *Mol. Biol. Cell* **6**, 1887–1902 (1995).

134. Kolarova, M., García-Sierra, F., Bartos, A., Ricny, J. & Ripova, D. Structure and Pathology of Tau Protein in Alzheimer Disease. *Int. J. Alzheimers. Dis.* **2012**, 1–13 (2012).

135. Mandelkow, E., von Bergen, M., Biernat, J. & Mandelkow, E.-M. Structural Principles of Tau and the Paired Helical Filaments of Alzheimer's Disease. *Brain Pathol.* **17**, 83–90 (2007).

136. Noble, W., Hanger, D. P., Miller, C. C. J. & Lovestone, S. The Importance of Tau Phosphorylation for Neurodegenerative Diseases. *Front. Neurol.* **4**, 1–11 (2013).

137. Bjørklund, G., Aaseth, J., Dadar, M. & Chirumbolo, S. Molecular Targets in Alzheimer's Disease. *Mol. Neurobiol.* **56**, 7032–7044 (2019).

138. Li, G., Yin, H. & Kuret, J. Casein Kinase 1 Delta Phosphorylates Tau and Disrupts Its Binding to Microtubules. *J. Biol. Chem.* **279**, 15938–15945 (2004).

139. Chen, D. *et al.* Tau local structure shields amyloid motif and controls aggregation propensity. *Nat. Commun.* **10**, 2493 (2019).

140. Li, W. & Lee, V. M. Y. Characterization of two VQIXXK motifs for tau fibrillization in vitro. *Biochemistry* **45**, 15692–701 (2006).

141. Bulic, B. *et al.* Development of Tau Aggregation Inhibitors for Alzheimer's Disease. *Angew. Chemie Int. Ed.* **48**, 1740–1752 (2009).

142. Congdon, E. E. & Sigurdsson, E. M. Tau-targeting therapies for Alzheimer disease. *Nat. Rev. Neurol.* **14**, 399–415 (2018).

143. Cioffi, F., Adam, R. H. I. & Broersen, K. Molecular Mechanisms and Genetics of Oxidative Stress in Alzheimer's Disease. *J. Alzheimer's Dis.* **72**, 981–1017 (2019).

144. Finkel, T. Signal transduction by reactive oxygen species. *J. Cell Biol.* **194**, 7–15 (2011).

145. Kishida, K. T. & Klann, E. Sources and Targets of Reactive Oxygen Species in Synaptic Plasticity and Memory. *Antioxid. Redox Signal.* **9**, 233–244 (2007).

146. Cheignon, C. *et al.* Oxidative stress and the amyloid beta peptide in Alzheimer's disease. *Redox Biol.* **14**, 450–464 (2018).

147. Wang, X. *et al.* Oxidative stress and mitochondrial dysfunction in Alzheimer's disease. *Biochim. Biophys. Acta* **1842**, 1240–1247 (2014).

148. Hung, C. H.-L. *et al.* A reciprocal relationship between reactive oxygen species and mitochondrial dynamics in neurodegeneration. *Redox Biol.* **14**, 7–19 (2018).

149. Teixeira, J. P., de Castro, A. A., Soares, F. V., da Cunha, E. F. F. & Ramalho, T. C. Future Therapeutic Perspectives into the Alzheimer's Disease Targeting the Oxidative Stress Hypothesis. *Molecules* **24**, 4410 (2019).

150. Bhatti, A. B. Vitamin Supplementation as an Adjuvant Treatment for Alzheimer's Disease. *J. Clin. diagnostic Res.* **10**, 7–11 (2016).

151. Tönnies, E. & Trushina, E. Oxidative Stress, Synaptic Dysfunction, and Alzheimer's Disease. *J. Alzheimer's Dis.* **57**, 1105–1121 (2017).

152. Collin, F., Cheignon, C. & Hureau, C. Oxidative stress as a biomarker for Alzheimer's disease. *Biomark. Med.* **12**, 201–203 (2018).

153. Deibel, M. ., Ehmann, W. . & Markesbery, W. . Copper, iron, and zinc imbalances in severely degenerated brain regions in Alzheimer's disease: possible relation to oxidative stress. *J. Neurol. Sci.* **143**, 137–142 (1996).

154. Cai, Z. Monoamine oxidase inhibitors: Promising therapeutic agents for Alzheimer's disease. *Mol. Med. Rep.* **9**, 1533–1541 (2014).

155. Hirvonen, J. *et al.* Assessment of MAO-B Occupancy in the Brain With PET and [11C]-L-Deprenyl-D2: A Dose-Finding Study With a Novel MAO-B Inhibitor, EVT 301. *Clin. Pharmacol. Ther.* **85**, 506–512 (2009).

156. Riederer, P. Monoamine Oxidase-B Inhibition in Alzheimer's Disease. *Neurotoxicology* **25**, 271–277 (2004).

157. Caraci, F., Copani, A., Nicoletti, F. & Drago, F. Depression and Alzheimer's disease: Neurobiological links and common pharmacological targets. *Eur. J. Pharmacol.* **626**, 64–71 (2010).

158. Zhang, P., Xu, S., Zhu, Z. & Xu, J. Multi-target design strategies for the improved treatment of Alzheimer's disease. *Eur. J. Med. Chem.* **176**, 228–247 (2019).

159. Pisani, L. *et al.* Targeting Monoamine Oxidases with Multipotent Ligands: An Emerging Strategy in the Search of New Drugs Against Neurodegenerative Diseases. *Curr. Med. Chem.* **18**, 4568–4587 (2011).

160. Wang, L. *et al.* Current understanding of metal ions in the pathogenesis of Alzheimer's disease. *Transl. Neurodegener.* **9**, 10 (2020).

161. Huang, X., Moir, R. D., Tanzi, R. E., Bush, A. I. & Rogers, J. T. Redox-active metals, oxidative stress, and Alzheimer's disease pathology. *Ann. N. Y. Acad. Sci.* **1012**, 153–163 (2004).

162. Yamamoto, A. *et al.* Iron (III) induces aggregation of hyperphosphorylated τ and its reduction to iron (II) reverses the aggregation: implications in the formation of neurofibrillary tangles of Alzheimer's disease. *J. Neurochem.* **86**, 1568–1568 (2002).

163. Adlard, P. A. & Bush, A. I. Metals and Alzheimer's Disease: How Far Have We Come in the Clinic? *J. Alzheimer's Dis.* **62**, 1369–1379 (2018).

164. Lovell, M. ., Robertson, J. ., Teesdale, W. ., Campbell, J. . & Markesbery, W. . Copper, iron and zinc in Alzheimer's disease senile plaques. *J. Neurol. Sci.* **158**, 47–52 (1998).

165. Matheou, C. J., Younan, N. D. & Viles, J. H. Cu2+ accentuates distinct misfolding of Aβ(1−40) and Aβ(1−42) peptides, and potentiates membrane disruption. *Biochem. J.* **466**, 233−242 (2015).

166. Multhaup, G. *et al.* The Amyloid Precursor Protein of Alzheimer's Disease in the Reduction of Copper(II) to Copper(I). *Science (80-.).* **271**, 1406−1409 (1996).

167. Choo, X. Y., Alukaidey, L., White, A. R. & Grubman, A. Neuroinflammation and Copper in Alzheimer's Disease. *Int. J. Alzheimers. Dis.* **2013**, 1−12 (2013).

168. Kitazawa, M., Cheng, D. & LaFerla, F. M. Chronic copper exposure exacerbates both amyloid and tau pathology and selectively dysregulates cdk5 in a mouse model of AD. *J. Neurochem.* **108**, 1550−1560 (2009).

169. Bush, A. *et al.* Rapid induction of Alzheimer A beta amyloid formation by zinc. *Science (80-.).* **265**, 1464−1467 (1994).

170. Seegar, T. C. M. *et al.* Structural Basis for Regulated Proteolysis by the α-Secretase ADAM10. *Cell* **171**, 1638-1648.e7 (2017).

171. Crouch, P. J. *et al.* Restored degradation of the Alzheimer's amyloid-β peptide by targeting amyloid formation. *J. Neurochem.* **108**, 1198−1207 (2009).

172. Mo, Z.-Y. *et al.* Low Micromolar Zinc Accelerates the Fibrillization of Human Tau via Bridging of Cys-291 and Cys-322. *J. Biol. Chem.* **284**, 34648−34657 (2009).

173. Kim, I. *et al.* Zinc stimulates tau S214 phosphorylation by the activation of Raf/mitogen-activated protein kinase-kinase/extracellular signal-regulated kinase pathway. *Neuroreport* **22**, 839−44 (2011).

174. Wang, T., Xu, S.-F., Fan, Y.-G., Li, L.-B. & Guo, C. Iron Pathophysiology in Alzheimer's Diseases. *Adv. Exp. Med. Biol.* **1173**, 67−104 (2019).

175. Liu, B. *et al.* Iron Promotes the Toxicity of Amyloid β Peptide by Impeding Its Ordered Aggregation. *J. Biol. Chem.* **286**, 4248−4256 (2011).

176. Wärmländer, S. K. T. S. *et al.* Metal binding to the amyloid-β peptides in the presence of biomembranes: potential mechanisms of cell toxicity. *JBIC J. Biol. Inorg. Chem.* **24**, 1189−1196 (2019).

177. Muñoz, P. *et al.* Effect of iron on the activation of the MAPK/ERK pathway in PC12 neuroblastoma cells. *Biol. Res.* **39**, 189−90 (2006).

178. Egaña, J. T., Zambrano, C., Nuñez, M. T., Gonzalez-Billault, C. & Maccioni, R. B. Iron-induced oxidative stress modify tau phosphorylation patterns in hippocampal cell cultures. *Biometals* **16**, 215−23 (2003).

179. Kuchibhotla, K. V. *et al.* Aβ Plaques Lead to Aberrant Regulation of Calcium Homeostasis In Vivo Resulting in Structural and Functional Disruption of Neuronal Networks. *Neuron* **59**, 214−225 (2008).

180. Yang, L., Wang, Z., Wang, B., Justice, N. J. & Zheng, H. Amyloid Precursor Protein Regulates Cav1.2 L-type Calcium Channel Levels and Function to Influence GABAergic Short-Term Plasticity. *J. Neurosci.* **29**, 15660−15668 (2009).

181. Wang, Y., Shi, Y. & Wei, H. Calcium Dysregulation in Alzheimer's Disease: A Target for New Drug Development. *J. Alzheimer's Dis. Park.* **7**, (2017).

182. Samad, N., Ishaq, S., Bano, S. & Manzoor, N. Calcium Regulation in Alzheimer's Disease: Mechanistic Understanding. *J. Coll. Physicians Surg. Pak.* **27**, 566−571 (2017).

183. Sciacca, M. F. M., Monaco, I., La Rosa, C. & Milardi, D. The active role of Ca 2+ ions in Aβ-mediated membrane damage. *Chem. Commun.* **54**, 3629−3631 (2018).

184. Morales, I., Guzmàn-Martì-nez, L., Cerda-Troncoso, C., Fari-as, G. A. & Maccioni, R. B. Neuroinflammation in the pathogenesis of Alzheimer's disease. A rational framework

for the search of novel therapeutic approaches. *Front. Cell. Neurosci.* **8**, 112 (2014).

185. Ji, K., Akgul, G., Wollmuth, L. P. & Tsirka, S. E. Microglia Actively Regulate the Number of Functional Synapses. *PLoS One* **8**, e56293 (2013).

186. Bamberger, M. E., Harris, M. E., McDonald, D. R., Husemann, J. & Landreth, G. E. A Cell Surface Receptor Complex for Fibrillar β-Amyloid Mediates Microglial Activation. *J. Neurosci.* **23**, 2665–2674 (2003).

187. El Khoury, J. B. *et al.* CD36 Mediates the Innate Host Response to β-Amyloid. *J. Exp. Med.* **197**, 1657–1666 (2003).

188. Hickman, S. E., Allison, E. K. & El Khoury, J. Microglial Dysfunction and Defective -Amyloid Clearance Pathways in Aging Alzheimer's Disease Mice. *J. Neurosci.* **28**, 8354–8360 (2008).

189. Medeiros, R. & LaFerla, F. M. Astrocytes: Conductors of the Alzheimer disease neuroinflammatory symphony. *Exp. Neurol.* **239**, 133–138 (2013).

190. Olabarria, M., Noristani, H. N., Verkhratsky, A. & Rodríguez, J. J. Concomitant astroglial atrophy and astrogliosis in a triple transgenic animal model of Alzheimer's disease. *Glia* **58**, 831–838 (2010).

191. Kummer, M. P. *et al.* Ear2 Deletion Causes Early Memory and Learning Deficits in APP/PS1 Mice. *J. Neurosci.* **34**, 8845–8854 (2014).

192. Rogers, J. *et al.* Inflammation and Alzheimer's disease pathogenesis. *Neurobiol. Aging* **17**, 681–686 (1996).

193. Heneka, M. T. *et al.* Neuroinflammation in Alzheimer's disease. *Lancet Neurol.* **14**, 388–405 (2015).

194. Summers, W., Koehler, A., Marsh, G., Tachiki, K. & Kling, A. Long-term hepatotoxicity of Tacrine. *Lancet* **333**, 729 (1989).

195. Bullock, R. *et al.* Rivastigmine and donepezil treatment in moderate to moderately-severe Alzheimer's disease over a 2-year period. *Curr. Med. Res. Opin.* **21**, 1317–1327 (2005).

196. Farlow, M. *et al.* Safety and tolerability of donepezil 23 mg in moderate to severe Alzheimer's disease. *BMC Neurol.* **11**, 57 (2011).

197. Camps, P. *et al.* Novel Donepezil-Based Inhibitors of Acetyl- and Butyrylcholinesterase and Acetylcholinesterase-Induced β-Amyloid Aggregation. *J. Med. Chem.* **51**, 3588–3598 (2008).

198. Kume, T. *et al.* Up-regulation of nicotinic acetylcholine receptors by central-type acetylcholinesterase inhibitors in rat cortical neurons. *Eur. J. Pharmacol.* **527**, 77–85 (2005).

199. Tiseo, P., Rogers, S. & Friedhoff, L. Pharmacokinetic and pharmacodynamic profile of donepezil HCl following evening administration. *Br. J. Clin. Pharmacol.* **46**, 13–18 (1998).

200. Kryger, G., Silman, I. & Sussman, J. L. Structure of acetylcholinesterase complexed with E2020 (Aricept®): implications for the design of new anti-Alzheimer drugs. *Structure* **7**, 297–307 (1999).

201. Galdeano, C. *et al.* Structural Determinants of the Multifunctional Profile of Dual Binding Site Acetylcholinesterase Inhibitors as Anti-Alzheimer Agents. *Curr. Pharm. Des.* **16**, 2818–2836 (2010).

202. Cummings, J., Lefevre, G., Small, G. & Appel-Dingemanse, S. Pharmacokinetic rationale for the rivastigmine patch. *Neurology* **69**, S10–S13 (2007).

203. Loy, C. & Schneider, L. Galantamine for Alzheimer's disease and mild cognitive

impairment. *Cochrane database Syst. Rev.* CD001747 (2006) doi:10.1002/14651858.CD001747.pub3.

204. Bullock, R. Efficacy and Safety of Memantine in Moderate-to-Severe Alzheimer Disease: The Evidence to Date. *Alzheimer Dis. Assoc. Disord.* **20**, 23–29 (2006).

205. Miguel-Hidalgo, J . ., Alvarez, X . ., Cacabelos, R. & Quack, G. Neuroprotection by memantine against neurodegeneration induced by β-amyloid(1–40). *Brain Res.* **958**, 210–221 (2002).

206. Song, M. S., Rauw, G., Baker, G. B. & Kar, S. Memantine protects rat cortical cultured neurons against β-amyloid-induced toxicity by attenuating tau phosphorylation. *Eur. J. Neurosci.* **28**, 1989–2002 (2008).

207. Joe, E. & Ringman, J. M. Cognitive symptoms of Alzheimer's disease: clinical management and prevention. *BMJ* **367**, l6217 (2019).

208. Aisen, P. S. *et al.* Effects of Rofecoxib or Naproxen vs Placebo on Alzheimer Disease Progression. *JAMA* **289**, 2819–2826 (2003).

209. Thies, W. & Bleiler, L. 2013 Alzheimer's disease facts and figures. *Alzheimer's Dement.* **9**, 208–245 (2013).

210. Chiang, K. & Koo, E. H. Emerging Therapeutics for Alzheimer's Disease. *Annu. Rev. Pharmacol. Toxicol.* **54**, 381–405 (2014).

211. Rosini, M., Simoni, E., Caporaso, R. & Minarini, A. Multitarget strategies in Alzheimer's disease: benefits and challenges on the road to therapeutics. *Future Med. Chem.* **8**, 697–711 (2016).

212. Harkany, T. *et al.* Mechanisms of ß-Amyloid Neurotoxicity: Perspectives of Pharmacotherapy. *Rev. Neurosci.* **11**, 329–382 (2000).

213. Jouanne, M., Rault, S. & Voisin-Chiret, A.-S. Tau protein aggregation in Alzheimer's disease: An attractive target for the development of novel therapeutic agents. *Eur. J. Med. Chem.* **139**, 153–167 (2017).

214. Jiang, T., Sun, Q. & Chen, S. Oxidative stress: A major pathogenesis and potential therapeutic target of antioxidative agents in Parkinson's disease and Alzheimer's disease. *Prog. Neurobiol.* **147**, 1–19 (2016).

215. Coimbra, J. R. M. *et al.* Highlights in BACE1 Inhibitors for Alzheimer's Disease Treatment. *Front. Chem.* **6**, 178 (2018).

216. Citron, M. Emerging Alzheimer's disease therapies: inhibition of β-secretase. *Neurobiol. Aging* **23**, 1017–1022 (2002).

217. Piton, M. *et al.* Alzheimer's Disease: Advances in Drug Development. *J. Alzheimer's Dis.* **65**, 3–13 (2018).

218. Imbimbo, B. P. & Giardina, G. A. M. γ-secretase inhibitors and modulators for the treatment of Alzheimer's disease: disappointments and hopes. *Curr. Top. Med. Chem.* **11**, 1555–70 (2011).

219. Wolfe, M. S. γ-Secretase as a Target for Alzheimer's Disease. *Adv. Pharmacol.* **64**, 127–153 (2012).

220. Eriksen, J. L. *et al.* NSAIDs and enantiomers of flurbiprofen target γ-secretase and lower Aβ42 in vivo. *J. Clin. Invest.* **112**, 440–449 (2003).

221. Pasqualetti, P. *et al.* A randomized controlled study on effects of ibuprofen on cognitive progression of Alzheimer's disease. *Aging Clin. Exp. Res.* **21**, 102–110 (2009).

222. Green, R. C. Effect of Tarenflurbil on Cognitive Decline and Activities of Daily Living in Patients With Mild Alzheimer Disease - A Randomized Controlled Trial. *JAMA* **302**, 2557 (2009).

223. Sivilia, S. *et al.* Multi-target action of the novel anti-Alzheimer compound CHF5074: in vivo study of long term treatment in Tg2576 mice. *BMC Neurosci.* **14**, 44 (2013).

224. Obregon, D. F. *et al.* ADAM10 Activation Is Required for Green Tea (−)-Epigallocatechin-3-gallate-induced α-Secretase Cleavage of Amyloid Precursor Protein. *J. Biol. Chem.* **281**, 16419−16427 (2006).

225. Gervais, F. *et al.* Targeting soluble Aβ peptide with Tramiprosate for the treatment of brain amyloidosis. *Neurobiol. Aging* **28**, 537−547 (2007).

226. Gupta-Bansal, R., Frederickson, R. C. A. & Brunden, K. R. Proteoglycan-mediated Inhibition of Aβ Proteolysis. *J. Biol. Chem.* **270**, 18666−18671 (1995).

227. Aisen, P. S. *et al.* Tramiprosate in mild-to-moderate Alzheimer's disease − a randomized, double-blind, placebo-controlled, multi-centre study (the Alphase Study). *Arch. Med. Sci.* **1**, 102−111 (2011).

228. Nalivaeva, N. N., Beckett, C., Belyaev, N. D. & Turner, A. J. Are amyloid-degrading enzymes viable therapeutic targets in Alzheimer's disease? *J. Neurochem.* **120**, 167−185 (2012).

229. Deane, R. J. Is RAGE still a therapeutic target for Alzheimer's disease? *Future Med. Chem.* **4**, 915−925 (2012).

230. Baranello, R. *et al.* Amyloid-Beta Protein Clearance and Degradation (ABCD) Pathways and their Role in Alzheimer's Disease. *Curr. Alzheimer Res.* **12**, 32−46 (2015).

231. Galasko, D. *et al.* Clinical trial of an inhibitor of RAGE-A interactions in Alzheimer disease. *Neurology* **82**, 1536−1542 (2014).

232. Gilman, S. *et al.* Clinical effects of A immunization (AN1792) in patients with AD in an interrupted trial. *Neurology* **64**, 1553−1562 (2005).

233. Wiessner, C. *et al.* The Second-Generation Active A Immunotherapy CAD106 Reduces Amyloid Accumulation in APP Transgenic Mice While Minimizing Potential Side Effects. *J. Neurosci.* **31**, 9323−9331 (2011).

234. Panza, F., Solfrizzi, V., Imbimbo, B. P. & Logroscino, G. Amyloid-directed monoclonal antibodies for the treatment of Alzheimer's disease: the point of no return? *Expert Opin. Biol. Ther.* **14**, 1465−1476 (2014).

235. Salloway, S. *et al.* Two Phase 3 Trials of Bapineuzumab in Mild-to-Moderate Alzheimer's Disease. *N. Engl. J. Med.* **370**, 322−333 (2014).

236. Doody, R. S. *et al.* Phase 3 Trials of Solanezumab for Mild-to-Moderate Alzheimer's Disease. *N. Engl. J. Med.* **370**, 311−321 (2014).

237. Novakovic, D. *et al.* Profile of gantenerumab and its potential in the treatment of Alzheimer's disease. *Drug Des. Devel. Ther.* **7**, 1359−64 (2013).

238. Jacobsen, H. *et al.* Combined Treatment with a BACE Inhibitor and Anti-A Antibody Gantenerumab Enhances Amyloid Reduction in APPLondon Mice. *J. Neurosci.* **34**, 11621−11630 (2014).

239. Ferrero, J. *et al.* First-in-human, double-blind, placebo-controlled, single-dose escalation study of aducanumab (BIIB037) in mild-to-moderate Alzheimer's disease. *Alzheimer's Dement. Transl. Res. Clin. Interv.* **2**, 169−176 (2016).

240. Sevigny, J. *et al.* The antibody aducanumab reduces Aβ plaques in Alzheimer's disease. *Nature* **537**, 50−56 (2016).

241. Budd Haeberlein, S. *et al.* Clinical Development of Aducanumab, an Anti-Aβ Human Monoclonal Antibody Being Investigated for the Treatment of Early Alzheimer's Disease. *J. Prev. Alzheimer's Dis.* **4**, 255−263 (2017).

242. Himmelstein, D. S., Ward, S. M., Lancia, J. K., Patterson, K. R. & Binder, L. I. Tau as a

therapeutic target in neurodegenerative disease. *Pharmacol. Ther.* **136**, 8–22 (2012).

243. Khan, A., Corbett, A. & Ballard, C. Emerging amyloid and tau targeting treatments for Alzheimer's disease. *Expert Rev. Neurother.* **17**, 697–711 (2017).

244. Wischik, C. M., Harrington, C. R. & Storey, J. M. D. Tau-aggregation inhibitor therapy for Alzheimer's disease. *Biochem. Pharmacol.* **88**, 529–539 (2014).

245. Atamna, H. & Kumar, R. Protective Role of Methylene Blue in Alzheimer's Disease via Mitochondria and Cytochrome c Oxidase. *J. Alzheimer's Dis.* **20**, S439–S452 (2010).

246. Ettcheto, M. *et al.* A Chronological Review of Potential Disease-Modifying Therapeutic Strategies for Alzheimer's Disease. *Curr. Pharm. Des.* **26**, 1286–1299 (2020).

247. Novak, P. *et al.* AADvac1, an Active Immunotherapy for Alzheimer's Disease and Non Alzheimer Tauopathies: An Overview of Preclinical and Clinical Development. *J. Prev. Alzheimer's Dis.* **6**, 63–69 (2019).

248. West, T. *et al.* Preclinical and Clinical Development of ABBV-8E12, a Humanized Anti-Tau Antibody, for Treatment of Alzheimer's Disease and Other Tauopathies. *J. Prev. Alzheimer's Dis.* **4**, 236–241 (2017).

249. Alam, R. *et al.* Preclinical characterization of an antibody [LY3303560] targeting aggregated Tau. *Alzheimer's Dement.* **13**, 592–593 (2017).

250. Imming, P., Sinning, C. & Meyer, A. Drugs, their targets and the nature and number of drug targets. *Nat. Rev. Drug Discov.* **5**, 821–834 (2006).

251. Alcaro, S., Bolognesi, M. L., García-Sosa, A. T. & Rapposelli, S. Editorial: Multi-Target-Directed Ligands (MTDL) as Challenging Research Tools in Drug Discovery: From Design to Pharmacological Evaluation. *Front. Chem.* **7**, 71 (2019).

252. Grossberg, G. T., Edwards, D. G. T. & Zhao, D. Q. Rationale for Combination Therapy With Galantamine and Memantine in Alzheimer's Disease. *J. Clin. Pharmacol.* **46**, 17S-26S (2006).

253. Deardorff, W. J. & Grossberg, G. A fixed-dose combination of memantine extended-release and donepezil in the treatment of moderate-to-severe Alzheimer's disease. *Drug Des. Devel. Ther.* **10**, 3267–3279 (2016).

254. Klein, J. Phenserine. *Expert Opin. Investig. Drugs* **16**, 1087–1097 (2007).

255. Greig, N. H. *et al.* The experimental Alzheimer drug phenserine: preclinical pharmacokinetics and pharmacodynamics. *Acta Neurol. Scand.* **102**, 74–84 (2000).

256. Thatte, U. Phenserine Axonyx. *Curr. Opin. Investig. drugs* **6**, 729–39 (2005).

257. Tweedie, D. *et al.* Cognitive Impairments Induced by Concussive Mild Traumatic Brain Injury in Mouse Are Ameliorated by Treatment with Phenserine via Multiple Non-Cholinergic and Cholinergic Mechanisms. *PLoS One* **11**, e0156493 (2016).

258. Becker, R. E. *et al.* (-)-Phenserine and Inhibiting Pre-Programmed Cell Death: In Pursuit of a Novel Intervention for Alzheimer's Disease. *Curr. Alzheimer Res.* **15**, 883–891 (2018).

259. Rosini, M. *et al.* Inhibition of Acetylcholinesterase, β-Amyloid Aggregation, and NMDA Receptors in Alzheimer's Disease: A Promising Direction for the Multi-target-Directed Ligands Gold Rush. *J. Med. Chem.* **51**, 4381–4384 (2008).

260. Bezprozvanny, I. The rise and fall of Dimebon. *Drug News Perspect.* **23**, 518 (2010).

261. Makhaeva, G. F. *et al.* Conjugates of γ-Carbolines and Phenothiazine as new selective inhibitors of butyrylcholinesterase and blockers of NMDA receptors for Alzheimer Disease. *Sci. Rep.* **5**, 13164 (2015).

262. Lecoutey, C. *et al.* Design of donecopride, a dual serotonin subtype 4 receptor

agonist/acetylcholinesterase inhibitor with potential interest for Alzheimer's disease treatment. *Proc. Natl. Acad. Sci.* **111**, E3825–E3830 (2014).

263. Giannoni, P. *et al.* Early administration of RS 67333, a specific 5-HT4 receptor agonist, prevents amyloidogenesis and behavioral deficits in the 5XFAD mouse model of Alzheimer's disease. *Front. Aging Neurosci.* **5**, 96 (2013).

264. King, M. V, Marsden, C. A. & Fone, K. C. F. A role for the 5-HT(1A), 5-HT4 and 5-HT6 receptors in learning and memory. *Trends Pharmacol. Sci.* **29**, 482–92 (2008).

265. Matsumoto, M. *et al.* Evidence for involvement of central 5-HT(4) receptors in cholinergic function associated with cognitive processes: behavioral, electrophysiological, and neurochemical studies. *J. Pharmacol. Exp. Ther.* **296**, 676–82 (2001).

266. Cho, S. & Hu, Y. Activation of 5-HT4 receptors inhibits secretion of β-amyloid peptides and increases neuronal survival. *Exp. Neurol.* **203**, 274–278 (2007).

267. Rochais, C. *et al.* Novel Multitarget-Directed Ligands (MTDLs) with Acetylcholinesterase (AChE) Inhibitory and Serotonergic Subtype 4 Receptor (5-HT 4 R) Agonist Activities As Potential Agents against Alzheimer's Disease: The Design of Donecopride. *J. Med. Chem.* **58**, 3172–3187 (2015).

268. Shoham, S., Bejar, C., Kovalev, E., Schorer-Apelbaum, D. & Weinstock, M. Ladostigil prevents gliosis, oxidative–nitrative stress and memory deficits induced by intracerebroventricular injection of streptozotocin in rats. *Neuropharmacology* **52**, 836–843 (2007).

269. Schneider, L. S. *et al.* Low-dose ladostigil for mild cognitive impairment. *Neurology* **93**, e1474–e1484 (2019).

270. Bolea, I. *et al.* Synthesis, Biological Evaluation, and Molecular Modeling of Donepezil and N -[(5-(Benzyloxy)-1-methyl-1 H -indol-2-yl)methyl]- N -methylprop-2-yn-1-amine Hybrids as New Multipotent Cholinesterase/Monoamine Oxidase Inhibitors for the Treatment of Alzheimer. *J. Med. Chem.* **54**, 8251–8270 (2011).

271. López López, L. I., Nery Flores, S. D., Silva Belmares, S. Y. & Sáenz Galindo, A. Naphthoquinones: Biological properties and synthesis of lawsone and derivatives — a structured review. *Vitae* **21**, 248–258 (2014).

272. Vukic, M. D. *et al.* Antibacterial and cytotoxic activities of naphthoquinone pigments from onosma Visianii clem. *EXCLI J.* **16**, 73–88 (2017).

273. Tandon, V. K., Chhor, R. B., Singh, R. V., Rai, S. & Yadav, D. B. Design, synthesis and evaluation of novel 1,4-naphthoquinone derivatives as antifungal and anticancer agents. *Bioorg. Med. Chem. Lett.* **14**, 1079–1083 (2004).

274. Campora, M., Francesconi, V., Schenone, S., Tasso, B. & Tonelli, M. Journey on Naphthoquinone and Anthraquinone Derivatives: New Insights in Alzheimer's Disease. *Pharmaceuticals* **14**, 33 (2021).

275. Checker, R., Sharma, D., Sandur, S. K., Khanam, S. & Poduval, T. B. Anti-inflammatory effects of plumbagin are mediated by inhibition of NF-kappaB activation in lymphocytes. *Int. Immunopharmacol.* **9**, 949–958 (2009).

276. Padhye, S., Dandawate, P., Yusufi, M., Ahmad, A. & Sarkar, F. H. Perspectives on medicinal properties of plumbagin and its analogs. *Med. Res. Rev.* **32**, 1131–1158 (2012).

277. Son, T. G. *et al.* Plumbagin, a novel Nrf2/ARE activator, protects against cerebral ischemia. *J. Neurochem.* **112**, 1316–1326 (2010).

278. Tamafo Fouegue, A. D., Ghogomu, J. N., Bikélé Mama, D., Nkungli, N. K. & Younang, E. Structural and Antioxidant Properties of Compounds Obtained from Fe 2+ Chelation by Juglone and Two of Its Derivatives: DFT, QTAIM, and NBO Studies. *Bioinorg. Chem. Appl.*

1–13 (2016).

279. Leopoldini, M., Russo, N. & Toscano, M. The molecular basis of working mechanism of natural polyphenolic antioxidants. *Food Chem.* **125**, 288–306 (2011).

280. Hennig, L. *et al.* Selective inactivation of parvulin-like peptidyl-prolyl cis/trans isomerases by juglone. *Biochemistry* **37**, 5953–5960 (1998).

281. Hamdane, M. *et al.* Pin1: A therapeutic target in Alzheimer neurodegeneration. *J. Mol. Neurosci.* **19**, 275–287 (2002).

282. Bermejo-Bescós, P. *et al.* In vitro antiamyloidogenic properties of 1,4-naphthoquinones. *Biochem. Biophys. Res. Commun.* **400**, 169–174 (2010).

283. Malik, E. M. & Müller, C. E. Anthraquinones As Pharmacological Tools and Drugs. *Med. Res. Rev.* **36**, 705–748 (2016).

284. Augustin, N. *et al.* Discovery of Helminthosporin, an Anthraquinone Isolated from Rumex abyssinicus Jacq as a Dual Cholinesterase Inhibitor. *ACS Omega* **5**, 1616–1624 (2020).

285. Jung, H. A. *et al.* Inhibitory activities of major anthraquinones and other constituents from Cassia obtusifolia against β-secretase and cholinesterases. *J. Ethnopharmacol.* **191**, 152–160 (2016).

286. Pickhardt, M. *et al.* Anthraquinones Inhibit Tau Aggregation and Dissolve Alzheimer's Paired Helical Filaments in Vitro and in Cells. *J. Biol. Chem.* **280**, 3628–3635 (2005).

287. Paranjape, S. *et al.* Inhibition of Tau Aggregation by Three Aspergillus nidulans Secondary Metabolites: 2,ω-Dihydroxyemodin, Asperthecin, and Asperbenzaldehyde. *Planta Med.* **80**, 77–85 (2014).

288. Scherzer-Attali, R. *et al.* Naphthoquinone-tyrptophan reduces neurotoxic Aβ*56 levels and improves cognition in Alzheimer's disease animal model. *Neurobiol. Dis.* **46**, 663–672 (2012).

289. Scherzer-Attali, R., Shaltiel-Karyo, R., Adalist, Y., Segal, D. & Gazit, E. Generic inhibition of amyloidogenic proteins by two naphthoquinone-tryptophan hybrid molecules. *Proteins Struct. Funct. Bioinforma.* **80**, 1962–1973 (2012).

290. Chioua, M. *et al.* Synthesis, Biological Assessment and Molecular Modeling of Racemic QuinoPyranoTacrines for Alzheimer's Disease Therapy. *ChemistrySelect* **3**, 461–466 (2018).

291. Nepovimova, E. *et al.* Multitarget drug design strategy: Quinone-tacrine hybrids designed to block amyloid-β aggregation and to exert anticholinesterase and antioxidant effects. *J. Med. Chem.* **57**, 8576–8589 (2014).

292. Li, S.-Y. *et al.* Design, synthesis and evaluation of novel tacrine–rhein hybrids as multifunctional agents for the treatment of Alzheimer's disease. *Org. Biomol. Chem.* **12**, 801–814 (2014).

293. Camps, P. *et al.* Huprine X is a novel high-affinity inhibitor of acetylcholinesterase that is of interest for treatment of Alzheimer's disease. *Mol. Pharmacol.* **57**, 409–17 (2000).

294. Pérez-Areales, F. J. *et al.* Design, synthesis and multitarget biological profiling of second-generation anti-Alzheimer rhein–huprine hybrids. *Future Med. Chem.* **9**, 965–981 (2017).

295. Tonelli, M. *et al.* Multitarget Therapeutic Leads for Alzheimer's Disease: Quinolizidinyl Derivatives of Bi- and Tricyclic Systems as Dual Inhibitors of Cholinesterases and β-Amyloid (Aβ) Aggregation. *ChemMedChem* **10**, 1040–1053 (2015).

296. Campora, M. *et al.* Multitarget Biological Profiling of New Naphthoquinone and Anthraquinone-Based Derivatives for the Treatment of Alzheimer's Disease. *ACS Chem. Neurosci.* **12**, 447–461 (2021).

297. Carta, A. *et al.* Synthesis and antiproliferative activity of 3-aryl-2-[1H(2H)-benzotriazol-1(2)-yl]acrylonitriles variously substituted: Part 4. *Farm.* **59**, 637–644 (2004).

298. Prachayasittikul, V. *et al.* Synthesis, anticancer activity and QSAR study of 1,4-naphthoquinone derivatives. *Eur. J. Med. Chem.* **84**, 247–263 (2014).

299. Singh, V. K., Verma, S. K., Kadu, R. & Mobin, S. M. Identification of unusual C−Cl⋯π contacts in 2-(alkylamino)-3-chloro-1,4-naphthoquinones: effect of N-substituents on crystal packing, fluorescence, redox and anti-microbial properties. *RSC Adv.* **5**, 43669–43686 (2015).

300. Shrestha-Dawadi, P. B., Bittner, S., Fridkin, M. & Rahimipour, S. On the Synthesis of Naphthoquinonyl Heterocyclic Amino Acids. *Synthesis (Stuttg).* 1468–1472 (1996).

301. Rivera-Ávalos, E. *et al.* Synthesis of Amino Acid–Naphthoquinones and In Vitro Studies on Cervical and Breast Cell Lines. *Molecules* **24**, 4285 (2019).

302. Havlíčková, L. & Arient, J. Anthraquinone dyes. Part VI. Nuclear alkylation of 1-aminoanthraquinone leuco-derivative. *J. Chem. Soc. C* 570–572 (1970) doi:10.1039/J39700000570.

303. Carpenter, T. S. *et al.* A Method to Predict Blood-Brain Barrier Permeability of Drug-Like Compounds Using Molecular Dynamics Simulations. *Biophys. J.* **107**, 630–641 (2014).

304. Di, L., Kerns, E. H., Fan, K., McConnell, O. J. & Carter, G. T. High throughput artificial membrane permeability assay for blood−brain barrier. *Eur. J. Med. Chem.* **38**, 223–232 (2003).

305. Cellamare, S. *et al.* Design, synthesis, and biological evaluation of glycine-based molecular tongs as inhibitors of Aβ1−40 aggregation in vitro. *Bioorg. Med. Chem.* **16**, 4810–4822 (2008).

306. Ellman, G. L., Courtney, K. D., Andres, V. & Featherstone, R. M. A new and rapid colorimetric determination of acetylcholinesterase activity. *Biochem. Pharmacol.* **7**, 88–95 (1961).

307. Convertino, M., Pellarin, R., Catto, M., Carotti, A. & Caflisch, A. 9,10-Anthraquinone hinders beta-aggregation: how does a small molecule interfere with Abeta-peptide amyloid fibrillation? *Protein Sci.* **18**, 792–800 (2009).

308. Tasso, B. *et al.* Quinolizidinyl derivatives of bi- and tricyclic systems as potent inhibitors of acetyl- and butyrylcholinesterase with potential in Alzheimer's disease. *Eur. J. Med. Chem.* **46**, 2170–2184 (2011).

309. Leonetti, F. *et al.* Homo- and hetero-bivalent edrophonium-like ammonium salts as highly potent, dual binding site AChE inhibitors. *Bioorg. Med. Chem.* **16**, 7450–7456 (2008).

310. Conejo-García, A. *et al.* Homodimeric Bis-Quaternary Heterocyclic Ammonium Salts as Potent Acetyl- and Butyrylcholinesterase Inhibitors: A Systematic Investigation of the Influence of Linker and Cationic Heads over Affinity and Selectivity. *J. Med. Chem.* **54**, 2627–2645 (2011).

311. Haviv, H., Wong, D., Silman, I. & Sussman, J. Bivalent Ligands Derived from Huperzine A as Acetylcholinesterase Inhibitors. *Curr. Top. Med. Chem.* **7**, 375–387 (2007).

312. Elsinghorst, P. W., González Tanarro, C. M. & Gütschow, M. Novel Heterobivalent Tacrine Derivatives as Cholinesterase Inhibitors with Notable Selectivity Toward Butyrylcholinesterase. *J. Med. Chem.* **49**, 7540–7544 (2006).

313. Scherzer-Attali, R. *et al.* Methylations of Tryptophan-Modified Naphthoquinone Affect Its Inhibitory Potential toward Aβ Aggregation. *J. Phys. Chem. B* **117**, 1780–1789 (2013).

314. Bolognino *et al.* A Prospective Repurposing of Dantrolene as a Multitarget Agent for Alzheimer's Disease. *Molecules* **24**, 4298 (2019).

315. Jasial, S., Hu, Y. & Bajorath, J. How Frequently Are Pan-Assay Interference Compounds Active? Large-Scale Analysis of Screening Data Reveals Diverse Activity Profiles, Low Global Hit Frequency, and Many Consistently Inactive Compounds. *J. Med. Chem.* **60**, 3879–3886 (2017).

316. Pisani, L. *et al.* Investigating alkyl nitrates as nitric oxide releasing precursors of multitarget acetylcholinesterase-monoamine oxidase B inhibitors. *Eur. J. Med. Chem.* **161**, 292–309 (2019).

317. Chuang, H. Y. K., Patek, D. R. & Hellerman, L. Mitochondrial monoamine oxidase. Inactivation by pargyline. Adduct formation. *J. Biol. Chem.* **249**, 2381–4 (1974).

318. Hubálek, F. *et al.* Inactivation of Purified Human Recombinant Monoamine Oxidases A and B by Rasagiline and Its Analogues. *J. Med. Chem.* **47**, 1760–1766 (2004).

319. Ittner, L. M. & Götz, J. Amyloid-β and tau — a toxic pas de deux in Alzheimer's disease. *Nat. Rev. Neurosci.* **12**, 67–72 (2011).

320. Dammers, C. *et al.* Selection and Characterization of Tau Binding ᴅ-Enantiomeric Peptides with Potential for Therapy of Alzheimer Disease. *PLoS One* **11**, e0167432 (2016).

321. Delarmelina, M. *et al.* Synthesis, antitumor activity and docking of 2,3-(substituted)-1,4-naphthoquinone derivatives containing nitrogen, oxygen and sulfur. *J. Braz. Chem. Soc.* **26**, 1804–1816 (2015).

322. Josey, B. J., Inks, E. S., Wen, X. & Chou, C. J. Structure–Activity Relationship Study of Vitamin K Derivatives Yields Highly Potent Neuroprotective Agents. *J. Med. Chem.* **56**, 1007–1022 (2013).

323. Yakkala, P. A., Giri, D., Chaudhary, B., Auti, P. & Sharma, S. Regioselective C–H alkylation and alkenylation at the C5 position of 2-amino-1,4-naphthoquinones with maleimides under Rh(III) catalysis. *Org. Chem. Front.* **6**, 2441–2446 (2019).

324. Lucki, N. C. *et al.* A cell type-selective apoptosis-inducing small molecule for the treatment of brain cancer. *Proc. Natl. Acad. Sci.* **116**, 6435–6440 (2019).

325. da Silva, C. C. *et al.* Antibacterial Activity of 2-Amino-1,4-naphthoquinone Derivatives Against Gram-Positive and Gram-Negative Bacterial Strains and Their Interaction with Human Serum Albumin. *J. Braz. Chem. Soc.* **31**, 1838–1851 (2020).

326. Gokmen, Z., Onan, M. E., Deniz, N. G., Karakas, D. & Ulukaya, E. Synthesis and investigation of cytotoxicity of new N - and S,S -substituted-1,4-naphthoquinone (1,4-NQ) derivatives on selected cancer lines. *Synth. Commun.* **49**, 3008–3016 (2019).

327. Schepetkin, I. A. *et al.* Synthesis, anticancer activity, and molecular modeling of 1,4-naphthoquinones that inhibit MKK7 and Cdc25. *Eur. J. Med. Chem.* **183**, 111719 (2019).

328. Tandon, V. K., Maurya, H. K., Verma, M. K., Kumar, R. & Shukla, P. K. 'On water' assisted synthesis and biological evaluation of nitrogen and sulfur containing hetero-1,4-naphthoquinones as potent antifungal and antibacterial agents. *Eur. J. Med. Chem.* **45**, 2418–2426 (2010).

329. Carmichael, J., DeGraff, W. G., Gazdar, A. F., Minna, J. D. & Mitchell, J. B. Evaluation of a tetrazolium-based semiautomated colorimetric assay: assessment of chemosensitivity testing. *Cancer Res.* **47**, 936–42 (1987).

330. Hoey, S. E., Williams, R. J. & Perkinton, M. S. Synaptic NMDA Receptor Activation Stimulates -Secretase Amyloid Precursor Protein Processing and Inhibits Amyloid- Production. *J. Neurosci.* **29**, 4442–4460 (2009).

331. Cox, C. J. *et al.* Dietary (-)-epicatechin as a potent inhibitor of βγ-secretase amyloid precursor protein processing. *Neurobiol. Aging* **36**, 178–87 (2015).

332. Chakraborty, H. & Chattopadhyay, A. Sensing Tryptophan Microenvironment of Amyloid

Protein Utilizing Wavelength-Selective Fluorescence Approach. *J. Fluoresc.* **27**, 1995–2000 (2017).

333. Dovey, H. F. *et al.* Functional gamma-secretase inhibitors reduce beta-amyloid peptide levels in brain. *J. Neurochem.* **76**, 173–181 (2009).

List of Pubblications

Reference 274: <u>Campora, M.,</u> Francesconi, V., Schenone, S., Tasso, B., Tonelli, M. Journey on Naphthoquinone and Anthraquinone Derivatives: New Insights in Alzheimer's Disease. *Pharmaceuticals* **14**, 33 (2021), doi: 10.3390/ph14010033.

Reference 296: <u>Campora, M.,</u> Canale, C., Gatta, E., Tasso, B., Laurini, E., Relini, A., Pricl, S., Catto, M., Tonelli, M. Multitarget Biological Profiling of New Naphthoquinone and Anthraquinone-Based Derivatives for the Treatment of Alzheimer's Disease. *ACS Chem. Neurosci.* **12**, 447–461 (2021), doi: 10.1021/acschemneuro.0c00624.